# INFORMATION TO USERS

This manuscript has been reproduced from the microfilm master. UMI films the text directly from the original or copy submitted. Thus, some thesis and dissertation copies are in typewriter face, while others may be from any type of computer printer.

**The quality of this reproduction is dependent upon the quality of the copy submitted.** Broken or indistinct print, colored or poor quality illustrations and photographs, print bleedthrough, substandard margins, and improper alignment can adversely affect reproduction.

In the unlikely event that the author did not send UMI a complete manuscript and there are missing pages, these will be noted. Also, if unauthorized copyright material had to be removed, a note will indicate the deletion.

Oversize materials (e.g., maps, drawings, charts) are reproduced by sectioning the original, beginning at the upper left-hand corner and continuing from left to right in equal sections with small overlaps. Each original is also photographed in one exposure and is included in reduced form at the back of the book.

Photographs included in the original manuscript have been reproduced xerographically in this copy. Higher quality 6" x 9" black and white photographic prints are available for any photographs or illustrations appearing in this copy for an additional charge. Contact UMI directly to order.

**UMI**

A Bell & Howell Information Company
300 North Zeeb Road, Ann Arbor MI 48106-1346 USA
313/761-4700 800/521-0600

# PHYSICALLY-BASED DYNAMIC MODEL FOR THE CONTROL OF CAVITY PRESSURE IN THERMOPLASTICS INJECTION MOLDING

By:
MEHDI RAFIZADEH

A Thesis Submitted to the Faculty of Graduate Studies
and Research in Partial Fulfilment of the
Requirements for the Degree of
Doctor of Philosophy

Department of Chemical Engineering
McGill University
Montreal, Canada

# ABSTRACT

The injection molding process, due to its versatility, cost effectiveness, and ability to produce precise complex articles is widely used in plastics processing. Mold cavity pressure is a good indicator of the processes taking place in the cavity and plays an important role in determining the quality of the molded articles. The dynamic modeling and control of cavity pressure, based on a physically-based approach, is studied in this research project. The work deals with the filling and packing phases.

A lumped physically-based model was developed in order to study the behavior of the system. The model is derived from conservation laws and incorporates a physical understanding of the process. The whole system was divided into subsystems including the hydraulic system, ram-screw, barrel, and polymer delivery system. It was found necessary to account for polymer melt elasticity as well as non-Newtonian behavior of the polymer melt flow. Consideration of the growing solid skin in the polymer delivery system was found to be necessary.

The dynamics of the cavity pressure during the filling phase were investigated and found to be non-linear and time-varying in relation to the hydraulic servo-valve opening which is the manipulated variable. The dynamic behavior of the cavity pressure is approximated by piece-wise linearization of the non-linear governing equations to derive a transfer function using the physically-based model which is of fifth order. Adaptive PI, PID, and IMC controllers were designed and tested for the control of the cavity pressure. Various tuning techniques, along with changes in set-point, were used to determine conservative settings for the PI and PID controllers.

A similar approach was used to study the dynamics of the cavity pressure during the packing phase. A sixth order transfer function, with piece-wise linearization, was derived to approximate the non-linear and time-varying behavior of the cavity pressure during packing. The adaptive PI, PID, and IMC controllers were successfully applied into the packing phase. The transition of the filling-to-packing was selected to be detected by the derivative of the cavity pressure and adaptive controllers were successfully used for this phase.

Two commonly used injection molding grade thermoplastics, polyethylene and polystyrene, were used in experimental part of this work for model validation and controller testing.

# RÉSUMÉ

Grâce à sa versatilite,ses coût avantageux et sa capacité de produire des articles de formes complexes, le moulage par injection est un procédé largement utilisé dans la production d'objets plastiques. La pression dans le moule est une bonne indication des procédés impliqués dans la cavité et joue un rôle important dans la détermination de la qualité des objets moulés. Un modèle dynamique a été développé et le contrôle de la pression dans le moule a été étudié dans ce projet. L'étude a porté sur le remplissage et le compactage du moule.

Un modèle à constantes distribuées a été développé pour cette étude à partir des lois de conservation et inclus une connaissance du procédé. Le système a été subdivisé en quatre parties: le système hydraulique, le la vis sans fin, le fourreau, et les conduits du moule. Il s'est avéré nécessaire de tenir compte de l'élasticité et des propriétés non-Newtoniennes du polymère dans le modèle. L'épaiseur de la couche de solidification du polymère dans le conduit d'admission du moule a été pris en considération dans le modèle.

Le comportement dynamique de la pression dans la cavité a été étudié pour la phase de remplissage. Cette pression s'est avérée non-linéaire et variant avec le temps quand la variable manipulée, la position de la vanne automatique, est modifiée. Ces équations furent ensuite linéarisees pour approximer la pression dans la cavité. Ces résultats ont été utilisés dans un modèle pour la dérivation d'une fonction de transfert du cinquième ordre. Des stratégies de contrôle adaptutif PI, PID et IMC ont été désignées et vérifiées pour contrôler la pression dans la cavité. Plusieurs techniques de d'ajustement ont été utilisées pour obtenir des valeurs conservatrices pour les contrôleurs PI et PID.

Une approche similaire a été appliquée pour étudier la dynamique de la pression durant le compactage du moule. Une équation du sixième ordre linéarisée fût dérivée pour approximer la pression dynamique non-linéaire dans le moule durant la phase de compactage. Des stratégies de contrôle adaptif PI, PID et IMC ont été appliquées avec succès. La transition de la phase du remplissage au compactage fût détectée par le changement de la valeur de la dérivée de la pression dans la cavité.

Le polyéthylène et le polystyrène, deux polymères utilisés à grande échelle dans le moulage par injection, ont été utilisés pour la validation du modèle et la vérification de la stratégie de contrôle.

# ACKNOWLEDGMENTS

Throughout this project, I have received a great amount of assistance, motivation, and scientific input from many people. I wish to convey my deep appreciation to them all, in particular to:

Professor Musa R. Kamal and Professor W. Ian Patterson, my research supervisors, for their patience, fruitful discussions, advice, and great interest throughout the course of this study. I would also like to thank them for their critical review of the thesis which instilled some measure of clarity and completeness to this work.

Mr. A. Gagnon and the staff of the machine and Mr. L. Cusmich, electronics workshop, for their assistance in the maintenance of the experimental equipment.

Dr. A. E. Varela, Mr. I. Ansari, Mr. F. Manero-Brito, Mr. M. Samara, Mr. H. Garmabi and the whole polymer group on the 5$^{th}$ floor, for their valuable discussion and comments throughout the project. I wish to thank Mr. F. Munaretto for his cooperation in proof reading this manuscript. Special thanks to Mr. F. Koran for translating the abstract into French.

The financial support provided by the Ministry of Culture and Higher Education of the Islamic Republic of Iran in the form of scholarship is also greatly appreciated.

Finally, I would like to express my deep gratitude to my family for their love, support, encouragement, and understanding.

# TABLE OF CONTENTS

# LIST OF TABLES

# LIST OF FIGURES

# CHAPTER 1

## INTRODUCTION AND THESIS OBJECTIVES

The last few decades have seen rapid development in the use of synthetic polymeric materials such that, the plastic production worldwide is doubled during the last two decades and reached 110 million ton in 1995 [1]. The growth in the use of polymers has been accomplished by developments and improvements in the processes to convert them into useful products. Polymer processing is concerned with the operations carried out to convert polymeric materials into finished consumer products. There are various plastics processing techniques which permit three dimensional control over the shape of the manufactured article of which injection molding is one of the most common and widely used operations. Its versatility and the significant fraction of the total industrial output of plastics that is molded make it one of the most important of the plastics fabrication operations. Automobile parts, electrical appliances, and medical equipment are some of the great variety of products that are manufactured using the injection molding process. The process, which can be automated, offers economy of operation with low labor cost, high production rates and good finished part quality. The process is used for thermoplastics, thermosetting resins, and rubbers. The thermoplastics injection molding is considered in this study.

## 1.1 A Brief Review of the Process

The injection molding machine consists of three parts: the hydraulic system, the injection molding unit, and the clamping unit [2]. The most common injection unit is the in-line reciprocating screw type. Figure 1.1 shows a simplified sketch of a typical horizontal single screw injection molding machine.

Solid polymer is supplied from a hopper, melted by means of heaters and screw rotation, and the melt is accumulated between the end of the screw and the injection molding nozzle at the end of the barrel. Screw rotation ceases and the polymer on the stationary screw continues to melt by heat conduction from the hot barrel. Hence this period is also called "soak" time. During the "filling" phase, the screw then moves forward and fills the mold. During the "packing" and "holding" phase, more melt is injected, and the melt is subsequently held under high pressure. The additional melt is injected to compensate for the shrinkage during the cooling of the article. A non-return valve at the end of screw prevents the polymer from flowing back to the plastication zone. Later, when the melt in the "gate", which is a narrow entrance to the mold, freezes, the melt within the mold is still at high pressure. As the melt cools and solidifies, the pressure drops. After gate freezing, screw rotation commences to generate melt for the next shot, then screw rotation ceases. Once the melt has frozen, the solidified part is ejected from the mold, and the mold is closed to accept the next shot. The molding cycle can be depicted graphically by the cavity pressure versus time diagram in Figure 1.2. It is a cyclic process characterized by the following phases: heating and melting of polymeric material, mixing and injection of the melt into a mold cavity, cooling and solidification, and ejection of the final part. The process is very complex due to the high degree of interaction between the material, machine, and process variables. Optimal performance of the injection molding process is characterized by consistent and repeatable cycles. Therefore, precise monitoring and efficient control are necessary for proper performance.

The present work is concerned mainly with dynamic simulation and control studies relating to the injection molding process. A brief review of other related areas

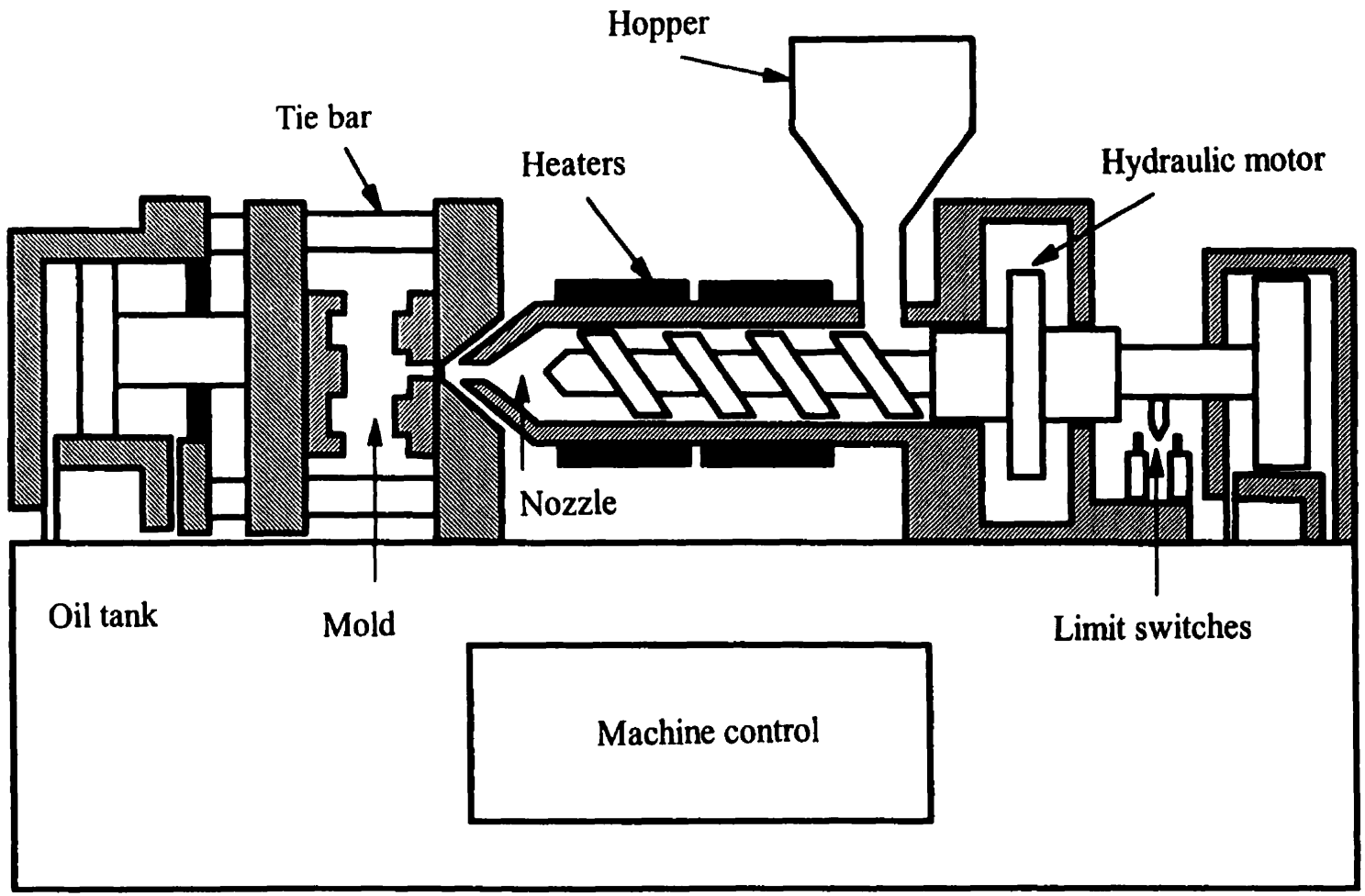


**Figure 1.1** Schematic single screw injection molding machine

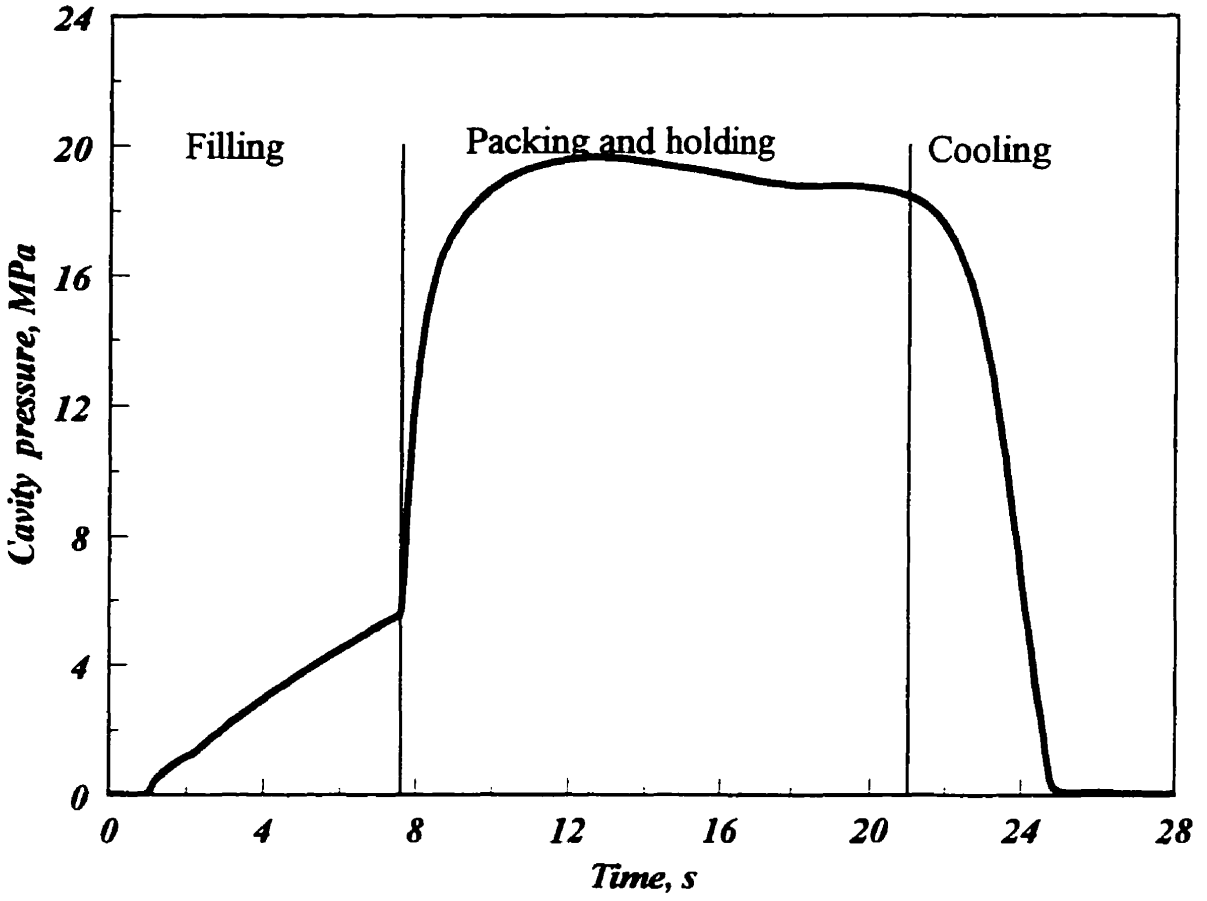


**Figure 1.2** Cavity pressure versus time

will be presented as necessary.

## 1.2 Modeling of the Process

A mathematical model of a system is a tool used to study the behavior of the actual system [3]. There are two methods for model construction: theoretical and experimental methods. Theoretical models are derived directly from basic principles while experimental models use correlations developed from experimental results.

### 1.2.1 Theoretical Modeling

Theoretical modeling is about understanding all the facts that are relevant to an actual system. The basic conservational laws are applied to the different processes in the system. Theoretical models can be categorized in two groups: distributive and lumped models. Distributive models take into consideration the spatial gradients of the dependent variables. Lumped models assume that the gradients of some dependent variables are zero in some space.

#### 1.2.1.1 Distributive Modeling

Different theoretical models, of varying complexity, have been proposed for the various phases of the injection molding process [8-21]. These theoretical distributive models for the phases of the injection molding cycle are attempts to predict the distribution of polymer pressure, temperature and velocity in the cavity and the barrel and their dependence on the resin properties, cavity shape, screw design and processing conditions. This approach leads to a good understanding of the process.

Barrie [4] performed a study of the melt flow behavior between the injection barrel and the mold entry. To understand the melt flow behavior, flow paths were separated into: a) the delivery channels from the injection barrel, and b) the cavity. He calculated the pressure drops using elementary non-Newtonian flow equations for straight and tapered circular channels and showed a comparison between the experimental and calculated results which were in good agreement. Donovan *et al* [5] studied the

plasticating phase in a reciprocating-screw injection molding machine. They concluded that the plasticating process is similar to transient plasticating extrusion behavior. Hence, better plasticating is achieved by a low screw rpm and a long rotation time rather than by a high screw rpm and a short rotation time. Donovan [6] presented a theoretical model for the transient melting behavior in a reciprocating-screw injection molding machine. A useful degree of correlation between the theory and experiment was demonstrated for various operating conditions. Williams and Lord [7,8] developed a finite difference analysis of the temperature, pressure, and velocity distributions for the flow of thermoplastics in straight and tapered, hot and cold walled circular flow channels and cavities. The formation of a layer of solidified plastic on the flow channel walls was detected in their model. Their modeling results were reasonably accurate when compared to data for plaque, disc, and telephone housing molds. Kamal *et al* [9] simulated the injection molding of thermoplastics in thin, rectangular cavities by two models. One is the numerical solution referred to as bounded radial flow model (BRFM). The second solution was based on potential theory. Hence, an analytical solution to the transport equation was depicted. They assumed that the polymer melt followed the Van der Waals equation of state extended for polymers. They compared their results with experimental data and good agreement was obtained. Ryan and Chung [10] presented a conformal mapping analysis of the mold filling behavior in rectangular cavities. This method was a relatively simple and direct method for the determination of the pressure distribution, temperature distribution, and filling time. They compared the results obtained by means of conformal mapping with both theoretical and experimental results previously reported in the literature. They inferred three additional results from their study. Firstly, the pressure distribution, flow pattern, melt front progression, and filling time were not significantly influenced by the gate dimensions. An increase in gate width corresponded to a slight increase in cavity pressure and consequently a small decrease in filling time. Secondly, the isothermal, inelastic analysis yielded a reasonably accurate approximation for the non-isothermal filling of thin rectangular cavities by viscoelastic molten polymers. Thirdly, incorporation of the convection terms in the energy equation

resulted in a more uniform temperature distribution over the entire mold cavity, but had relatively little effect on the overall filling time. Kamal and Lafleur [11] outlined some of the significant developments associated with computer simulation of the thermoplastics injection molding process. They discussed the mathematical simulation which involves writing of the relevant continuity, momentum, and energy equations in the mold cavity and delivery system. They emphasized that knowledge of the morphological, crystallization, and orientation phenomena of the polymer were necessary to predict the microstructure and ultimate properties of the molded article. They made some simplifying assumptions to reduce the complexity of governing equations. Lafleur and Kamal [12,13] proposed such a model that was capable of describing moldability parameters and characteristics of the final product. They considered the viscoelastic behavior and crystallization of the polymer using the White-Metzner modification of the Maxwell model and the Avrami equation. They experimentally tested the accuracy of the model. Their model included the filling, packing, and cooling phases. Gogos *et al* [14] modeled the flow of an isothermal and incompressible power-law fluid in the mold cavity, during the filling phase. They gave special attention to the flow region near the advancing melt front, in order to obtain better insight of the fountain effect, during which the fluid flows from center to the walls of the cavity. Their results of the simulation of the flow front region were in qualitative agreement with experimental results. Titomanlio *et al* [15] described the packing-holding phase on the basis of an extension of the Lord and Williams analysis of mold filling [7,8]. Crystallization was not explicitly accounted for in the energy equation. The reduction of cooling rate by the effect of crystallization heat release was, however, approximately accounted for by means of a suitable reduction of thermal diffusivity. They solved their model numerically. Kamal and Chu [16] developed a two-dimensional mathematical model to evaluate the effects of viscoelasticity, non-isothermality, and fountain flow on the structure of the flow filed. They simulated using the no-slip and slip boundary conditions and showed that a slip boundary condition is necessary to alleviate the singularities in the flow structure. They also indicated that the predicted stress profiles were significantly

influenced by the viscoelasticity of the polymer melt. Huilier *et al* [17] proposed a model for the packing phase in injection molding of thermoplastics. Their model held for amorphous as well as for crystalline polymers with known kinetics of crystallization. Their model predicted quite accurately the pressure evolution recorded on an experimental mold of simple geometry. Chiang *et al* [18,19] demonstrated a unified theoretical model to simulate the filling and packing phases of the injection molding process. For pressure-volume-temperature (PVT) behavior, the classical empirical equation of state proposed by Tait was used. Their model was based on a hybrid finite-element/finite-difference numerical solution of the generalized Hele-Shaw flow of a compressible viscous fluid under non-isothermal conditions. Their predicted pressure history over the entire filling and packing phases was generally in good agreement with corresponding experimental results. Kamal and Papathanasiou [20] presented the application of boundary fitted curvilinear coordinates (BFCC) to the modeling of the filling phase of injection molding of a viscoelastic material in a cavity of complex shape. Their model considered viscoelastic, non-isothermal flow with an advancing free surface in a cavity of complex shape with an insert. They showed satisfactory agreement between experimental and simulated results, with larger discrepancies occurring toward the end of filling and at longer injection times. Titomanlio [21] performed a simulation with reference to filling, packing/holding and cooling phases on the basis of Lord and Williams [7,8] model. They took the effect of pressure into account on both viscosity and crystallization kinetics.

The advantage of distributive theoretical models is that they can be developed for a process or a plant that is not yet built or available for experimentation. Such models are useful in the analysis, optimization, and design of processing parameters, such as filling time, injection rate, injection and clamping pressure, melt and mold temperatures, solidification time, etc, in order to improve overall productivity of the molding operation. They usually describe the behavior of the polymer melt after the nozzle. Constant nozzle pressure is one of common assumptions of some of these models. In a few cases, the models are coupled with principles of polymer science to yield predictions regarding

physical properties of the molded articles, such as crystallinity, residual stresses, tensile modulus, etc. They are not, however, appropriate for real-time control applications. They normally lead to a set of non-linear partial differential governing equations; numerical solutions are usually required with considerable computational efforts. Despite the growing power of computers to perform more complex calculations faster, it takes hours, even days sometimes, to solve these equations and reach to final solution. Therefore, these models are not usually suitable for process control purposes.

### 1.2.1.2 Lumped Modeling

The alternative approach to the theoretical model is lumped modeling of the injection molding machine. In spite of existence of a great number of published works in the field of distributive modeling, the research in lumped modeling is less comprehensive. Shankar and Paul [22], in the first place, presented a deterministic non-linear lumped parameter mathematical model. Their state model was based on a seventh order non-linear system with the seven state variables of hydraulic injection pressure, screw position, screw velocity, barrel pressure, flow through the relief valve, hydraulic back pressure and the volume of the polymer in the cavity. They estimated most by the model parameters from experimental data. The simulation results were qualitatively in agreement with experimental results. Furthermore, they did not show the control application of their model. Wang *et al* [23] presented a simulation using an approach similar to that of Shankar and Paul [22]. However, their simulation involved modeling of air shots. They used a four-constant viscosity model. Chiu *et al* [24] developed a non-linear mathematical model for the filling phase. They formulated their model using the Reynolds transport theorem. The mold filling process was approximated by the transient phenomenon of the non-Newtonian flow through a closed conduit. The process was divided into two parts: the actuation system and the mold filling process. The model was an eight order non-linear system with eight state variables: spool position, supply pressure, injection pressure, screw position, screw velocity, barrel temperature, volume of polymer in the cavity, and polymer flow rate.

They found five of the model parameters by the model fitting method. Comparison between the experimental results and the theoretical simulation indicated that the non-linear model gave a reasonable representation of the mold filling dynamics when acrylonitrile-butadiene-styrene (ABS) was injected into a disk-shaped mold. Wei *et al* [25] derived a non-linear mathematical model employing the Reynolds transport theorem for a microcomputer controlled servo-pump injection molding machine. The variable displacement pump was used in the actuation system of the injection molding machine because of its advantages, such as energy saving, lower noise, and high efficiency. Servo-pump pressure and control flow were proportional to its input voltage. This was the first time that a servo-pump machine was modeled. Their model was a sixth-order non-linear system with six state variables: servo-pump flow rate, injection pressure, screw position, screw velocity, barrel pressure, and polymer melt flow rate. Six parameters of the model were obtained by the model fitting method. It provided a good representation of the servo-pump controlled injection molding machine dynamics. Woll and Cooper [26] derived a multi-variable, non-linear model for the injection molding machine. They related the mold cavity pressure pattern to the barrel temperature and holding pressure. The model included the filling, packing, and cooling phases for a rectangular ASTM flame bar. The packing and cooling phases were considered to occur concurrently. A first order model was assumed for the ram velocity.

The above lumped approach for modeling leads to simultaneous non-linear ordinary differential equations. Such equations are more suitable for control applications than distributive parameter models.

### 1.2.2 Experimental Modeling

The drawback of theoretical models is the enormous effort required to develop such models. Furthermore, these models involve many parameters that sometimes are difficult to estimate theoretically. The alternative approach is an experimental model or identification method. The experimental determination of the dynamic behavior of a process from input-output signals is referred to as system identification. Experimental

modeling avoids many of the difficulties and hypotheses necessary in theoretical modeling, but experimental models are like black boxes where the estimated parameters are without physical meaning. The experimental model is generally valid for the conditions where the system identification takes place, unless the process is linear and time invariant which is usually not the case. Experimental methods can be classified into classical deterministic and modern parametric groups.

Classical identification methods are based on deterministic perturbations of the input signal such as step, pulse, and sinusoidal changes [27,28]. A first order plus dead time or second order system plus dead time are widely used for modeling chemical processes. The graphical or non-linear regression fitting methods are used to estimate the gain, time constant, and dead time. A disadvantage of the deterministic methods is that they are useful mainly when the system has small amounts of noise. Moreover, it is difficult to choose the best order for the system among higher order systems. Therefore, in practice, some features of the process may not be adequately described.

Variables in most processes are subject to random disturbances (noises) which cannot be described by deterministic modeling. Parametric identification methods provide a noise model in addition to the process model [29]. Hence, the estimation of the process model parameters is more reliable. The pseudo-random binary signal (PRBS), which consists of a series of positive and negative step changes of different durations, is widely accepted as the test signal. The advantage of the PRBS is that it has a rich and predetermined frequency spectrum, but the testing duration of a PRBS is much longer than a step test.

The unknown values in deterministic and parametric methods can be estimated off-line or on-line. In the off-line approach, model parameters are calculated using the experimental data. These values are used for controller design without further changes. In the on-line approach, the unknown values are calculated continuously during the operation of the process. Hence, on-line measurement is required. However, the amount of calculation effort is a critical factor. The on-line approach is useful for non-linear and time-varying systems.

## 1.3 Injection Molding Control

In injection molding, consistency and repeatability from cycle to cycle are important objectives of process control. Hence, some important variables should be controlled to assure the performance of the machine. So far, researchers have investigated the dynamics and control of various variables of the process under different conditions.

A detailed discussion of injection molding variables and control is given in the next chapter. For the moment, it should be mentioned that polymer melt pressure at some points in the cavity is one of the best variables to be controlled. Paulson [30] studied the various variable measurements. He concluded that the cavity pressure is the best variable for process to understand what is going on in the process and it determines many final molded article properties. Keyes [31] discussed the available process control equipment as well as different possible variables which could be used to control product properties. He briefly described adaptive and computer based control and their effect on the part quality. Mold cavity pressure, injection melt pressure, holding pressure, injection velocity, injection ram position, and melt temperature were considered as variables in his studies. He suggested that cavity pressure is one of the most significant variables to control.

## 1.4 Thesis Objectives

The present thesis is a part of ongoing research related to injection molding, which has been in progress in the Chemical Engineering Department at McGill University for last two decades. Injection molding process control is a significant part of this effort due to the industrial demands and lack of complete and suitable controller for the process.

Controlling cavity pressure is an effective control strategy for the injection molding process. The importance of cavity pressure arises because of its close interaction with most of the process variables and its influence on important microstructural aspects, such as orientation and crystallinity and final properties such as

surface characteristic, and mechanical properties. Hence, the control of cavity pressure is the motivation for the present study.

The objective of this research project is to obtain a physically-based model representation of the injection molding process and to use this model for control purposes. The work involves phenomenological analysis and takes note of theoretical models and considerations.

The specific objectives of the present research were:

(1) To develop an appropriate dynamic physically-based model which relates cavity pressure to the machine variables, particularly servo-valve opening, during filling.

(2) To develop an appropriate dynamic physically-based model which relates cavity pressure to the machine variables, particularly servo-valve opening, during packing and holding.

(3) To test the utility of the above models for control purposes.

(4) To design the controller for cavity pressure control in the filling and packing phases.

(5) To simulate the closed loop control behavior and search for an optimum control strategy and performance.

(6) To apply the model and the controller to a laboratory size injection molding machine.

## 1.5 Thesis Overview

The present work incorporates the results of a large number of experiments. A detailed lumped mathematical model of the injection molding process is used to explain some of the observed phenomena and pursue control studies.

The text is divided into seven chapters. Chapter One introduces the injection molding process and the need for process control. In addition to the general background, it contains the scope and objectives of the present study. Injection molding variables and control are discussed in chapter Two. A critical review of the literature is also presented in chapter Two. Chapter Three describes the existing injection molding machine and

related instrumentation as well as the incorporated computer system. The experimental procedure and material characteristics are described in this chapter. Chapter Four gives the details of the theoretical model of the injection molding system, including the hydraulic system, which is judged to be suitable for control purposes. Chapter Five introduces the results of control studies of the filling phase using different process variables in conjunction with various controllers. Chapter Six deals with the dynamics and control of the packing phase. Chapter Seven summarizes the conclusions and the original contributions of this work and offers recommendations for future work.

# CHAPTER 2

# REVIEW OF INJECTION MOLDING PROCESS VARIABLES AND CONTROL

## 2.1 Introduction

In injection molding, consistency and repeatability from cycle to cycle are important objectives of process control. Considerable effort has been expended to obtain an understanding of the interactions between the process variables and the operating conditions. Control of at least some of these variables is essential for achieving reliable product quality. The following section discusses the important injection molding variables and efforts to control them.

## 2.2 Injection Molding Process Variables and Control

The injection molding process is a complex process in which material, machine, and process interact with each other to produce the final molded article. Jordan *et al* [32] used a specially instrumented injection molding machine to study the effect of the hydraulic system on the quality of molded parts. Although they did not use any closed loop control, they demonstrated the practical value of good hydraulic control. They statistically improved the part size consistency and concluded that for critical molding applications, occasional or constant accurate monitoring of the hydraulic system

could be excellent insurance against sudden, inexplicable loss of control. Peter [33] installed some thermocouples on the screw tip and barrel end cup, and studied the effect of screw speed, hydraulic pressure, and barrel temperature on the polymer melt temperature. Moreover, he studied the effects of hydraulic back pressure, screw speed, and barrel temperature on the plastication time. However, he did not try to control the injection molding machine. Allen and Vanputte [34] statistically designed an experiment to obtain quantitative results to establish the relationship between the molding variables and the material physical properties, such as tensile load at failure, and ball-drop impact strength. They concluded that knowing the cavity pressure profile contributed significantly to a better understanding of the injection molding process. Mahoney [35] identified relationships between cavity, nozzle, and hydraulic pressure. He tried to control the article volume by controlling some machine variables, but he did not employ a closed loop control. Plant and Maher [36] instrumented an injection molding machine with 28 transducers and studied the relationships between the nozzle polymer pressure and temperature, screw rpm, back pressure, cavity pressure, and part size. They concluded that monitoring mold cavity pressure proved to be an essential aid in determining the correct gate freeze-off time and overall cycle time. Moreover, they showed that cavity pressure reacts to changes in all machine variables, e.g. injection pressure, injection rate, screw rpm and cushion.

The injection molding process involves, as described by many works, a number of steps and complex interaction between resin and process variables. Hence, it is convenient to classify the variables into smaller groups. One of the possible classification is [37]:

(1) Resin variables - properties of the processing resin such as density, rheological behavior, thermal properties.

(2) Machine variables - machine related variables, such as hydraulic pressure, screw rpm, screw speed, barrel temperature, back pressure, and mold temperature.

(3) Process variables - variables related to the condition of the material during the process, such as nozzle melt pressure and temperature, cavity pressure, and melt

temperature in the mold cavity.

(4) Final article properties - properties of the final molded product such as density, part size, tensile strength, surface quality, optical properties, etc.

(5) Disturbances - all undesired perturbations which occur during processing such as pump and valve leakage, voltage fluctuation, electrical noise, etc.

Figure 2.1 shows the hierarchy of these classified variables.

Different algorithms can be suggested for the closed loop control of the injection molding process. The quality and dimensions of the final article are the ultimate goals of injection molding control. Control of the resin variables is an upstream task and cannot be done in this process. Therefore, one may try to control machine or process variables or final article properties. The process itself can affect the material properties. The changes in the resin variables can be treated as the disturbances for the chosen feedback closed loop. Figure 2.2 suggests some possible closed loop algorithms. It is assumed that $G_1$, $G_2$, and $G_3$ are the transfer functions between the sequence of hydraulic system, machine, process, and final article variables. The first choice is machine variable control. The relation of variables with final article properties is interrupted by the process variables. Hence, it cannot reject the input disturbances to the actual process. Due to a lack of suitable and/or commercial sensors for the final article properties, it is currently very difficult to measure the final article properties on-line. Therefore, the process variables are the best candidates for the closed loop control of the process.

Davis [38] discussed briefly the control of polymer velocity, cavity pressure, and the injection ram. He observed that cavity pressure provides an indication of certain aspects of part quality, such as part weight and density. Paulson [39] concluded the need to control process variables and suggested that plastic melt pressure was a very important indicator of process variation and, therefore, of subsequent product variations. Unfortunately, commercial machines are equipped mainly with machine variable control systems. Sanschagrin [40] tried to identify the most important input parameters of the conventional injection molding process. He studied the influence of ten input

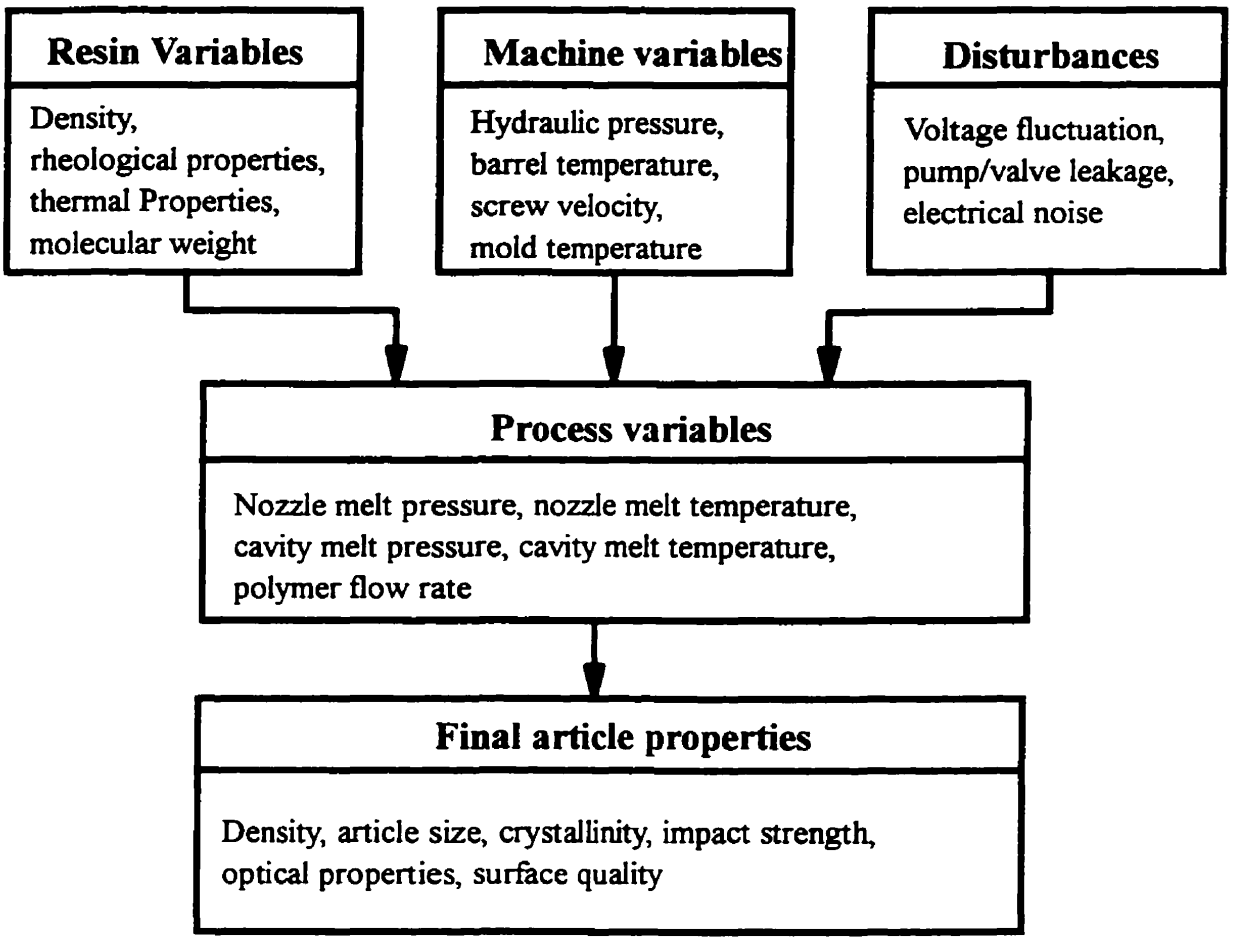


**Figure 2.1** Relationships of the injection molding variables

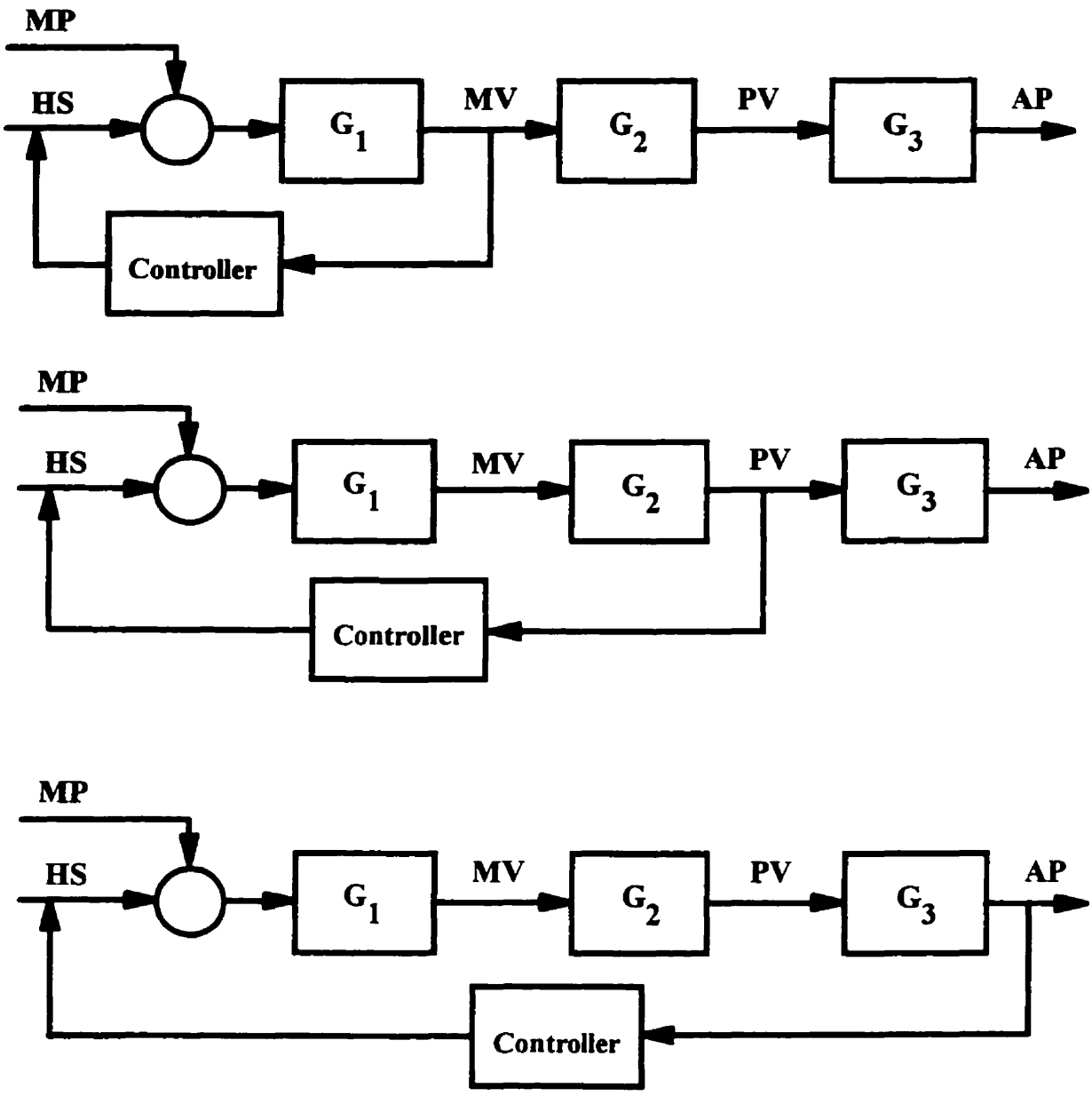


MP = Resin properties, HS = Hydraulic system, MV = Machine variables
PV = Process variables, AP = Article properties

**Figure 2.2** Closed loop control alternatives for injection molding process

parameters on three output variables. The input variables included back pressure, holding pressure, injection time, open mold time, shot size, clamping pressure, injection pressure, screw speed, and boost cut-off. The output parameters were part weight, maximum cavity pressure, and maximum mold opening. He concluded that maximum cavity pressure and part weight followed similar dependence on most input parameters. Consequently, he defined and executed three closed loop controls which were injection speed, holding pressure, and boost cut-off. Agrawal *et al* [41] reviewed control strategies employed in the injection molding machine. They grouped the control variables into all-phase control, phase dependent control, and cycle to cycle control. All-phase control includes variables that must be monitored and controlled at all times. Barrel and melt temperatures which are fundamental variables in the injection molding process, need to be continuously controlled and held to a specific level. Control of variables that are triggered during a specific phase are categorized under phase dependent control. Ram velocity, cavity pressure, and peak cavity pressure are examples of the phase dependent variables. Cavity pressure is the most widely employed closed loop process control method. Since it is a direct indicator of what is occurring inside the mold. Cavity pressure is sensitive to changes in injection pressure, screw speed, back pressure, and cushion. Cycle-to-cycle control is defined to include those control strategies wherein corrective actions are taken in the subsequent cycle based on the information from the present cycle. Shot size control and statistical process control fall in this category.

### 2.2.1 Melt Temperature Control

Gomes *et al* [42,43,44] installed a thermocouple in the injection screw tip to measure the polymer melt temperature inside the nozzle. They used deterministic and parametric experimental modeling methods to determine the dynamics of melt temperature. They found that the melt temperature was strongly affected by the front zone barrel heater and that the interaction between the front zone heater and other heaters was negligible. They designed and applied a proportional-integral-derivative (PID)

controller and other classical techniques to control the melt temperature, and produced satisfactory results. Later, Ruscitti [45] installed four band heaters on the barrel and a number of thermocouples as well as a Vanzetti infrared sensor at various positions in the nozzle. He employed these devices to study the dynamics and control of melt temperature. Experimental results for control of the polymer melt temperature were qualitatively good. Lu and Tsai [46] developed a multivariable self-tuning control method to improve performance of a temperature control system for the barrel in the injection molding process. A multivariable mathematical model of the heated barrel was obtained from the energy balance. The unknown system parameters in the model were identified by the recursive least-squares estimation method. Computer simulation and experimental results were presented to show that proposed method is feasible and effective. Bulgrin and Richards [47] addressed themselves to a programmable logic control (PLC) with PID controller for the barrel temperature control. They applied an energy balance over the barrel. Then, the governing partial differential boundary value equations were simplified. A $16^{th}$ order state controller was derived for the four zone barrel. The state variables used in this implementation were the temperatures at the heater bands, the outer layer of the barrel, the middle layer of the barrel, and the inner layer of the barrel which was in contact with the melt, for each of the four zones. A system identification method was used to calculate the values of matrices in state space formulation. Finally, they successfully applied the controller to the barrel temperature control of an injection molding machine.

### 2.2.2 Ram Screw Velocity Control

Abu Fara [48] derived a model to describe ram screw velocity dynamics with only a gain term. The model is given by:

$$C_t = G.M_t \tag{2.1}$$

where, $C_t$ is the controlled variable, the ram velocity at sampling instance t, $M_t$ is the manipulated variable, the servo-valve opening at sampling time instance t, and G is the

process gain corresponding to different step changes in the valve opening. He also gave a time series model of the form:

$$C(k) = 0.3M(k-1) + (1 - 0.4B)a(k) \tag{2.2}$$

where M(k-1) is the servo-valve opening at the (k-1)$^{th}$ sample, B is the backward shift operator, and a(k) is the random noise value at the k$^{th}$ sample. The sampling rate was 10 ms. Constants 0.3 and 0.4 were calculated by system output.

Wang *et al* [49] reported a fourth order transfer function between ram velocity and M, the voltage to the servo-valve:

$$G(s) = \frac{c(s)}{M(s)} = \frac{2.144 \times 10^{11}}{(s+125)(s+1138)[(s+383)^2+1123^2]} \tag{2.3}$$

c is the controlled variable, the ram velocity. They assumed that the ram velocity was linear and time-invariant, thus neglecting the effect of the increasing cavity pressure during filling on the ram velocity during injection. Pandelidis and Agrawal [50] designed a self-tuning controller for the ram velocity control. The simulation results followed a varying velocity profile closely. Pandelidis and Agrawal [51] used the ram velocity models of Abu Fara and Wang *et al* to obtain an optimal controller. They demonstrated the effectiveness of the proposed anticipatory control algorithm by applying it to a PID controller. The simulation results showed that the optimal controller tracks the trajectory set-point. However, they did not test their results experimentally, and the non-linearity and time-varying characteristics of ram velocity during filling were ignored. Zhang *et al* [52] described a methodology to obtain an adaptive controller for the control of ram velocity during the filling phase. They presented results of the controller performance for simple linear injection profiles and more complex stepped injection profiles. It was observed that the adaptive controller followed the set profile, however the coefficient of variation was unusually high. They did not explain why the coefficient of variation was high.

### 2.2.3 Polymer Melt Flow Rate Control

Shankar [53] attempted to control the polymer melt flow rate into the cavity during the filling phase of molding. A fifth order linear model of the filling phase was developed to simulate dynamic behavior of the process. The control of melt flow rate was not satisfactory and it was concluded that the controller design based on linear state variable feedback was not applicable to this case because of the highly non-linear nature of the filling phase. The melt flow rate could not be measured directly and was estimated by the multiplication of screw displacement by the nozzle cross-section area. The control results were not satisfactory. In a further attempt, he tried to calculate the polymer melt flow rate by taking into consideration the compressibility effect in the nozzle. Results were qualitatively good, yet the desired control action was not achieved. Speight *et al* [54] suggested that the melt front position might be inferred by monitoring different pressure sensors in a mold cavity, along the downstream. They argued that the final performance was determined by how efficiently the polymer melt flows into the cavity. The full algorithm to determine the polymer melt front position was a specific combination of the inferred polymer melt compression measurement, linear screw position and the rate of change of nozzle melt pressure. However, they did not show this algorithm in view of commercial sensitivity. It should be mentioned that these algorithms are only applicable for the filling phase.

### 2.2.4 Mold Temperature Control

Gao *et al* [55,56] installed a number of fast response thermocouples both at the mold surface and inside the mold metal to measure the mold surface temperatures and mold metal temperatures. They evaluated the temperature variation in the mold, in both space and time. Since it is difficult to develop a strategy to control temperature distribution at all points and times they considered a number of alternative parameters such as mold surface cycle averaged temperature, mold surface peak temperature, mold partial cooling time, mold metal cycle averaged temperature, and mold metal peak temperature. A first order plus dead time was fitted to model the dynamic behavior of

the system. The PID and Dahlin methods were applied and the performance of the Dahlin controller was slightly better than that of the PID.

### 2.2.5 Melt Pressure Control

Most of the control studies have been associated with the control of melt pressure at various positions in the system. Harry [57] carried out a study to determine which of the injection molding variables can best predict product characteristics, particularly part weight. While monitoring the screw position and cavity pressure at two locations, the process was perturbed to permit variations in the output. He found that the average cavity pressure is a potentially stronger algorithm factor than the peak pressure or the maximum screw forward position. The pressure near the gate seemed to exert a stronger influence than the downstream pressure, which is in agreement with many other studies. Kamal *et al* [58,59] carried out an early study of hydraulic and nozzle pressure dynamics. They performed deterministic modeling methods to obtain a dynamic model of the hydraulic pressure. They found both first and second order plus dead time models for the step input in servo-valve opening. The latter model is described by the following equation:

$$P_H = G\left[1 - \frac{\tau_1\tau_2}{\tau_1-\tau_2}\left(\frac{1}{\tau_2}e^{-\frac{t}{\tau_1}} - \frac{1}{\tau_1}e^{-\frac{t}{\tau_2}}\right)\right] + G_1\left[\frac{1}{(1-\xi^2)^{1/2}\tau_3}e^{\frac{-\xi t}{\tau_3}}\sin\left((1-\xi)^{1/2}\frac{t}{\tau_3}\right)\right] \quad (2.4)$$

where $P_H$ is the hydraulic pressure, G and $G_1$ are process gains, $\tau_1$, $\tau_2$, and $\tau_3$ are time constants and $\xi$ is a damping factor. The first term of Equation (2.4) accounts for the second order part of the response while the second term is the oscillatory, valve induced, component. Although physical considerations supported the use of the above equation, better agreement with experimental data was obtained from a first order plus dead time with oscillatory component model:

$$P_H = G(1 - e^{-(t-D)/\tau}) + G_1\left[\frac{1}{(1-\xi^2)^{1/2}\tau_1} e^{\frac{-\xi t}{\tau_1}} \sin\left((1-\xi)^{1/2}\frac{t}{\tau_1}\right)\right] \quad (2.5)$$

where D is the dead time.

They also modeled the nozzle pressure as an overdamped second order system:

$$P_N = G\left[1 - \frac{\tau_1\tau_2}{\tau_1 - \tau_2}\left(\frac{1}{\tau_2} e^{-\frac{t}{\tau_1}} - \frac{1}{\tau_1} e^{-\frac{t}{\tau_2}}\right)\right] \quad (2.6)$$

where $P_N$ is the nozzle pressure, and as a first order plus dead time model:

$$P_N = G\left(1 - e^{-\frac{t-D}{\tau}}\right) \quad (2.7)$$

They carried out stochastic experiments on the nozzle pressure and produced similar results to those obtained from step tests. The stochastic experiments yielded the following nozzle pressure model:

$$P_N(k) = \frac{6.62 - 1.00B}{1 - 0.68B} U(k-2) + \frac{1}{1 - 0.97B} a(k) \quad (2.8)$$

where B is a backward difference operator, U(k) is the manipulated variable (servo-valve opening) at sampling time k, and a(k) is the random noise value at sampling time k. The sampling rate was 10 ms. They concluded that it is preferable to conduct control using nozzle pressure rather than hydraulic pressure.

Later, Kamal *et al* [60,61] carried out a more detailed study to determine the dynamics of cavity pressure. They concluded deterministic and parametric experimental modeling on cavity pressure and obtained the following first order plus dead time model:

$$P_c(t) = K_1 t + K_2\left(1 - e^{-\frac{t-D}{\tau}}\right) \quad (2.9)$$

where $P_c$ is the cavity pressure, $K_1$ is the ramp slope, $K_2$ is process gain, $\tau$ is the process time constant, and D is the dead time. They also fitted the data to a second order model

plus dead time:

$$P_c(t) = K_1 t + K_2 \left[ 1 - \frac{\tau_1 \tau_2}{\tau_1 - \tau_2} \left\{ \frac{1}{\tau_2} e^{-\frac{t-D}{\tau_1}} - \frac{1}{\tau_1} e^{-\frac{t-D}{\tau_2}} \right\} \right] \qquad (2.10)$$

They obtained the following parametric model for cavity pressure:

$$P_c(k) = \frac{0.628 - 1.059B - 1.536B^2}{1 - 0.591B} U(k-1) + \frac{1}{1 - 0.40B} a(k) \qquad (2.11)$$

They experimented with proportional and integral (PI) feedback control. The experimental cavity pressure followed the set-point closely in the beginning of the filling phase, then it became increasingly oscillatory. This was attributed to the non-linearity and time-varying nature of the process. To overcome this problem, a gain scheduling control strategy was devised such that the gain was reduced throughout the injection phase. However, an explicit expression for the reduction of the gain was not given.

Haber and Kamal [62,63] carried out a statistical study of cavity pressure fluctuation from cycle to cycle. They coupled the use of a servo-valve in the hydraulic system with a microprocessor to reduce the peak cavity variation. The control strategy was employed from cycle-to-cycle, rather than within the cycle.

Abu Fara *et al* [64,65] developed a strategy for the control of the cavity pressure throughout the injection molding cycle. They used a first order plus dead time experimental model for the cavity pressure. A classical PI controller was designed, implemented and tested experimentally. The results were reasonably good. The switch from filling to packing was found to be best based on the rate of change of the cavity pressure. However, the control response during packing seemed to be a strong function of the packing set-point profile. When a fourth order polynomial for the pressure profile was used, the results were very good.

Smud *et al* [66] used clamp pressure (or clamp force) to manipulate the cavity pressure, instead of the most common approach of using one or more hydraulic servo-valves. A least squares procedure was used to fit the process response data to first

order plus dead time model. They considered the proportional and integral (PI), simplified model predictive control (SMPC), and conservative model based control (CMBC). They used a different set of tuning constants depending on whether the controlled variable was over or under the set-point. The integral of square error was used as the optimization criterion. The performance of the action control technique was satisfactory, and the simulated and experimental results were in close agreement.

Wu *et al* [67] employed a cavity pressure pattern based approach to develop an expert system, in an attempt to extract information not seen by the operator and emulate the expert's reasoning through heuristic techniques with the aid of nozzle pressure and ram position. The logic was to develop a method to distinguish between the standard cavity pressure pattern and non-standard one and to provide the operators or machine controller with the necessary information to correct the set-up until a standard pressure pattern was achieved.

Chiu *et al* [68] used a first order plus dead time model and designed a PI controller as well as an adaptive model following controller (AMFC) for the cavity pressure in the filling phase. They compared the performance of these two controllers and concluded that the control response of AMFC provided better tracking of the set-point. They applied the tests for the simple set-point profile in the fixed operating conditions with simple cavity geometries.

Srinivasan *et al* [69] proposed a learning control for the cavity or nozzle pressure during the filling phase. Learning control strategy is a new controller structure which is very effective for controlling periodic processes. Hence, sometimes it is called repetitive control. The learning control is applied on a cycle-to-cycle basis. Therefore, the current injection molding cycle is improved by the information from the last cycle. The improved accuracy was directly attributed to the fact that the corrective action at any point in time depends significantly on the error at corresponding instants during the previous cycle, as a result of the learning function within the controller and the cycle delay block. The simulation results showed that the application of learning control to the control of the cavity pressure during the injection phase is feasible. However,

experimental evaluation of the effectiveness of learning control was not demonstrated. Due to the cycle-to-cycle nature of the controller, there is no possible improvement within an injection cycle.

Gao *et al* [70,71] used a recursive identification method to find a discrete-time transfer function model of an injection molding machine. A dynamic model was found for the entire filling phase. An indirect adaptive self-tuning control strategy was used so that the time-varying behavior of the process could be examined. Having the parametric process model, the pole-placement method was used to obtain the controller. Two open-loop experiments were conducted to examine the time-varying and non-linear behavior of the process. They proposed the following discretized transfer function:

$$y(k) = a_1 y(k-1) + a_2 y(k-2) + b_0 u(k-1-ntd) + b_1 u(k-2-ntd) \qquad (2.12)$$

where y is the cavity pressure at the gate, ntd is the number of sampling instants that equals the dead time, and u is the manipulated variable (servo-valve opening). A set of experiments was done to investigate the effect of different forgetting factors. The results of the cavity pressure control revealed that the cavity pressure followed the set-point profile very well. Later, Patterson *et al* [72] extended the same approach for the control of the cavity pressure at the gate during the packing phase. The derivative of the cavity pressure was used to determine the transition from the filling to the packing phase. When this value exceeded a threshold of 8.6 MPa/s it triggered the switch to the packing profile. The experimental results showed that the cavity pressure closely followed the set-point during the packing phase.

Kamal *et al* [73] studied, for the first time, the manipulation of cavity pressure during cooling (after gate freezing) by changing the coolant temperature or coolant flow rate. Due to the large thermal mass of the mold, it is not possible to manipulate the pressure during cooling within a cycle. Thus, they manipulated it over the successive cycles. The relationship between controlled pressure cooling time (CPCT) and the coolant temperature was modeled as first order plus dead time. An experimental

closed loop control to track a changing set-point profile was carried out. The step set-point change occurred at cycle 20 and the experimental pressure profile followed it after 5 cycles.

Hu and Vogel [74] established a physical basis for a control model of pressure during the packing phase of the injection molding cycle. They used a modeling approach similar to that developed by Shankar and Paul [22]. The major assumptions were that hydraulic valve pressure response during the packing phase was a first order system, that the screw assembly mass was neglected during the acceleration period encountered during packing, that frictional forces opposing screw motion were proportional to velocity, and that the melt and mold wall temperatures were constant during packing. Introducing some of these assumptions produced some major errors. However, it allowed them to develop a system of linear, time-invariant differential equations to represent the behavior of the system. Therefore, classical controller design methods were applied to obtain control parameters. Some of the model parameters were identified experimentally using the injection molding machine. A PID controller was designed and during the experiments the controlled variable exhibited a large overshoot that was attributed to the linear model used in controller design.

Seaman *et al* [75] explored the role that multi-objective optimization can play in the control of repetitive manufacturing processes. Their research concentrated on the plastication phase. The PID controller has been very successful and widely accepted for handling a single objective function. They used the Kuhn-Tucker conditions (for non-dominance) and the Gordan's theorem of the alternative to find non-dominated points of operation. A seventh order model was derived for the melt pressure with respect to the servo-valve opening using input/output from the injection molding machine. They used an auto-regressive model (ARX) available in the identification toolbox in MATLAB [76]. Two objective functions were chosen: minimize the integral time absolute error and minimize controller effort. The multi-objective optimization algorithm was used to tune a PID controller to meet the specified objective functions. They applied the controller to control the melt pressure at 3000 psi by manipulating the servo-valve

voltage, the result of the multi-objective tuned controller was superior to the normally tuned PID controller with ITAE criteria.

Coates and Speight [77] presented introductory steps towards intelligent process control of the injection molding of polymers. In-process measurements of melt and hydraulic pressure in the injection phase, was shown to provide a sensitive means of monitoring changes in the process and changes in the polymer feedstock. They observed correlations between the real-time process measurements, in the form of specific time integral of melt and hydraulic pressures and product quality such as a product weight or dimensions. The model was validated in both the laboratory and factory environments for a range of polymers, injection molding technologies and complexities of product. Such correlations could form the basis of meaningful statistical process control for injection molding or a viable closed loop control strategy.

### 2.2.6 Final Article Properties Control

Ricketson and Wang [78] conducted a study to understand and control the molded part shrinkage. Using a multiple regression method, the following model was derived to estimate part thickness, y:

$$y = b_0 + b_1 x_1 + b_2 x_2 + b_3 x_3 + b_{12} x_1 x_2 + b_{13} x_1 x_3 + b_{23} x_2 x_3 \qquad (2.13)$$

where $x_1$, $x_2$, and $x_3$ are packing pressure, mold temperature, and barrel temperature, respectively. They found that packing pressure had a greater effect on part thickness than the other variables. They used a recursive method to recalculate the model coefficients. Experimentally, their controller, which was not specified, was claimed to be very effective in reducing the variation in the distribution of part thickness.

Wang and Wang [79] derived a semi-mechanistic process model based on a numerical scheme and on-line data acquisition using a simplified thermodynamic model for describing the PVT properties of polymers. The model was used to predict the thickness of injection molded parts. In controlling the process, an empirical linear equation was constructed to convert the volumetric shrinkage to corresponding part

thickness based on experimental observations. Using on-line linear regressional analysis, the coefficients of the empirical equation were updated when a drift was detected by the predictive model. The error was applied to determine the proper hydraulic packing pressure level for the next cycle. They successfully tested this semi-mechanistic process control model on several amorphous materials.

Devos [80] tried to provide some answers to the problems of flexibility and quality control. They used the PVT principle without using PVT data. They created a process control unit which modifies and directly adjusts the polymer pressure in the cavity, in real-time. The basic model was built during preliminary experiments. Then the model precision increased during continuous real production. This was they used the auto-adaptive definition for their command system because it improved accuracy during continuous real production. They tested the controller for the control of weight of a standard dumbbell-shaped specimen during different phases of production. They concluded that it was possible to use polymers with different viscosity to produce plastic parts with constant weight.

Yakemoto *et al* [81] regarded the temperature variation as a primary cause leading to the fluctuation of product quality. They analyzed the theoretical importance of the control to predict the effect of temperature variation on final product quality. Based on the theoretical prediction prior to the mold filling phase, a simple holding pressure control to solve the fluctuation of product weight was developed.

Recently, Varela *et al* [82,83] presented a methodology to estimate cavity melt temperature and part weight in the injection molding of amorphous thermoplastics. Temperature profiles across the cavity thickness were estimated using the surface temperature data. Fitting the cycle-to-cycle values of average mold-cavity temperature and peak cavity pressure to a Tait equation of state yielded a model to find the part weights. Then, Varela [84] tried to control the molded part weight. The part weight was controlled through the use of a control strategy for the cavity pressure and the part weight model, together with the on-line estimation of the bulk temperature. He applied a self-tuning algorithm with an observer for controlling the cavity pressure time

profile to a set-point trajectory. The control over part weight was qualitatively good.

Taghizadegan [85] conducted a statistical approach for injection molding process. He used an ASTM impact-strength plaque shaped mold. He modeled plaque weight in the canonical form with respect to injection pressure, plastication screw speed, and injection velocity. He used results of 150 open loop shots in the modeling. The model was used in a closed loop control strategy and the part-to-part weight variation was decreased.

## 2.3 Selection of the Best Controlled Variable

The complicated interactions between process, machine, and material determines the quality of the final molded article. The process variables include hydraulic pressure, ram screw velocity, ram screw displacement, nozzle pressure, melt temperature, and cavity pressure.

The melt temperature can be normally controlled by the voltage to the band heaters installed on the barrel. The time constant of this process is large and should be controlled all the time not only within a cycle. In practice, the individual and separate closed loop control of each band heater is sufficiently effective to keep each barrel zone temperature around the set-point. Moreover, a small deviation of band heater set-point temperature causes very little change in the melt temperature in the nozzle. This small deviation can be treated as a disturbance, and the control action on the other controlled variable rejects this disturbance.

The changes in the hydraulic oil flow rate into the injection cylinder are reflected as hydraulic pressure changes. The hydraulic pressure changes then propagate to the rest of the process via the ram screw system. In the meantime, the displacement and velocity of the ram screw are affected by the changes in the hydraulic pressure. Pressure starts to build in the nozzle due to a pressure increase in the back of the screw. This pressure pushes polymer melt into the polymer delivery system including the sprue, runner, gate, and mold cavity. During the filling phase, the pressure in the cavity increases gradually with the filling of the cavity by the polymer melt. The pressure in the cavity rises

dramatically as soon as the mold is filled. Figure 2.3 shows the relationships between process variables schematically. Although the system is single input and multi-output, all process variables cannot be controlled at the same time with different objectives due to interaction between them. Hence, only one of the process variables can be controlled. Of course, controlling one of the five variables implies that other variables are also being controlled without predetermined set-point profiles.

Hydraulic pressure may be controlled. However, it is far from the mold cavity and cannot detect any disturbances between the hydraulic system and the mold cavity. Although, the ram velocity may be controlled, disturbances such as back-flow, leakage, temperature changes, and polymer melt compression in the nozzle can cause a perturbation of polymer melt flowing into the cavity. Moreover, during the packing phase, the ram screw velocity drops to approximately zero and cannot be used as the controlled variable. Control of the polymer melt flow rate is preferable. Unfortunately, there is no practical transducer to measure this variable. Estimation of the polymer flow rate via ram displacement is possible. However, inferential control of the polymer flow rate has not been successful. It has been shown that the cavity pressure is the best candidate as the controlled variable [31,34,36,35,39]. It is possible to measure and control the cavity pressure. The cavity pressure clearly determines what is happening in the cavity. The microstructure and product quality are directly related to the cavity pressure pattern.

In the light of above arguments, cavity pressure is judged to be the best candidate as the controlled variable during the injection molding cycle. However, the chosen process variable is highly non-linear and time-varying. These characteristics cause problems in the design and implementation of classical closed loop control. In the literature [65,66], researchers have mostly used experimental linear time invariant models, even though the process is strongly non-linear. This means that the controller should be implemented close to the identification condition, otherwise the controller performance deteriorates. Some advanced methods are also reported in the literature [67-74]. The self-tuning method uses on-line parameter approximation and the results

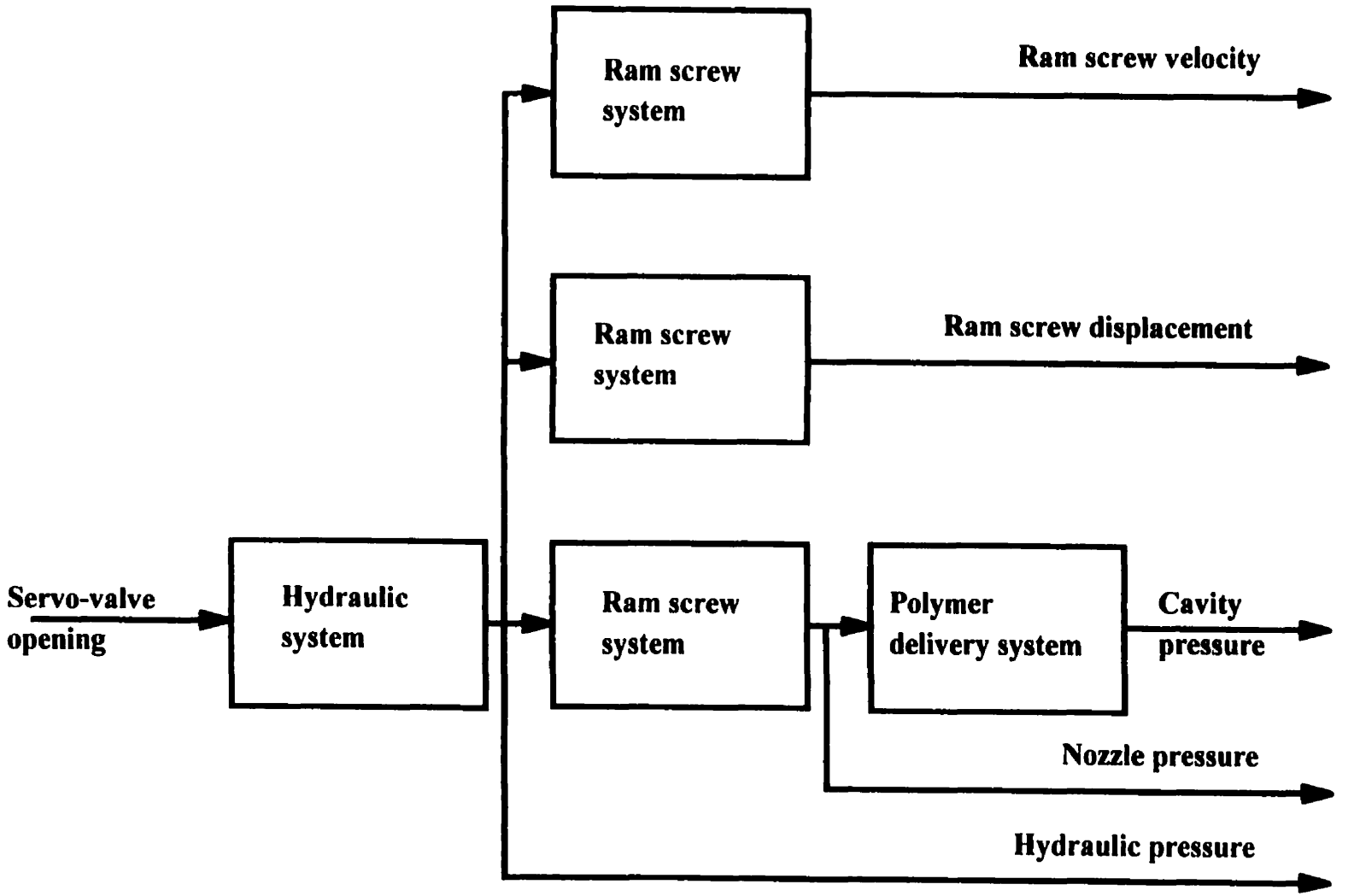


**Figure 2.3** Relationship between process variables

of self-tuning control are promising. The controller design, using identification methods, is blind and looks like a black box. The fitted parameters do not reflect the physical meaning and the experimental modeling method does not give the functionality of parameters to the physical properties. Therefore, theoretical modeling, according to physically-based conservation laws, should give real and physical meaning to the gains and time constants. For theoretical modeling, a lumped approach seems suitable because it leads to ordinary differential equations.

# CHAPTER 3

# EXPERIMENTAL

## 3.1 Introduction

Modern injection molding operations are often automated to the extent that one operator can supervise the operation of many machines. Commercial control systems with considerable power and complexity are widely installed on the injection molding machines. No commercially available molding machine control system has the degree of flexibility of operation that is required for research purposes. Therefore, a custom injection molding control system has been installed on an existing injection molding machine in order to satisfy research objectives.

This chapter describes the existing injection molding machine instrumentation, the microcomputer system, the properties of the materials used, and the experimental procedure.

## 3.2 Injection Molding Machine

The experimental work is carried out on a Danson-Metalmec reciprocating screw injection molding machine. A schematic of the machine is shown in Figure 3.1. Some specifications of the machine are listed in Table 3.1.

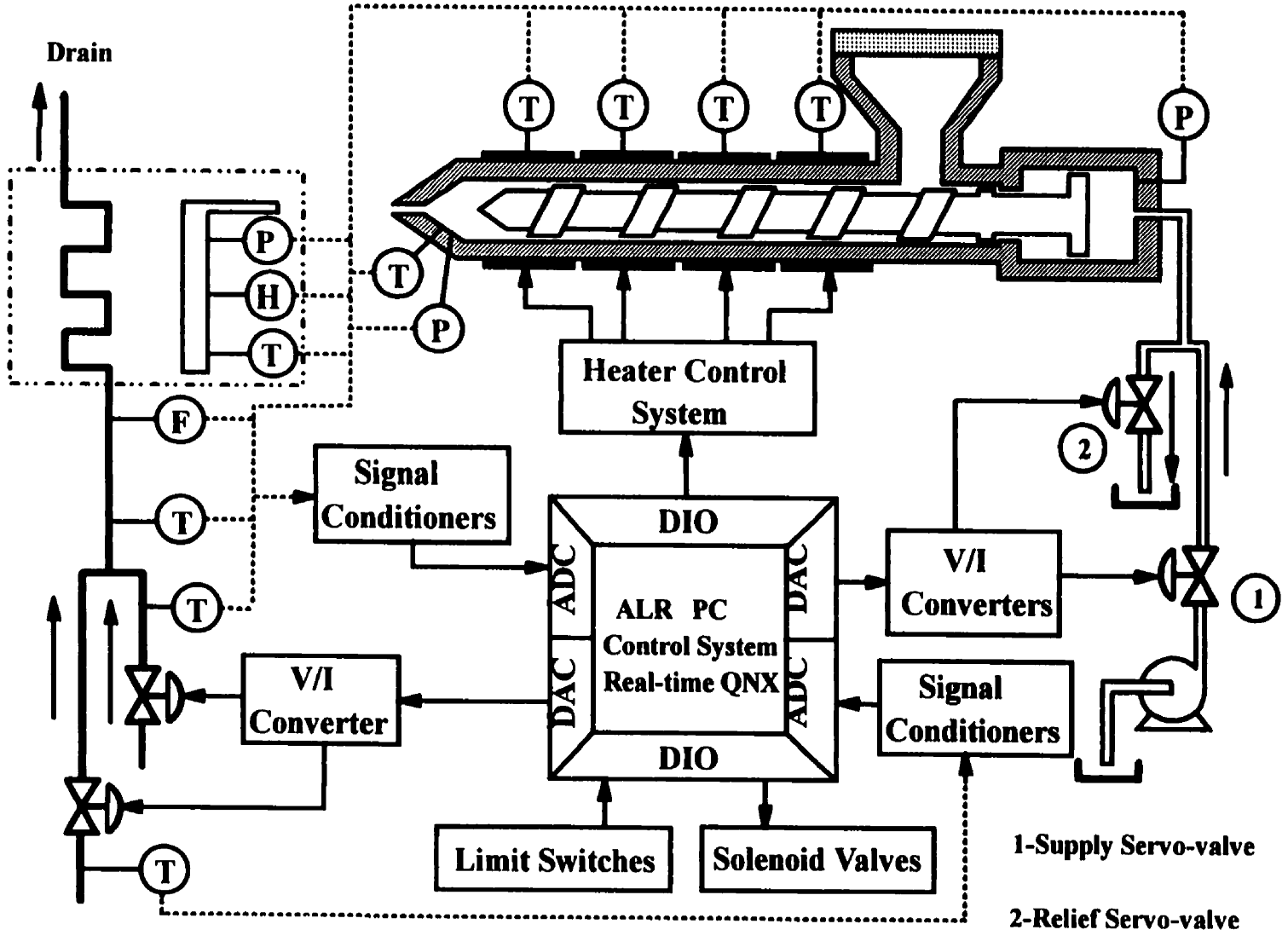


**Figure 3.1** McGill injection molding machine

| Machine Model | Danson-Metalmec 60-SR |
|---|---|
| Capacity | 2 1/3 oz ( 66.1 g ) |
| Screw Diameter | 1.375" ( 0.035 m ) |
| Screw L/D Ratio | 15/1 |
| Screw Rotation Speed | 40 - 150 rpm |
| Clamping Force | 60 T ( 53386 kN ) |
| Hydraulic Pump | Sperry-Vickers vane pump |
| Pump Capacity | 8 gpm ( 1.82 $m^3$/hr ) flow at 2000 psi ( 13.8 Mpa ) pressure |
| Electric Motor | 20 hp ( 14.92 kw ), 3 phase, 60 hz |
| Servo-valves | Moog A076-103 and 760-103A 10 gpm ( 2.28 $m^3$/hr ) flow at 1000 psi ( 0.9 Mpa ) pressure |

**Table 3.1** - Injection molding machine specifications

The whole system consists of two parts: injection molding machine including: 1) hydraulic system, 2) screw and barrel, 3) mold and coolant system; instrumentation including: 1) sensors, 2) computer hardware interfaces, and 3) software.

The machine can be operated either in the manual, semi-automatic, or automatic mode. The machine sequencing is controlled by timers, limit switches and relays. The injection, holding, and cooling durations are set by the corresponding timers on the machine. The limit switches are used to determine the completion of certain machine movements, such as mold closing and opening, carriage advancement, and plastication. There are nine limit switches listed in Table 3.2, with their positions and conditions.

The screw rotation speed is set manually by a hand wheel on the screw speed valve. There are four 220 volt electric band heaters installed on the barrel, numbered 1 to 4 from the nozzle toward the hopper.

### 3.2.1 Hydraulic System

The original hydraulic system was modified to include a hydraulic servo-valve, Moog A076-103, called SV1 [86]. Another servo-valve, Moog 760-103A, called SV2, was installed to facilitate cavity pressure control, especially during the packing phase, for which one servo-valve does not provide enough manoeuvrability [37]. Both valves have a 10 U.S. gallons per minute (37.85 l/min) capacity at a rated pressure drop of 1000 psi (6.2 MPa) Figure 3.2 shows the modified and existing hydraulic system of the machine and Table 3.3 gives the description of the parts in the hydraulic system.

The configuration of the nine manual valves in the hydraulic system determines which servo-valve will act as the supply or relief servo-valve. Table 3.4 shows the possible configurations for the hydraulic system.

Figure 3.3 shows a schematic of the hydraulic system and relative positions of the servo-valves and manual valves. For using SV1 as supply servo-valve and SV2 as relief servo-valve, a small improvement should be done in the operation of the hydraulic system which is shown as the dotted line in Figure 3.3. Each servo-valve can be completely closed (0% open) or completely open (100% open). However, to avoid the

| Switch | Function | Position |
|---|---|---|
| LS1 | Mold safety cover | NC |
| LS2 | Mold open | NC |
| LS3 | Pressure switch (up), Mold closed | NO |
| LS4 | Carriage forward | NC |
| LS5 | Screw back | NC |
| LS6 | Screw forward | NC |
| LS7 | Carriage back | NO |
| LS8 | Pressure switch (Down) | NO |
| LS9 | Same as LS3 | NC |
| NC = Normally Closed, NO = Normally Open | | |

**Table 3.2** - Limit switches function and position

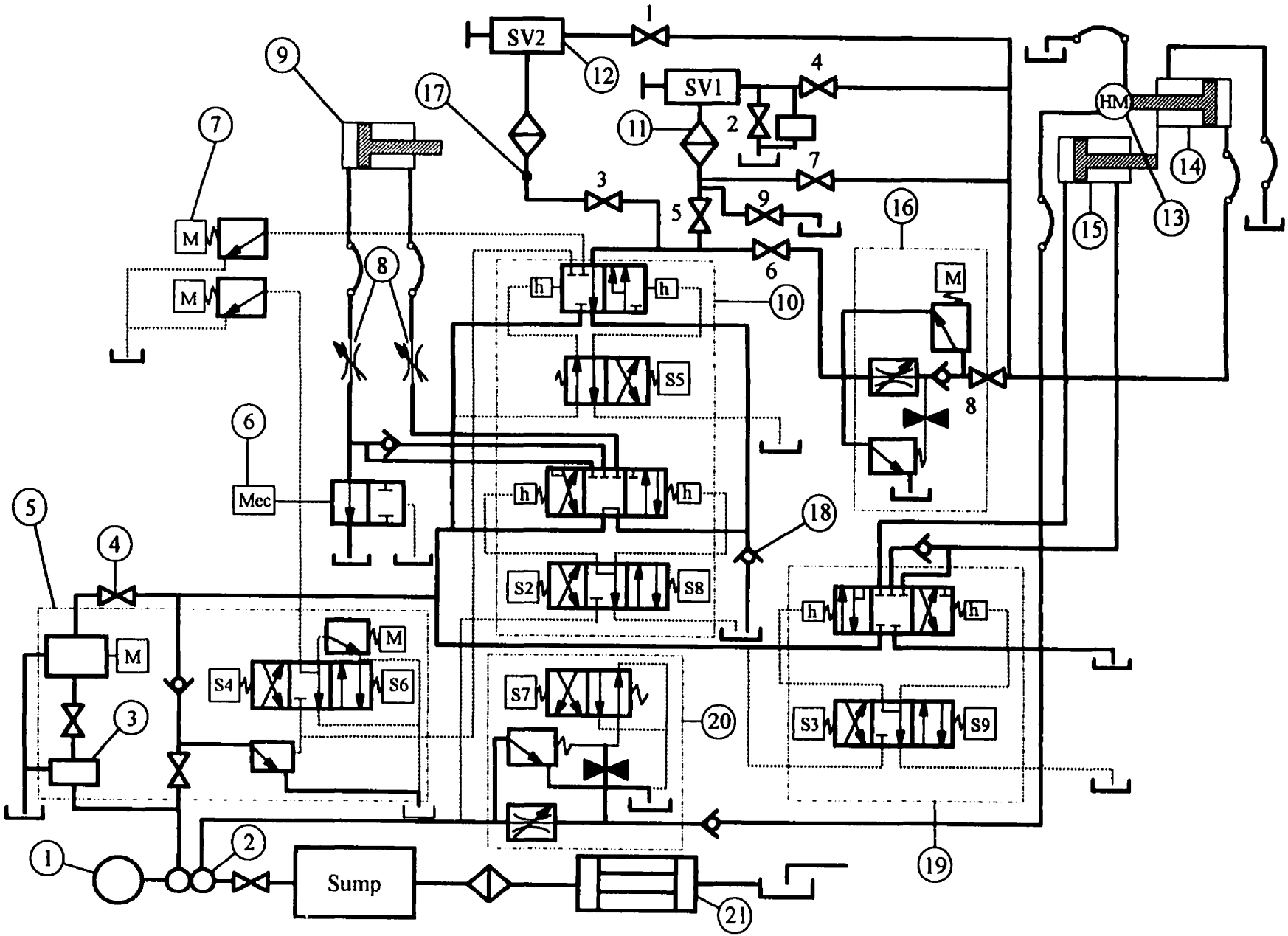


**Figure 3.2** Hydraulic system, see Table 3.3 for part definition

| Part No. | Description |
|---|---|
| 1 | Electric motor |
| 2 | Pump |
| 3 | Safety valve |
| 4 | Ball valve |
| 5 | Main pressure distributer |
| 6 | Hydraulic safety pilot operated |
| 7 | Injection relief valve |
| 8 | Clamp speed adjusting valve |
| 9 | Clamp cylinder |
| 10 | Main Pressure relief valve with two pilots |
| 11 | Filter |
| 12 | Servo-valve |
| 13 | Hydraulic motor |
| 14 | Injection cylinder |
| 15 | Carriage cylinder |
| 16 | Injection speed and screw back pressure regulating valve |
| 17 | Pressure transducer |
| 18 | Check valve |
| 19 | Injection carriage forward and return valve |
| 20 | Screw drive regulating valve |
| 21 | Heat exchanger |

**Table 3.3** - Description of hydraulic parts in Figure 3.2

| Function | | Manual valve positions | |
|---|---|---|---|
| | | Position | Valves |
| 1 | SV1 as supply valve<br>SV2 is not in circuit | Open | 4, 5 |
| | | Closed | 1, 2, 3, 6, 7, 8, 9 |
| 2 | SV2 as supply valve<br>SV1 is not in circuit | Open | 1, 3 |
| | | Closed | 2, 4, 5, 6, 7, 8, 9 |
| 3 | SV1 as supply valve<br>SV2 as relief valve | Open | 4, 5 |
| | | Closed | 1, 2, 3, 6, 7, 8, 9 |
| 4 | SV2 as supply valve<br>SV1 as relief valve* | Open | 1, 2, 3, 7 |
| | | Closed | 4, 5, 6, 8, 9 |
| 5 | No servo-valve<br>Original machine configuration | Open | 6, 8 |
| | | Closed | 1, 2, 3, 4, 5, 7, 9 |
| * The existing position during experiments | | | |

**Table 3.4** - Position and function of each manual valve

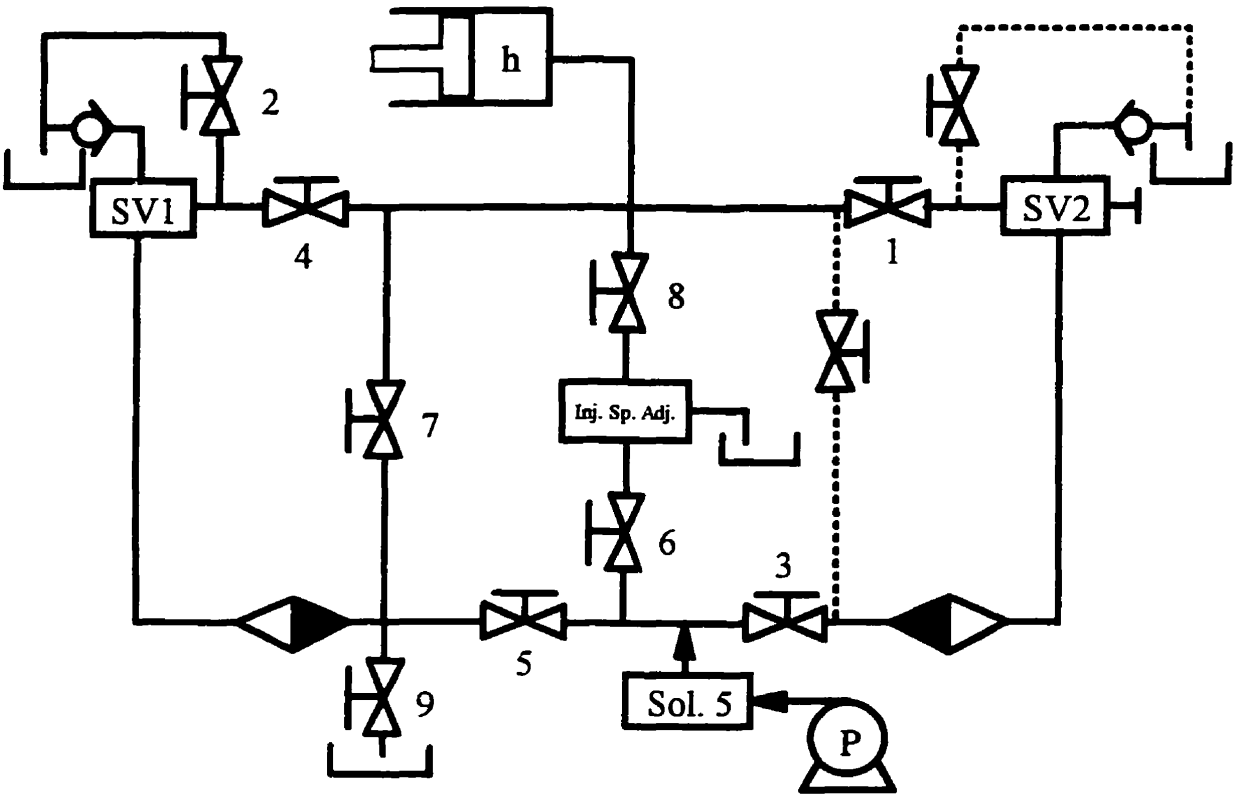


Inj. Sp. Adj. = Injection Speed Adjusting Valve

**Figure 3.3** Schematic hydraulic system

dead zone of the valves, the range 0.5 - 99.5% opening is applied to the servo-valves. Both of the servo-valves are linear, i.e. their openings are linearly proportional to the supplied current.

There are five solenoid valves to divert the hydraulic oil in the correct direction with respect to the existing phase during the cycle. Table 3.5 gives the function of the each valve when the corresponding solenoid is activated.

### 3.2.2 Barrel and Screw

The two original band heaters on the barrel are replaced with four band heaters [45]. One is in the solid conveying zone at the rear of the barrel, one is installed in the melting zone of barrel, and two are in the metering zone of barrel at the front. The band heater located at the nozzle has twice the power of the other band heaters to supply proper heating power in the nozzle. The band heaters are all supplied 220 volt AC current. A barrel temperature dynamic model is developed in relation to the percentage of maximum power delivered to each heater. Heat transfer to the polymer is influenced by the effective heat transfer area, screw rpm velocity, thermal properties of the polymer, and the barrel temperature profile. Band heater temperature is the most effective means to reach the desired melt temperature.

### 3.2.3 Mold and Coolant Systems

The coolant water adjusts the mold metal temperature. Figure 3.4 shows a schematic of the coolant system. Cold water, hot water, and mixed water temperatures, and mixed water flow rate were measured. Two manual valves were installed before the cold and hot water lines to adjust the maximum flow rate of each flow. The flows of cold and hot water were controlled by two control valves which had equal percentage trim and are pneumatically operated. The coolant temperature has a much larger effect than coolant flow rate on the rate of heat removal in the metal mold [87]. Hence, coolant temperature was chosen as the controlled variable instead of coolant flow rate. The relationship between percentage of control valve openings was:

| Solenoid No. | Function |
|---|---|
| S1 | None |
| S2 | Mold close |
| S3 | Carriage backward |
| S4 | Switch to high pressure |
| S5 | Screw forward |
| S6 | Switch to low pressure |
| S7 | Screw backward |
| S8 | Mold open |
| S9 | Carriage forward |

**Table 3.5** - Solenoid valve functions

D/A = Digital to Analog converter
A/D = Analog to Digital converter
V/ I = Voltage to Current converter
I /P = Current to Pressure converter
T = Thermocouple
F = Flowmeter

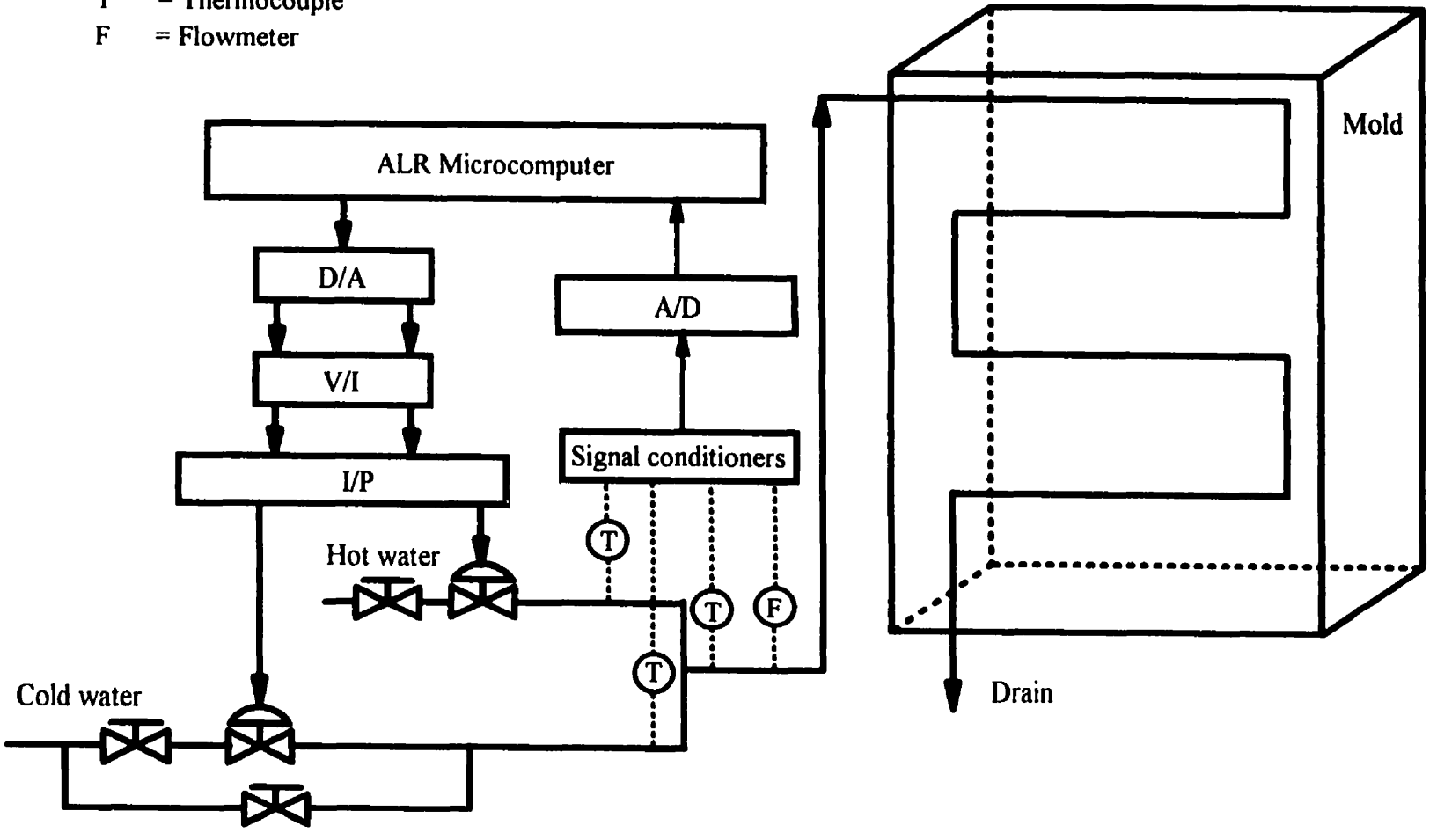


**Figure 3.4** Schematic coolant system

$$CV_c = 100 - CV_h \tag{3.1}$$

where $CV_c$, and $CV_h$ are control valve openings of the cold water and hot water lines, respectively.

## 3.3 Instrumentation

There are sensors to measure different variables. The injection molding machine is interfaced with a microcomputer system to achieve the following tasks:

(1) Data acquisition

(2) Machine sequencing control

(3) Control of the different phases of the injection cycle

The microcomputer system can be separated into two parts: system hardware, and system software, which are described separately.

### 3.3.1 Sensors

The sensors could be divided into several categories: 1) temperature sensors, 2) pressure transducers, 3) the screw position and velocity sensors, and 4) flowmeter.

Five melt pressure transducers were used in this study. Four are Dynisco pressure transducers and the fifth was a GP:50 pressure transducer [88,89]. The first transducer was mounted on the output of the pump, while the second transducer was installed just before the supply servo-valve. The third one was mounted on the injection cylinder to measure the hydraulic pressure. The fourth transducer was located in the nozzle to measure the nozzle pressure. Finally, the last one was installed in the mold cavity near the gate to measure the polymer melt pressure.

The transducers were calibrated prior to installation to verify their gauge factors and linearity. A dead weight tester was used to calibrate these transducers [90]. Table 3.6 gives the model and serial number of each pressure transducer, its range of measurement and the calibration equation. The calibration data is given in Appendix A.

Twelve thermocouples were used to measure temperature at different points in the

machine. All thermocouples were type E except for the one installed in the nozzle which was type K. All the thermocouples were ungrounded to minimize noise pick up. Four thermocouples were mounted on the barrel, one for each heater zone. Three thermocouples were installed in the mold coolant system to measure the hot water, cold water, and the coolant water temperatures. Three thermocouples measure the polymer melt temperature inside the mold cavity. The mold cavity thermocouples have a NANMAC pencil-probe-eroding structure which is isolated from the mold metal. One was placed close to the gate, one in the middle of the cavity, and the last one was close to the end of the cavity. Figure 3.5 shows the place of the sensors inside the mold cavity. One thermocouple was mounted to measure the mold metal temperature. Another thermocouple, type K, was installed in the nozzle. The thermocouple tip protruded into the polymer melt.

The screw displacement and velocity were two other important parameters. A Markite, model 4709, linear displacement transducer was used to measure the ram displacement during the injection molding cycle. A linear velocity transducer, TRANS-TEK Model 112-001, was installed to measure the screw velocity in different phases.

A Compak 8500 flow transducer, supplied by Axel Johnson Inc., was installed in the coolant system to measure coolant water flow rate.

### 3.3.2 System Hardware

An ALR (micro-channel bus) computer, 33 MHz with an i80486DX CPU, was chosen to host the data acquisition and control system. Two data acquisition boards from Analog Devices, RTI220, were mounted for the task of data acquisition. They were selected for their large input/output capacity. Each data acquisition board has a maximum of 64 inputs and 16 outputs. The boards can generate an interrupt to the computer when an analog-to-digital conversion is completed. Two data acquisition boards were installed to have one board for rapidly varying signals, such as pressure, and the other board for slowly changing signals, such as barrel temperatures. Therefore, system has multi-rate sampling ability. Two differential amplifiers transform the signal

| Sensor | Sensor location and calibration equation | |
|---|---|---|
| PT435A - 3M S/N 297231 3000 psi | Location | After pump |
| | Equation | P = 113.38 * mv - 401.88 |
| PT435A - 3M S/N 226385 3000 psi | Location | Before supply servo-valve |
| | Equation | P = 90.80 * mv - 123.98 |
| PT422A-7.5M S/N 195678 750 psi | Location | Injection cylinder |
| | Equation | P = 23.95 * mv - 49.36 |
| PT435A -10M S/N 160039 10000 psi | Location | Nozzle |
| | Equation | P = 304.84 * mv - 212.70 |
| GP:50 - 142 S/N 1546D2 5000 psi | Location | Cavity gate |
| | Equation | P = 149.10 * mv - 37.03 |
| Markite Model 4709 | Location | Barrel |
| | Equation | L = 0.6147 * mv - 1.2265 |
| TRANS-TEK 112-001 | Location | Barrel |
| | Equation | V = 0.209 * mv - 0.004 |
| Compak 8500 | Location | Coolant water circuit |
| | Equation | Q = 110.44 * v |

**Table 3.6** - Sensor calibrations

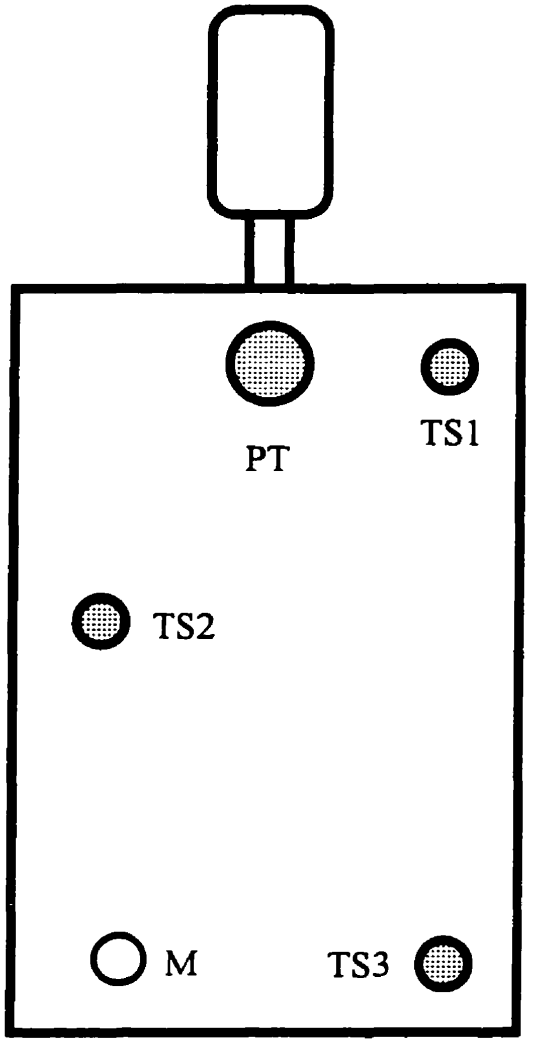


**Figure 3.5** Placement of the sensors inside the cavity mold
PT = Pressure transducer
TS = Surface thermocouple
M = Metal thermocouple

from the pressure transducers to the range of 0-5 volt, before entering the RTI220 board. The RTI220 boards convert the entering signals to numeric forms. Digital input/output signals are delivered through Analog Devices, RTI217, which has 32 input/output lines.

### 3.3.3 Software Structure

A multi-tasking operating system was judged to be essential for achieving a good data acquisition and control system for this complex process [91]. This allowed individual tasks to be associated with particular program modules. The modular programming approach permits easy modification and expansion.

The QNX 4.1 operating system, from QNX Software Systems Ltd., was chosen [92]. QNX is real-time multitasking, POSIX operating system running on IBM PC compatible computers [93]. POSIX is the acronym for Portable Operating System Information Exchange. The QNX structure is in a micro-kernel, modular form. Thus it is easy to add, rename or modify a control process (task) without modifying the programs for other tasks. In QNX, time management is based on a system timer maintained by the operating system. A process can create timers, arm them with a time interval, and remove timers. QNX allows processes to share portions of memory. This is an effective way to communicate and share dynamic information among processes. All the tasks were written in WATCOM C language running under the QNX 4.1 operating system. The remarkable advantages of QNX kernel are [94]:

(1) Inter process communication (IPC): communication can be handled in three forms: messages, proxies, and signals. *Send()*, *Receive()*, and *Reply()* are the C-language routines for sending data, receiving data, and for replying, respectively [95].

(2) Process scheduling.

(3) First-level-interrupt handling: the kernel receives a hardware-interrupt request before any driver or system manager.

The real-time part of the software was developed by Gao [96]. Programs have been developed to enable several functions, the most important ones are: (1) data

acquisition manipulation, (2) memory management, (3) data transfer among input/output devices, and (4) real-time processing. The file named *IMM* (Injection Molding Machine) performs the user interface task. *IMM* distributes all the necessary information to various tasks from user input through the keyboard. A major function of this task is to display relevant process information so that the user can monitor and adjust the process. *IMM* creates three sub-processes: *barreltemp*, *statdip2*, and *variable*. Program *barreltemp* is responsible for the information display regarding barrel heaters; *statdip2* is responsible for the machine status display such as injection cycle information; program *variable* is responsible for the distribution of all the relevant information to other tasks; *variable* also runs real-time programs which are in direct interaction with hardware. Figure 3.6 shows the hierarchy of these programs.

The *moldtemp.control* controls the coolant water temperature to the mold by manipulating the cold and hot water flow via two control valves.

The *pcontrol* controls the cavity pressure. This task operates at a high priority. It starts to work when it receives an injection start signal from the machine. It determines the output to both supply and relief valves to force the cavity pressure to follow the set-point profile. Details on the cavity pressure and control are discussed in Chapter 5.

The *heater* is responsible for the control of the barrel zone temperatures.

The *cycle* is responsible for all the cyclic movement of the injection machine based on its current status and the information provided by the user. The cyclic information received is the injection, packing, cooling and recycling durations. The current status provided to the user include the current phase of the machine operation and its fraction of completion. The task also adjusts the data acquisition rate according to the different molding phases and provides cyclic information to all phase-related control tasks. However, constant sampling rate is used during control experiments.

The *RTI217* is loaded into memory but suspended, and it becomes active when the computer receives a hardware interrupt caused by a limit switch status change. Based on information from the user interface and display task, it activates different solenoid

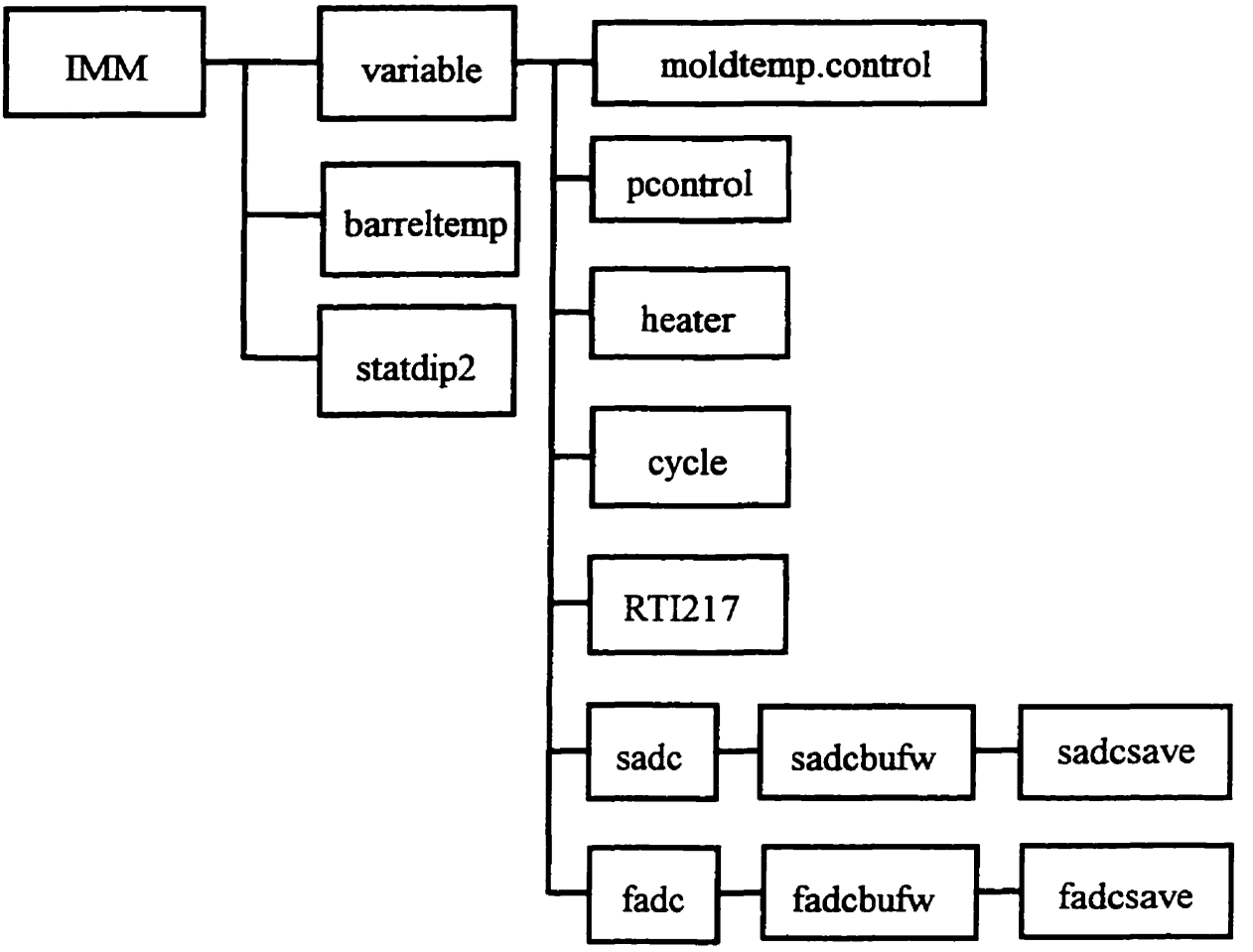


**Figure 3.6** Hierarchy of the computer control tasks

valves for machine movement and provides limit switch information for the display task.

The *fadc* and *sadc* are responsible for all the data collection based on the A/D rate, specified by the user interface task and the machine *cycle* task, for the fast and slow changing data, respectively. The *fadcbufw* and *sadcbufw* provide circular queues for keeping fast and slow changing data temporarily, respectively. The *fadcsave* and *sadcsave* save data from the queues maintained by *fadcbufw* and *sadcbufw*, respectively, onto hard disk using the file information specified by the user interface and display task.

## 3.4 Materials

Two type of polymers have been used in this study. An injection molding grade high density polyethylene resin, supplied by Dupont Canada as Sclair 2908. This resin has been employed in a large number of injection molding studies carried out in the Department of Chemical Engineering at McGill University [97,98]. A substantial amount of data is available regarding the fundamental properties and processing characteristics of this resin. Some of these properties are given in Table 3.7 [99].

Commercial injection molding grade polystyrene, Styron 685D supplied by Dow Chemical, was the second material used in this research. The manufacturer provided the property data shown in Table 3.8 [100].

## 3.5 Experimental Procedure

The experimental procedure was outlined at the start of each specific experimental section. The general operating conditions which were set at the beginning of each experiment were:

(1) Put the manual valves in the hydraulic system in the required positions.

(2) Open the coolant water for the heat exchanger located in the hydraulic system to keep hydraulic oil temperature from rising.

(3) Set the barrel temperature set-points for the four band heaters.

(4) Set the coolant temperature set-point for keeping constant mold temperature.

| Property | ASTM test method | Value |
|---|---|---|
| Solid density | D1505 | 0.96 g/cm$^3$ |
| Melt index | D1238 | 7.3 dg/min |
| Grid flow number | Du Pont | 20 cm |
| Bulk density | ---- | 0.61 g/cm$^3$ |
| Tensile yield, 50 mm/min | D1248 | 29 Mpa |
| Elongation, 50 mm/min | D1248 | 1200% |
| Tensile Impact | D1822 | 10 j/cm$^2$ |
| Flexural Stiffness | D747 | 965 Mpa |
| Hardness | D1706 | D 65 |
| Softening point | D1525 | 129 °C |
| Low temp. brittleness point | D746 | <-70°C |

**Table 3.7** - Physical properties of the polyethylene, Sclair 2908

| Property | ASTM method | Value SI unit |
|---|---|---|
| Yield tensile strength | D638 | 56.5 Mpa |
| Ultimate tensile strength | D638 | 56.5 Mpa |
| Ultimate elongation | D638 | 2.4 % |
| Tensile modulus | D638 | 3350 Mpa |
| IZOD impact strength (notched) @23°C | D256 | 24.0 J/M |
| Deflection temp. (annealed) @1.82 Mpa | D648 | 103 °C |
| Vicat softening point | D1525 | 108 °C |
| Melt flow rate | D1238 | 1.6 g/10 min |
| Specific gravity | D792 | ---- |

**Table 3.8** - Some properties of the polystyrene, Styron 685D

(5) Set the timers for the different component of each cycle including: injection, packing, cooling, and recycling durations.

(6) Define the data sampling time interval, which can be changed in different parts of the cycle.

(7) Turn on the required channels to collect data.

# CHAPTER 4

# DEVELOPMENT OF THE THEORETICAL MODEL

## 4.1 Introduction

A suitable mathematical model is necessary to carry out the control studies. Lumped parameter models which result in ordinary differential equations are more suitable for control system design. The numerical computation time for such models are less than those of a distributed model, and they can be analyzed more easily. This chapter deals with the development of such a theoretical model. The model includes filling, packing and holding, and cooling phases. Models for each phase were developed using the principles of conservation of mass, momentum, and energy. Criteria for transition from one phase to the next were defined as:

(1) Transition from the filling to the packing phase occurs when the mold cavity has filled with the polymer melt.

(2) Transition from the packing to the cooling occurs when the polymer melt in the gate has solidified completely.

Ordinary differential equations were developed for the filling and packing phases and solved using the Runge-Kutta fourth order method on a digital computer. The following sections develop the detailed analytic lumped model for dynamics of the molding process dynamics.

## 4.2 Filling Phase Model

In the filling phase, hydraulic oil is pumped into the injection cylinder with the action of hydraulic pump. Two servo-valves in the hydraulic circuit determine the flow rate of hydraulic oil into the injection cylinder, and thus the injection rate. The flow of hydraulic oil into the injection cylinder results in forward motion of the screw, as the screw is rigidly connected to the piston. This, in turn, pushes the polymer melt in the barrel through the nozzle into the sprue and runner. Figure 4.1 shows the schematic of the machine. The whole system is divided into subsystems in the modeling part. The subsystems are the injection cylinder, the ram-screw, the hydraulic system, and the polymer delivery system.

### 4.2.1 Injection Cylinder Model

The integral form of the mass conservative law [101], given below in one-dimensional form, is the basis of analysis of the flow in the injection cylinder:

$$0 = \frac{d}{dt}\int_{cv} \rho \, dv + (\rho A U)_{output} - (\rho A U)_{input} \tag{4.1}$$

where A is the cross-sectional area, *cv* is the control volume, dv is the differential volume, t is the average time, U is flow velocity, and $\rho$ is density. Figure 4.2 shows a close view of the injection cylinder. Applying the above equation to the injection cylinder gives:

$$\frac{V_h}{\beta_h}\frac{dP_h}{dt} = q_h - A_h\frac{dz}{dt} \tag{4.2}$$

where the injection cylinder itself is the control volume, as shown in Figure 4.2, $A_h$ is the injection cylinder cross area, $P_h$ is the pressure inside the injection cylinder called hydraulic pressure, $q_h$ is the hydraulic oil flow rate into the injection cylinder, $V_h$ is the injection cylinder volume, z is the screw position, $\beta_h$ is the bulk modulus of the hydraulic

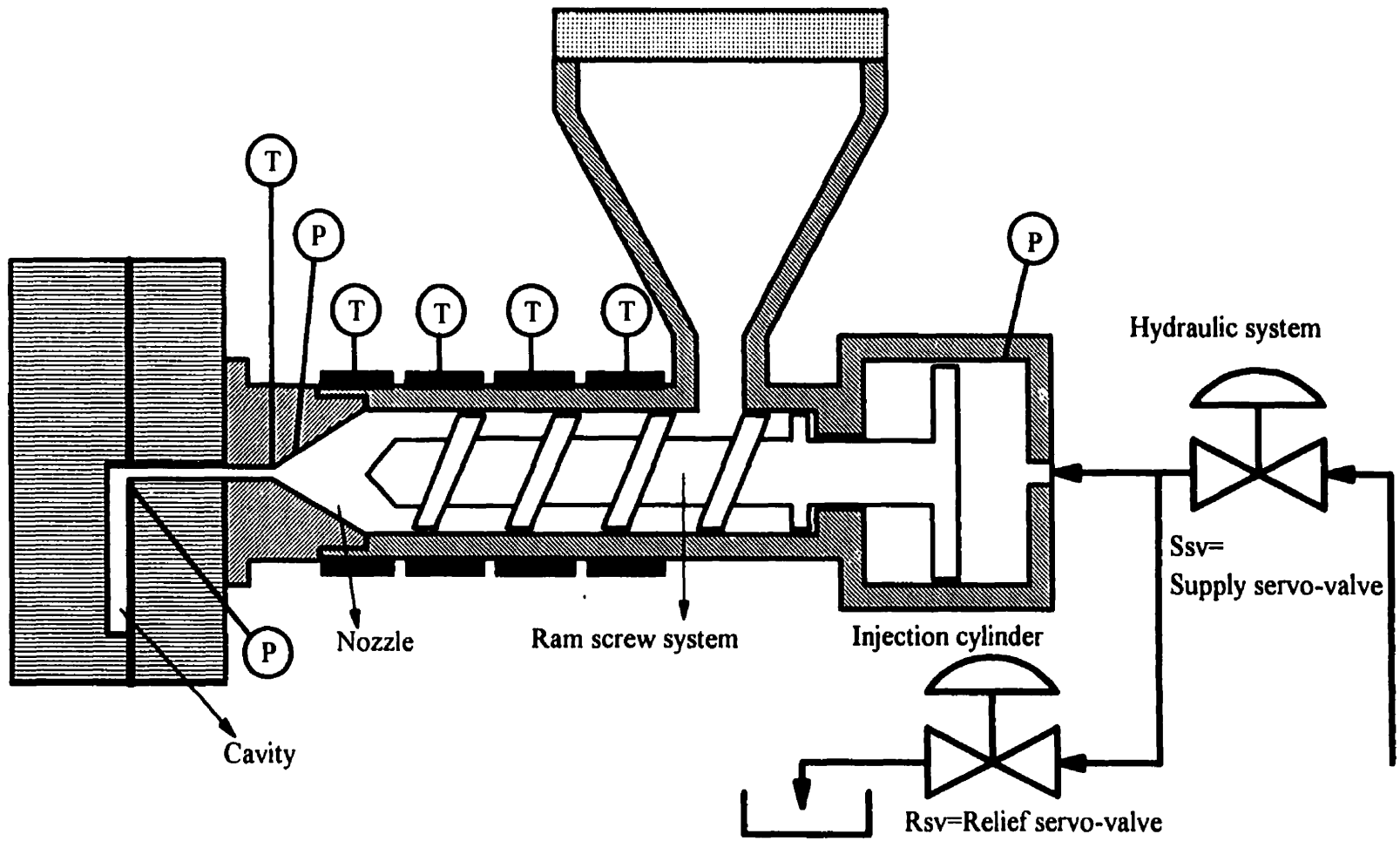


**Figure 4.1** Shematic of the machine

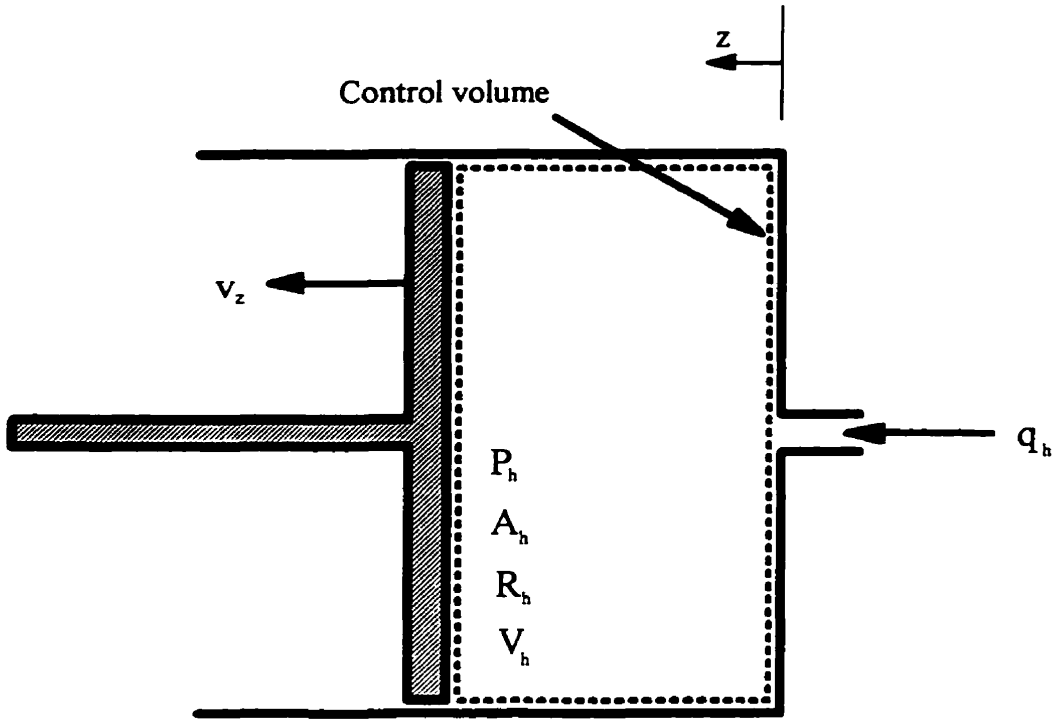


**Figure 4.2** Schematic of injection cylinder

oil, which is available as a function of temperature and pressure, defined as:

$$\beta_h = \frac{dP}{\frac{d\rho}{\rho}} \tag{4.3}$$

The injection cylinder volume, $V_h$ is changing due to the screw movement. Instantaneous $V_h$ is:

$$V_h = V_{h_0} + A_h z \tag{4.4}$$

where $V_{h0}$ is the initial volume of the injection cylinder. The major assumptions in deriving this model are: the injection cylinder body is rigid and there is no expansion due to high pressure, the density of the hydraulic oil is uniform throughout the injection cylinder, the injection cylinder is isothermal and there is no leakage between the screw and injection cylinder.

### 4.2.2 Ram-Screw Model

The hydraulic pressure moves the screw forward but the pressure at the nozzle and the friction force oppose its movement. Figure 4.3 shows the schematic ram-screw system. Applying Newton's second law to the screw results:

$$M\frac{dv_z}{dt} = A_h P_h - A_n P_n - f_v \tag{4.5}$$

where $A_n$ is the nozzle cross-sectional area, $f_v$ is the friction force against the screw system movement, M is the ram-screw system mass, $P_n$ is the pressure inside the nozzle called nozzle pressure, $v_z$ is the screw velocity. The friction force $f_v$ includes the viscous friction due to shearing the polymer melt between the screw and barrel and the mechanical friction in the fitting, which is negligible in comparison to the viscous friction force. Abu Fara [48] calculated the friction force by approximating flow in the ram system as axial annular Couette flow. This model considers the polymer melt to be sheared in the annular space between two coaxial cylinders with the inner cylinder (the

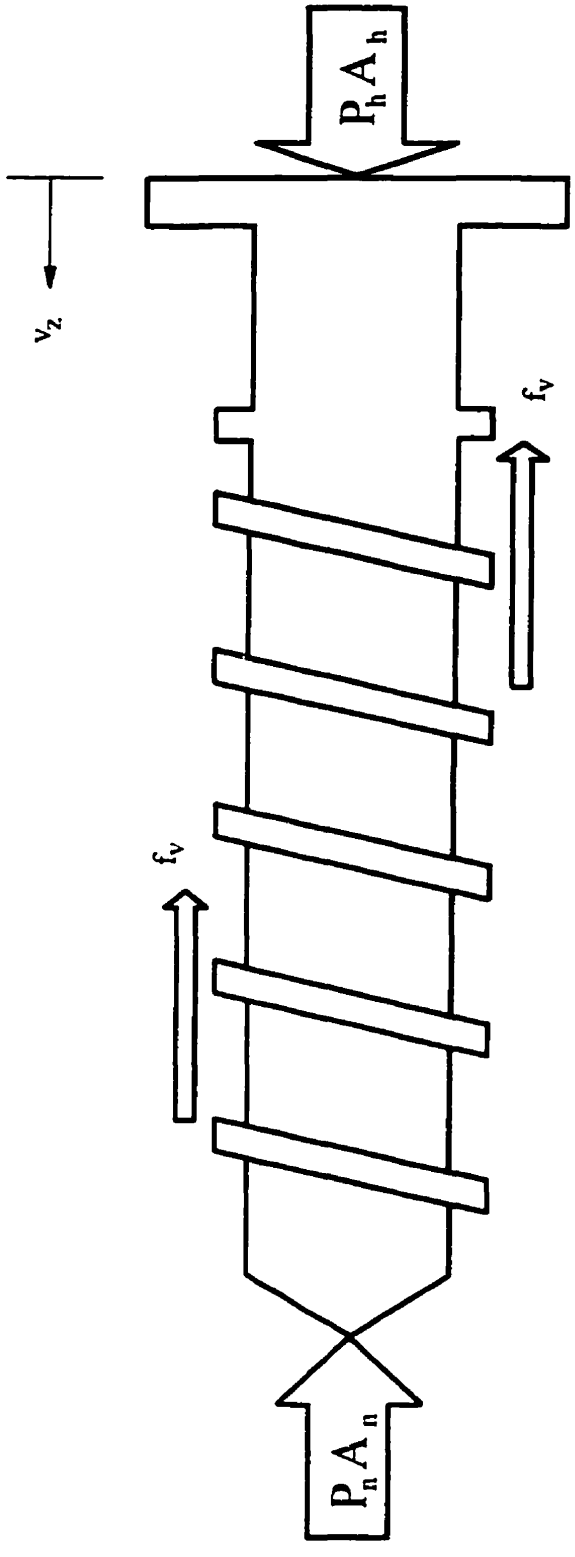


**Figure 4.3** Schematic of the ram screw system

screw) moving at velocity $v_z$. The equation of motion for this case is:

$$\begin{aligned} 0 &= -\frac{1}{r}\frac{\partial}{\partial r}\left(-r.\eta\frac{\partial v}{\partial r}\right) \\ v &= 0 \quad @ \quad r = R_n \\ v &= v_z \quad @ \quad r = k_r R_n \end{aligned} \tag{4.6}$$

where $k_r$ is ratio of screw radius to the inside barrel radius, r is the radial distance from the screw center, $R_n$ is the barrel radius, and $\eta$ is polymer melt viscosity. The major assumptions in deriving this equation are: the flow is one dimensional, temperature is constant, there is no slip at the barrel wall, the velocity gradient is radial, the polymer melt is incompressible, and the polymer flow between the screw and the barrel is steady. The polymer melt viscosity obeys the shear thinning power law, which is:

$$\eta = \eta_0 \dot{\gamma}^{n-1} = k_a e^{-\frac{\Delta E}{RT}} \dot{\gamma}^{n-1} \tag{4.7}$$

where $\eta_0$ is polymer viscosity at the shear rate equals 1 $s^{-1}$, $k_a$ and $\Delta E/R$ are the power law constants, and n is the power law index. The viscous force is:

$$f_v = 2\pi\eta_0 R_n^{1-n}(L_0+z)\left(\frac{(s-1)v_z}{k_r^{1-s}-1}\right)^n \tag{4.8}$$

where $L_0$ is the initial length of screw inside the barrel and $(L_0+z)$ is the instantaneous screw length inside the barrel, and s is 1/n. The resin characteristics were evaluated at an average temperature of the polymer melt film between the screw and the inside surface of the barrel. The average temperature was estimated using an expression developed by Tadmor and Klein [102]:

$$T_{avg} = T_m + (T_b - T_m)\frac{\frac{A_4}{2} + e^{-A_4}\left(1 + \frac{1}{A_4}\right) - \frac{1}{A_4}}{A_4 + e^{-A_4} - 1} \qquad (4.9)$$

$$A_4 = \frac{\Delta E}{R} \times \frac{1}{T_m\, n}$$

where $T_{avg}$ is the average temperature, $T_m$ is the melting point of the polymer, $T_b$ is the barrel temperature.

The ram displacement is simply calculated by integrating its velocity:

$$\frac{dz}{dt} = v_z \qquad (4.10)$$

### 4.2.3 Nozzle Model

The head of the barrel, where polymer melt accumulates, is called the nozzle. Figure 4.4 shows a schematic of the nozzle. The integral form of the mass conservation law is applied to the nozzle and gives:

$$\frac{V_n}{\beta_p}\frac{dP_n}{dt} = A_n\frac{dz}{dt} - q_p \qquad (4.11)$$

where $A_n$ is the nozzle cross-sectional area, $q_p$ is polymer melt flow rate which flows out of the nozzle, $V_n$ is the nozzle volume, and $\beta_p$ is polymer melt bulk modulus. The major assumptions in deriving this equation are: the nozzle body is rigid, the nozzle is isothermal, and the polymer density is uniform throughout the nozzle. The volume of the nozzle, $V_n$, is changing according to:

$$V_n = V_{n_0} - A_n z \qquad (4.12)$$

where $V_{n0}$ is the initial volume of the nozzle. The injection molding machine geometry is listed in appendix B.

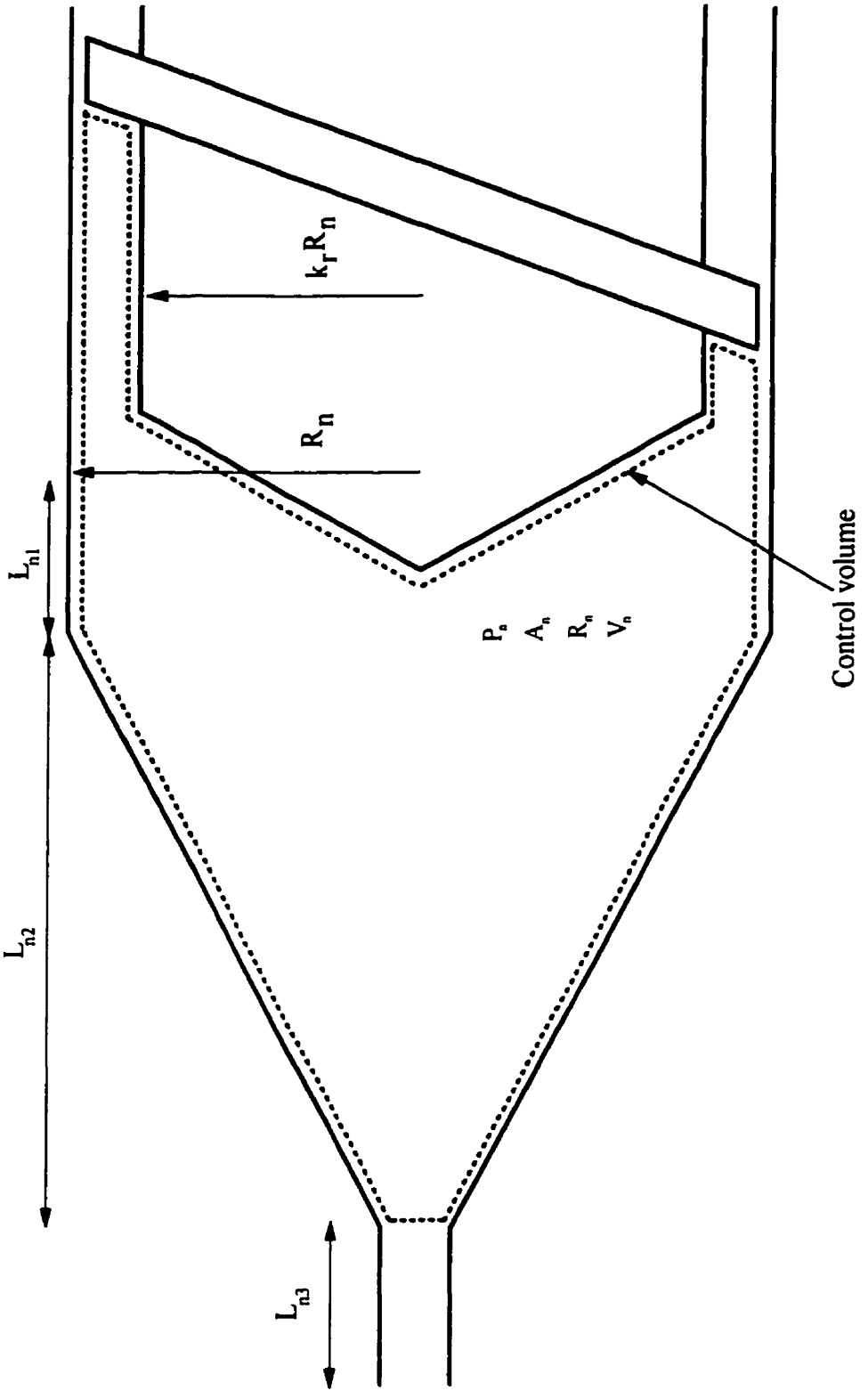


**Figure 4.4** Schematic of the nozzle diagram

### 4.2.4 Hydraulic System Model

Figure 4.5 shows the essential hydraulic system, indicating the curvature in the real system. Based on this figure the complete analysis of the system was done including losses such as those due to elbows, etc. The output pressure of the hydraulic pump is constant by controlled by an unloading valve, hence, the pressure before supply servo-valve, point s in Figure 4.5, is constant. A pressure transducer was installed at point s to measure the pressure at this point, called supply pressure, $P_s$. The configuration of the hydraulic circuit and servo-valve openings determines the hydraulic oil flow rate, $q_h$, into the injection cylinder. The following assumptions can be applied for the treatment of the hydraulic system: the flow is isothermal, the hydraulic oil flow in the hydraulic system is laminar and fully-developed (typically the Reynolds number is 300), flow is one dimensional, and the hydraulic oil is an incompressible fluid. In this case Bernoulli's equation can be applied to model the hydraulic system:

$$\frac{P_1}{\rho g} + \frac{\alpha_1}{2g} V_1^2 + y_1 = \frac{P_2}{\rho g} + \frac{\alpha_2}{2g} V_2^2 + y_2 + \sum h_f + \sum h_m \qquad (4.13)$$

where $h_f$ is friction head loss, $h_m$ is minor head loss, g is gravity acceleration, P is pressure, V is the flow velocity, y is height, and $\alpha$ is the kinetic energy correction factor. $h_f$ is calculated by Darcy-Weisbach equation and the definition of $h_m$ is:

$$h_f = f \frac{L}{d} \frac{V^2}{2g}$$
$$h_m = \frac{\Delta P}{\rho \cdot g} \qquad (4.14)$$

where d is the tube diameter and L is the length of the tube. The pressure drop of the servo-valves is calculated using the following equation [103]:

$$q = k_v i \sqrt{\Delta P} \qquad (4.15)$$

where i is the servo-valve opening and $k_v$ is the valve constant. The pressure drop of hydraulic filters installed in the inlet of the valves is calculated by [104]:

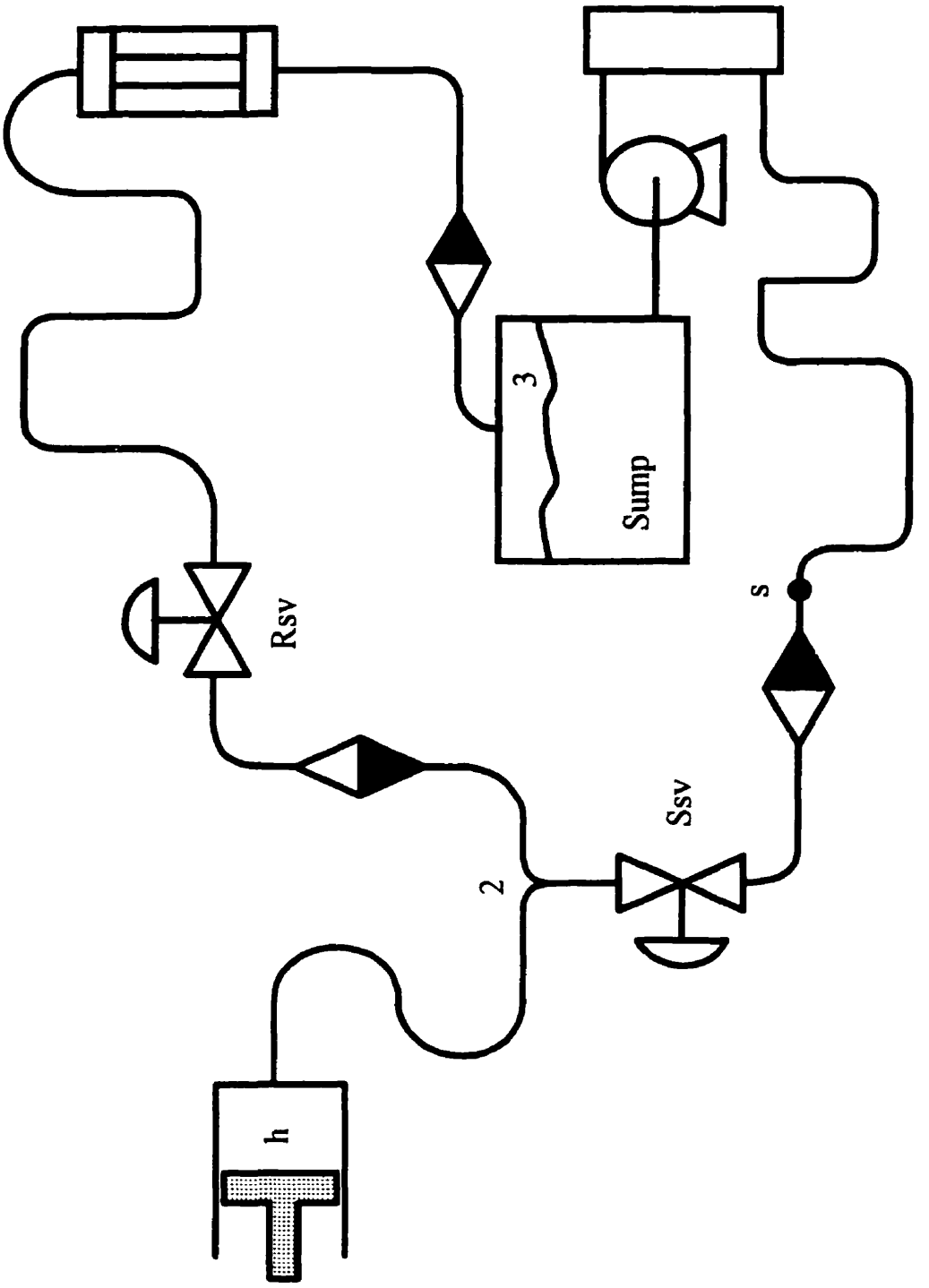


**Figure 4.5** Simplified hydraulic system

$$\Delta P = A_3 q^3 + A_2 q^2 + A_1 q + A_0 \tag{4.16}$$

where $A_0$ through $A_3$ are constants.

The Bernoulli relationship in this case can be applied to calculate the flow rate between points s, 2, h (see Figure 4.5) which results in the following:

$$\begin{aligned} P_s - P_2 &= C_{s2} q^2 \\ P_2 - P_h &= C_{2h} q_h^2 \\ P_2 - P_3 &= C_{23} q_2^2 \end{aligned} \tag{4.17}$$

where $C_{s2}$, $C_{2h}$, and $C_{23}$ are the flow coefficients for the various flow segments including skin friction force, valve and filter as well as minor friction forces, q is the hydraulic oil flow rate through the supply servo-valve, and $q_2$ is the hydraulic oil flow rate through the relief servo-valve. They are obtained from Bernoulli's relation according to the following equation:

$$\begin{aligned} C_{s2} &= \textit{Minor Losses} + \textit{Filter} + \textit{Friction} + \textit{Potential} \\ C_{s2} &= A_3 q + A_2 + \frac{1}{(k_v i_s)^2} + \frac{\rho_o k_{s2}}{2 g A_t^2} + \left( A_1 + \frac{8 \mu L_{s2}}{\pi R_t^4} \right) \frac{1}{q} + (A_0 + y_2 \rho_o g) \frac{1}{q_2} \\ C_{2h} &= \textit{Minor Losses} + \textit{Friction} + \textit{Expansion} + \textit{Potential} \\ C_{2h} &= \frac{\alpha_h \rho_o}{2 A_h^2} - \frac{\alpha_2 \rho_o}{2 g A_t^2} + \left( 1 - \frac{R_t}{R_h} \right)^2 \frac{\rho_o}{2 A_t^2} + \frac{8 \mu L_{2h}}{\pi R_t^4} \frac{1}{q_h} + \rho_o g (y_h - y_2) \frac{1}{q_h^2} \\ C_{23} &= \textit{Minor Losses} + \textit{Filter} + \textit{Friction} + \textit{Potential} + \textit{Heat Exchanger} \\ C_{23} &= A_3 q_2 + \left( \frac{-\alpha_2 \rho_o}{2 A_t^2} + \frac{1}{(k_v i_R)^2} + A_2 + \frac{\rho_o k_{23}}{2 A_t^2} \right) + \left( \frac{8 \mu L_{23}}{\pi R_t^4} + A_1 + \frac{8 \mu L_{exc}}{\pi R_{exc}^4 n_t} \right) \frac{1}{q_2} \\ &\quad + \left( (y_3 - y_2) \rho_o g + A_o \right) \frac{1}{q_2^2} \end{aligned} \tag{4.18}$$

where $A_t$ is the cross sectional area of the pipe in the hydraulic system, $i_s$, and $i_R$ are the supply and relief servo-valve openings, respectively, $k_{s2}$ is the minor loss coefficient

between point s and 2, $k_{23}$ is the minor loss coefficient between points 2 and 3, $L_{s2}$ is the pipe length between points s and 2, $L_{2h}$ is the length of pipe between points 2 and h, $L_{23}$ is the pipe length between points 2 and 3, $L_{exc}$ is the length of the heat exchanger in the hydraulic system, $n_t$ is the number of tubes in the heat exchanger, $R_{exc}$ is the radius of tube in the heat exchanger, $R_h$ is the injection cylinder radius, $R_t$ is the radius of pipe in the hydraulic system, $y_2$ is the height of point 2, $y_3$ is the height of point 3, $y_h$ is the height of point h, $\mu$ is the hydraulic oil viscosity, and $\rho_o$ is the hydraulic oil density. Algebraic arrangement of Equation (4.17) provides a relationship to calculate $q_h$:

$$q_h = \left[\frac{P_s - P_n - C_{2h} q_h^2}{C_{s2}}\right]^{0.5} - \left[\frac{P_h + C_{2h} q_h^2}{C_{23}}\right]^{0.5} \tag{4.19}$$

The hydraulic system geometry is listed in appendix B.

### 4.2.5 Polymer Delivery System Model

The polymer delivery system includes the sprue, runner, gate, and mold cavity. Figure 4.6 shows the polymer delivery system. In modeling the flow inside the polymer delivery system, it is assumed that polymer flow is one dimensional and laminar as well as isothermal. The pseudo-steady approximation is used [105]. The flow equation can be described as:

$$\Delta P = k_t \, q_p^n \tag{4.20}$$

where $k_t$ is the summation of instantaneous k-values, and k is the coefficient which relates the flow rate to the pressure drop in that part of the channel.

The nozzle is divided into three parts, see Figure 4.4, with three different k-values to analyze the flow behavior. The first part has a constant diameter; the pressure drop is calculated by the Hagen-Poiseuille equation for the power law fluid in a pipe:

$$\Delta P = k_{n_1} q_p^n = 2\eta_0 \left(L_{n_1} - z\right) \left[\frac{s+3}{\pi R_n^{s+3}}\right]^n q_p^n \tag{4.21}$$

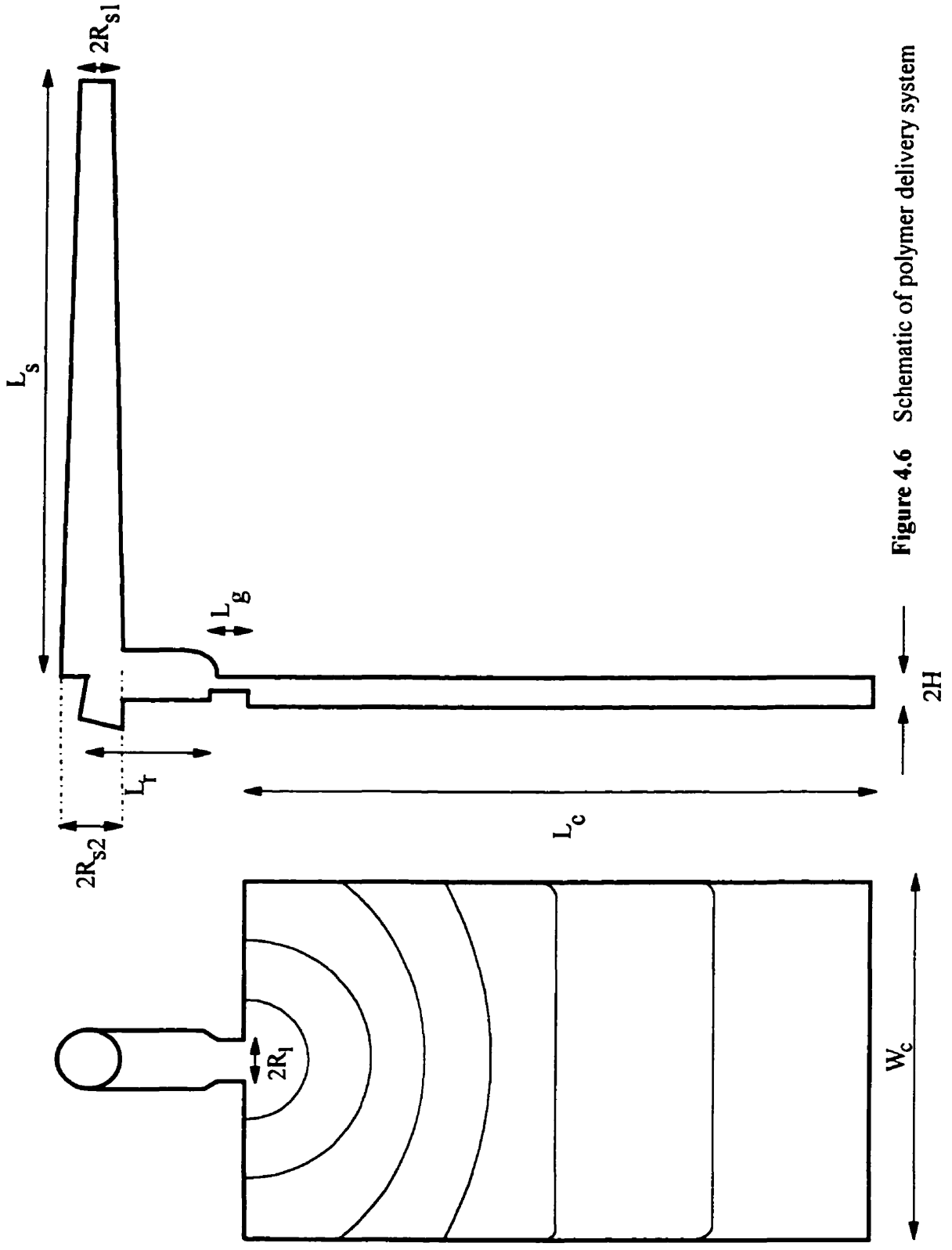


**Figure 4.6** Schematic of polymer delivery system

where $L_{n1}$ is the length of the first part of the nozzle.

The second part of the nozzle has a considerable convergence. Using the fully-developed flow formula for power law fluid is far from reality. There have been some attempts to derive some simple formula to calculate the pressure drop [106,107]. In this research study, a similar approach to that of Kwon *et al* [108] is used to find the pressure drop. A $\theta$-averaged force balance has been first introduced to obtain an average pressure drop due to converging flow. The elastic effect in terms of the normal-stress difference, $N_1$, has been incorporated in the final formula. The final pressure drop formula is:

$$\Delta P = \left(\frac{1}{R_1^{3n}} - \frac{1}{R_2^{3n}}\right) \times \left( \frac{2\eta_0}{3n\tan\omega}\left[\frac{n+1}{2n\pi I\tan\omega}\right]^n + \frac{2\eta_0(1-\cos^{n+3}\omega)}{3n(n+3)\sin^{n+3}\omega}\left[\frac{n+1}{2n\pi I}\right]^n \right) \times q_p^n + \frac{4\psi E}{3f(\sin\omega)^{2+f+\frac{f}{n}}}\left[\frac{n+1}{2n\pi I}\right]^f \left(\frac{1}{R_1^{3f}} - \frac{1}{R_2^{3f}}\right) \times q_p^f \tag{4.22}$$

where

$$I = \frac{2}{3}\frac{(1-\cos\omega)^2(1+2\cos\omega)}{\sin^2\omega}\frac{n+1}{3n+1}$$

$$E = \int_0^{\omega} \cos^{f+1}\theta \, \sin^{\frac{f}{n}+1}\theta \, d\theta \tag{4.23}$$

$$N_1 = \psi \dot{\gamma}^f$$

where f is normal stress power law index, $N_1$ is the first normal-stress difference, $\psi$ is the constant in the normal stress power law, and $\omega$ the is converging angle of the channel. Appendix C gives details of the derivation of this equation.

The third part of the nozzle has a constant diameter, and Equation (4.21) is applied to calculate the pressure drop in this part.

The sprue is diverging with a very small angle, and the fully-developed power law flow assumption is used to calculate pressure drop in the sprue [109], as follows:

$$\Delta P = \frac{2\eta_0}{3n}\left[\frac{s+3}{\pi}\right]^n \frac{L_s}{R_{s_2}-R_{s_1}}\left(\frac{1}{R_{s_1}^{3n}}-\frac{1}{R_{s_2}^{3n}}\right) \tag{4.24}$$

where $L_s$ is the length of sprue, $R_{s1}$, and $R_{s2}$ are the radius of sprue cross-section at two ends.

The runner is a pipe with constant diameter and its pressure drop can be calculated by Equation (4.21). The gate pressure drop is calculated by Equation (4.21), using the hydraulic radius for the gate section.

The flow in the mold cavity is divided into two different sections: the radial flow section and the one-dimensional flow between two parallel plates. Figure 4.6 shows the flow pattern inside the mold cavity. In the radial flow section, the pressure drop is determined by an approach similar to Equation (4.22). The normal stress effect is taken into consideration, and the result is:

$$\Delta P = \frac{\eta_0}{H(1-n)}\left[\frac{2n+1}{2n\pi H^2}\right]^n \left(r^{1-n}-R_1^{1-n}\right)q_p^n + \frac{n\psi}{f(f+n)}\left[\frac{2n+1}{2n\pi H^2}\right]^f \left(\frac{1}{R_1^f}-\frac{1}{r^f}\right)q_p^f \tag{4.25}$$

where H is half the thickness of the mold cavity.

In the second part of the cavity, the flow is between two parallel plates. Using the equation of motion, the pressure drop can be calculated as:

$$\Delta P = \left[\frac{2n+1}{2w_c n}\frac{1}{H^{\frac{1}{n}+2}}\right]^n \eta_0 L_c q_p^n \tag{4.26}$$

where $L_c$ is the mold cavity length, and $w_c$ is the cavity width.

Bernoulli's equation is used to evaluate the polymer melt flow rate between the nozzle and the instantaneous polymer front during filling and yields:

$$q_p = \left[ \frac{P_n - \frac{\alpha_f \rho q_p^2}{2A_f^2} - \rho g y_f}{k_t} \right]^{\frac{1}{n}} \tag{4.27}$$

where $A_f$ is the front cross area, $y_f$ is the height of the front flow, and $\alpha_f$ is kinetic energy correction factor. The definition of $\alpha$, the kinetic energy correction factor, is:

$$\alpha = \frac{1}{A} \int\int \left( \frac{u}{V_{avg}} \right)^3 dA \tag{4.28}$$

For a power law fluid flow inside a pipe, the kinetic energy correction factor is:

$$\alpha = \frac{3(3n+1)^2}{(2n+1)(5n+3)} \tag{4.29}$$

Inside the cavity, when the fluid flow front is rectangular, the kinetic energy correction factor is:

$$\alpha = \frac{6(2n+1)^2}{(3n+2)(4n+3)} \tag{4.30}$$

During filling, the mass of polymer in the polymer delivery system at any instant equals the total amount of polymer mass flow through the nozzle from the beginning of filling. If the flow is assumed incompressible, the volume of polymer in the cavity, $V_p$, is:

$$V_p = \int_0^t q_p \, dt \tag{4.31}$$

Hence, the flow rate of polymer during filling is:

$$\frac{dV_p}{dt} = q_p \tag{4.32}$$

Polymer delivery system geometry is given in appendix B.

### 4.2.6 Summary of the Filling Phase Equations

The following set of state equations governs the polymer melt and hydraulic oil during the filling phase:

$$\begin{aligned}
\frac{dP_h}{dt} &= F_1 = \frac{\beta_h}{V_h}\left(q_h - A_h\frac{dz}{dt}\right) \\
\frac{dv_z}{dt} &= F_2 = \frac{1}{M}\left(A_h P_h - A_n P_n - f_v\right) \\
\frac{dz}{dt} &= F_3 = v_z \\
\frac{dP_n}{dt} &= F_4 = \frac{\beta_p}{V_n}\left(A_n\frac{dz}{dt} - q_p\right) \\
\frac{dV_p}{dt} &= F_5 = q_p
\end{aligned} \tag{4.33}$$

This fifth order state equations describe the filling phase of the injection molding process. It is a set of non-linear ordinary differential equations. This set of equations is shown in block diagram form in Figure 4.7. Each block represents a process element whose behavior can be expressed by a differential or algebraic equation. For example, consider the block whose output is the velocity in Figure 4.7. The input to this block is the summation of three terms which are $A_hP_h$, $-f_v$, and $-A_nP_n$. The output, $v_z$ is found by integration of the input with respect to time and dividing by M. This is equivalent to Equation (4.5).

## 4.3 Packing Phase Model

### 4.3.1 Mold Cavity Model

In the packing phase, the cavity is already filled and compression of polymer in the cavity starts. The melt flow rate drops and the pressure in the cavity increases very rapidly. It is assumed that the cavity pressure is uniform throughout the cavity. Therefore, the following equation is added from the integral form of the mass balance

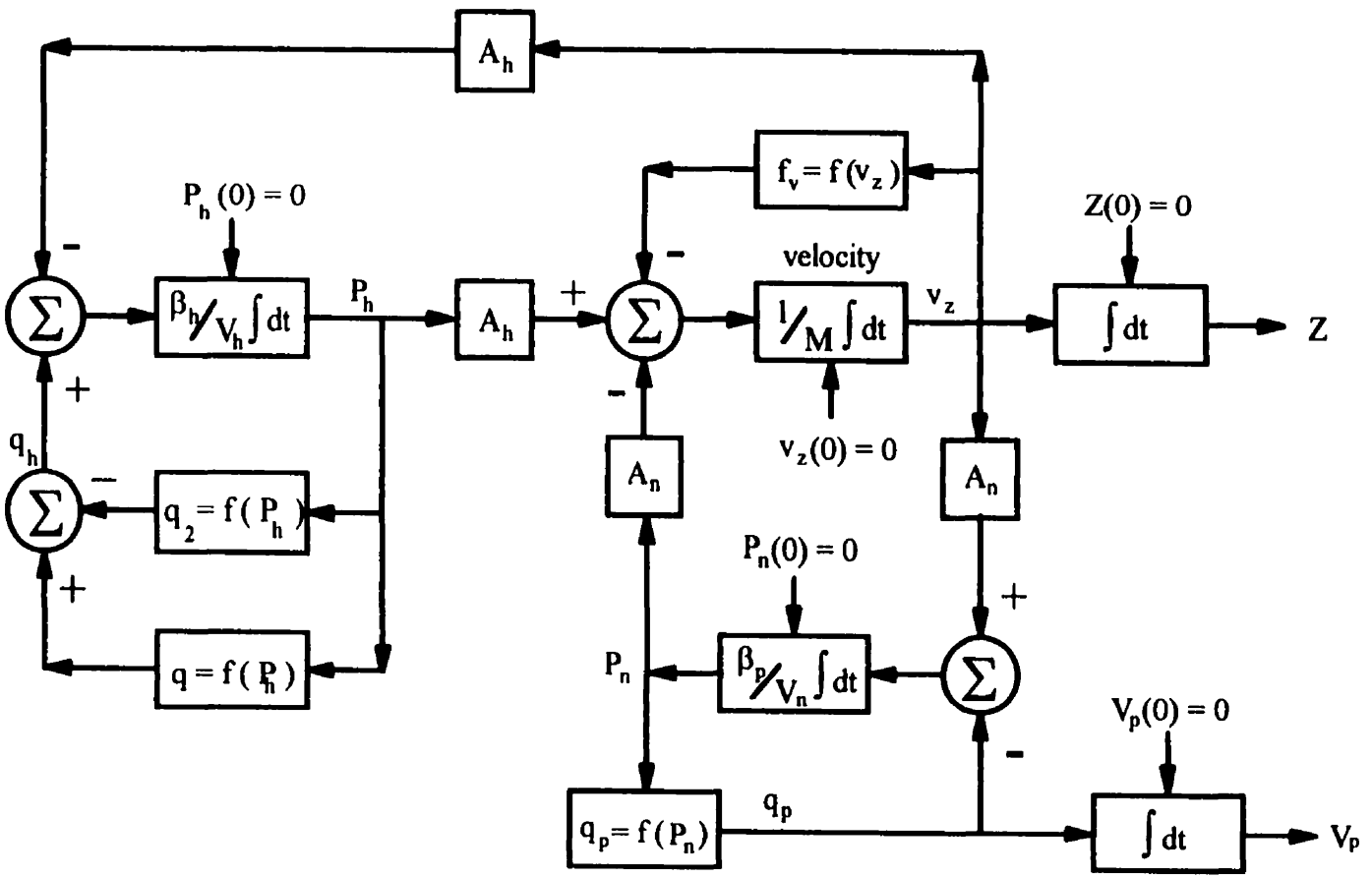


**Figure 4.7** Block diagram of the filling phase model

for the cavity after filling:

$$\frac{dP_c}{dt} = \frac{\beta_p}{V_t} q_p \tag{4.34}$$

where $P_c$ is the cavity pressure and $V_t$ is the total volume of polymer delivery system. The major assumptions in this equation are that the polymer delivery system body is rigid and that polymer density is uniform throughout the mold cavity. The polymer melt flow rate, in this phase, is mostly determined by the pressure difference between the nozzle and the cavity:

$$q_p = \left[ \frac{P_n - P_c - \frac{\alpha_f \rho q_p^2}{2A_f^2} - \rho g y_f}{k_t} \right]^{\frac{1}{n}} \tag{4.35}$$

### 4.3.2 Summary of the Packing Phase Equations

In view of the above, during the packing phase the following set of state equations is employed:

$$\begin{aligned}
\frac{dP_h}{dt} &= F_1 = \frac{\beta_h}{V_h}\left(q_h - A_h \frac{dz}{dt}\right) \\
\frac{dv_z}{dt} &= F_2 = \frac{1}{M}(A_h P_h - A_n P_n - f_v) \\
\frac{dz}{dt} &= F_3 = v_z \\
\frac{dP_n}{dt} &= F_4 = \frac{\beta_p}{V_n}\left(A_n \frac{dz}{dt} - q_p\right) \\
\frac{dP_c}{dt} &= F_5 = \frac{\beta_p}{V_t} q_p
\end{aligned} \tag{4.36}$$

Figure 4.8 shows this set of equations in block diagram form. During the packing phase, the polymer melt flow rate decreases dramatically and the polymer solidifies on the wall

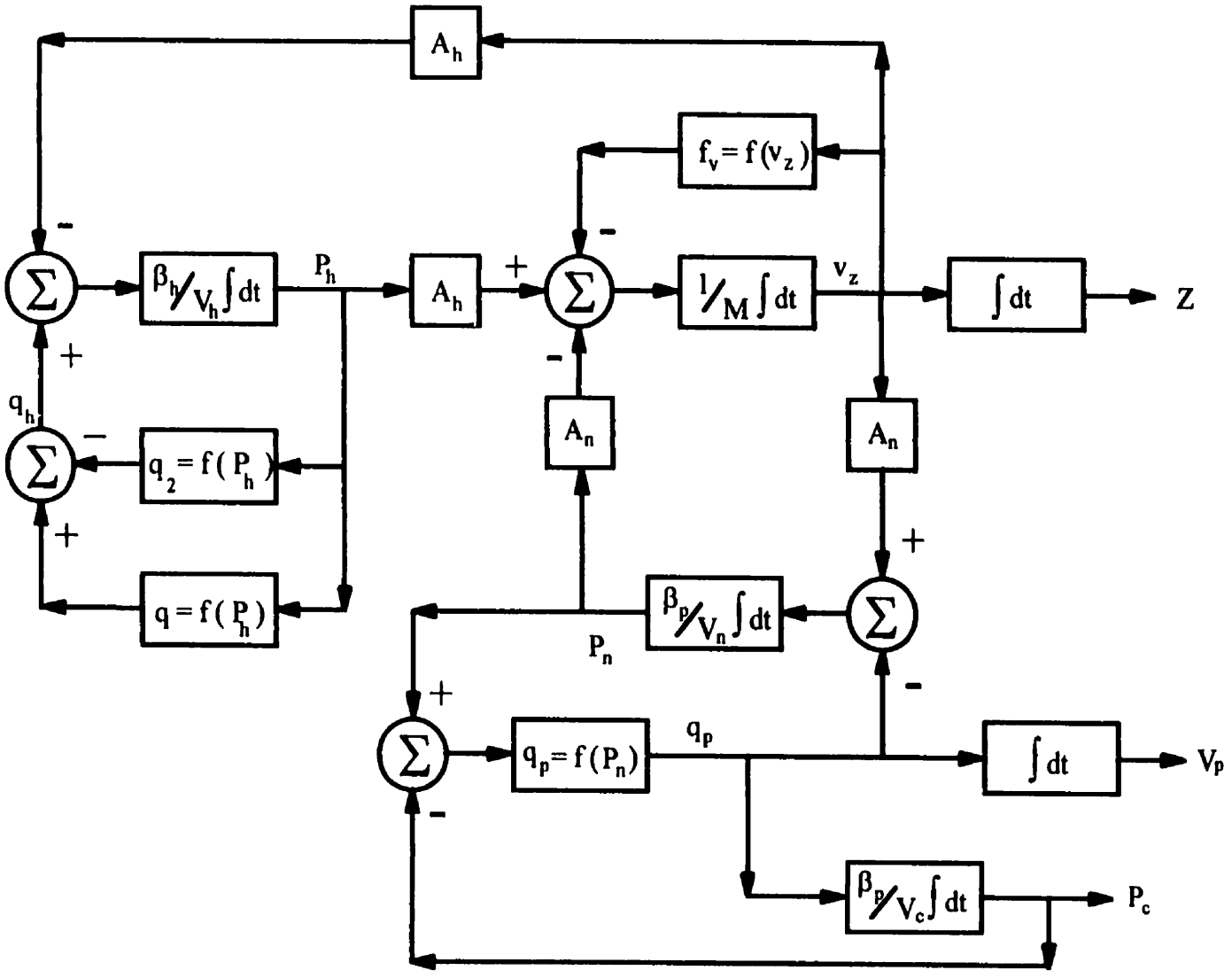


**Figure 4.8** Block diagram of the packing phase model

of the sprue and runner. This reduces the flow cross-sectional areas. The reduction of radius can be analyzed by energy balance in the polymer delivery system. In the following section, the analysis for semi-crystalline polymer is introduced. The treatment is simpler for strictly amorphous polymers since the heat of crystallization does not contribute to the energies of the system.

### 4.3.3 Solidification of Polymer Melt in the Sprue and Runner

Solidification of the polymer melt in the polymer delivery system reduces the flow cross-section. Hence, the resistance against the polymer flow increases. Figure 4.9 shows a schematic cross section of the sprue. The energy balance at the solid-melt interface is used to calculate the reduction of radius. The high density polyethylene is a semi-crystalline polymer. Hence, a variable thermal diffusivity is used, instead of the latent heat of crystallization. The following equation summarizes the treatment of heat transfer and crystallization in the sprue and runner:

$$
\begin{aligned}
C_p \rho \frac{\partial T}{\partial t} &= \frac{1}{r}\frac{\partial}{\partial r}\left(kr\frac{\partial T}{\partial r}\right) \\
T &= T_{melt} \quad @ \quad t = 0 \\
\frac{\partial T}{\partial r} &= 0 \quad @ \quad r = 0 \\
h(T - T_{mold}) &= -k\frac{\partial T}{\partial r} \quad @ \quad r = R
\end{aligned}
\qquad (4.37)
$$

where $C_p$ is the heat capacity of the polymer melt, h is convection heat transfer coefficient, k is the thermal conductivity of the polymer melt, T is the local temperature, $T_{melt}$ is the initial polymer melt temperature, and $T_{mold}$ is the mold metal temperature. The major assumptions in deriving the above equation are: heat transfer is one dimensional in the radial direction; the mold metal temperature is constant; the initial temperature is uniform; flow effects in the energy equation during packing are considered to be negligible. With variable thermal properties Equation (4.37) is solved numerically using the Crank-Nicholson implicit finite difference method [110], which is

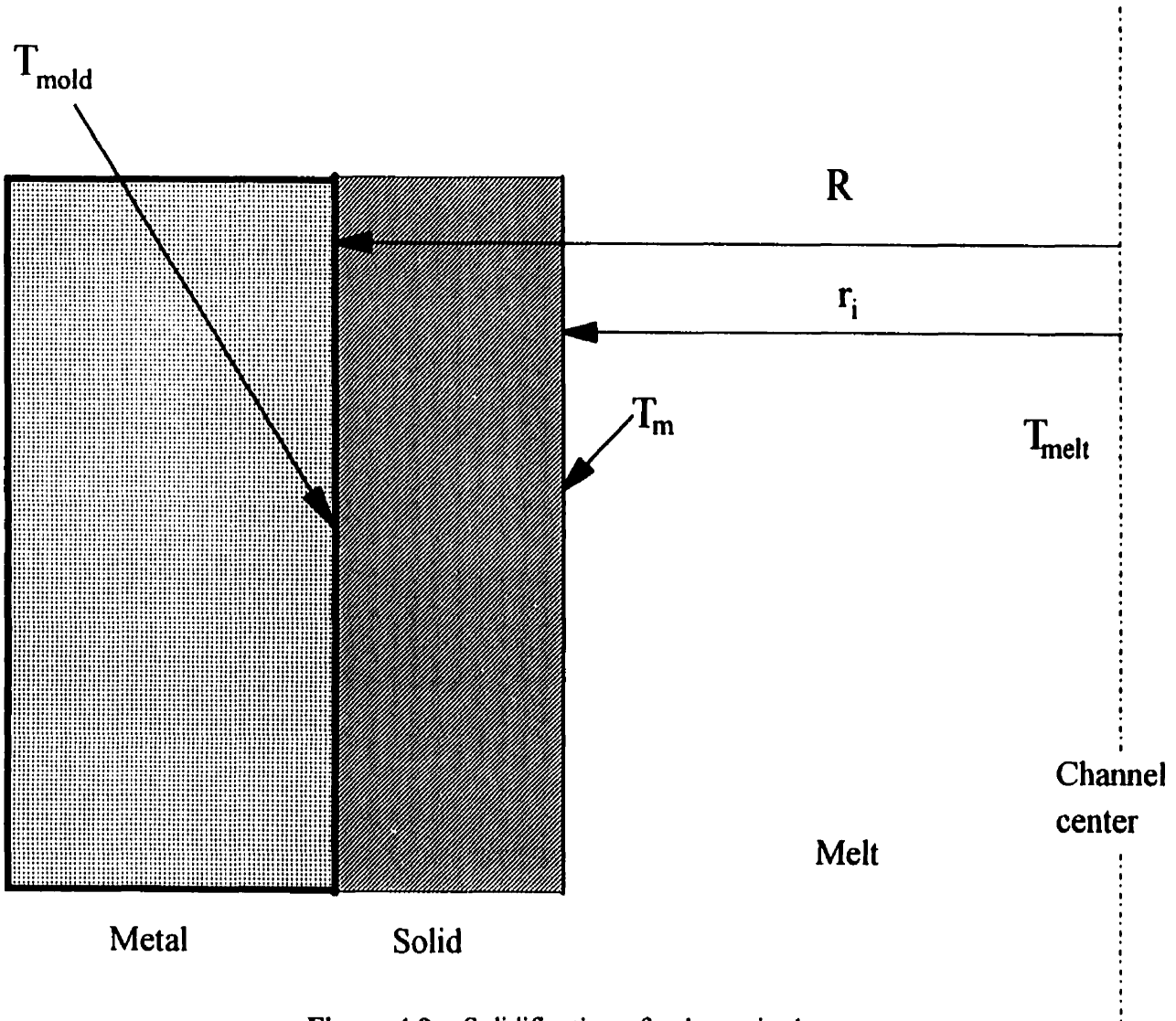


**Figure 4.9** Solidification of polymer in the sprue

unconditionally stable.

The finite difference representation of Equation (4.37) is given by:

$$-\frac{i+1}{2i}\lambda_{i+1}T_{i+1,n+1}+\left(1+\frac{i+1}{2i}\lambda_{i+1}+\frac{1}{2}\lambda_i\right)T_{i,n+1}-\frac{1}{2}\lambda_i T_{i-1,n+1} = \frac{i+1}{2i}\lambda_{i+1}T_{i-1,n}+\left(1-\frac{i+1}{2i}\lambda_{i+1}-\frac{1}{2}\lambda_i\right)T_{i,n}+\frac{1}{2}\lambda_i T_{i+1,n} \tag{4.38}$$

$$\begin{aligned} T_0 &= T_1 \\ T_n &= \frac{h\Delta r T_{mold}+kT_{n-1}}{h\Delta r+k} \\ T_1 &= T_{melt} \quad @ \quad t = 0 \end{aligned} \tag{4.39}$$

where $\lambda_i$ is $\alpha_i.\Delta t/\Delta r^2$; thermal diffusivity of polymer, $\alpha_i=k_i/\rho C_p$, is an experimentally determined function of temperature; n and i are time and location grid number, respectively.

In order to estimate the thickness of the solid skin near the wall, it is assumed the solidification temperature $T_m$ is 110°C. At higher temperature the material is considered to be a melt. The average melt temperature is calculated by the following equation:

$$T_{avg} = \frac{1}{R_m}\int_0^{R_m} T.dr \tag{4.40}$$

where $R_m$ is the radius of the melt part. The finite difference formula for this equation is:

$$T_{avg} = \frac{\dfrac{T_m^2-T_j^2}{2(T_{j+1}-T_j)}+\dfrac{T_o+T_j}{2}+\sum_{k=1}^{j-1}T_k}{j+\dfrac{T_m-T_j}{T_{j+1}-T_j}} \tag{4.41}$$

where j is the grid number for which $T_{j+1} \le T_m \le T_j$.

The average temperature is used to calculate the viscosity of polymer melt. The gate is approximated by its hydraulic radius. Therefore, Equation (4.37) is also applicable for the gate.

## 4.4 Cooling Phase Model

The cavity is modeled as two parallel plates. Figure 4.10 shows the cavity during the cooling phase. The major assumptions are: heat transfer is one dimensional and perpendicular to the cavity walls; the mold metal temperature is constant; and the cavity initial temperature is uniform throughout the cavity. The governing equation and its boundary conditions are:

$$
\begin{aligned}
C_p \rho \frac{\partial T}{\partial t} &= \frac{\partial}{\partial y}\left(k \frac{\partial T}{\partial y}\right) \\
T &= T_{melt} \qquad @ \qquad t = 0 \\
\frac{\partial T}{\partial y} &= 0 \qquad @ \qquad y = 0 \\
h\left(T - T_{mold}\right) &= -k \frac{\partial T}{\partial y} \qquad @ \qquad y = H
\end{aligned}
\tag{4.42}
$$

A variable thermal diffusivity is used to account for the crystallization. With a variable thermal diffusivity, the above equation must be solved numerically. The Crank-Nicholson implicit finite difference method is used to solve it numerically. The finite difference formula for this equation is:

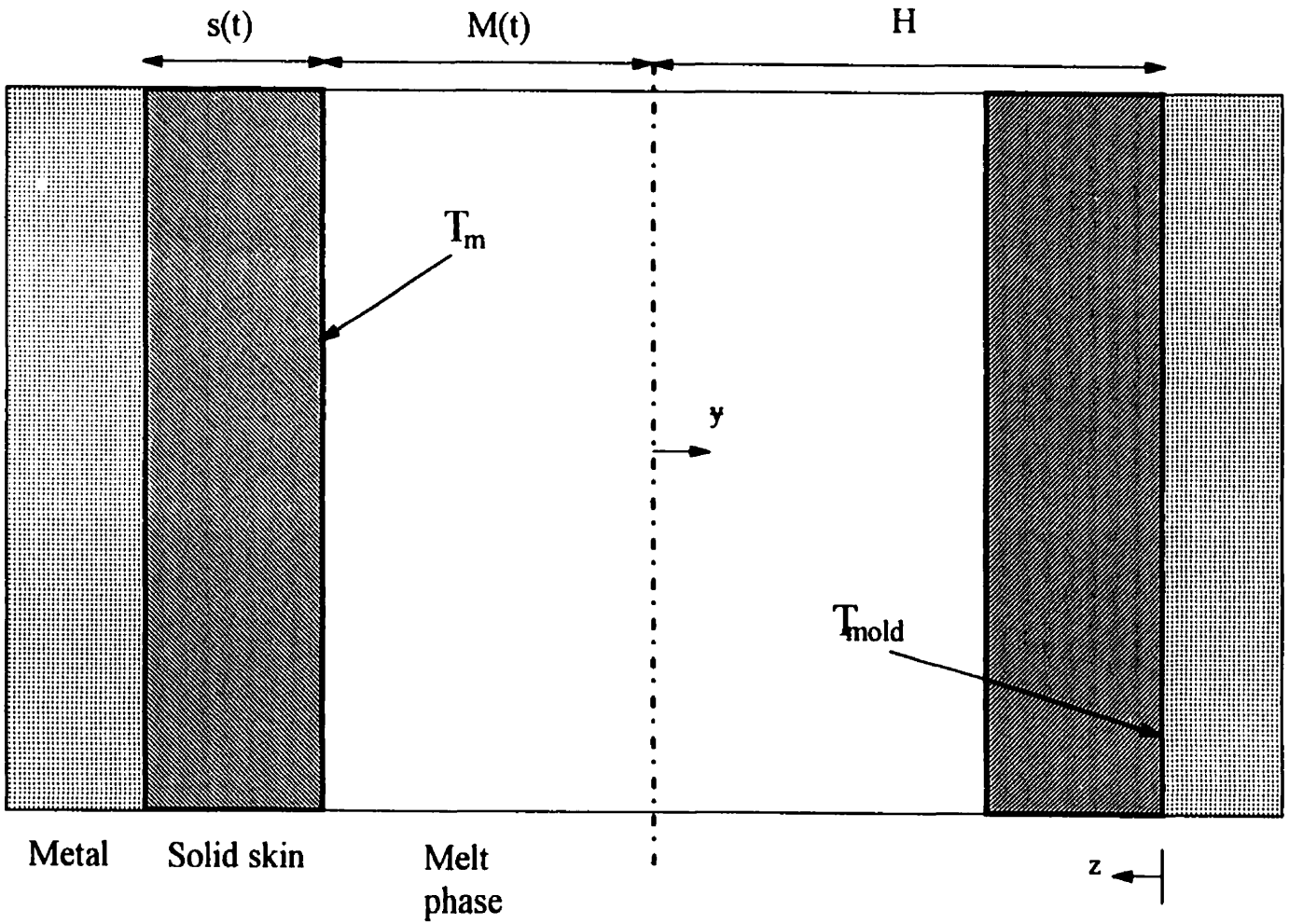


**Figure 4.10** Cavity mold during the cooling phase

$$
\begin{aligned}
-\lambda_{i+1}T_{i+1,n+1}+(1+\lambda_{i+1}+\lambda_i)T_{i,n+1}-\lambda_i T_{i-1,n+1} &= \\
\lambda_{i+1}T_{i+1,n}+(1-\lambda_{i+1}-\lambda_i)T_{i,n}+\lambda_i T_{i-1,n} & \\
T_0 = T_1 & \\
T_n = \frac{h\Delta y T_{mold}+kT_{n-1}}{h\Delta y+k} & \\
T_i = T_{melt} \quad @ \quad t = 0 &
\end{aligned}
\tag{4.43}
$$

To calculate the solid skin thickness near the cavity wall, it is assumed that wherever temperature is less than $T_m = 110°C$, the polymer is solid and the rest of the cavity is filled with polymer melt. This calculation starts as soon as the filling phase finishes. After the gate has frozen, the cavity is isolated from the rest of the process. Hence, the mass of the polymer in the cavity is constant during the cooling phase. The average polymer temperature in the cavity is calculated from the following equation:

$$
T_{avg} = \frac{1}{H_m}\int_0^{H_m} T.dy \tag{4.44}
$$

The finite difference formula of this equation is:

$$
T_{avg} = \frac{\dfrac{T_m^2-T_j^2}{2(T_{j+1}-T_j)}+\dfrac{T_o+T_j}{2}+\sum_{k=1}^{k-1}T_i}{j+\dfrac{T_m-T_j}{T_{j+1}-T_j}} \tag{4.45}
$$

where j is the grid number for which $T_{j+1} \leq T_m \leq T_j$. The average temperature in the cavity was calculated numerically, and the experimentally determined P-V-T relationship for the polymer was used to calculate the pressure during the cooling phase [111]. The total polymer mass inside the cavity during cooling is constant because the cavity was isolated from the rest of the process. For the polyethylene, a fitted polynomial of the experimental data was used. Appendix D gives the complete physical and rheological properties of Sclair 2908 polyethylene.

For the polystyrene, Styron 685D, which is an amorphous thermoplastic, the P-V-T behavior has been modeled using the double-domain Tait equation [112,113], which is:

$$v(T,P) = v_0(T)\left(1 - 0.0894\ln\left[1 + \frac{P}{B(T)}\right]\right) \qquad (4.46)$$

Characterization of the polystyrene is listed in appendix D.

## 4.5 Method of Solution

The equations describing the three phases of the injection molding process were solved on a digital computer. The non-linear equations for the various phases were solved using a Runge-Kutta fourth order method. A program which solves the set of non-linear differential equations was written in WATCOM-C running under QNX.

The numerical solution process was initiated with the filling phase. The supply pressure was input to the program and measured before the supply servo-valve in the hydraulic system. The instantaneous flow resistance in the polymer delivery system was calculated to find the polymer melt flow rate. Cavity pressure was zero until polymer melt filled the sprue and runner. The integration continues until the cavity was filled. The flow cross-section reduction due to solidification in negligible at high fill rates, but should be taken into account at fill rates close those that produce short shot. At this time the governing equations for the packing phase were introduced instead of the filling phase equations. The final values of the filling phase were the initial values for the packing phase. The same integration method was applied to the differential equations during packing. During the packing phase, the reduction of the radius in the sprue and runner were calculated. The integration method was continued until the gate completely froze. At this point, the cavity was isolated and the polymer specific volume (or density) remained constant. The average temperature in the cavity was calculated numerically, and the P-V-T relationship for the polymer was used to calculate the pressure during the cooling phase. Figure 4.11 shows the computer simulation procedure.

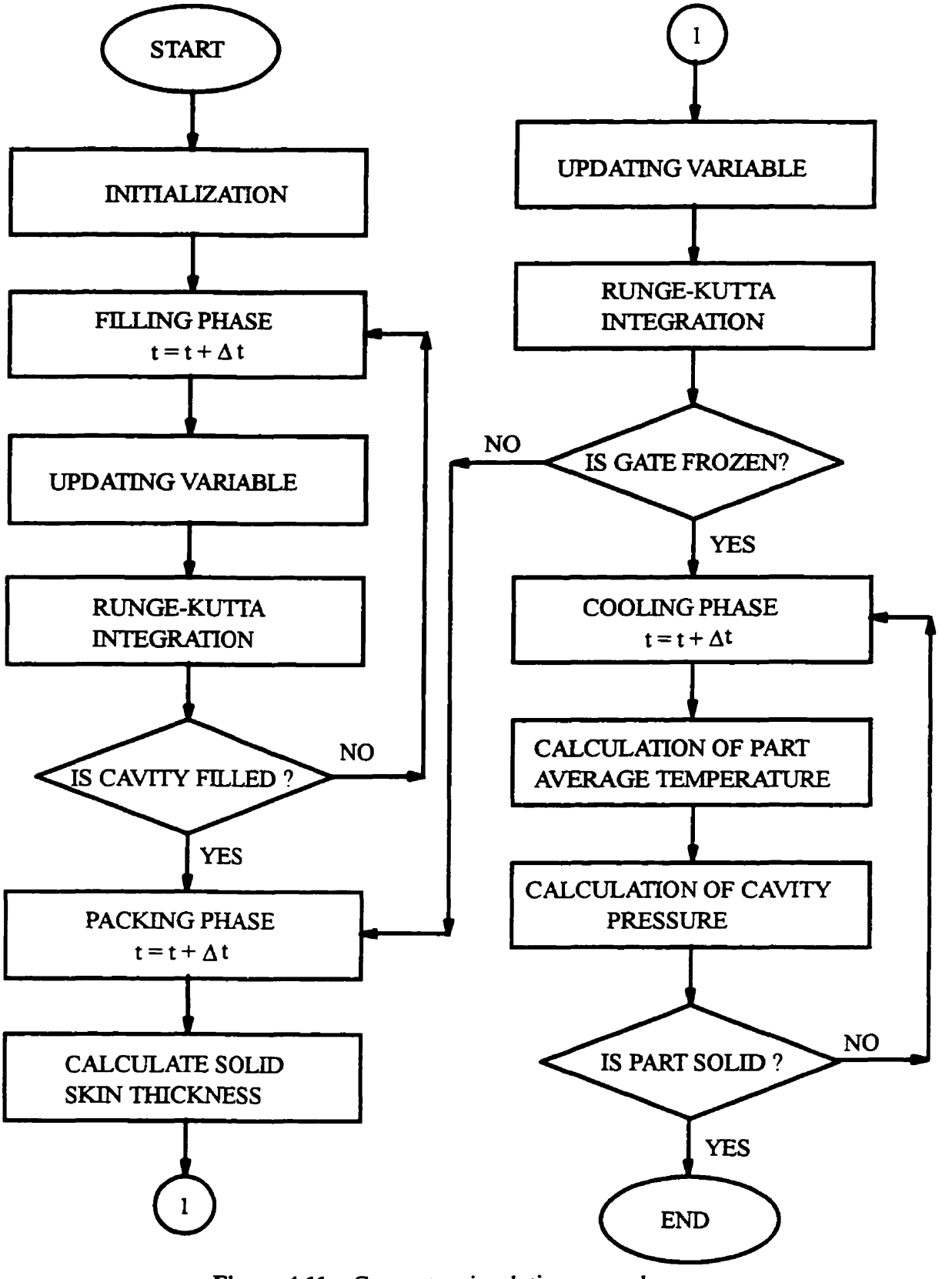


**Figure 4.11** Computer simulation procedure

## 4.6 Model Validation

Experimental data was obtained from the Danson Metalmec injection molding machine, model 60-SR. Variables of the injection molding process was collected using the computer. The set of variables sampled was: a) supply pressure, b) hydraulic pressure, c) screw position, d) screw velocity, e) nozzle temperature, f) nozzle pressure, g) cavity pressure. At the start of each run, the variables to be monitored were entered. The computer system samples these variables during all phases including filling, packing, and cooling phases. Different sampling rates can be used for the various phases.

A number of runs were made at various supply and relief servo-valve openings. Data were collected for pressure in the cavity, nozzle, and injection cylinder as well as for the velocity and position of the screw.

Typical predicted and experimental results are shown in Figures 4.12 a and b. Figure 4.12a shows the hydraulic and nozzle pressures. In the beginning of the filling phase, the simulation and experimental results are in very good agreement. Figure 4.13 shows the same figure in a larger time scale for better comparison. The experimental hydraulic pressure shows some noise due to the hydraulic pump. The transition from filling to packing in simulation is fast compared to the actual process. The isothermal assumption may explain the difference. During packing, simulation pressure is somewhat higher than the experimental values. The reason could be the underestimation of some resistances in the hydraulic system or the change in behavior of elements with time. The simulation ends at t=25 s, when the hydraulic oil flow is diverted from the injection cylinder due to the start of the cooling phase and isolation of the cavity from the rest of the process.

The predicted and experimental nozzle pressures are generally in good agreement. According to the model, the transition from filling to packing is less sluggish than the experimental results. The noise which is seen in the experimental hydraulic pressure trace is not seen in the nozzle experimental pressure trace. The viscous flow in the screw region filters this noise. The slight changes in the hydraulic pressure have no effect on the movement of the screw because of dominance of the nozzle pressure and

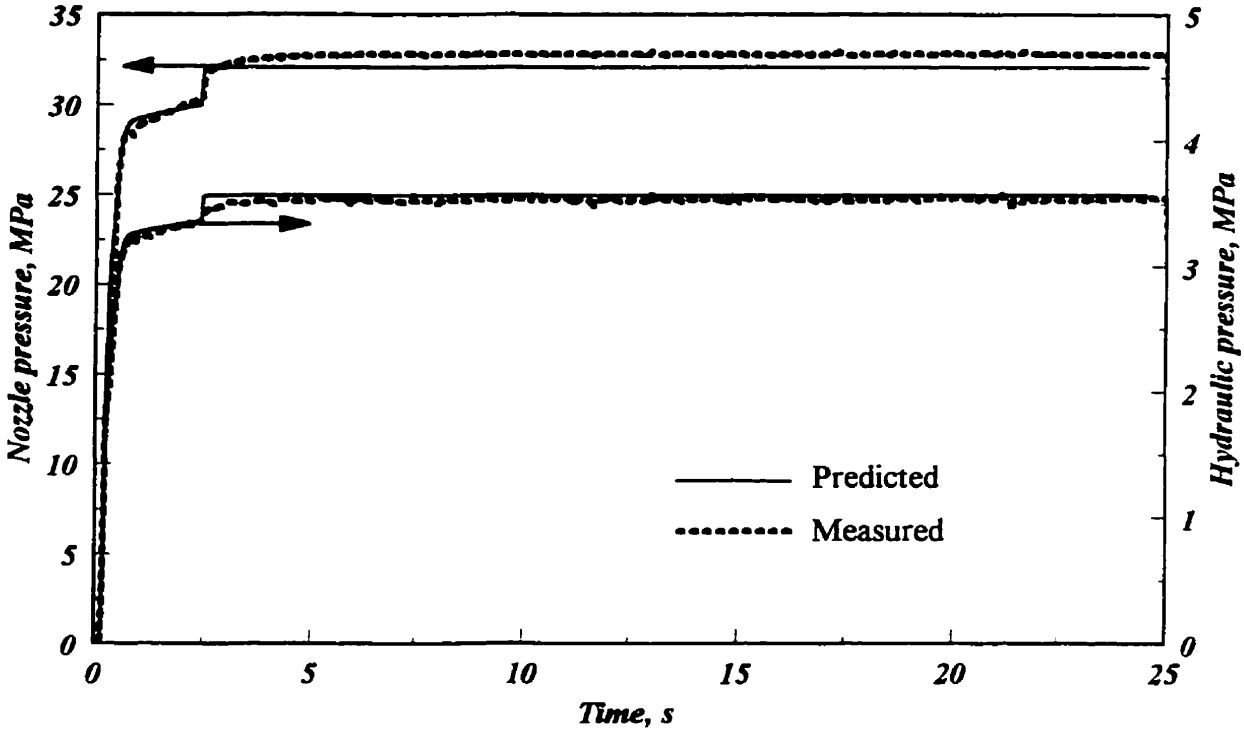


Figure 4.12a Nozzle and hydraulic pressures

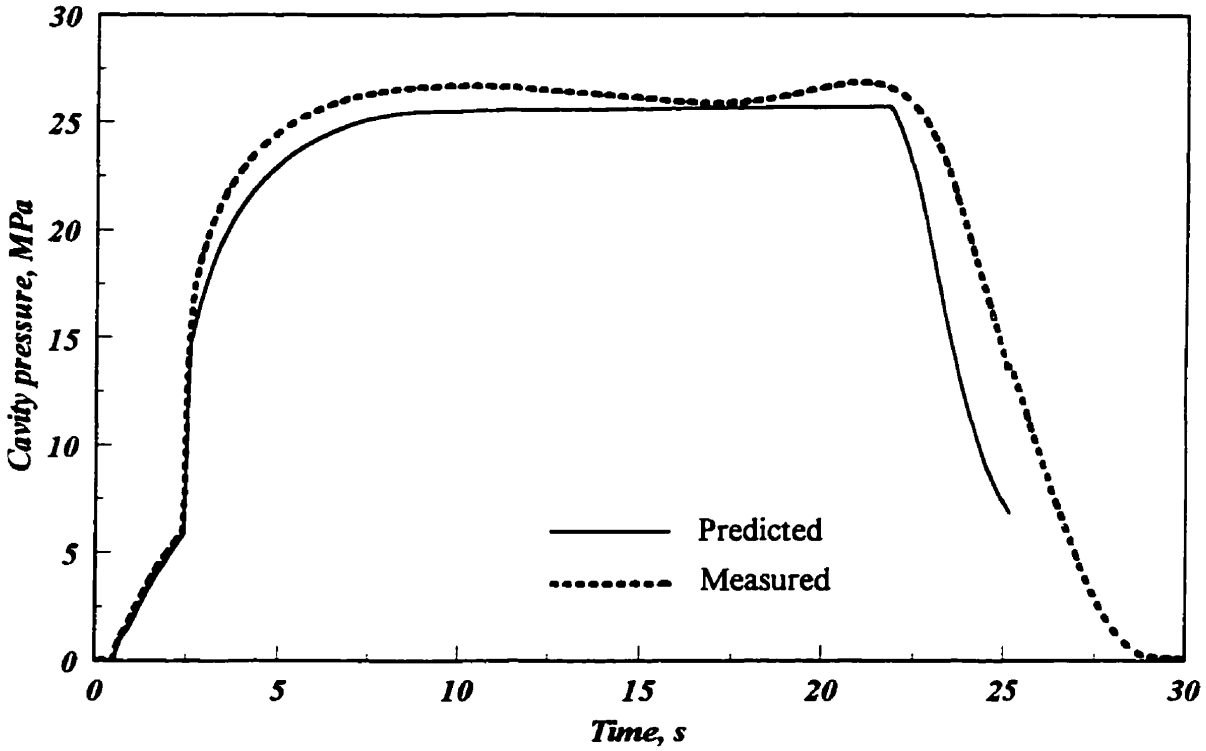


Figure 4.12b Cavity pressure

**Figure 4.12** Hydraulic, nozzle, and cavity pressures, Ssv=90%, Rsv=0%

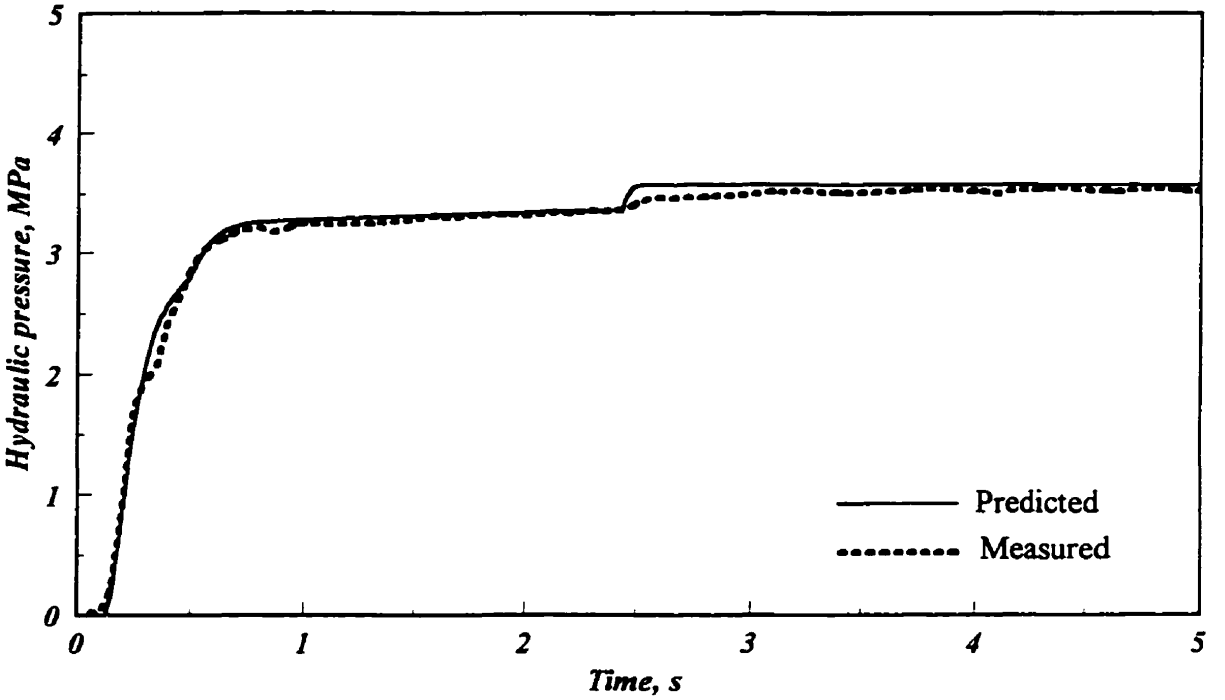


Figure 4.13a Hydraulic pressure

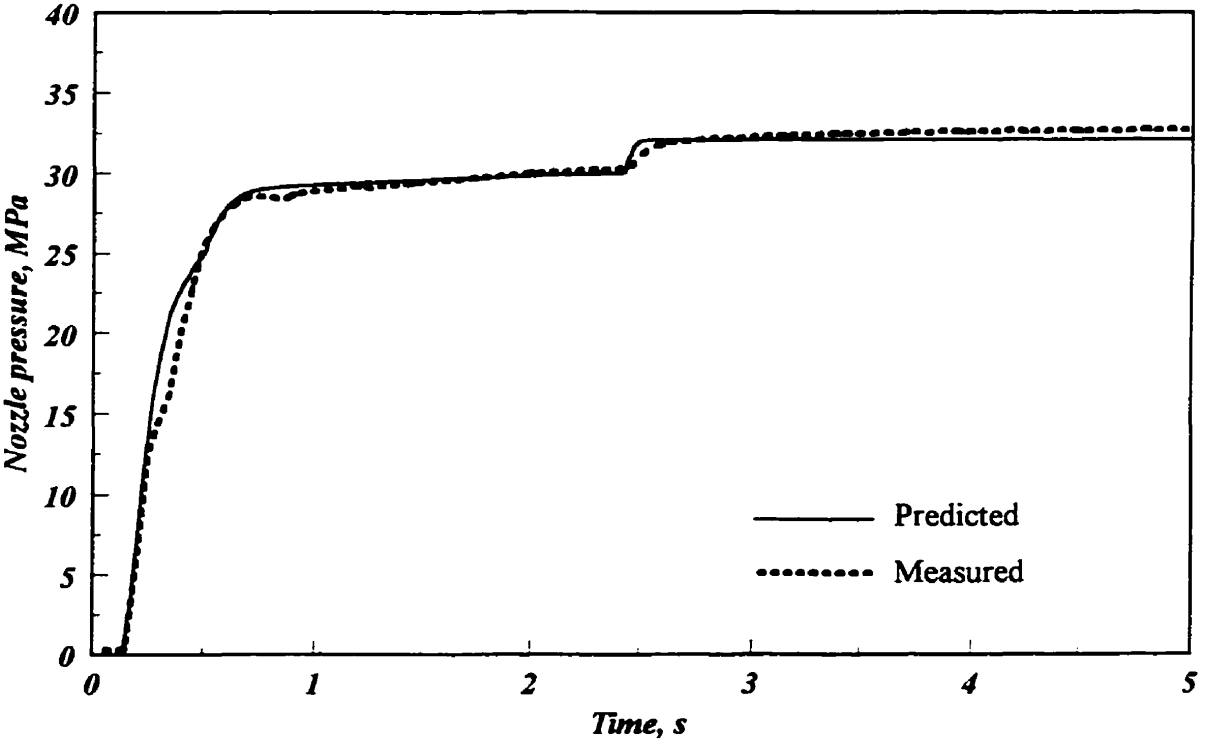


Figure 13b Nozzle pressure

**Figure 4.13** Large scale of hydraulic and nozzle pressures, Ssv=90%, Rsv=0%

viscous friction. The simulated nozzle pressure is somewhat lower than expected, probably due to an over-estimation of the screw friction force.

The simulated cavity pressure is generally in good agreement with experimental data (see Figure 4.12b). The cavity pressure during the filling phase is shown on an expanded scale in Figure 4.14a. Figure 4.14a shows that the pressure drop in the runner and sprue is slightly over-estimated giving the observed off-set. Figure 4.14b shows the modeling result without considering the normal stress and the polymer solidification in the sprue. As expected, the simulated cavity pressure was higher and the filling time was shorter than experimental values when the normal stress was ignored. In the absence of the solidification effect inside the sprue and runner, the simulated cavity pressure rose rapidly to reach the nozzle pressure. The solidification increases the resistance between the nozzle and the cavity and decreases the flow to the cavity. It seems that the solidification rate in the calculation is a little higher because the simulated cavity pressure is lower than the measured levels during packing. During cooling, the simulated and experimental pressure profiles follow similar patterns, but the experimental pressure is larger than the simulation. This also is explained by a solidification rate that is too high. The probable cause of this is the assumption that mold metal temperature is constant. The model calculation stops when the cavity average temperature reaches the melting temperature because of unavailability of P-V-T data below this temperature for the solid polymer. Figures 4.15 shows the evolution of the ram screw displacement and velocity. The simulated and experimental displacements are in good agreement. Initially, the experimental velocity is larger because the barrel is partially filled with the solid granular polymer and the frictional resistance is lower than that used in this simulation. The actual displacement is larger than predicted by the model. This is probably due to the isothermal assumption. The experimental velocity is noisy because it is obtained by electronically differentiating the displacement.

Figure 4.16 shows the hydraulic, nozzle, and cavity pressures, respectively for another set of processing conditions (supply and relief servo-valve openings equal 80% and 15%, respectively). The quality of the agreement between prediction and experimental data

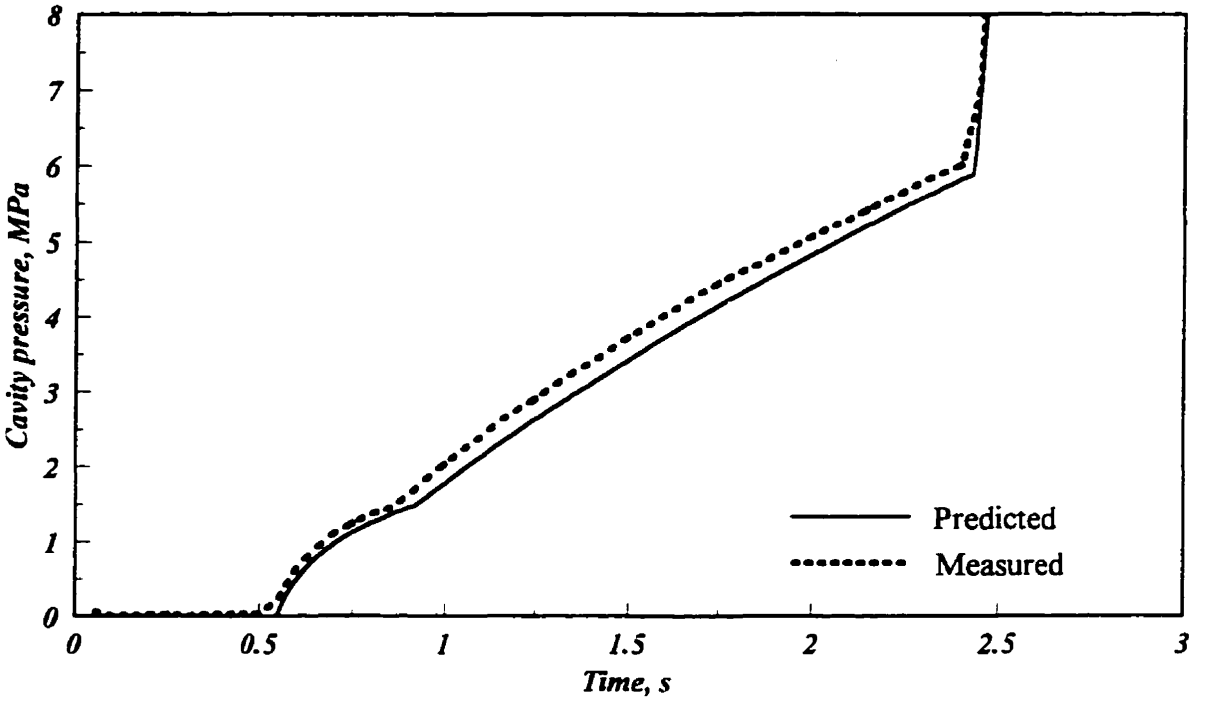


Figure 4.14a Large scale of cavity pressure during the filling

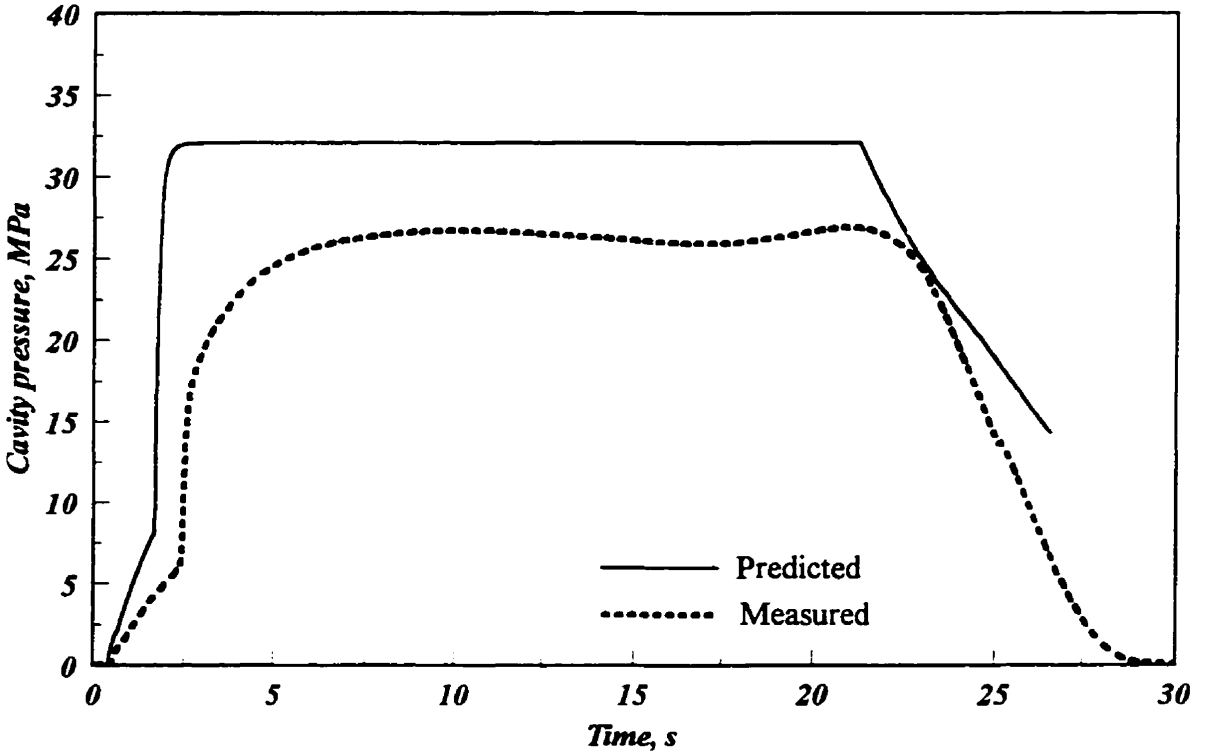


Figure 4.14b Cavity pressure without normal stress and solidification

**Figure 4.14** Cavity pressure in different conditions, Ssv=90%, Rsv=0%

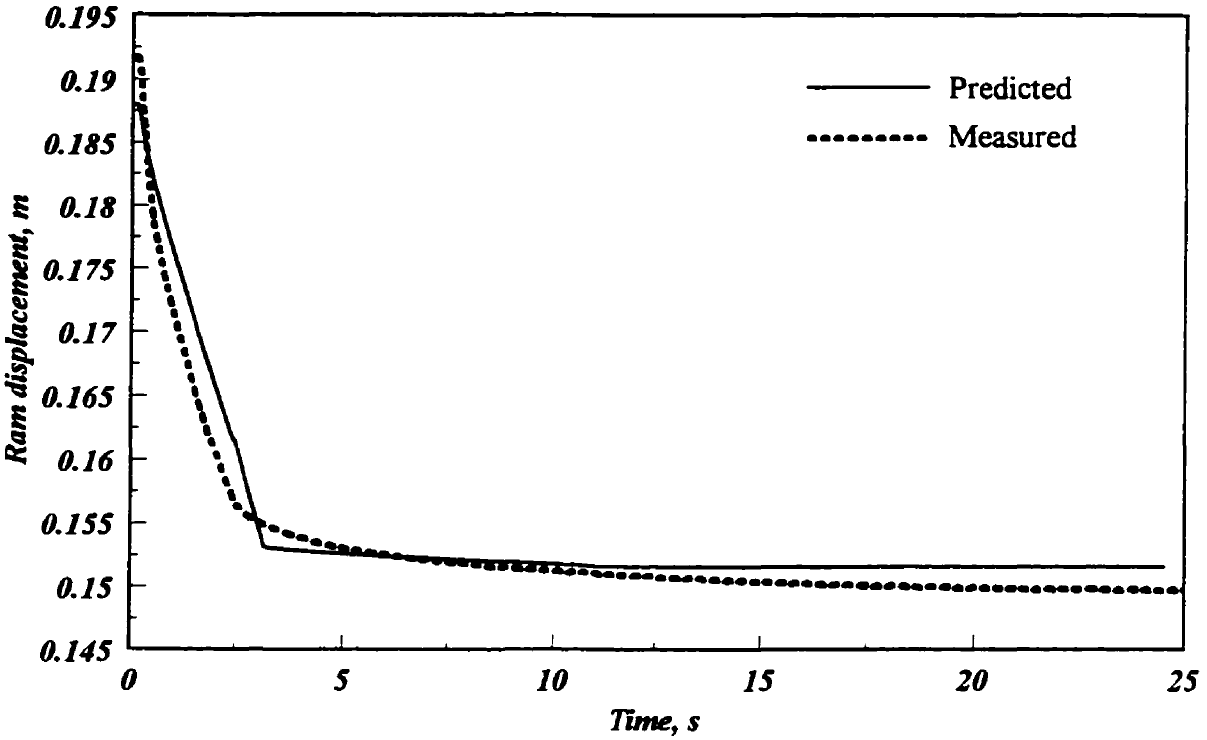


Figure 4.15a Ram screw displacement

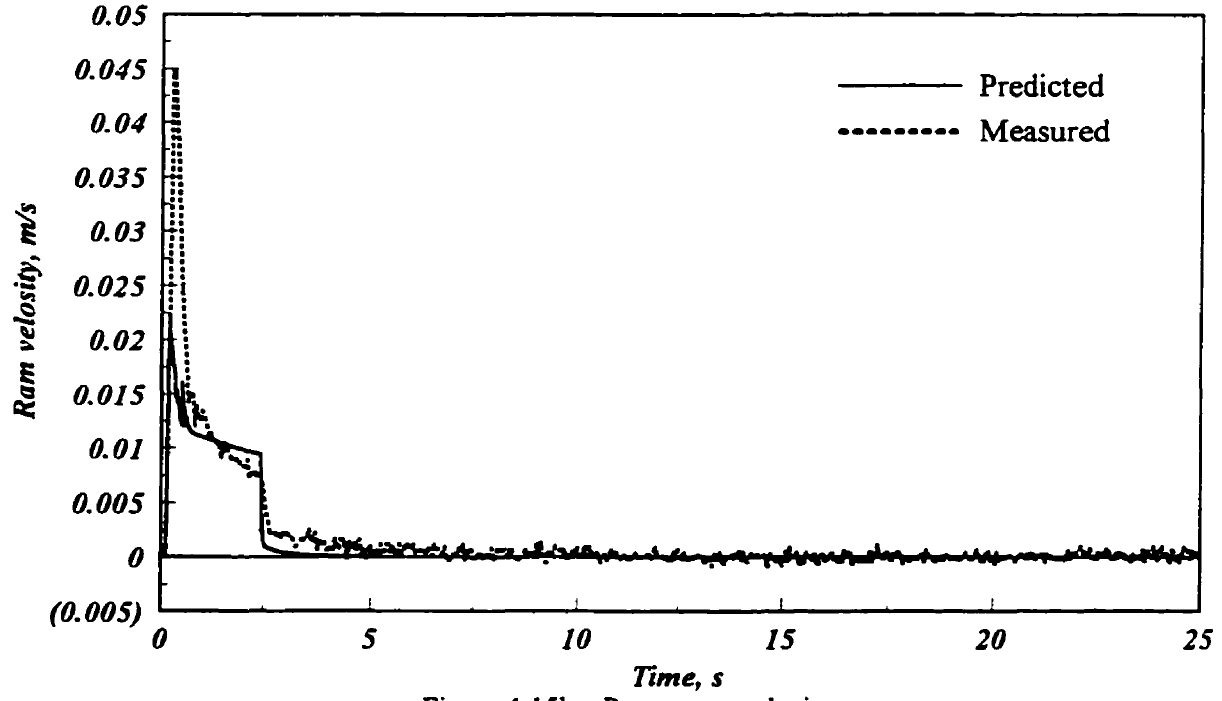


Figure 4.15b Ram screw velocity

**Figure 4.15** Ram screw position and velocity Ssv=90%, Rsv=0% open

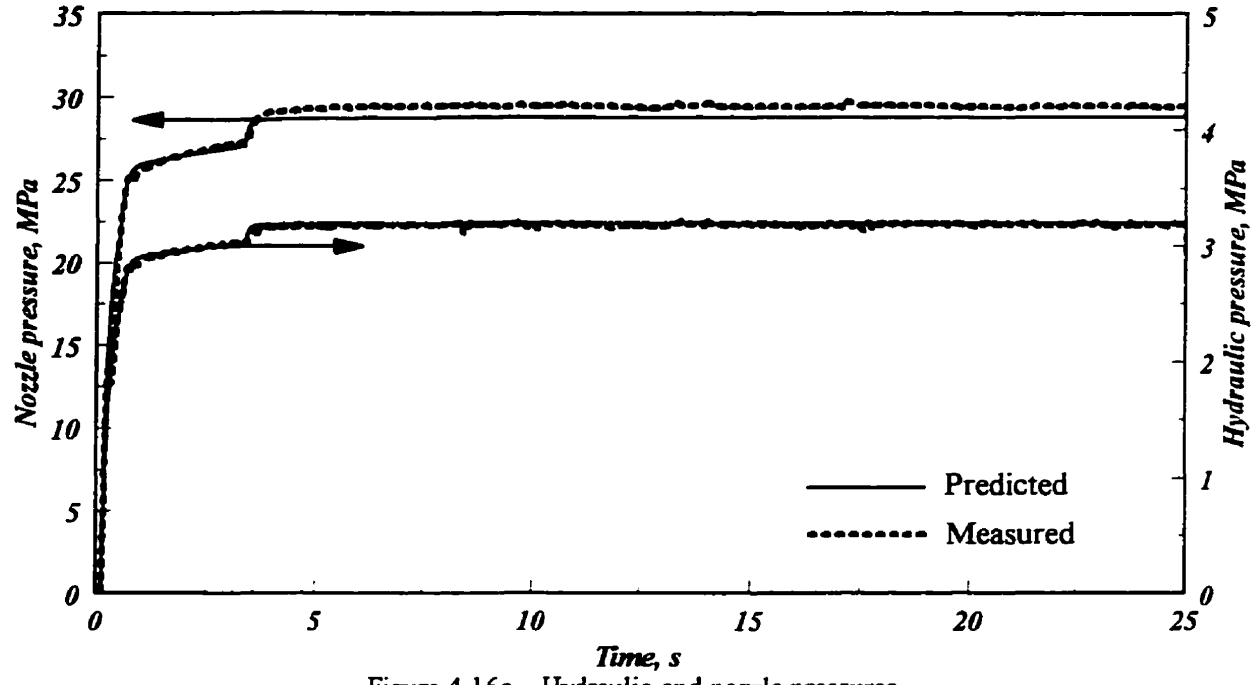


Figure 4.16a Hydraulic and nozzle pressures

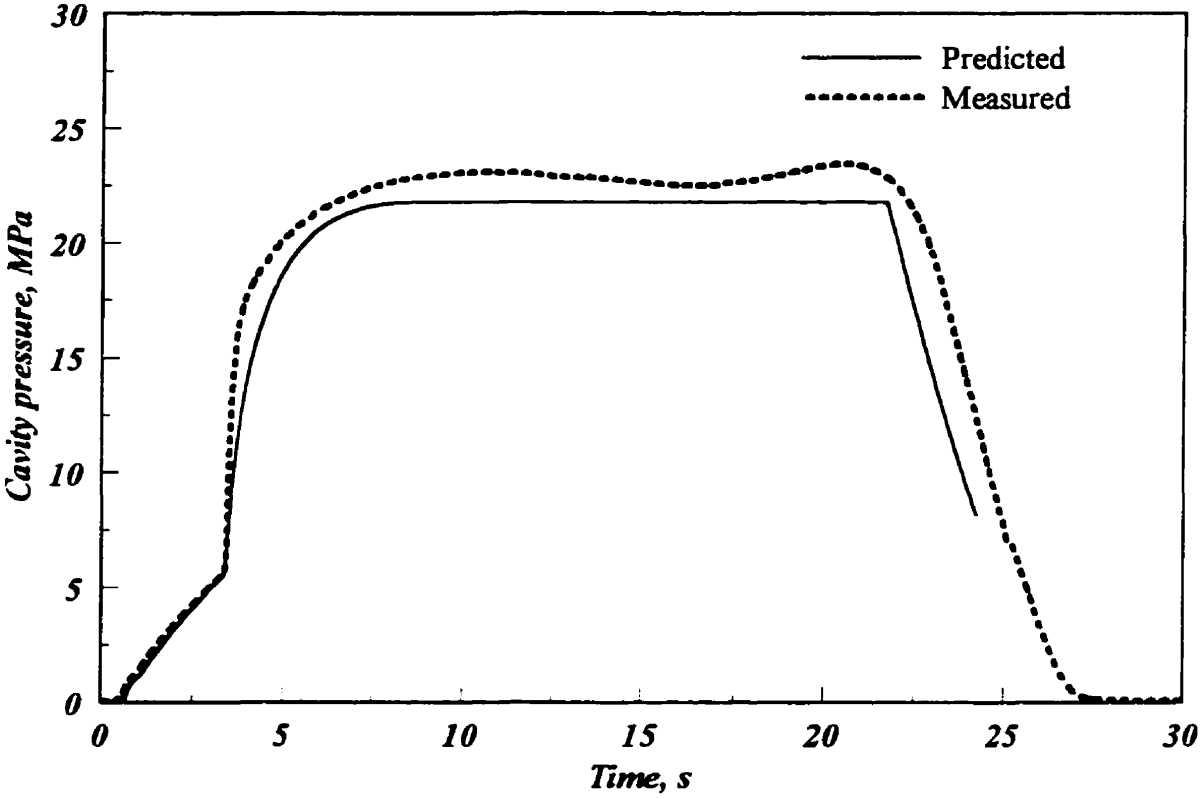


Figure 4.16b Cavity pressure

**Figure 4.16** Hydraulic, nozzle, and cavity pressures, Ssv=80%, Rsv=15%

is similar to the case discussed above.

Some experiments have also been done to validate the modeling of the polystyrene injection. Figures 4.17 shows the comparison of the experimental and simulation results. Figure 4.17a shows the comparison between the simulated and experimental injection and nozzle pressures. They are generally in good agreement. The cavity pressure comparison for simulation and experimental data is shown in Figure 4.17b.

## 4.7 Conclusions

A physically-based model for the simulation of the complete injection molding process, including all phases, has been developed. The model considers the hydraulic system, the ram screw system, the nozzle, cavity, and the polymer melt delivery system. In the hydraulic system, all pressure drops and relevant details are included. In the polymer delivery system, the normal stresses in the diverging part of the nozzle and the radial flow part of the cavity are taken into consideration. The solidification of the polymer melt in the polymer delivery system is accounted for during packing. Two distinct cases for the semicrystalline and amorphous thermoplastics polymers are considered. The predictions of the model are in good agreement with the experimental data.

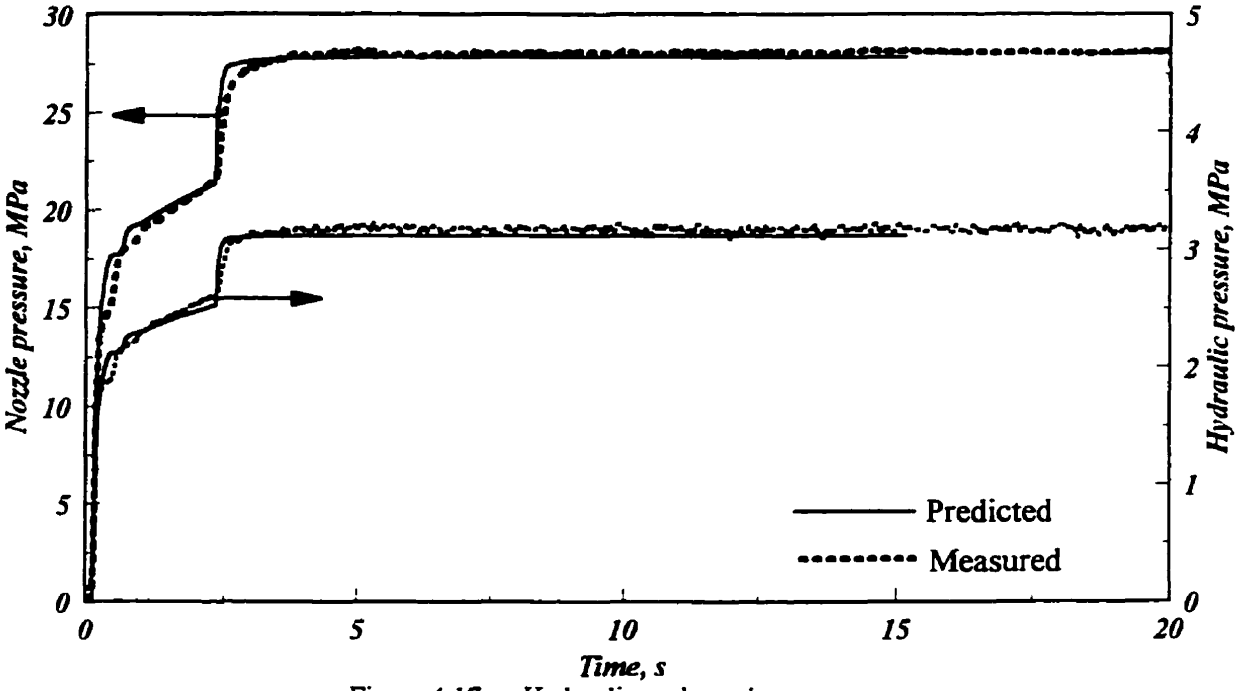


Figure 4.17a Hydraulic and nozzle pressures

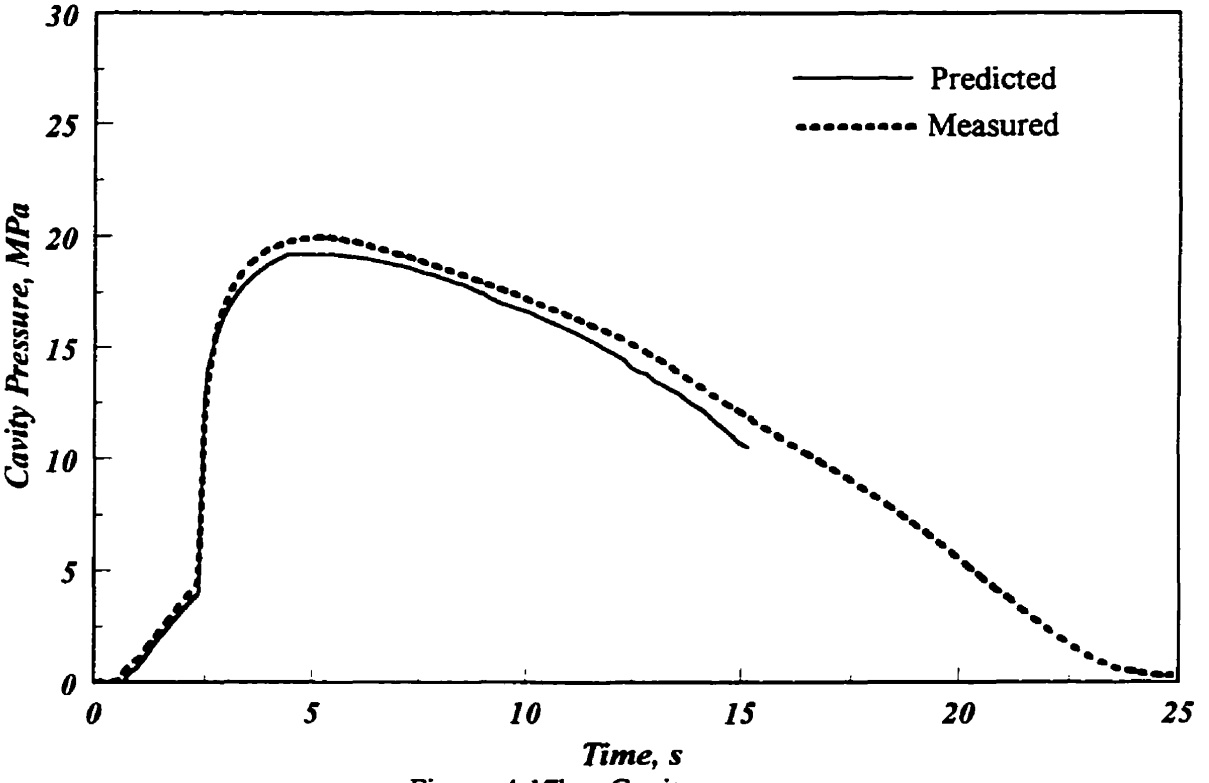


Figure 4.17b Cavity pressure

**Figure 4.17** Hydraulic, nozzle, and cavity pressure pressures for Polystyrene Ssv=40%, Rsv=10%

# CHAPTER 5

# DYNAMICS AND CONTROL OF THE FILLING PHASE

## 5.1 Introduction

The process control problem consists of two parts: first, a mathematical model of the process is identified, then a control strategy is designed based on the knowledge obtained from the modeling stage. The previous chapter presented the complete modeling of the molding cycle. This chapter gives the procedure of deriving a transfer function from the developed mathematical model. This transfer function is a linear one with time-varying parameters. The transfer function is a mathematical description of the relation between the manipulated variable and controlled variable. Then, various control strategies are discussed and used to design controllers to control the cavity pressure profile during the filling phase. The design procedure is followed by a simulation of filling phase control. The last section covers the experimental application of the different controllers to the injection molding process during the filling phase. The controllers are applied to the machine using a microcomputer system. A digital controller is used in conjunction with the discretized transfer functions of the process model and controller.

## 5.2 Dynamics of Cavity Gate Pressure

In Chapter 4, a simple physically based model for injection molding process was discussed. The model showed, Equation (4.33), the strong non-linearity and time-varying behavior of the injection molding process.

The control problem being addressed in this work is the control of polymer pressure at the mold cavity gate. In the existing machine, the pressure is varied by opening or closing the servo-valves. With this method of control, pressure can be controlled by changing the servo-valve openings. In other words, servo-valve opening is the manipulated variable and cavity pressure is the controlled variable. The next step is to derive a transfer function showing the relation between the manipulated and controlled variables. Servo-valve dynamics should be included in the mathematical model. The dynamic bahavior of the servo-valve is discussed in the following section.

### 5.2.1 Servo-Valve Dynamics

The servo-valves are complex devices that exhibit high-order, non-linear responses. If a first, second, or even third order transfer function is selected to represent servo-valve dynamics, still only an approximation to actual response is possible. Fortunately, for most physical systems, the servo-valve is not the primary dynamic element, so it is only necessary to represent valve response throughout a relatively low frequency spectrum, less than 100 cps [114]. Therefore, a first order expression is usually adequate:

$$q(s) = \frac{Valve\ gain}{\tau s + 1} i(s) \qquad (5.1)$$

where i is the servo-valve opening, q is the flow rate through the servo-valve, s is the Laplace transform variable, and $\tau$ is the servo-valve time constant. Valve gain is the product of the valve constant by the square root of pressure drop across the servo-valve. Thus, the transient behavior of the servo-valve is described by the following differential equation:

$$\frac{dq}{dt} = \frac{1}{\tau} q + \frac{k_v \sqrt{\Delta P}}{\tau} i \qquad (5.2)$$

### 5.2.2 The Non-Linear State Equations

Section 4.2.6 gives a summary of filling phase equations. An effective control

system is dependent upon an understanding of the process dynamics. A dynamic model of the injection molding machine is required to conduct the control studies. The following set of non-linear state equations governs the polymer melt and hydraulic oil during the filling phase:

$$\frac{dq_r}{dt} = F_1 = -\frac{1}{\tau} q_r + \frac{k_v\sqrt{P_h}}{\tau}\, i_R$$

$$\frac{dq_s}{dt} = F_2 = -\frac{1}{\tau} q_s + \frac{k_v\sqrt{P_s - P_h}}{\tau}\, i_S$$

$$\frac{dP_h}{dt} = F_3 = \frac{\beta_h}{V_{h0} + A_h z}\{q_s - q_r - A_h v_z\}$$

$$\frac{dz}{dt} = F_4 = v_Z \qquad \textbf{(5.3)}$$

$$\frac{dv_z}{dt} = F_5 = \frac{1}{M}\left[A_h P_h - A_n P_n - 2\pi\eta_0 R_n^{1-n}(L_0 + z)\frac{(s-1)^n}{(k_r^{1-s}-1)^n} v_z^n\right]$$

$$\frac{dP_n}{dt} = F_6 = \frac{\beta_p}{V_{n0} - A_n z}\left[A_n v_z - \sqrt[n]{\frac{P_n}{k_t}}\right]$$

$$P_{gate} = \left(1 - \frac{k_{ct}}{k_t}\right) P_n$$

where $F_1$ through $F_6$ are state equations, $P_{gate}$ is cavity pressure at gate and the output, and $q_r$ and $q_s$ are hydraulic oil flow rates through relief and supply servo-valves, respectively.

The above set of governing equations is based on the laws of conservation and includes basic information of process physics. The first two equations describe the dynamic behavior through supply and relief servo-valves, respectively. The third and sixth equations are mass balances around on the injection cylinder and the nozzle, respectively. The fifth equation is Newton's second law applied to the screw. The last equation relates the cavity pressure to the nozzle pressure. The controlled variable is cavity pressure, which is measured at the cavity gate. The manipulated variable is the

supply servo-valve opening. The relief servo-valve opening is specified by the following relationship to the supply servo-valve [96]:

$$i_R = 0.2\times(100 - i_s) + 0.4 \tag{5.4}$$

The filling phase, therefore, is a single input-single output (SISO) system for cavity pressure with respect to valve control signal.

### 5.2.3 Model Validation

The above set of non-linear differential equations was solved numerically using a Runge-Kutta 4$^{th}$ order method. Figure 5.1 shows the comparison of the solution of this set of equations with experimental results given a step change in the supply servo-valve opening. The agreement is good, and the theoretical model describes the dynamics of the process well. To conduct the control studies, a transfer function is required. The Laplace transformation technique is widely used for this purpose. However, this technique is applicable only to linear differential equations. Therefore, in the following section, a linearized model is developed.

## 5.3 Model Linearization

Although much work has been done in the area of non-linear control theory for system design, much of the theory is applicable to simple low order systems. For the case considered here, a linearized model is used. A linear model is most accurate near the point of linearization. The non-linear model can be expressed as:

$$\frac{d\underline{x}}{dt} = \underline{F}(\underline{x},\underline{u}) \tag{5.5}$$

Linearizing Equation (5.5) produces:

$$\Delta\frac{dx}{dt} = \underline{A}\ \Delta x + \underline{B}\ \Delta u \tag{5.6}$$

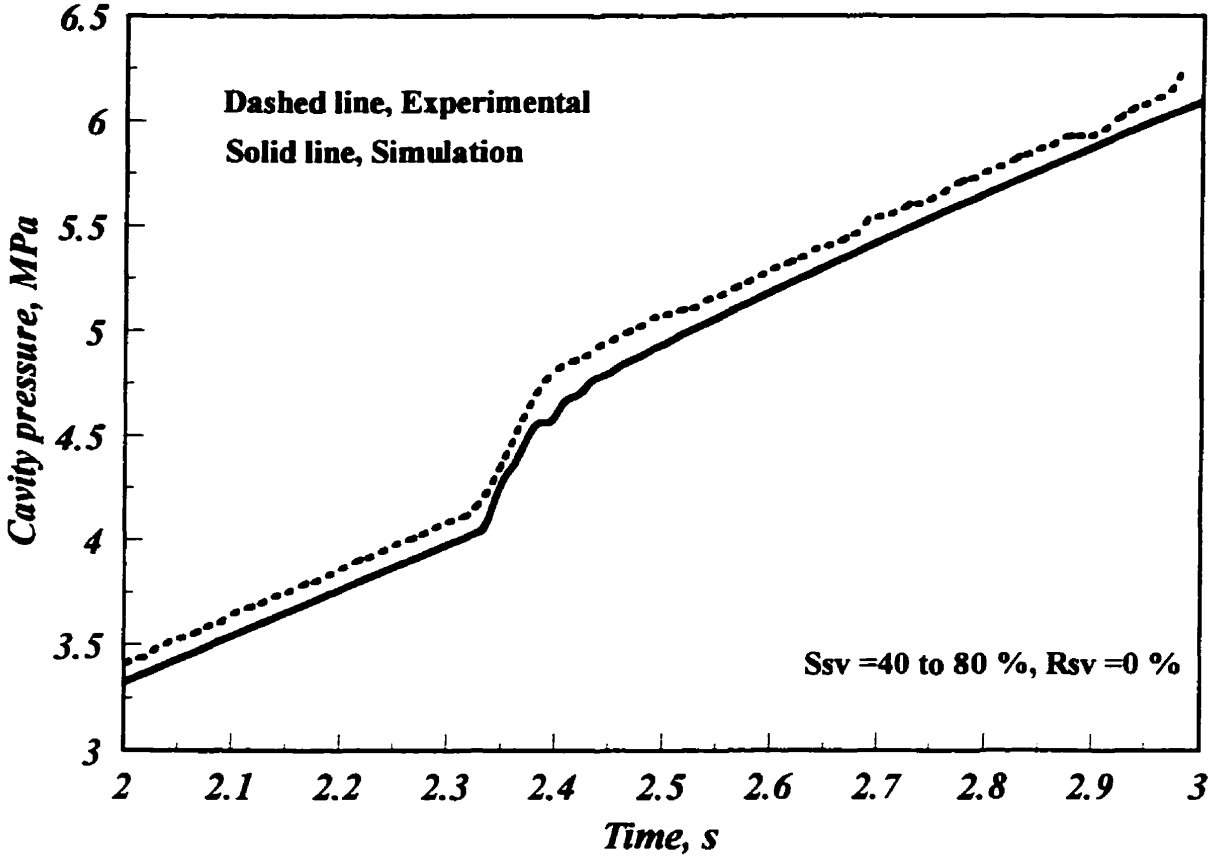


**Figure 5.1** Comparison of non-linear model and experiment

where $\underline{A}$ and $\underline{B}$ are 6×6 and 6×2 matrices in this case, respectively. Entries of these matrices are given by:

$$\underline{A} = [a_{ij}] = \left[\frac{\partial F_i}{\partial x_j}\right]_{x^0,u^0} \qquad i=1,6 \quad j=1,6$$
$$\underline{B} = [b_{ij}] = \left[\frac{\partial F_i}{\partial u_j}\right]_{x^0,u^0} \qquad i=1,6 \quad j=1,2 \tag{5.7}$$

which $x^0$, and $u^0$ are operating point values. Applying these equations to the Equation set (5.3) gives the following equations:

$$\begin{aligned}
\frac{dQ_r}{dt} &= -\frac{1}{\tau}Q_r + \frac{a}{\tau}H + \frac{b}{\tau}R \\
\frac{dQ_s}{dt} &= -\frac{1}{\tau}Q_s - \frac{c}{\tau}H + \frac{d}{\tau}T \\
\frac{dH}{dt} &= -eQ_r + fQ_s - gZ - iV \\
\frac{dZ}{dt} &= V \\
\frac{dV}{dt} &= jH - kZ + lV - mN \\
\frac{dN}{dt} &= nZ + pV - qN \\
P_c &= rN
\end{aligned} \tag{5.8}$$

The deviation variables are defined as:

$$\begin{aligned}
T &= i_S - i_{s0} & R &= i_R - i_{R0} & P_c &= P_{gate} - P_{gate0} \\
Q_r &= q_r - q_{r0} & Q_s &= q_s - q_{s0} & H &= P_h - P_{h0} \\
Z &= z - z_0 & V &= v_z - v_{z0} & N &= P_n - P_{n0}
\end{aligned} \tag{5.9}$$

The various parameters are defined below:

$$a = \frac{k_v i_{R0}}{2\sqrt{P_{h0}}} \qquad b = k_v\sqrt{P_{h0}}$$

$$c = \frac{k_v i_{S0}}{2\sqrt{P_s - P_{h0}}} \qquad d = k_v\sqrt{P_s - P_{h0}} \tag{5.10}$$

$$e = \frac{\beta_h}{V_{h0} + A_h z_0} \qquad f = \frac{\beta_h}{V_{h0} + A_h z_0}$$

and

$$g = \frac{\beta_h A_h (q_{S0} - q_{r0} - A_h V_{z0}}{(V_{h0} + A_h z_0)^2} \qquad i = \frac{\beta_h A_h}{V_{h0} + A_h z_0}$$

$$j = \frac{A_h}{M} \qquad k = \frac{2\pi\eta_0 R_n^{1-n}(s-1)^n v_{z0}^n}{M(k_r^{1-s} - 1)^n} \tag{5.11}$$

$$l = \frac{2\pi\eta_0 R_n^{1-n}(s-1)^n (L_0 + z_0) n v_{z0}^{n-1}}{M(k_r^{1-s} - 1)^n} \qquad m = \frac{A_n}{M}$$

and

$$n = \frac{\beta_p A_n \left( A_n v_{z0} - \sqrt[n]{\frac{P_{n0}}{k_t}} \right)}{(v_{z0} - A_n z_0)^2} \qquad p = \frac{\beta_p A_n}{V_{z0} - A_n z_0} \tag{5.12}$$

$$q = \frac{\beta_p \sqrt[n]{\frac{P_{n0}}{k_t}}}{(V_{z0} - A_n z_0) n P_{n0}} \qquad r = 1 - \frac{k_{ct}}{k_t}$$

The linearized set of equations (in Laplace transformed form) is:

$$
\begin{aligned}
s\ Q_r(s) &= -\frac{1}{\tau}Q_r(s) + \frac{a}{\tau}H(s) + \frac{b}{\tau}R(s) \\
s\ Q_s(s) &= -\frac{1}{\tau}Q_s(s) - \frac{c}{\tau}H(s) + \frac{d}{\tau}T(s) \\
s\ H(s) &= -eQ_r(s) + fQ_s(s) - gZ(s) - iV(s) \\
s\ Z(s) &= V(s) \\
s\ V(s) &= jH(s) - kZ(s) - lV(s) - mN(s) \\
s\ N(s) &= nZ(s) + pV(s) - qN(s) \\
P_c(s) &= r\ N(s)
\end{aligned}
\tag{5.13}
$$

With the linear set of equations in hand, the control study can be pursued for controller design. The Laplace transform techniques is normally to be used to determine transient responses from the ordinary differential equation model. Taking the Laplace transform of this set of equations and algebraic manipulation yields the transfer function which relates the controlled variable (the cavity pressure at the gate) to the manipulated variable (supply servo-valve opening):

$$
P_c(s) = \frac{rj(n+ps)}{DEN.}(df + 0.2eb)T(s) = \frac{n_1 s + n_2}{\tau(s-r_1)(s-r_2)(s-r_3)(s-r_4)(s-r_5)}\ T(s)
$$

$$
\begin{aligned}
DEN. = {} & \tau s^5 + (\tau l + \tau q + 1)s^4 \\
& + [\tau k + \tau ql + \tau mp + l + q + ea + cf + \tau ji]s^3 \\
& + [kq\tau + mn\tau + k + ql + mp + (ea + cf)(l + q) \\
& + \tau jq + \tau jiq + ji]s^2 \\
& + [kq + mn + (ea + cf)(k + lq + mp) + \tau jgq + gj + jiq]s \\
& + [(ea + cf)(kq + mn) + jgq]
\end{aligned}
\tag{5.14}
$$

The above represents a linear and time-invariant system and can be used for control purposes. It is useful to have relationship for each root of denominator of Equation (5.14). However, attempts to find analytical expression for $r_i$ was not successful due to lack of analytical solution for fifth order equation. To estimate the accuracy and utility of this linearized model the non-linear and linear models are

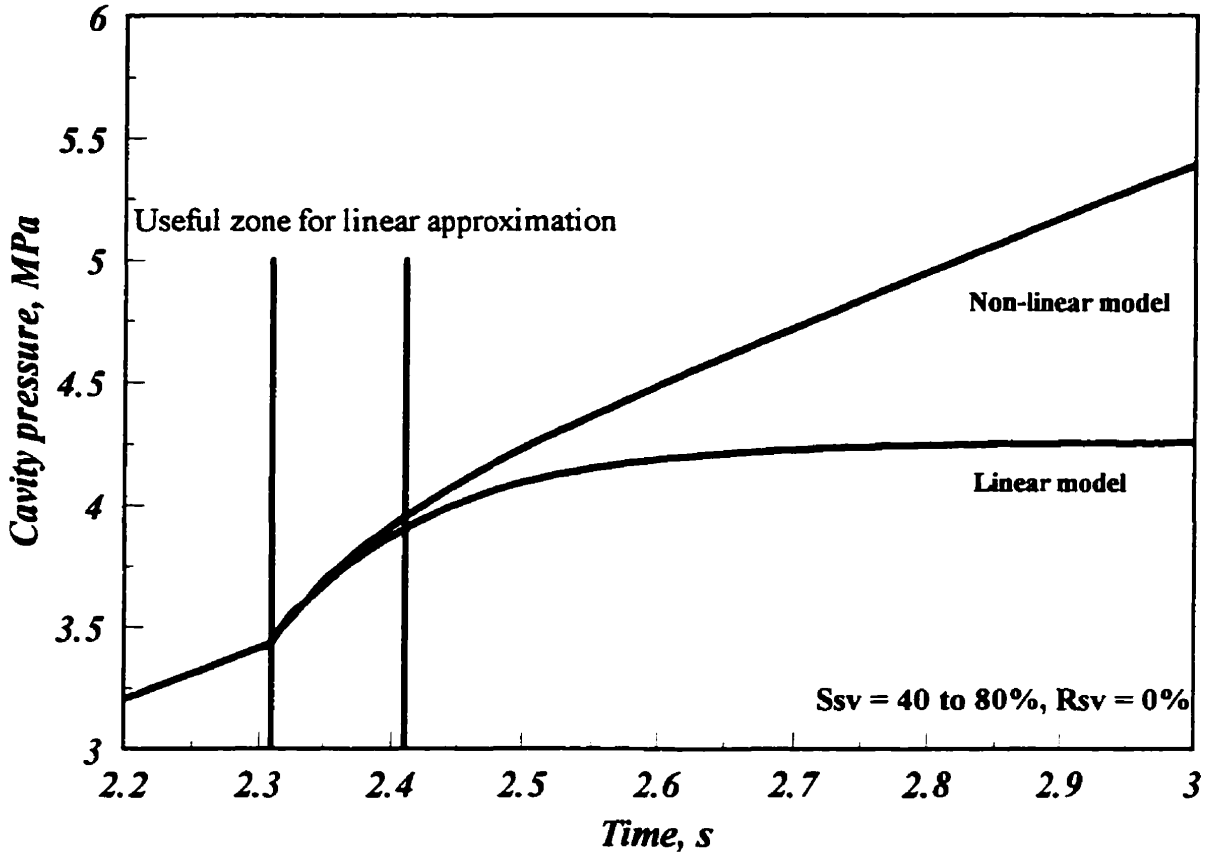


**Figure 5.2** Comparison of non-linear and linear models

compared for a step change in servo-valve opening in Figure 5.2. The solution for the linear model can be obtained by integration of the whole set in Equations (5.8) or taking the inverse Laplace transform of Equation (5.14). Inspection of Figure 5.2 reveals that the linear model initially follows the non-linear model very well, then it deviates substantially. Hence, due to the non-linearity of the process, only the first 0.1 seconds of the linear model approximates the non-linear model. This suggests that, at least every 0.1 second, the model parameters should be changed and updated because of the time-varying and non-linear characteristics of the system. In other words, along the selected set-point, linearization parameters are calculated every 0.1 s. Therefore, the physically-based approach suggests an adaptive approach to the strategy of injection molding control. The transfer function is of fifth order and has one zero and five poles. Table 5.1 gives the numerical values of a typical transfer function for $i_s$=40% and $i_R$=15%, at time 2.3 s, for the high density polyethylene. It is obvious that the only zero of the system is very close to the fifth root. Due to lack of analytical expression for roots and zero, one cannot correspond zero and pole to specific machine or process parameters. However, same event has been observed for polystyrene which suggests this cancelled zero and pole are machine related parameters rather than process. They essentially cancel each other out and the transfer function will be a fourth order system without any zero:

$$P_c(s) = \frac{n_1}{\tau(s-r_1)(s-r_2)(s-r_3)(s-r_4)} T(s) \qquad (5.15)$$

The fourth order transfer function was used to conduct the control studies.

## 5.4 Discrete Transfer Function

The discrete forms of the dynamic model for cavity pressure was derived from the corresponding continuous model utilizing the z-transform method. The discretization variable z is defined as:

where $\Delta t$ is sampling time interval.

| | |
|---|---|
| Zero | $-4.769\times10^{-4}$ |
| First pole | $-20.487+230.93\times i$ |
| Second pole | $-20.487-230.93\times i$ |
| Third pole | -72.773 |
| Fourth pole | -12.346 |
| Fifth pole | $-4.725\times10^{-4}$ |

**Table 5.1** - Roots of transfer function, $i_s=40\%$, $i_R=15\%$, t=2.3 s

$$z \triangleq e^{s\Delta t} \tag{5.16}$$

To discretize the transfer function, Equation (5.15) is expanded via partial fractions, as:

$$G(s) = \frac{n_1}{\tau(s-r_1)(s-r_2)(s-r_3)(s-r_4)} = \frac{n_1}{\tau}\left[\frac{As+B}{s^2-2as+a^2+b^2} + \frac{C}{s-r_3} + \frac{D}{s-r_4}\right] \tag{5.17}$$

where

$$r_1 = a+bi \qquad , \qquad r_2 = a-bi \tag{5.18}$$

and A, B, C, and D are:

$$\begin{aligned}
A &= \frac{(r_4-r_3)(r_3+r_4-2a)}{DEN.} \\
B &= \frac{(r_4-r_3)[r_3r_4+4a^2-2a(r_4+r_3)-(a^2+b^2)]}{DEN.} \\
C &= -\frac{-r_3r_4-(2a-r_4)(r_3+r_4)+2ar_3+a^2+b^2}{DEN.} \\
D &= \frac{-r_3r_4-(2a-r_3)(r_3+r_4)+2ar_4+a^2+b^2}{DEN.} \\
DEN. &= (r_4-r_3)\left[r_3^2r_4^2+(a^2+b^2)[r_4^2+r_3^2-2a(r_4+r_3)]-2ar_3r_4(r_3+r_4-2a)\right. \\
&\quad \left.+(a^2+b^2)^2\right]
\end{aligned} \tag{5.19}$$

The discretization with zero order hold is:

$$G(z) = \frac{n_1}{\tau}\left[\frac{b_1z^{-1}+b_2z^{-2}}{1+a_1z^{-1}+a_2z^{-2}} + \frac{d_1z^{-1}}{1+c_1z^{-1}} + \frac{f_1z^{-1}}{1+e_1z^{-1}}\right] \tag{5.20}$$

where

$$a_1 = -2e^{a\Delta t}\cos b\Delta t \qquad a_2 = e^{2a\Delta t}$$

$$b_1 = \frac{-B}{a^2+b^2} - e^{a\Delta t}\left[\frac{A}{b}\sin b\Delta t + \frac{B}{b}\frac{a}{a^2+b^2}\sin b\Delta t - \frac{B}{a^2+b^2}\cos b\Delta t\right]$$

$$b_2 = \frac{Ae^{a\Delta t}}{a^2+b^2}\left[\frac{B}{A}e^{a\Delta t} - \frac{B}{A}\cos b\Delta t - \frac{a^2+b^2+\frac{aB}{A}}{b}\sin b\Delta t\right] \qquad (5.21)$$

$$c_1 = -e^{r_3\Delta t} \qquad d_1 = \frac{C}{-r_3}\left(1-e^{r_3\Delta t}\right)$$

$$e_1 = -e^{r_4\Delta t} \qquad f_1 = \frac{D}{-r_4}\left(1-e^{r_4\Delta t}\right)$$

Finally, the rearrangement of Equation (5.20), with zero-order hold, gives the discretized transfer function:

$$G(z) = \frac{g_1 z^{-1} + g_2 z^{-2} + g_3 z^{-3} + g_4 z^{-4}}{1 + h_1 z^{-1} + h_2 z^{-2} + h_3 z^{-3} + h_4 z^{-4}} \qquad (5.22)$$

The relationships for $g_1$, $g_2$, $g_3$, $g_4$, $h_1$, $h_2$, $h_3$, and $h_4$ are:

$$g_1 = \frac{n_1}{\tau}(b_1 + d_1 + f_1) \qquad g_2 = \frac{n_1}{\tau}(b_1e_1 + b_1c_1 + b_2 + d_1e_1 + d_1a_1 + f_1c_1 + f_1a_1)$$

$$g_3 = \frac{n_1}{\tau}(b_1c_1e_1 + b_2e_1 + b_2c_1 + d_1a_1e_1 + d_1a_2 + f_1a_1c_1 + f_1a_2) \qquad (5.23)$$

$$g_4 = \frac{n_1}{\tau}(b_2c_1e_1 + d_1a_2e_1 + f_1a_2c_1)$$

$$h_1 = e_1 + c_1 + a_1 \qquad h_2 = c_1e_1 + a_1e_1 + a_1c_1 + a_2$$

$$h_3 = a_1c_1e_1 + a_2e_1 + a_2c_1 \qquad h_4 = a_2c_1e_1$$

Figure 5.3 shows the discrete transfer function coefficients for the high density polyethylene. The points, in Figure 5.3, are coefficients for the linearized values for every 0.1 s for $i_s$ 80% and $i_R$ 10%, and solid lines are a least-squares fit to the points that were used in the control algorithm. During control, these parameters are updated in each

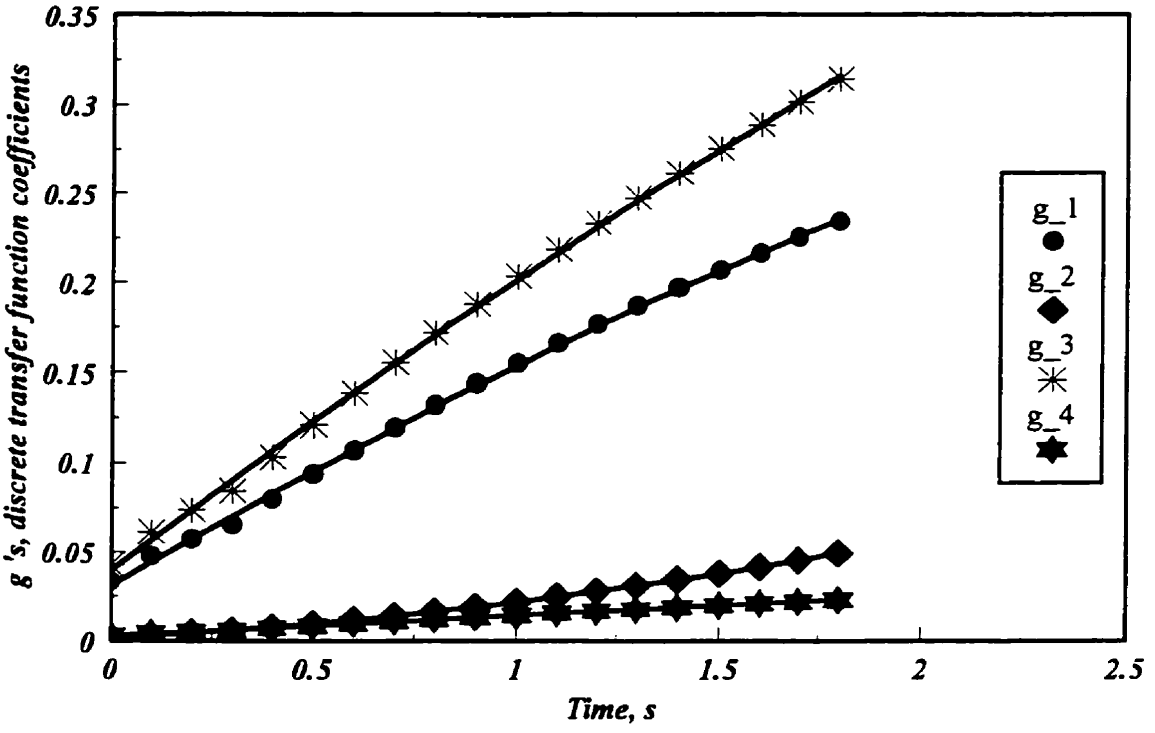


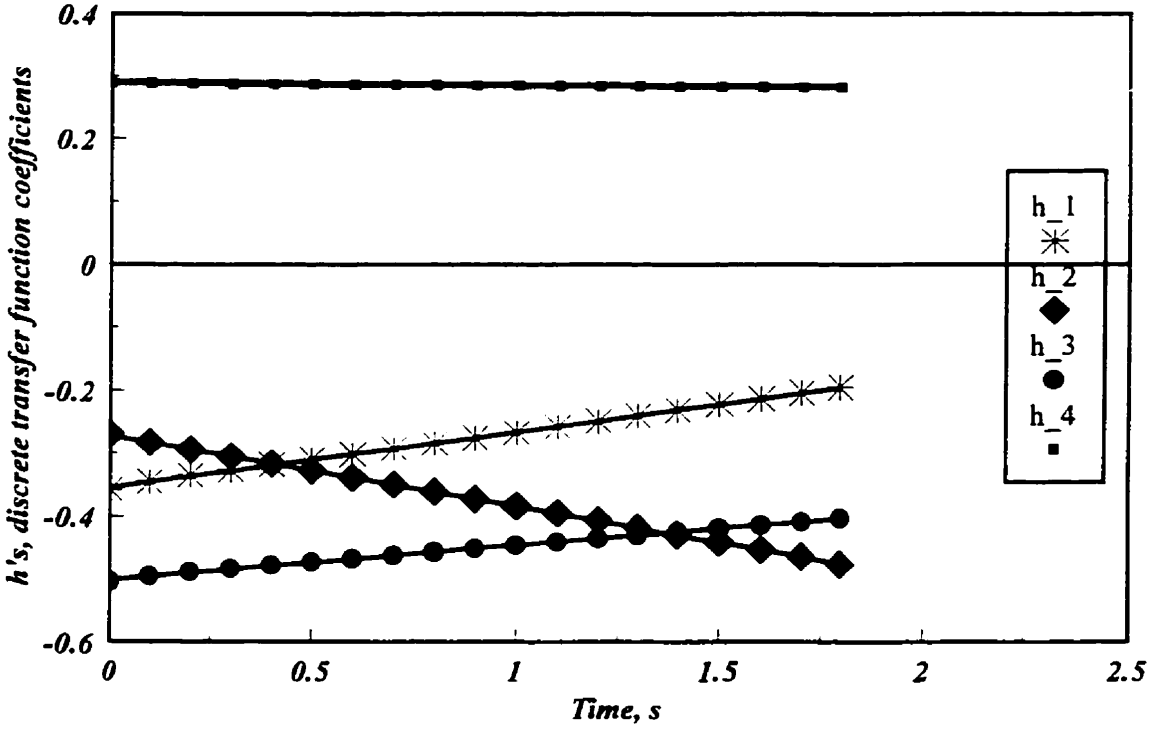


**Figure 5.3** Discrete transfer function coefficients

sampling time using fitted curves.

## 5.5 Controller Selection and Design

Once the process model is available, the next step is to design a control system for the process. There are variety of procedures to determine controller type and settings which are described in control textbooks and in the literature. Process dynamics, the requirement of the closed loop performance, and the designer's personal judgement usually indicate the controller structure. The proportional (P) controller is a very simple controller with one tuning parameter. Most of the time, it produces offset; hence, it is rarely used in chemical industry. The proportional and integral (PI) controller is one of the simplest controllers that normally gives good results for chemical processes. Controller gain and controller integral time constant are setting parameters to be determined. The proportional, integral and derivative (PID) controller is, so far one of the most popular controllers. It involves three parameters: controller gain, integral time constant, and derivative time constant. There are different methods to obtain these parameters. The internal model control (IMC) method is becoming widely used for chemical process control due to its simplicity (only one parameter to be determined) and its robustness in handling model errors. PI and PID controllers, with different tuning procedures, and IMC are used in the control of the injection molding process in this work. A brief review of these controllers is given below. Details can be found elsewhere [27,28]. The tuning procedure can depend on the set-point profile. Hence, it is necessary to chose a suitable and reasonable profile based on the machines limitations.

### 5.5.1 Filling Pressure Profile

Inspection of the open loop results reveal that cavity pressure during filling is close to a linear ramp. Therefore, a ramp is a good initial set-point profile to investigate the control of the process. The maximum slope for the ramp is 3.72 MPa/s, for $i_s$ 99.5% and $i_R$ 0%. The minimum filling rate is determined by the need to avoid a short shot and

corresponds to a slope 0.60 MPa/s for $i_s$ 40% and $i_R$ 25%. Hence, the set-point time profile must be within these predetermined limits. Figure 5.4 shows the limitation of the machine and the practical range of set-points. The chosen set-point ramp is 2.76 MPa/s, corresponding to $i_s$ 80% and $i_R$ 10%. However, some non-linear set-points profiles are applied to evaluate the ability of the controller for tracking a trajectory. A complex geometry mold cavity is used in order to evaluate the designed controller in realistic, practical applications.

### 5.5.2 PI Controller Design

This controller is also known as the proportional-plus-reset controller. Its actuating signal is related to the error by the equation:

$$m(t) = k_c e(t) + \frac{k_c}{\tau_I}\int_0^t e(t)\,dt + m_s \qquad (5.24)$$

where $k_c$ is the proportional gain of controller, $m_s$ is controller's bias signal (its actuating signal when there is no error), and $\tau_I$ is the integral time constant or reset time. The larger is the gain $k_c$, the higher will be the sensitivity of the controller's actuating signal to error e(t). The integral action causes the controller output m(t) to change, as long as an error exists in the process output. Therefore, such a controller can eliminate even small errors. In general, smaller values of $\tau_I$ are favoured for better performance. The transfer function form of a PI controller is given by:

$$G_c(s) = k_c\left(1 + \frac{1}{\tau_I s}\right) \qquad (5.25)$$

Figure 5.5 summarizes pictorially the standard closed loop control. Some criterion is needed to establish the comparison of alternative controller tuning. For every process control application, two type of criteria can be distinguished: a) steady-state performance criteria, and b) dynamic response performance criteria. The principal steady state performance criterion is usually zero error at steady state. The evaluation of dynamic

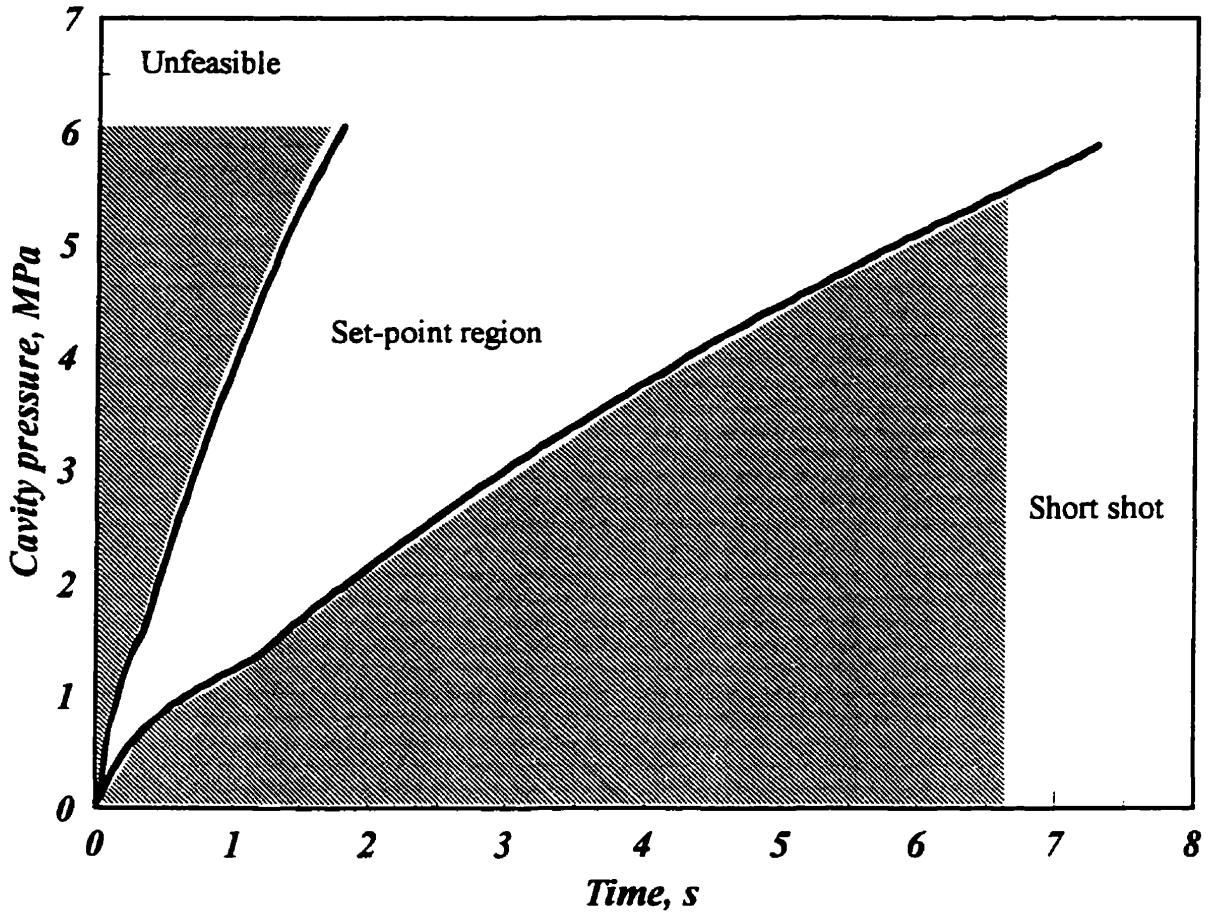


**Figure 5.4** Limitation of set point selection during filling

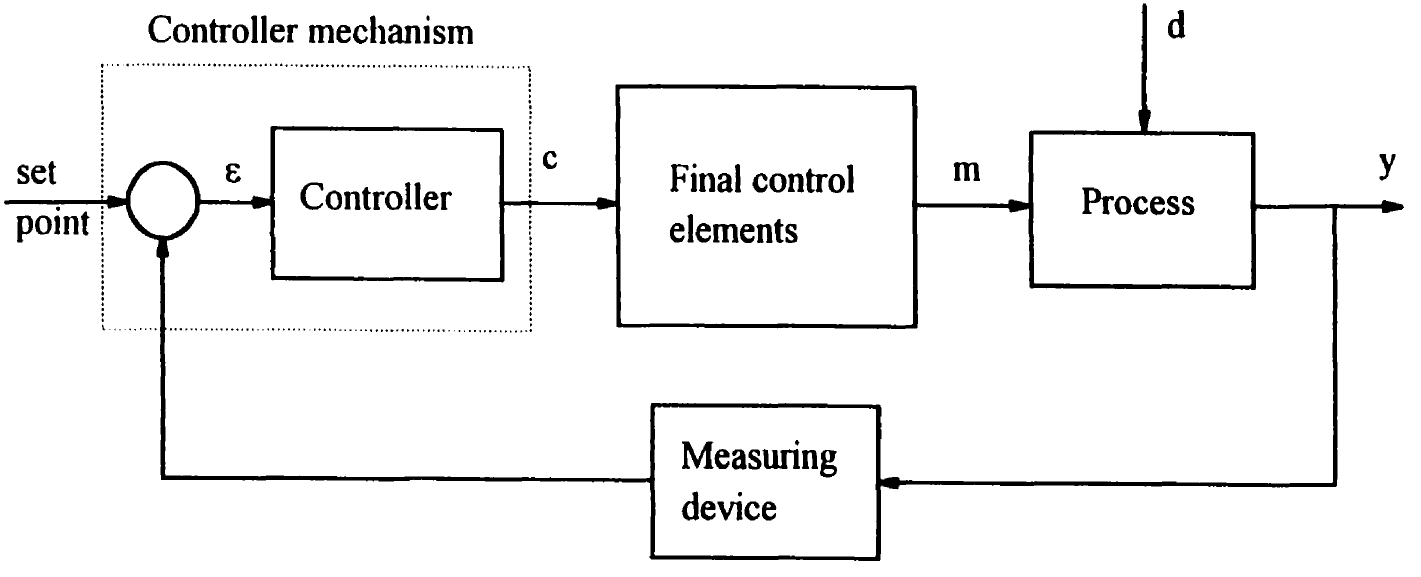


**Figure 5.5** Feedback closed loop control of a process

performance of a closed loop system is based on two types of commonly used criteria:

(1) Criteria that use only a few points of the response. They are simpler, but only approximate. The most often quoted are: overshoot, rise time, setting time, and decay ratio.

(2) Criteria that use the entire closed loop response. These are more precise but also more cumbersome to use.

The most commonly used criteria which employs the complete closed loop response involve some sort of integration of the error, for example:

(1) Integral of the time weighted absolute error (ITAE), where:

$$ITAE = \int_0^{\infty} t|e(t)|\,dt \tag{5.26}$$

(2) Integral of the square error (ISE), where:

$$ISE = \int_0^{\infty} e^2(t)\,dt \tag{5.27}$$

Therefore, after selecting the type of controller, the values of the adjustable parameters are determined using the MATLAB FMINS [115] command so as to minimize the ITAE, or ISE of the system's response. Which one of the criteria should be used depends on the required characteristics of the system. The ITAE or ISE value is normally calculated for the step change in the set-point of the process. This approach is common in classical process control and leads to a conservative and good tuning. Figure 5.6 shows a typical closed loop response of the molding process to a step change in the set-point. However, for this study, a step change in ramp set-point is another possibility. Figure 5.7 shows a typical closed loop response of the process to step change in the ramp set-point. Although these different methods produce somewhat different results, the experimental results show close performances for the two tuning methods. Figure 5.8 shows the PI controller parameters versus time, for two cases, using the ITAE and ISE optimization criteria. Zero time corresponds to the instant that

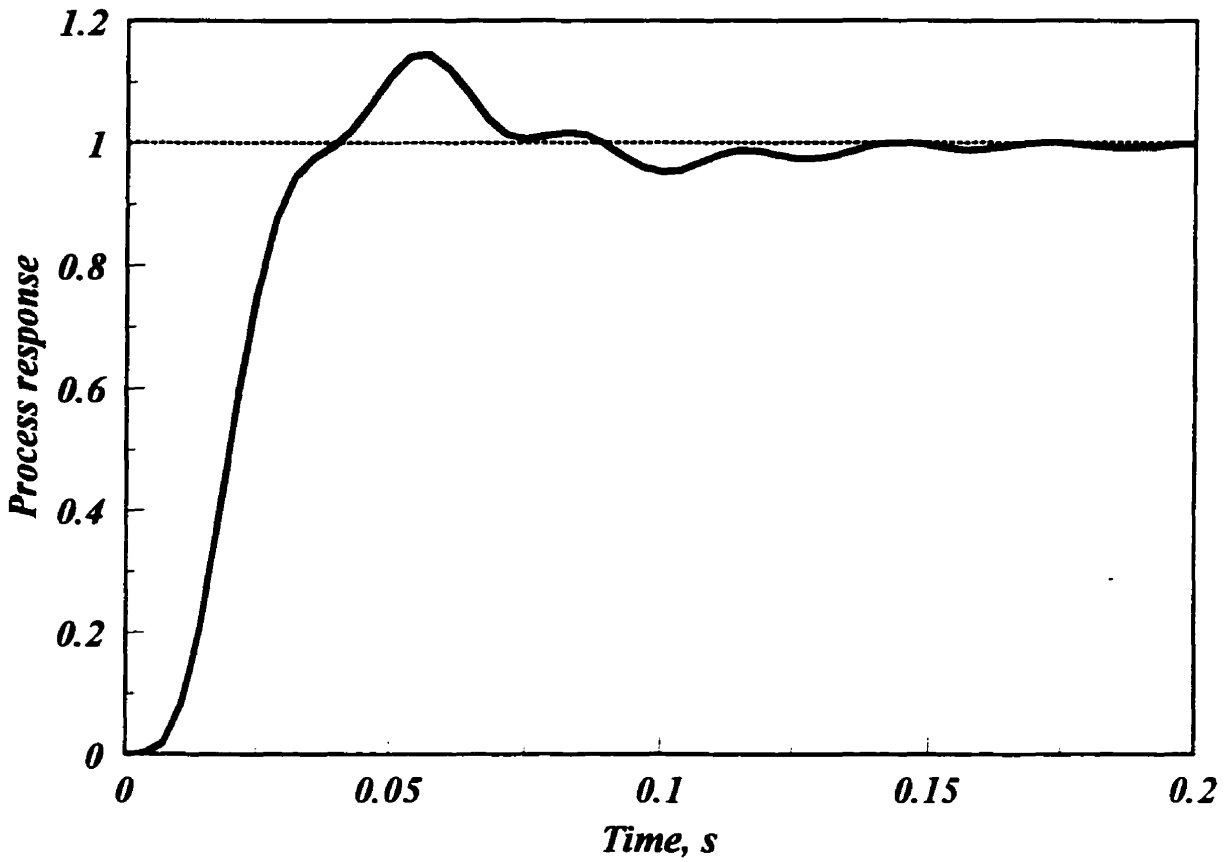


**Figure 5.6** Closed loop response using step change in set point

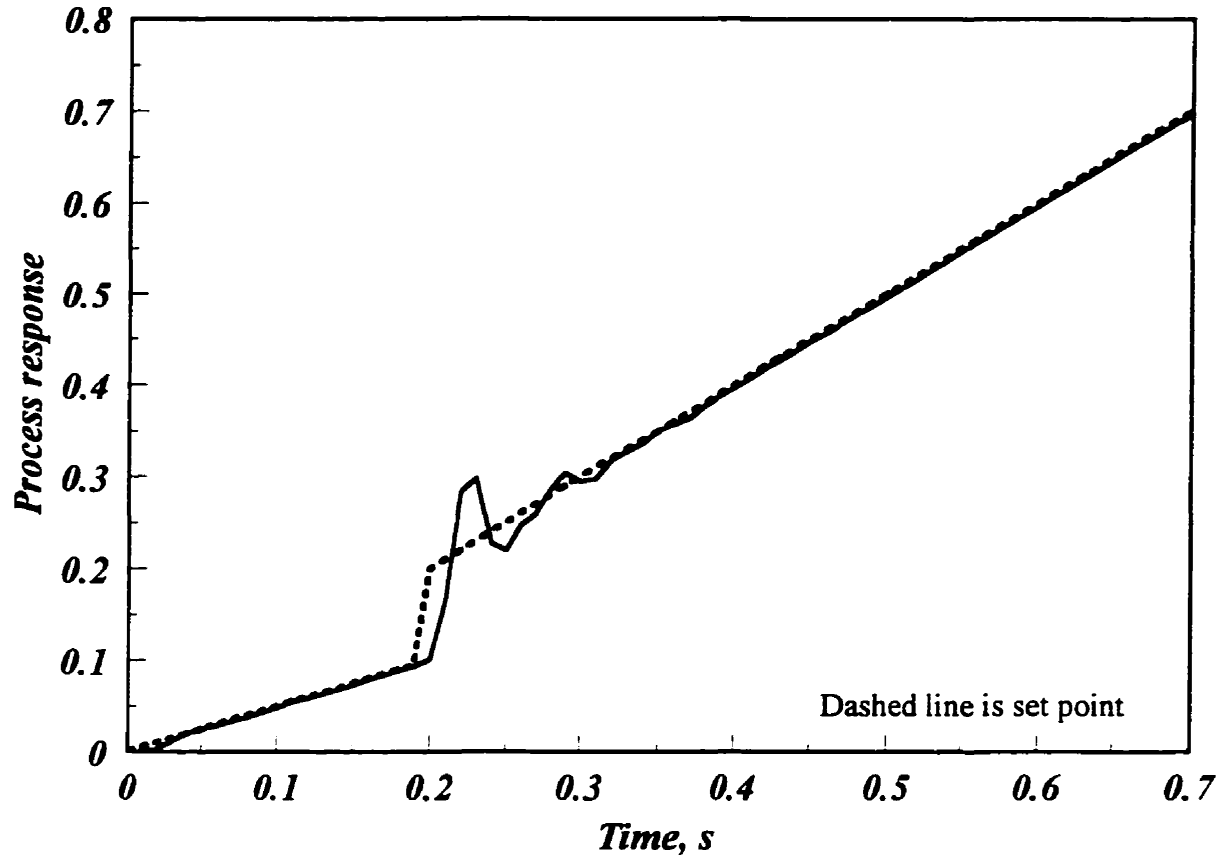


**Figure 5.7** Closed loop response using step change in the ramp set-point

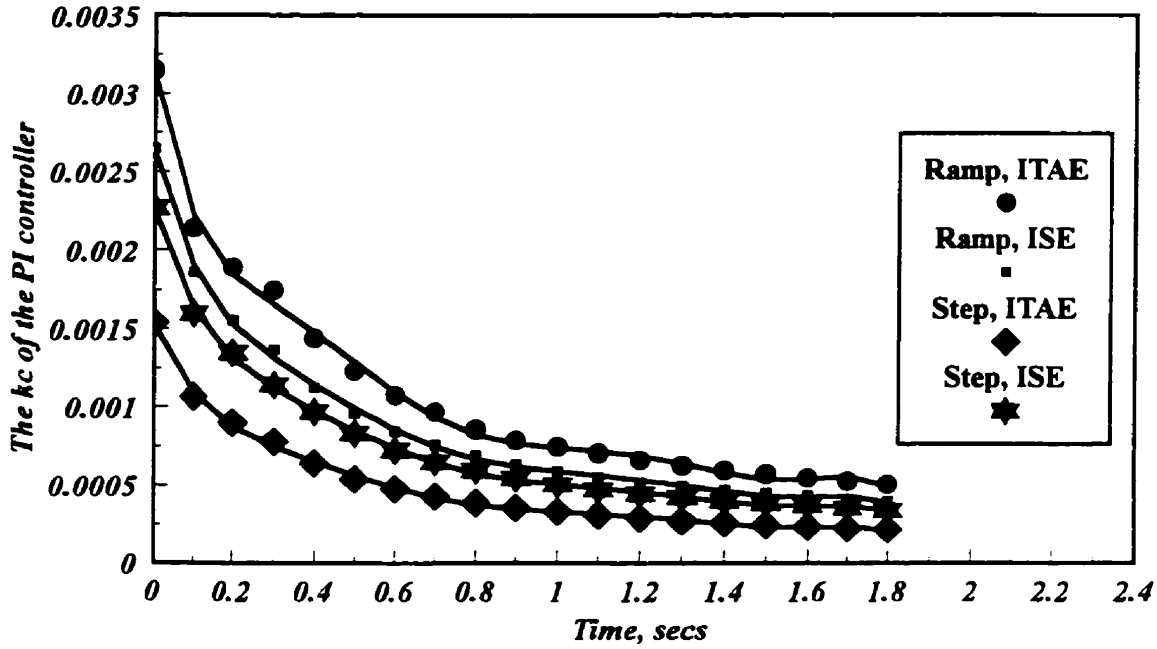


Figure 5.8a PI controller gains

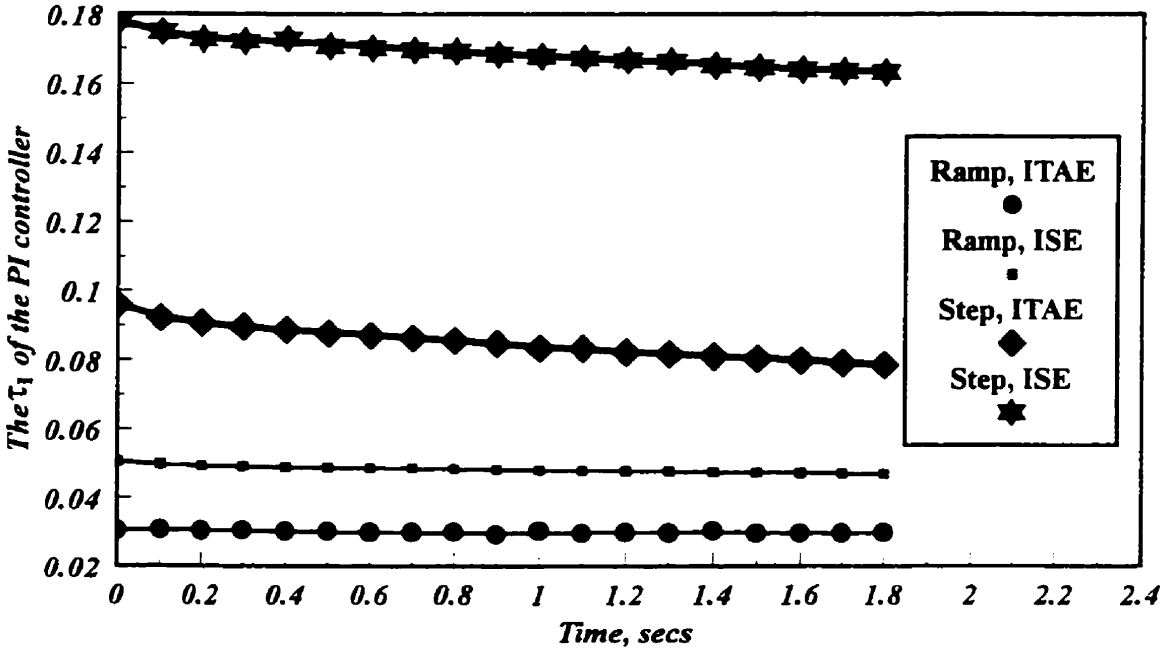


Figure 5.8b PI controller integral time constants

**Figure 5.8** PI controller settings

the polymer melt reaches the pressure transducer. The points, in Figures 5.8 and 5.9, are tuning for the linearized values for every 0.1 s, and solid lines are a least-squares fit to the points for use in the control algorithm. During the control the settings are updated in each sampling time. The controller gain decreases for all tuning methods, due to the increase in process gain. Also, the integral time continuously decreases. However, for the set-point ramp tuning, the reduction is so small to be seen in graph. Despite the different results, the performances of all controllers are good. Therefore, set-point ramp tuning is somewhat slightly superior to set-point step tuning.

### 5.5.3 PID Controller

In industrial practice, this is commonly known as proportional plus reset plus rate controller. The output of this controller is given by:

$$m(t) = k_c e(t) + \frac{k_c}{\tau_I}\int_0^t e(t)\,dt + k_c \tau_D \frac{de}{dt} + m_s \qquad (5.28)$$

where $\tau_D$ is the derivative time constant. With the presence of the derivative term, the PID controller anticipates what the error will be in the immediate future and applies a control action which is proportional to the current rate of change in the error. Due to this property, the derivative control action is sometimes referred to as anticipatory control. However, it suffers from two effects: a) it gives no control action for a constant non-zero error, and b) for a noisy response, it yields large control action. The transfer function of a PID controller is:

$$G_c(s) = k_c\left(1 + \frac{1}{\tau_I s} + \tau_D s\right) \qquad (5.29)$$

For tuning the PID controller parameters, the same procedures, which were used for the PI controller, are used. The values of controller adjusted parameters are selected using ITAE and ISE integral performance criteria for the two different types of set-points. Figure 5.9 shows the settings for PID controllers. Figure 5.9a shows gains for different

tuning criteria. Figure 5.9b and 5.9c show integral and derivative time constants, respectively.

### 5.5.4 IMC Controller

The IMC design method is based on an assumed process model and relates the controller settings to the model parameters in a straightforward manner [116]. The IMC approach has two important additional advantages: a) it explicitly takes into account model uncertainty, b) it allows the designer to trade off control system performance against control system robustness to process changes and modeling errors. Figure 5.10 shows the IMC method in a simplified block diagram form. G and $\tilde{G}$ are the transfer functions of the real process and the model, respectively. The model response $\tilde{c}$ is subtracted from the actual response c and the difference, $c-\tilde{c}$, is used as the input signal to the controller, which has a transfer function $G_c^*$. This block diagram can be converted into the conventional feedback control loop, if $G_c$ is:

$$G_c = \frac{G_c^*}{1 - G_c^* \tilde{G}} \tag{5.30}$$

The IMC controller is designed in two steps: 1) the process model is factored as:

$$\tilde{G} = \tilde{G}_+ \times \tilde{G}_- \tag{5.31}$$

where $\tilde{G}_+$ contains time delay and any right-half plane zeros; 2) the controller is specified as:

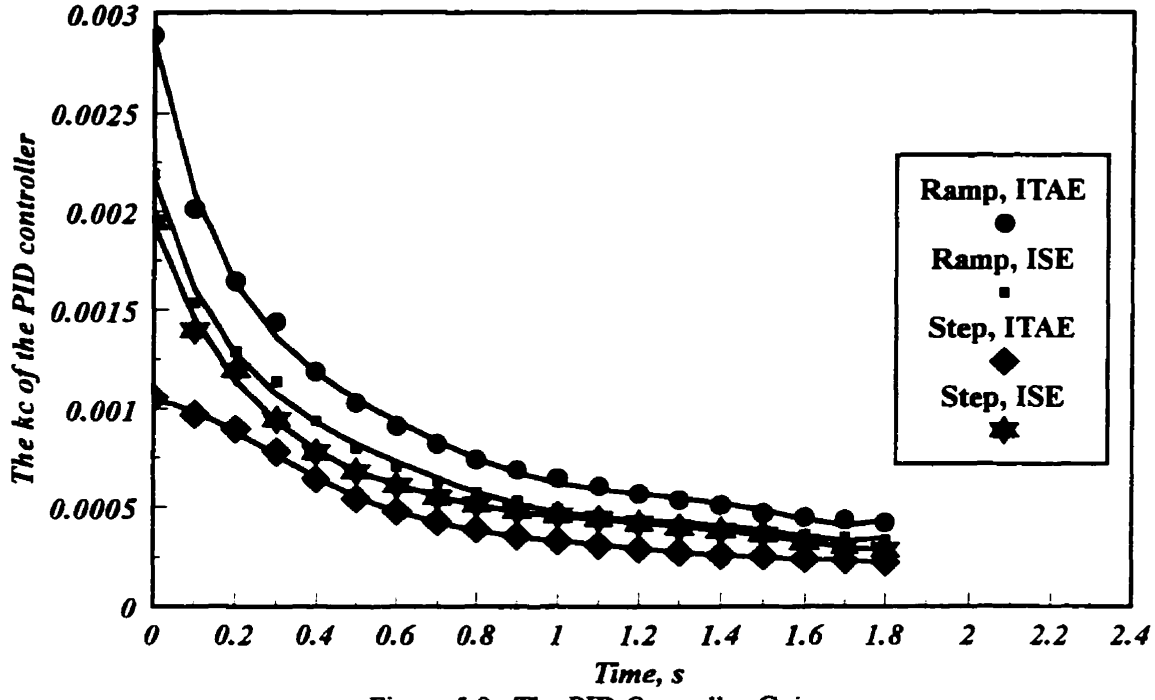


Figure 5.9a The PID Controller Gain

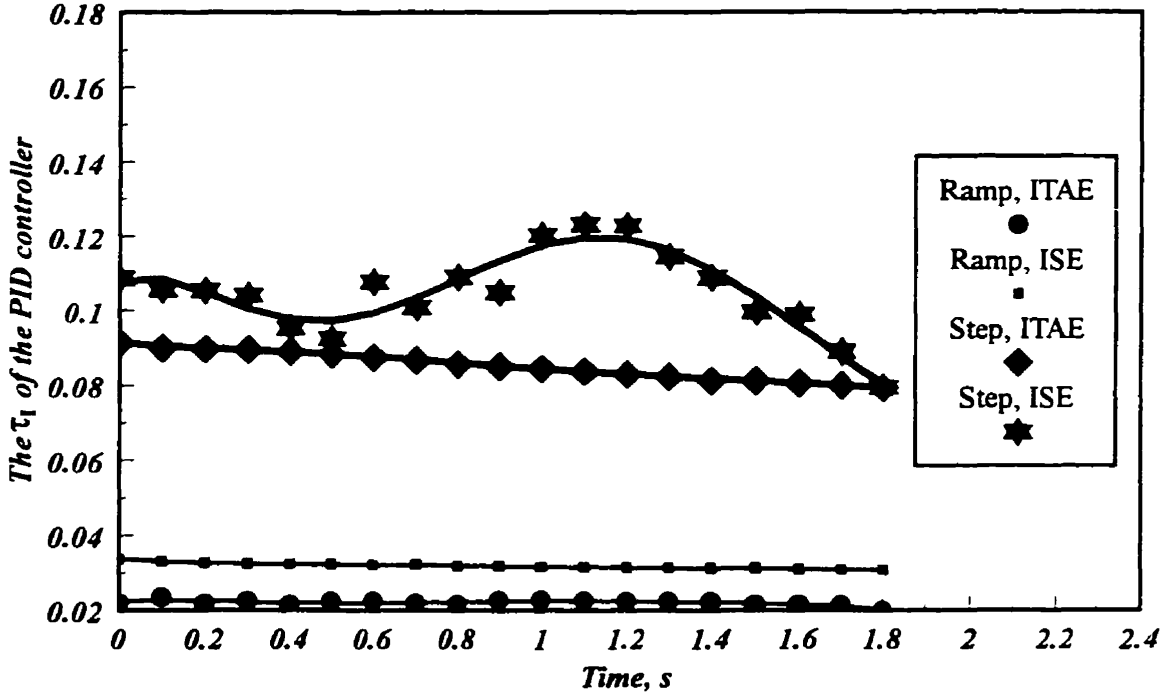


Figure 5.9b The PID Controller Integral Time Constant

**Figure 5.9** PID controller settings

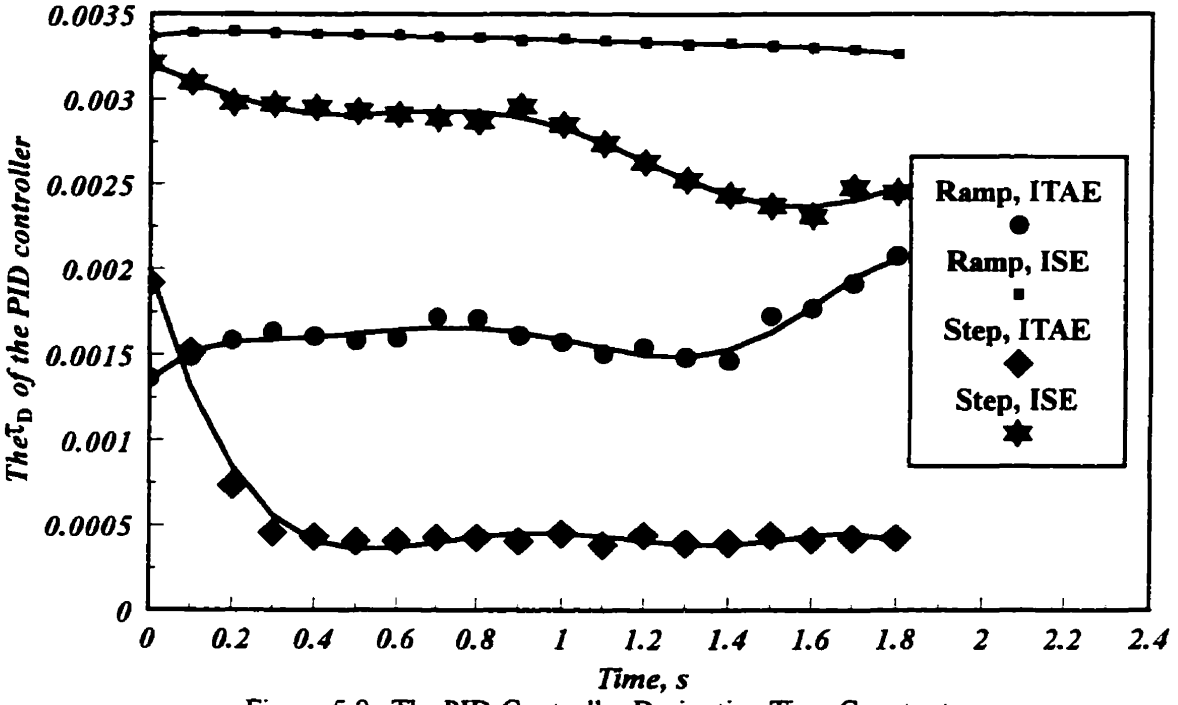


Figure 5.9c The PID Controller Derivative Time Constant

**Figure 5.9** The PID controller settings

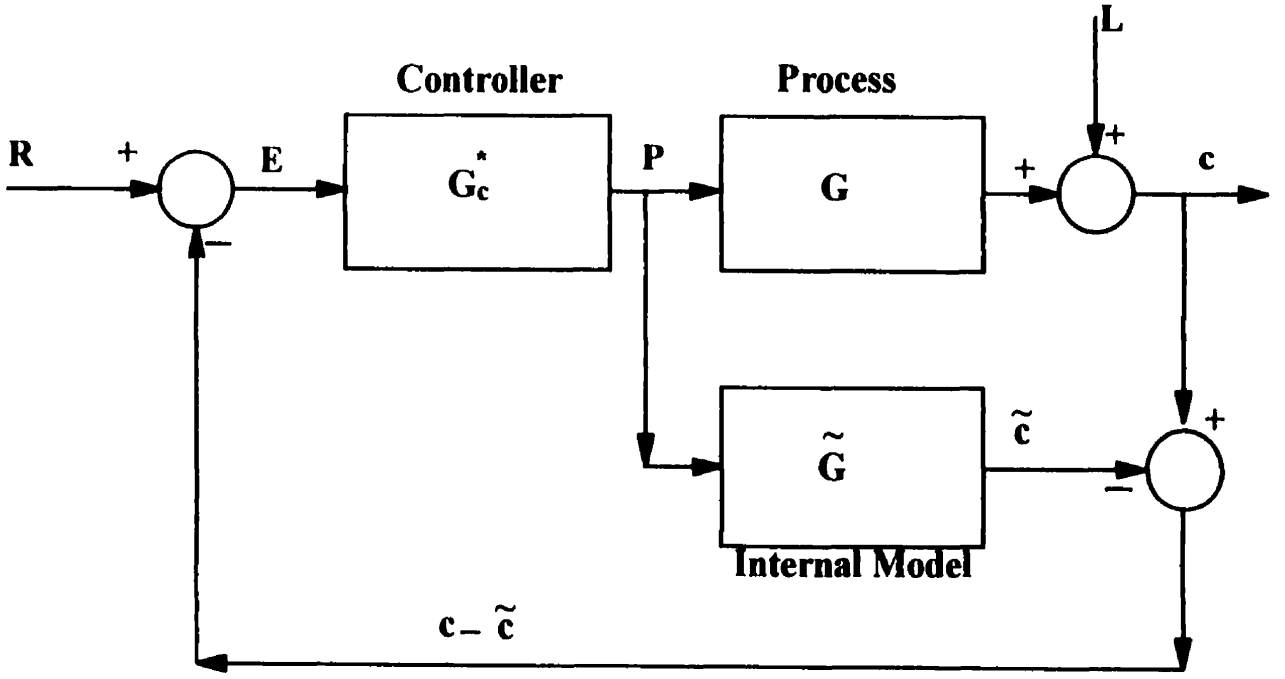


**Figure 5.10** Simplified block diagram of IMC method

$$G_c^* = \frac{1}{G_-} f_i$$
$$f_i = \frac{1 - a_{IMC}}{1 - a_{IMC}\, z^{-1}} \tag{5.32}$$

where $f_i$ is a low-pass filter with a steady-state gain of one.

To design the IMC controller, the discretized process model is used. Then, the final IMC controller is:

$$G_c = \frac{1 - a_{IMC}}{1 - z^{-1}} \times \frac{1 + h_1 z^{-1} + h_2 z^{-2} + h_3 z^{-3} + h_4 z^{-4}}{g_1 + g_2 z^{-1} + g_3 z^{-2} + g_4 z^{-3}} \tag{5.33}$$

where $a_{IMC}$ is the low pass filter parameter and was set experimentally with testing different values for $a_{IMC}$. During control, values of $g_i$, and $h_i$ are updated in each sampling time.

## 5.6 Filling Phase Control Experiments

The results of the control studies presented in the previous section indicated the feasibility of accurate control of cavity pressure during the filling phase. The objective of this part of the study, covered in this section, is to perform a series of control experiments using PI, PID and IMC controllers to verify the control results and to demonstrate experimentally the feasibility of pressure control during the filling phase of the injection molding cycle.

Closed loop control experiments for the cavity pressure were carried out using the injection molding machine and the associated microcomputer system described in chapter 3. The following results and discussion is for high density polyethylene. The results for polystyrene are given in section 5.8. The control laws for the PI, PID, and IMC controllers with the optimum tuned parameters obtained in the tuning section were scaled for implementation on the QNX operating system based microcomputer for 16-bit

arithmetic. The following experiments were performed:

(1) Control of cavity pressure using PI and PID controllers with different tuning methods and IMC controller with ramp set-point.

(2) Applying the controller for a non-linear set-point during the filling phase.

(3) Applying the controller to a complex mold cavity.

### 5.6.1 Discretized Form of the Controllers

The general analog form of the PI controller is given in Equation (5.24). A discrete PI controller can be obtained by approximating the integral in Equation (5.24) using the backward rectangular integration rule:

$$m(k) = k_c\left(e(k) + \frac{\Delta t}{\tau_I}\sum_{i=1}^{i=k} e(i)\right) + m_s \qquad (5.34)$$

where $\Delta t$ is the sampling interval and equals 10 ms because it is much less than dominant time constant of the process which is approximately 60 ms, see Figure 5.1. The backward difference is used because it always gives stable z-transfer function for stable continuous transfer function. This equation is known as the position form of the PI algorithm, because at each sampling instant it calculates the actual or absolute value of the controller output signal. An alternative form for the PI control algorithm is the so called velocity form. It calculates the incremental change of the controller output signal with respect to its previous value. Writing Equation (5.34) for the $k^{th}$ and the $(k-1)^{th}$ sampling instants and obtaining the difference gives the velocity form of the controller as follows:

$$m(k) = m(k-1) + k_c\left(1 + \frac{\Delta t}{\tau_I}\right)e(k) - k_c e(k-1) \qquad (5.35)$$

The velocity form of the algorithm is preferred because it has the following advantages over the position form:

(1) The velocity algorithm unlike, the position form, does not require the steady state

value of the actuator position.

(2) The position form with its summation of the errors produces integral wind-up and special attention is required. But, the velocity form is protected against integral wind-up because control action changes all the time until it becomes saturated. Therefore, as soon as the error changes sign, the control action can return within the control range in one sampling period.

Applying the same approach for the PID analog form, Equation (5.28), gives the following difference equation for this controller:

$$m(k) = m(k-1) + k_c\left(1 + \frac{\Delta t}{\tau_I} + \frac{\tau_D}{\Delta t}\right)e(k) - k_c\left(1 + \frac{2\tau_D}{\Delta t}\right)e(k-1) + \frac{\tau_D}{\Delta t}e(k-2) \qquad (5.36)$$

For the IMC controller, the z-transform transfer function is given in Equation (5.33). Using the backward operator definition $z^{-1}$, m(k-1)=$z^{-1}$ m(k), yields the following equation:

$$\begin{aligned} m(k) \;=\; & m(k-1) + \frac{1}{g_1}\{-g_2 m(k-1) + (g_2 - g_3)m(k-2) + (g_3 - g_4)m(k-3) \\ & + g_4 m(k-4)\} \\ & + \frac{1-a_{IMC}}{g_1}\{e(k) + h_1 e(k-1) + h_2 e(k-2) + h_3 e(k-3) + h_4 e(k-4)\} \end{aligned} \qquad (5.37)$$

values of $g_i$, and $h_i$ are updated in each sampling time. The settings and model parameters which are used in digital controllers are calculated by using continuous plant model. This is applicable due to the small value of sampling period. Furthermore, constant sampling time is used during the filling and packing phases experiments.

## 5.7 Results and Discussions

A number of experiments were conducted to examine the performance and effectiveness of the controllers for high density polyethylene. The controller was applied digitally using the micro-computer system. All the software was written in WATCOM

C running under the QNX operating system. Figure 5.11 shows the experimental result of applying the PI step tuned controller with the ITAE criterion. Figure 5.11a shows the experimental cavity pressure and the selected set-point. After small fluctuation around the set-point, the cavity pressure follows the set-point very well. Figure 5.11b shows the output command of the controller or manipulated variable. Figures 5.12, 5.13, and 5.14 show the experimental results for other PI controllers, step or ramp servoproblem tuned with ITAE and ISE criteria. One open loop cavity pressure profile is shown beside the closed loop result in Figure 5.13. With the closed loop cavity pressure profiles, the servo-valve opening first decreases to overcome the high slope of open loop behavior. Subsequently, it increases and finally is more or less constant around 60% $i_s$. Accordingly, the important part of the control activity takes place in the beginning of the each cycle.

In order to have a better view of controller action, the measured controlled variable error is shown in the lower part of Figure 5.11b. The maximum error is less than 0.2 MPa and the maximum cavity pressure is around 5.5 MPa. The error is high in the beginning and decreases toward the end of filling. Figures 5.15 through 5.18 show the experimental results for the PID step tuned controller with ITAE and ISE and the PID ramp servoproblem tuned controllers with ITAE and ISE, respectively. The PID result is very good. The best performance is obtained with the IMC controller, as shown in the Figure 5.19. The $a_{IMC}$ was experimentally determined to have a value of 0.5. The average error, maximum error, and standard deviation of the error for the different controllers are given in Table 5.2. The average errors of all the controllers are approximately the same. The largest maximum error is given by the PI step tuned controller, the smallest is given by the IMC controller. The IMC controller has the least standard deviation, which implies better performance. Although there are other methods to compare different controller performances [117] which is out of the scope of this study. Figures 5.20 through 5.23 show the results for cycle numbers 9, 27, 39, and 51, respectively. Clearly, the ability of the controller does not deteriorate over the period under consideration.

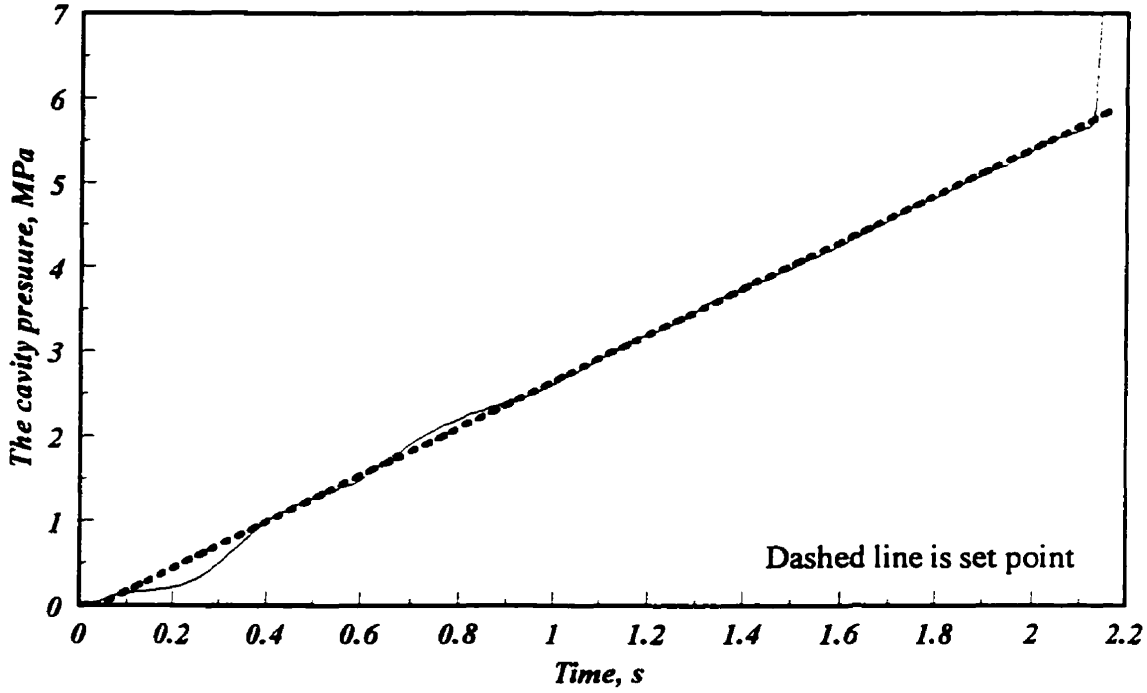


Figure 5.11a Measured cavity pressure

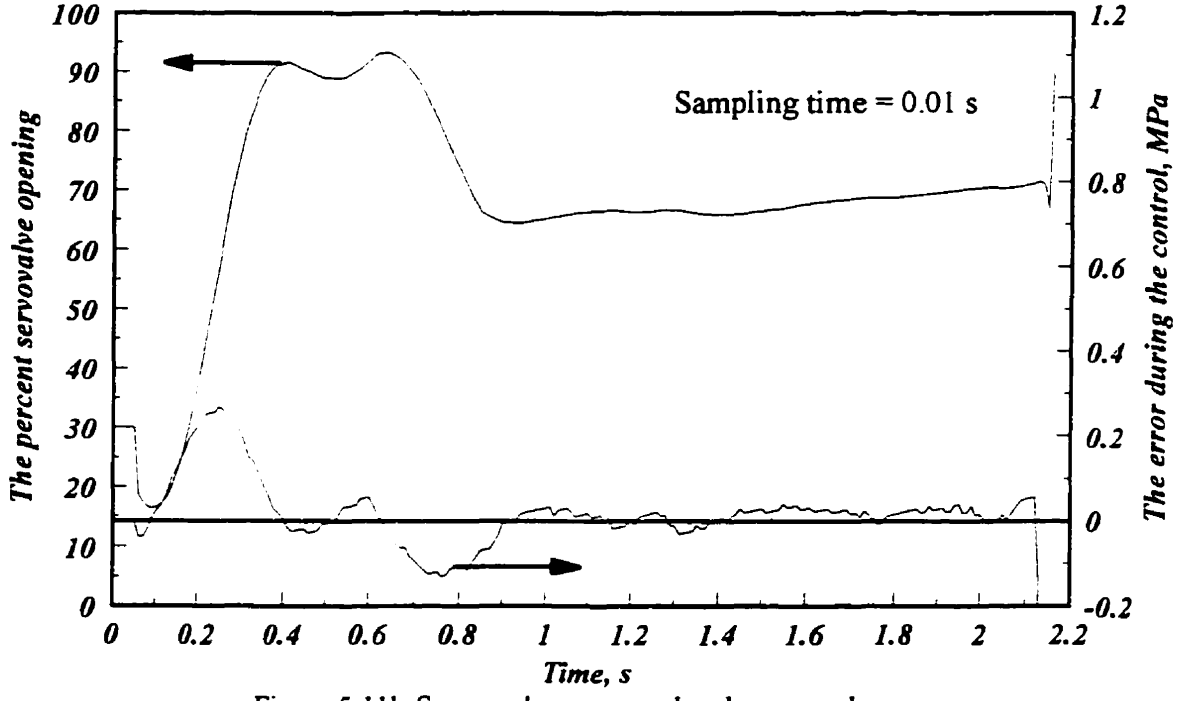


Figure 5.11b Servo-valve command and measured error

**Figure 5.11** PI step servoproblem tuned controller with ITAE criteria

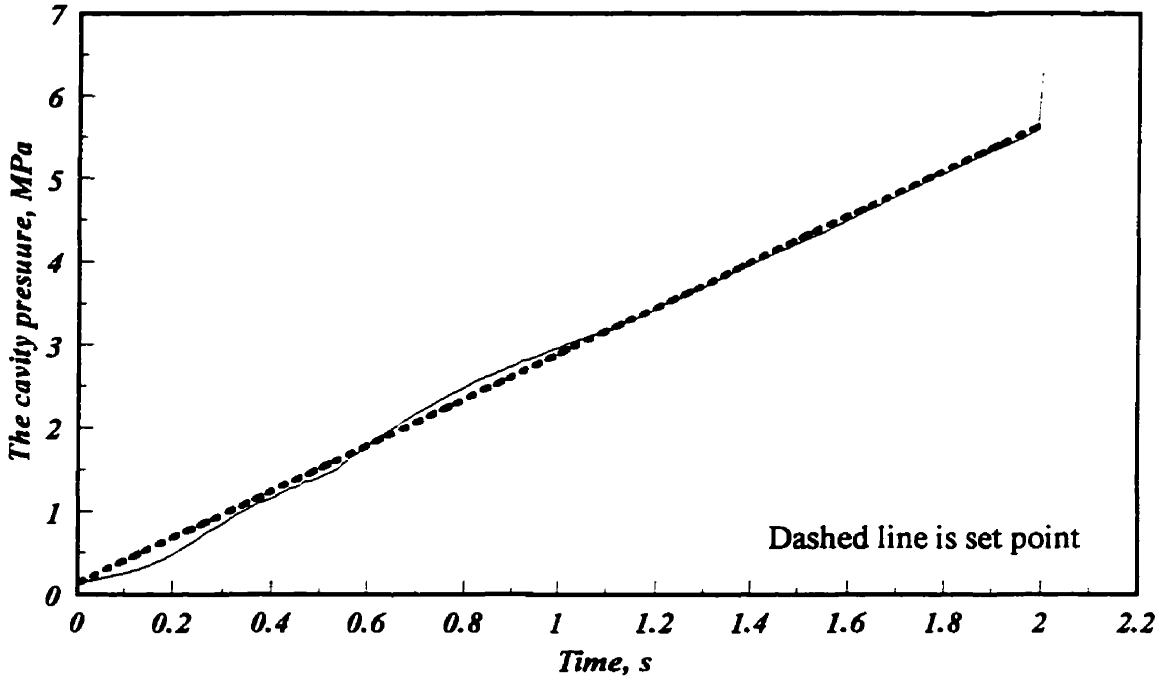


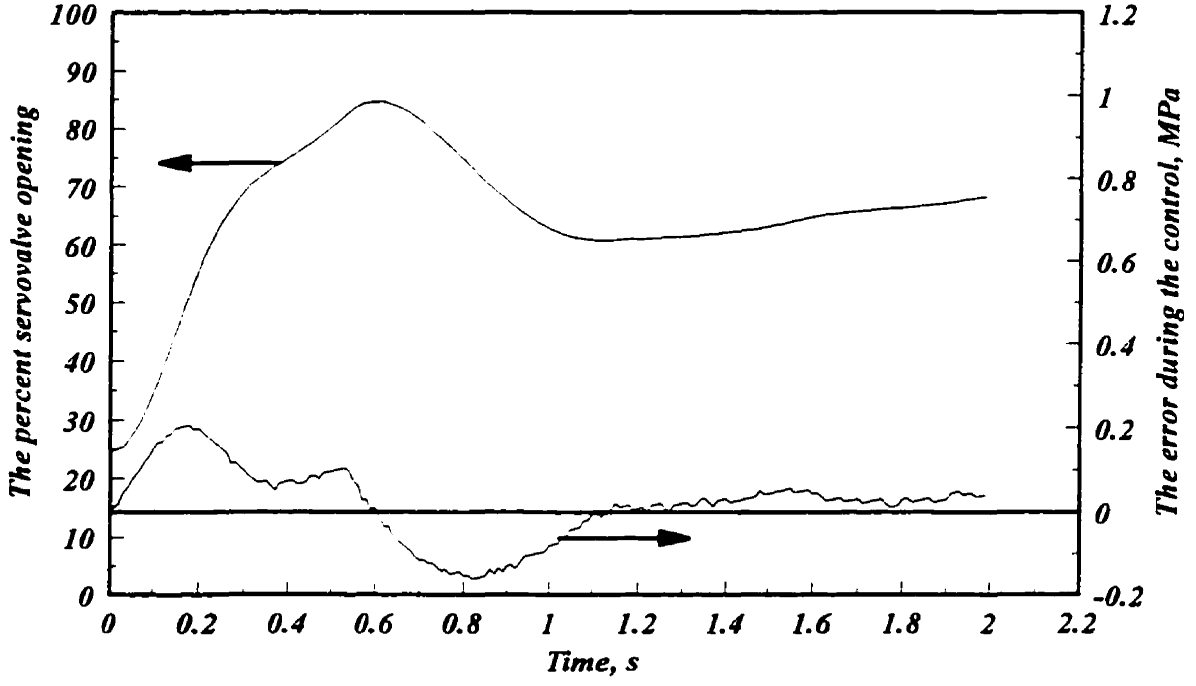


**Figure 5.12** PI step servoproblem tuned controller with ISE criteria

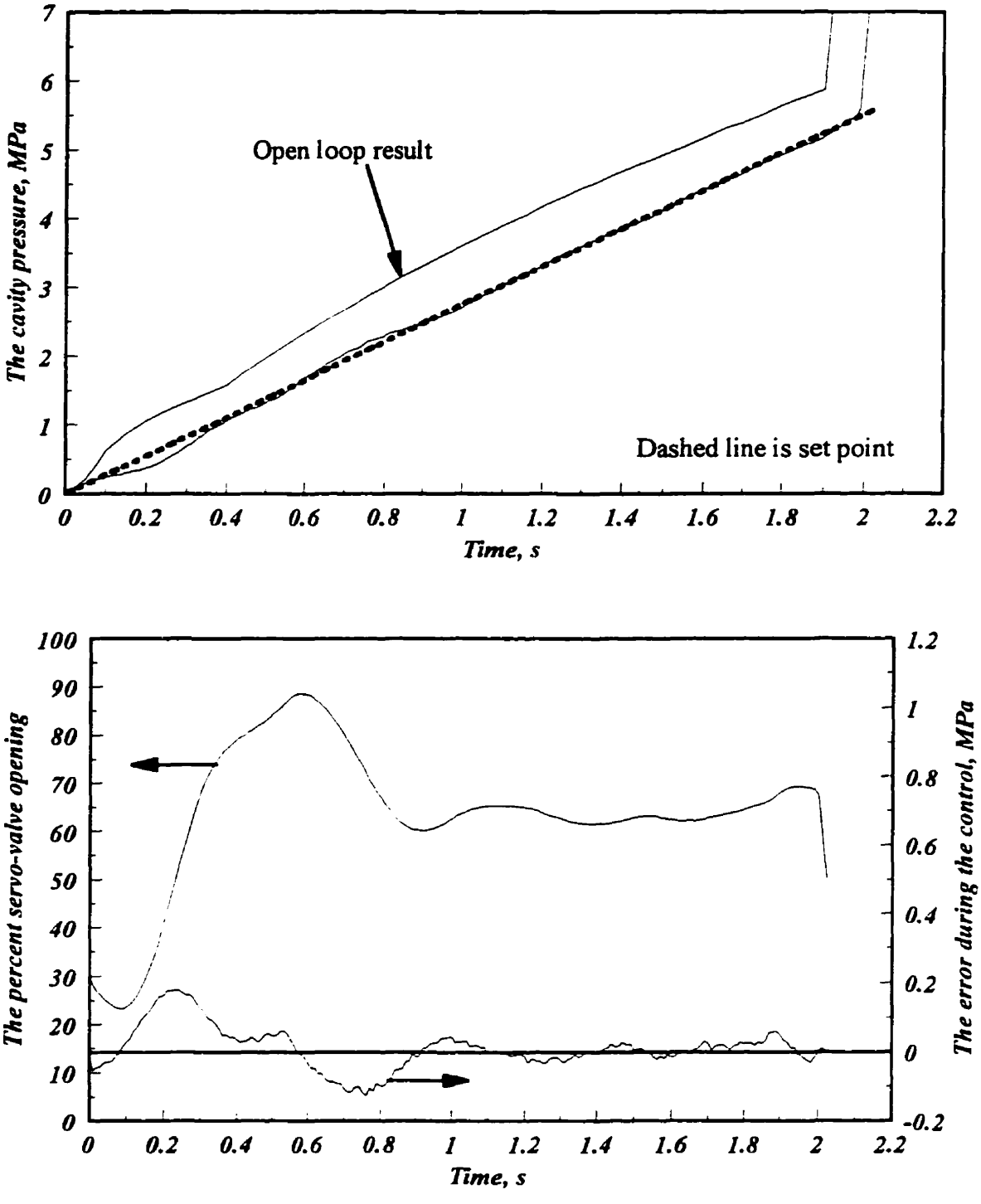


**Figure 5.13** PI ramp servoproblem tuned controller with ITAE criteria

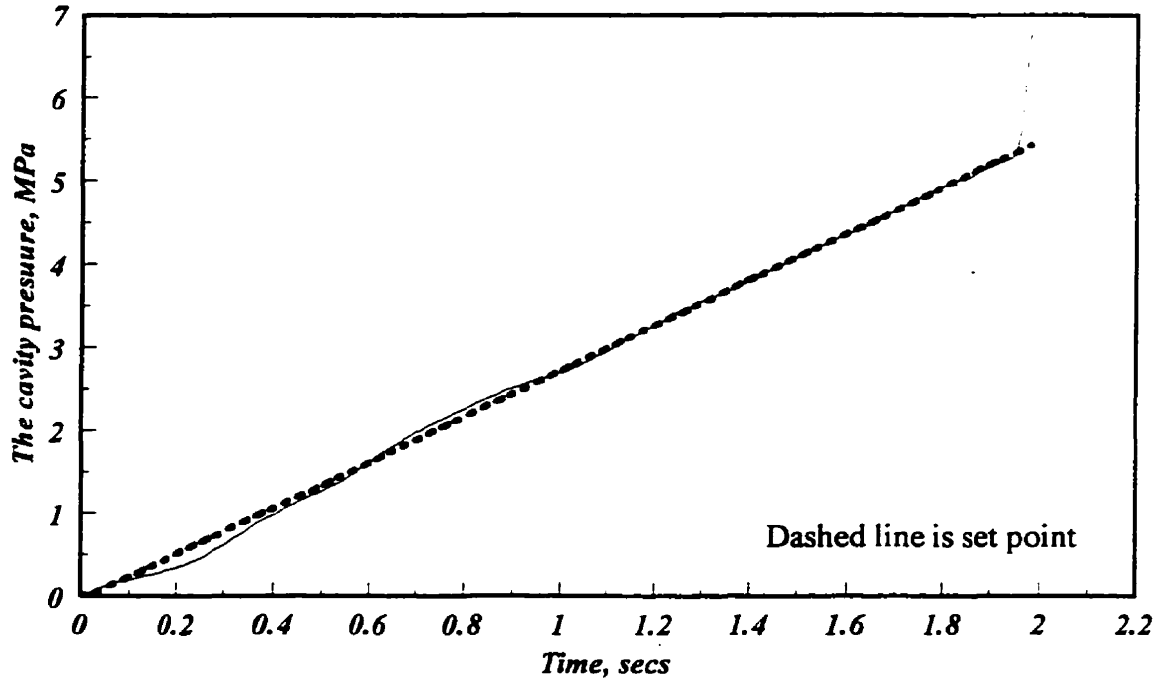


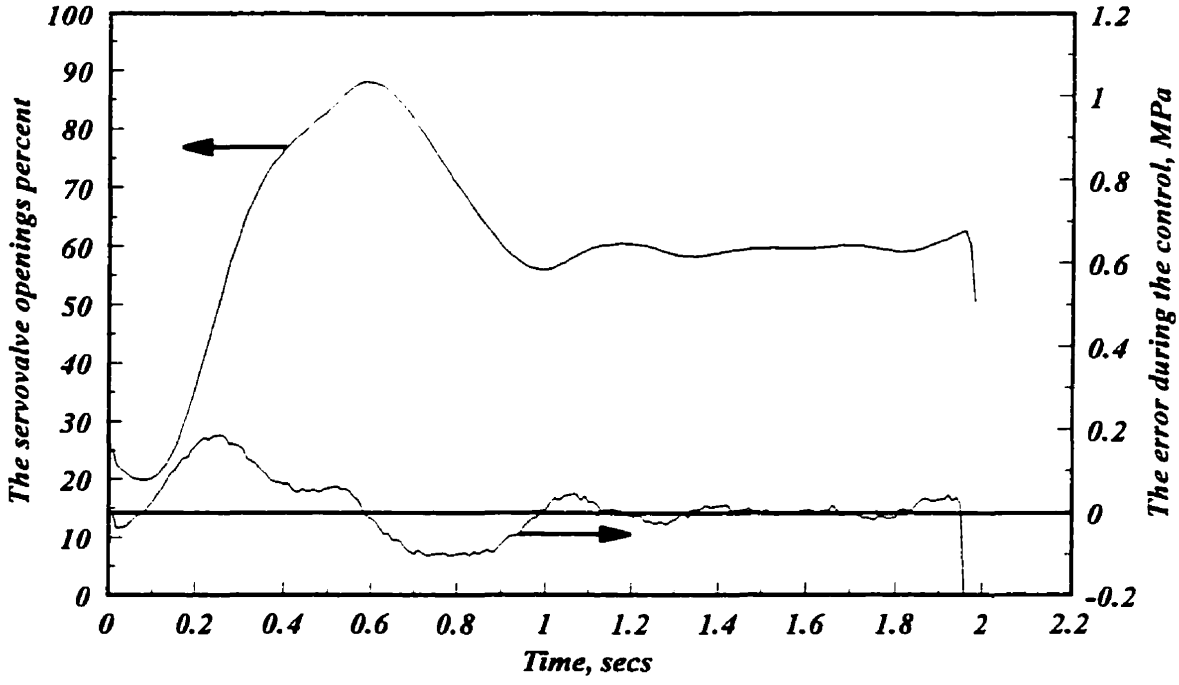


**Figure 5.14** PI ramp servopriblem tuned controller with ISE

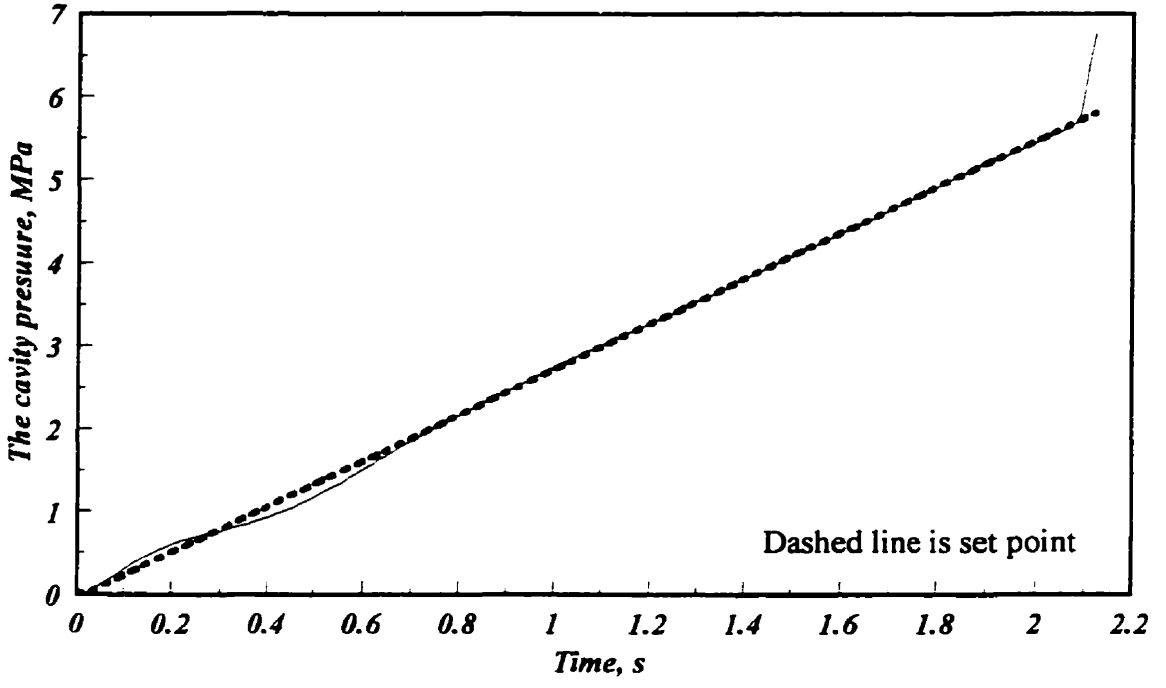


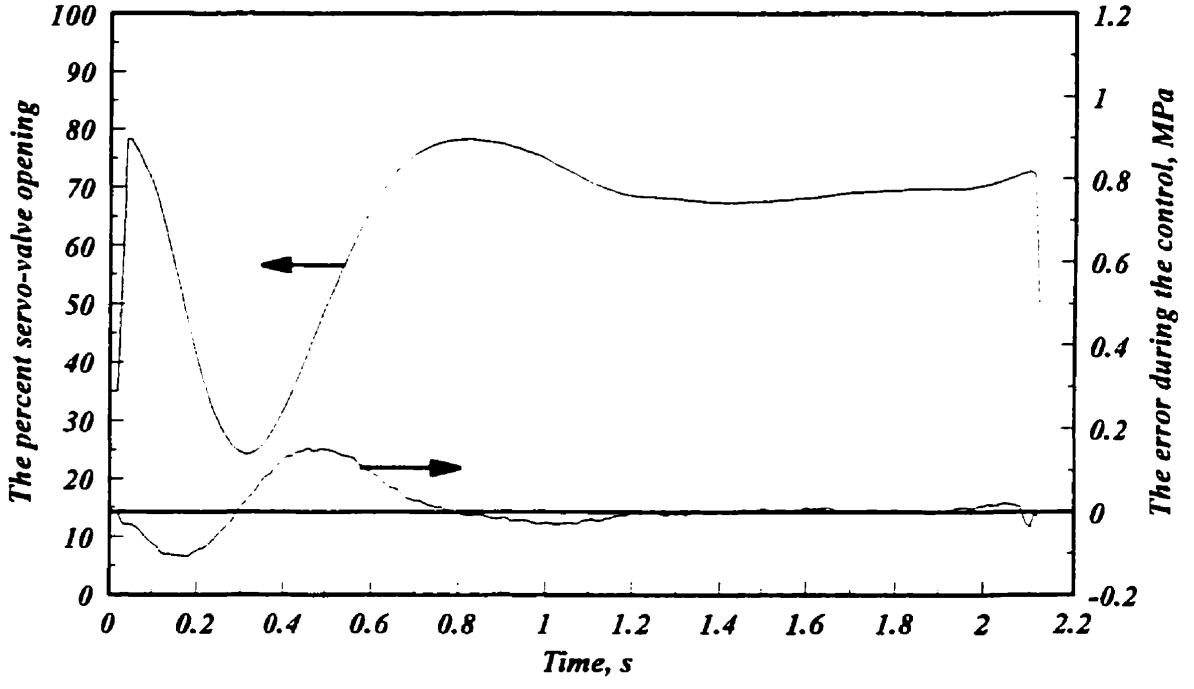


**Figure 5.15** PID step servoproblem tuned controller with ITAE criteria

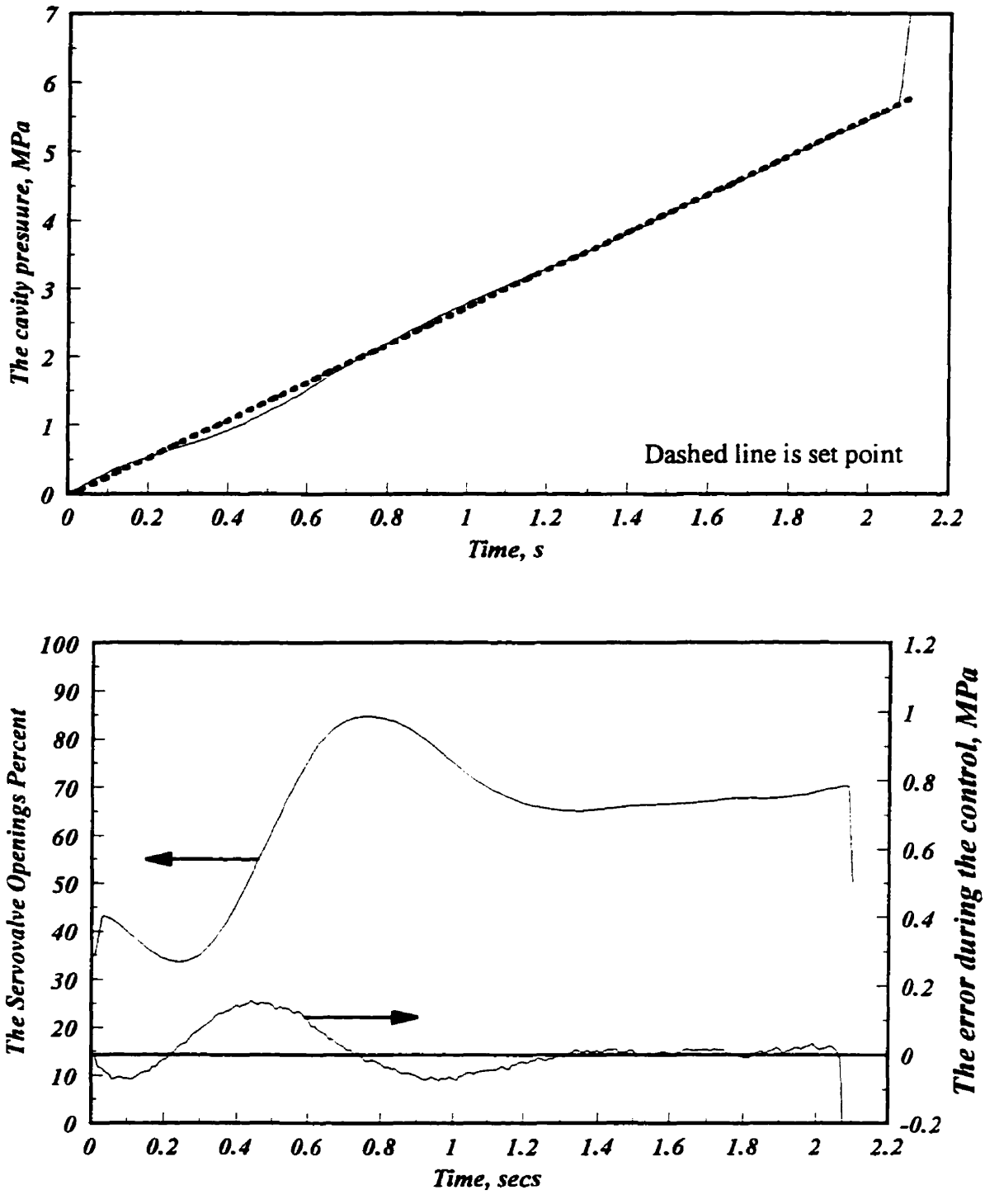


**Figure 5.16** PID step servoproblem tuned controller with ISE criteria

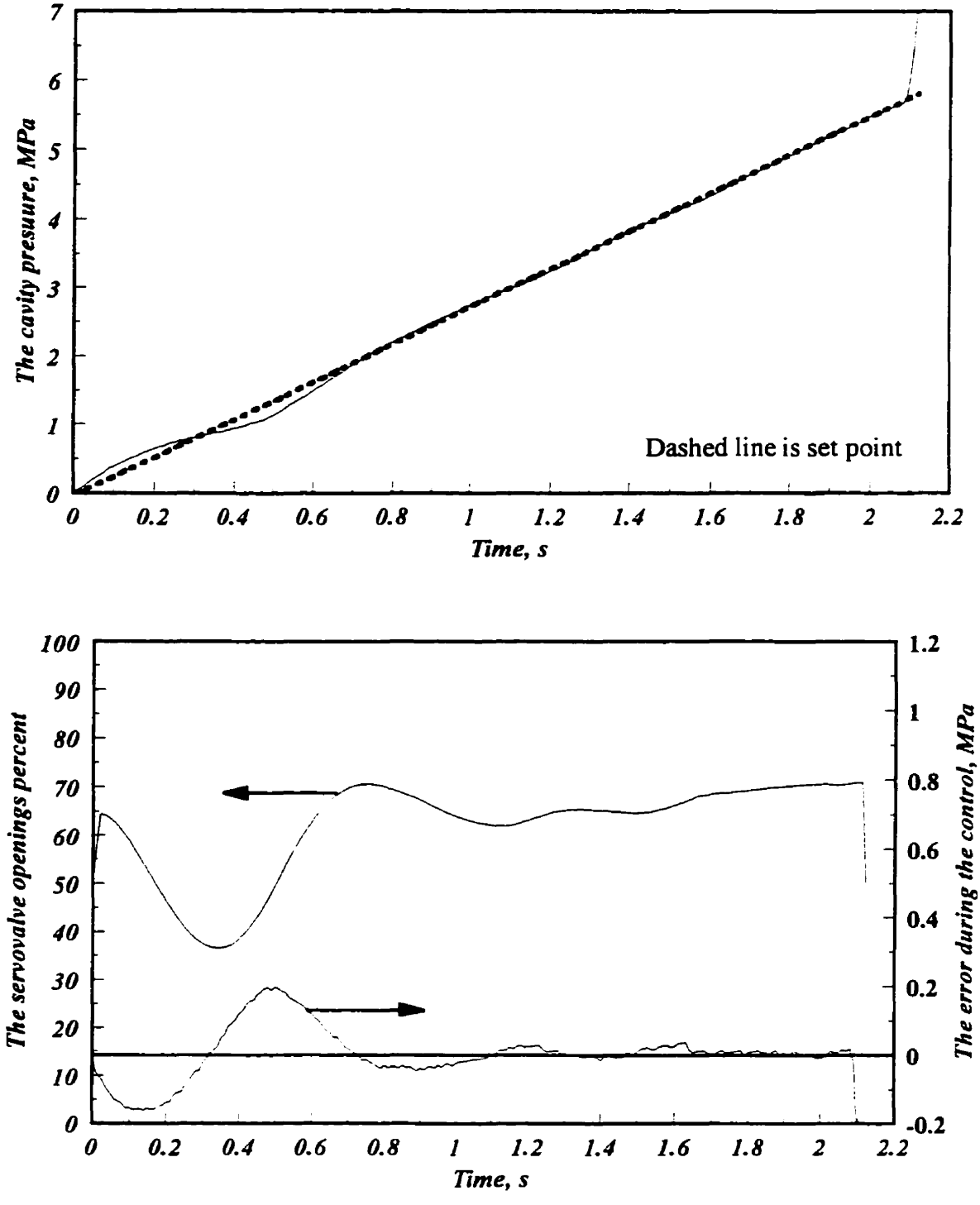


**Figure 5.17** PID ramp servoproblem tuned controller with ITAE criteria

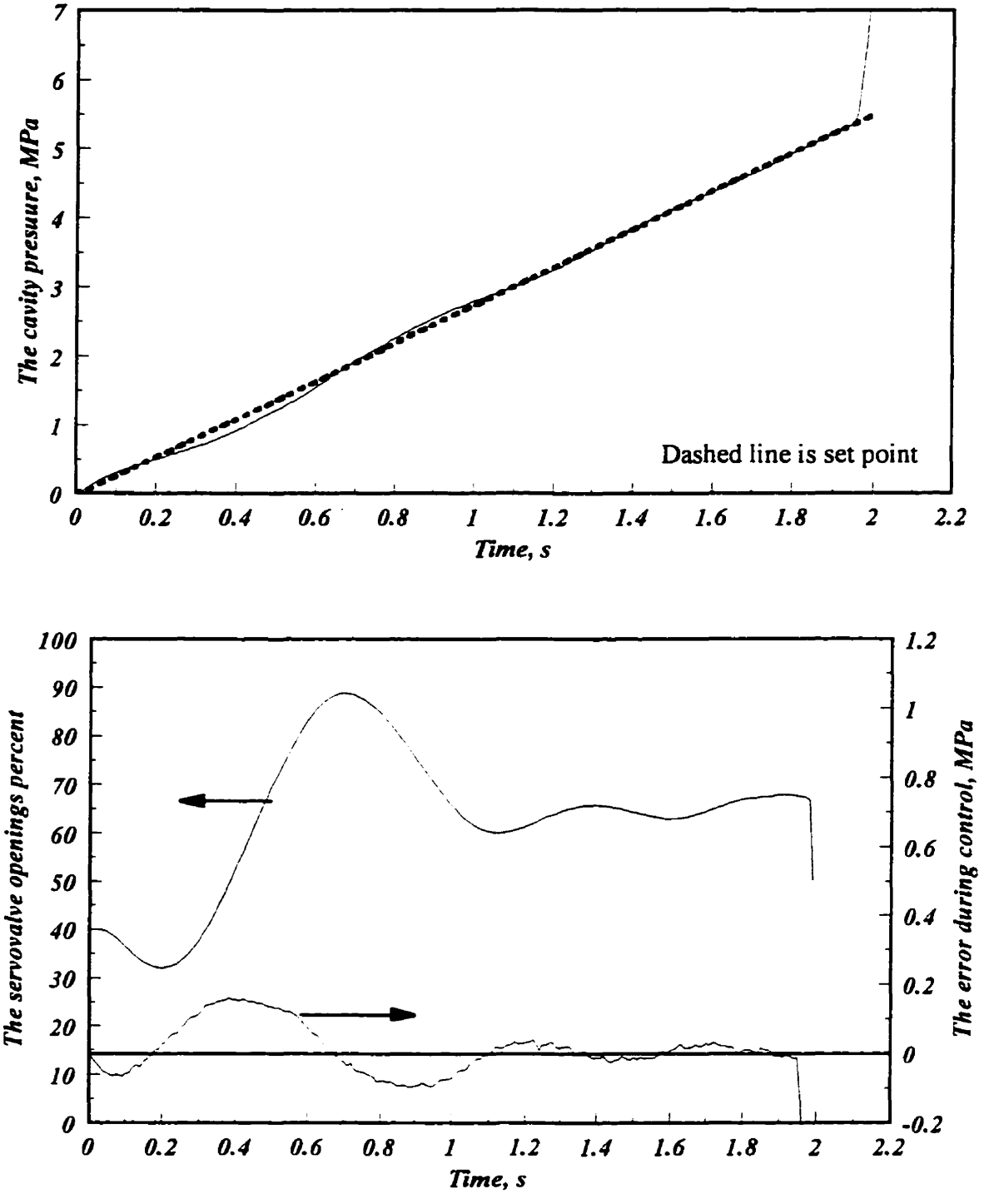


**Figure 5.18** PID ramp servoproblem tuned controller with ISE criteria

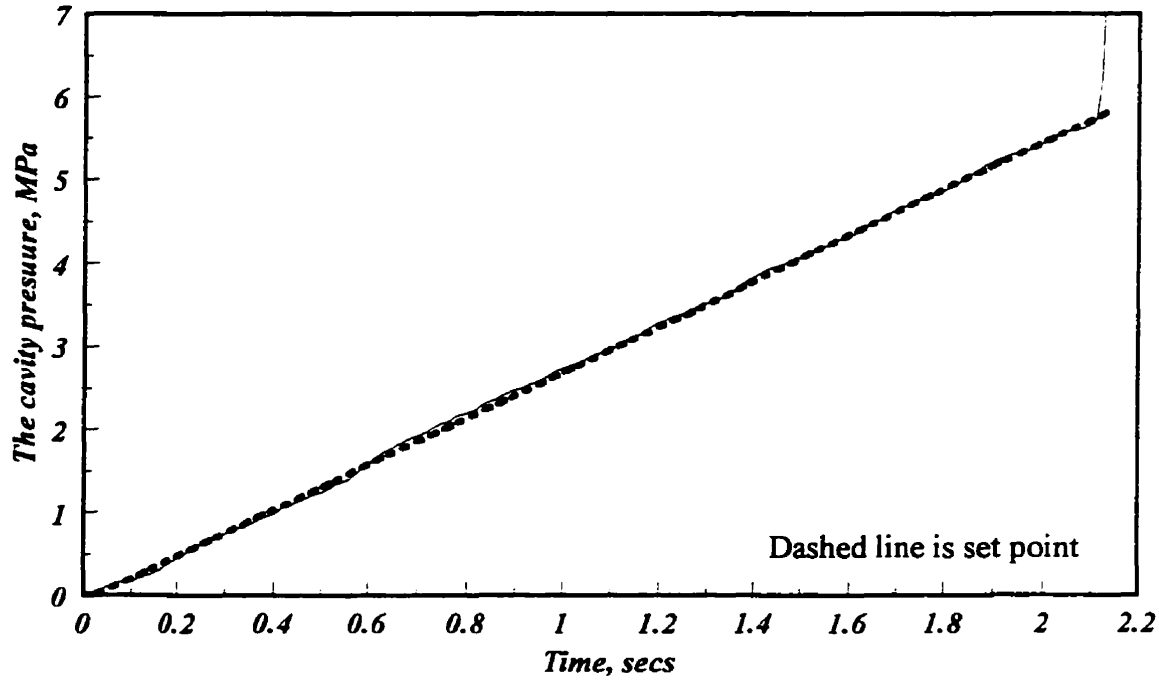


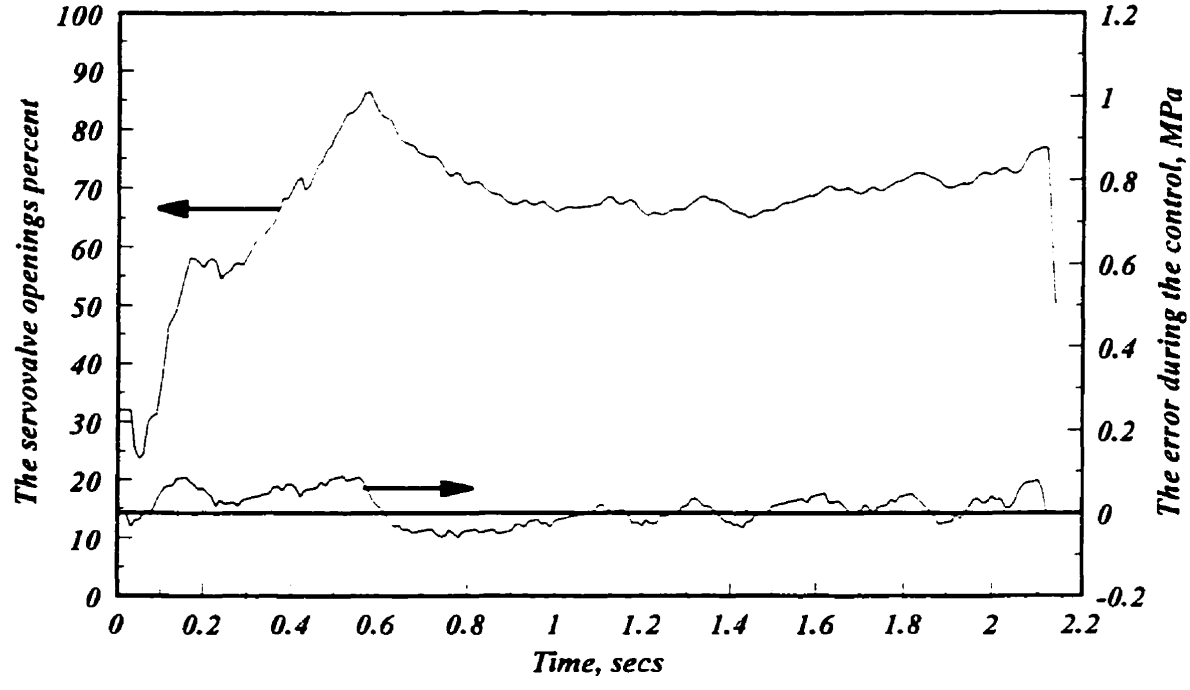


**Figure 5.19** IMC controller, a $_{IMC}$=0.5

| Controller Type | | Average Error | Maximum Error | Standard Deviation |
|---|---|---|---|---|
| | IMC | 0.0127 | 0.0885 | 0.0377 |
| Set Point Ramp Tuning | PI, ITAE | 0.0116 | 0.1806 | 0.0609 |
| | PI, ISE | 0.0122 | 0.1870 | 0.0662 |
| | PID, ITAE | 0.0124 | 0.1992 | 0.0743 |
| | PID, ISE | 0.0127 | 0.1621 | 0.0675 |
| Set Point Step Tuning | PI, ITAE | 0.0194 | 0.2710 | 0.0738 |
| | PI, ISE | 0.0183 | 0.2068 | 0.0856 |
| | PID,ITAE | 0.0117 | 0.1543 | 0.0553 |
| | PID, ISE | 0.0111 | 0.1555 | 0.0597 |

**Table 5.2** - Comparison between different controller performances

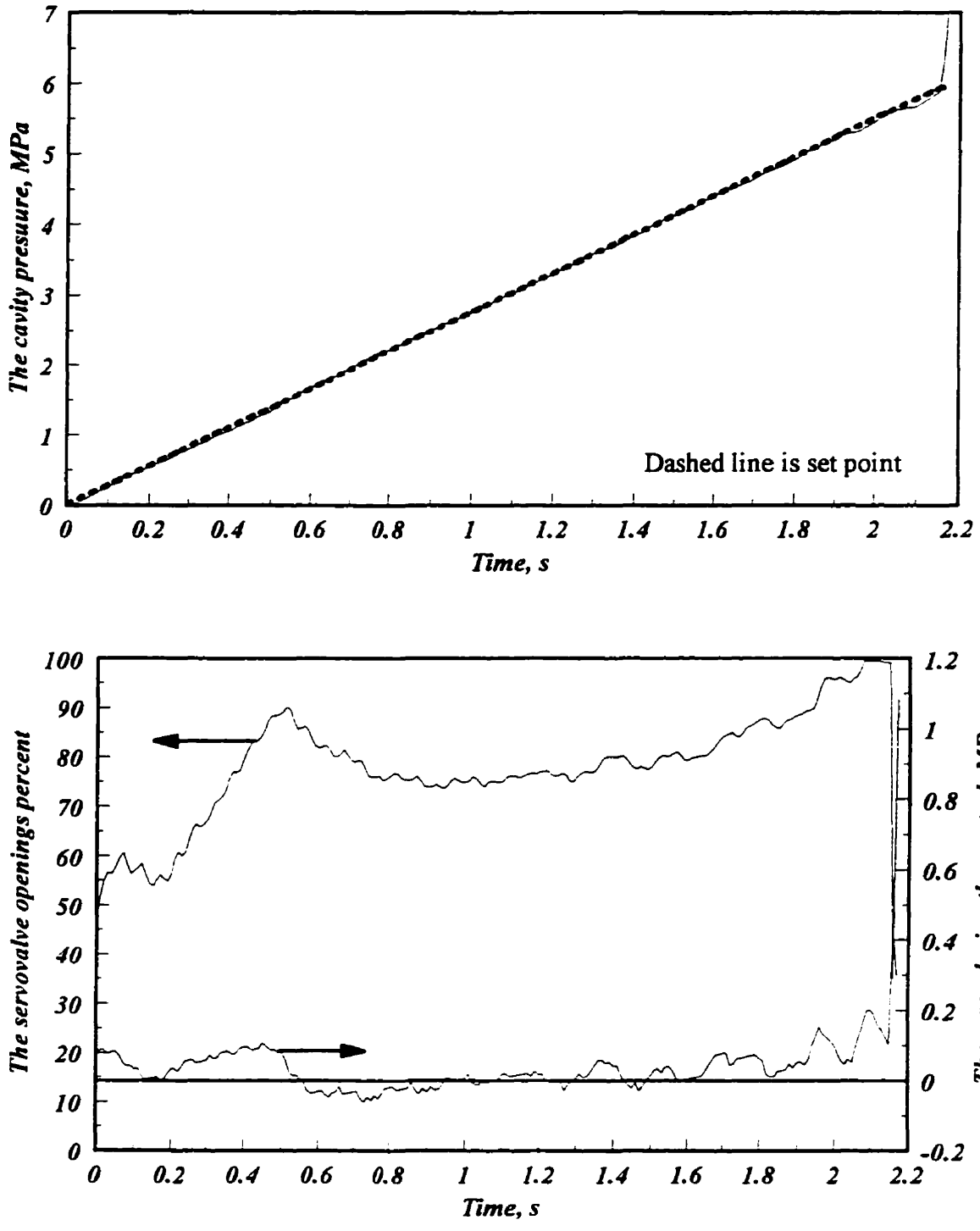


**Figure 5.20** IMC controller, cycle number 9

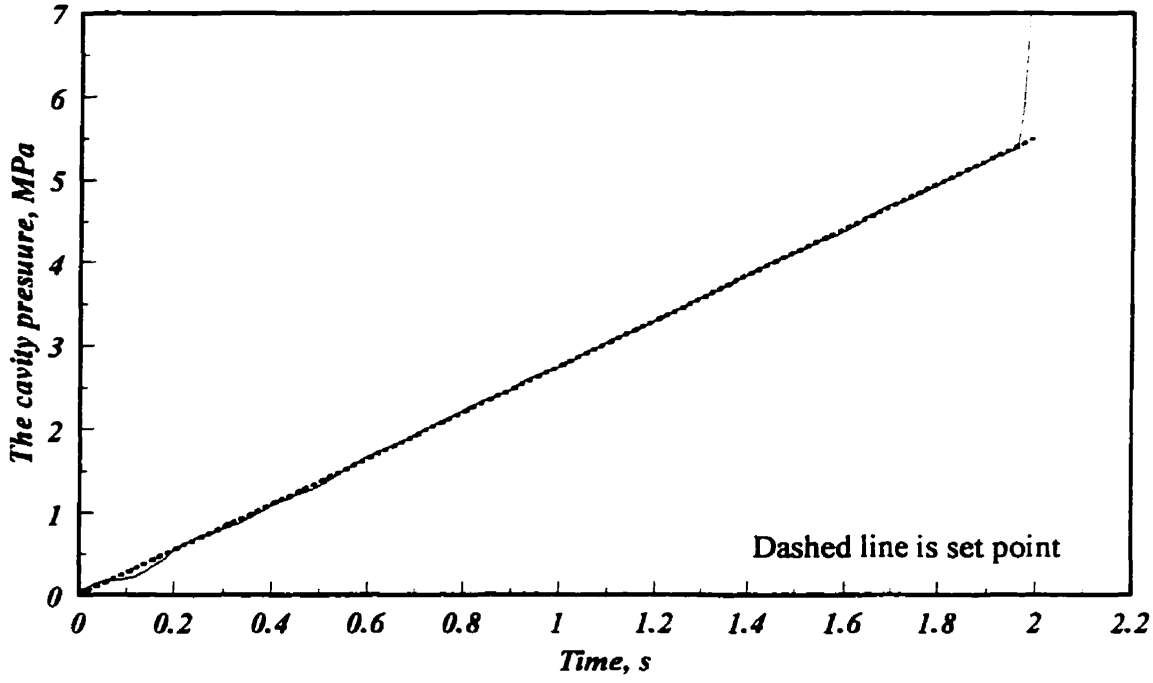


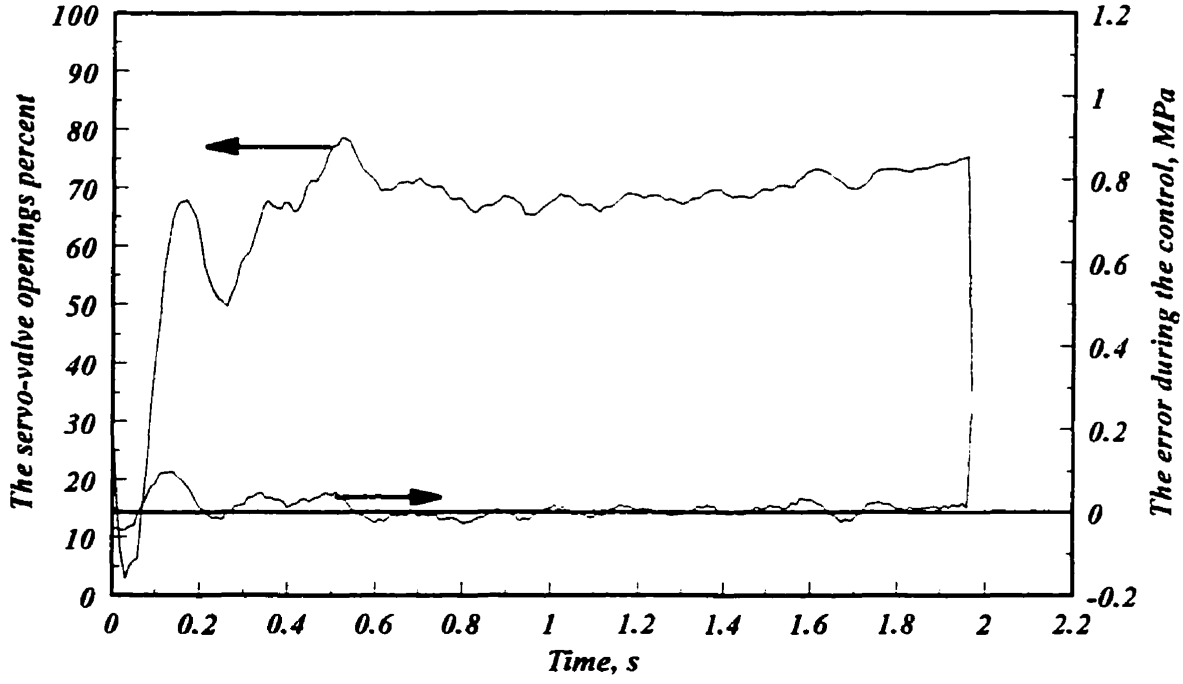


**Figure 5.21** IMC controller, cycle number 27

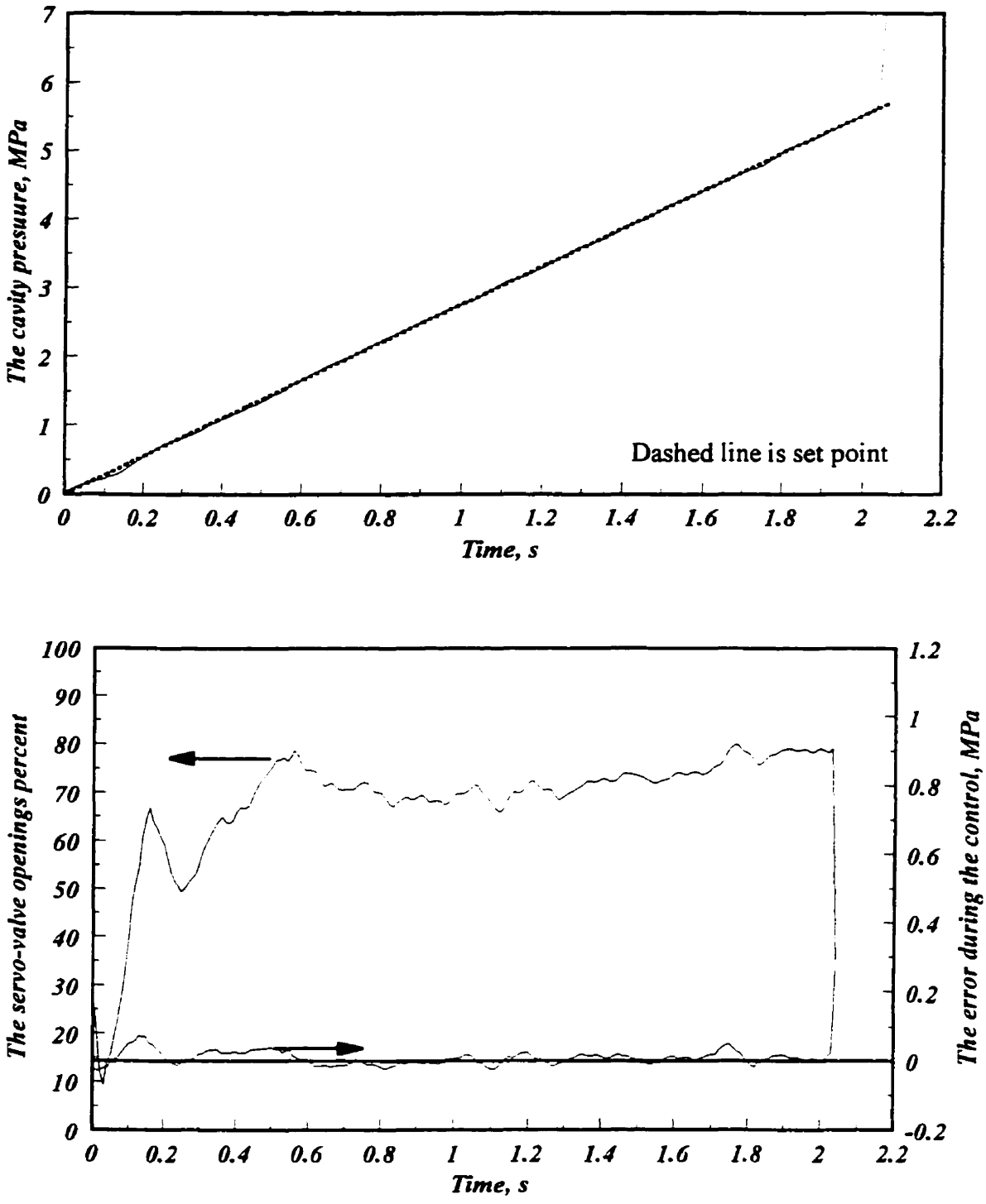


**Figure 5.22** IMC controller, cycle number 39

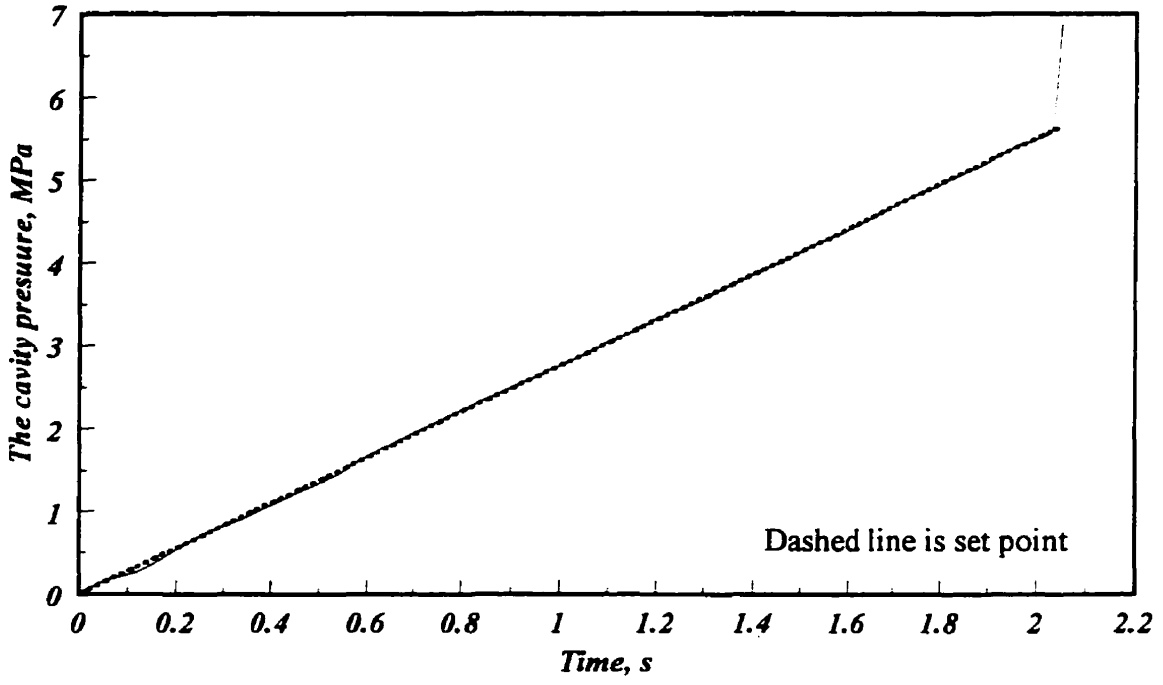


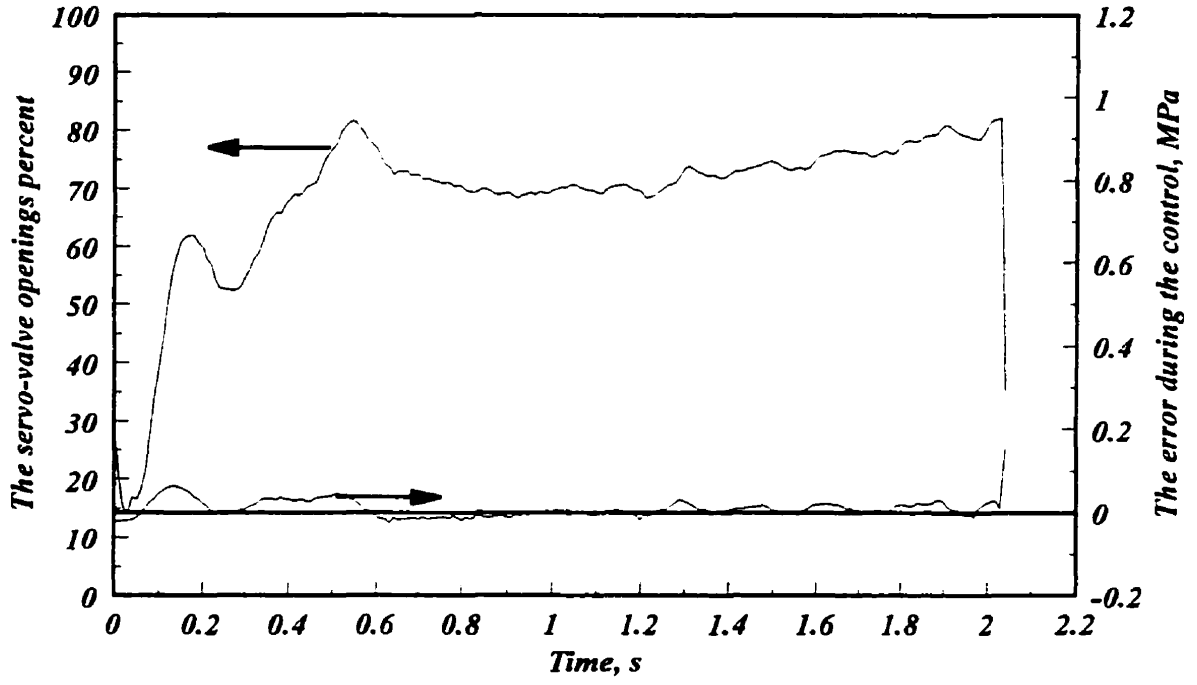


**Figure 5.23** IMC controller, cycle number 51

To study the effectiveness of the controller, a non-linear set-point is used. Figure 5.24 shows the result. In the beginning, the set-point is linear with a slope of 1.72 MPa/s. After a while, the set-point has a step equal to 0.34 MPa to a new slope of 2.41 MPa/s. The cavity pressure follows the set-point very well prior to the jump. At the step in the set-point, there is a time delay which is related to system dynamics. Then, the profile reaches the set-point again. The servo-valve opening shows saturation at the step in the set-point. This is due to setting a slope higher than the physical capacity of the machine. To evaluate a more realistic set-point, the step in Figure 5.24 is replaced by a third order polynomial. Figure 5.25 shows the result for the new non-linear set-point. The experimental cavity pressure follows the set-point very well, although some saturation is still evident.

The last part of experiment was to apply the IMC controller on a cavity with irregular shape. Figure 5.26 shows the irregular cavity. Figure 5.27 shows the result of the experiment. The cavity pressure follows the set-point very good. The value of $a_{IMC}$ in this case was 0.7.

## 5.8 Control Studies for Polystyrene

The second material used in this research was polystyrene, which is an amorphous thermoplastic polymer. The transfer function for polystyrene during the filling phase is the same as Equation (5.14). This derived transfer function is the fifth order and has one zero and five poles similar to Equation (5.14) for polyethylene. Table 5.3 gives the numerical values of a typical transfer function for $i_s$ 80% and $i_R$ 10% at time 1.4 s, for the polystyrene. It is obvious that the only zero of the system is very close to the fifth root. They essentially cancel each other out and the transfer function is a fourth order system without any zero:

$$P_c(s) = \frac{n_1}{\tau(s-r_1)(s-r_2)(s-r_3)(s-r_4)} T(s) \qquad (5.38)$$

The fourth order transfer function was used to conduct control studies.

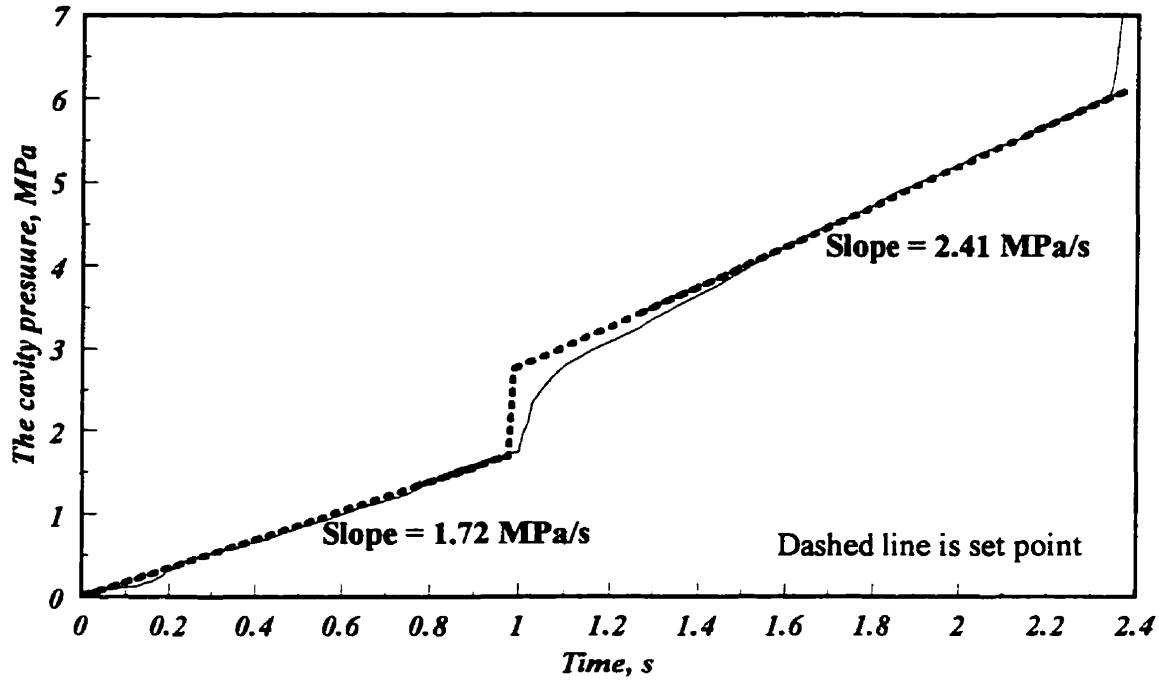


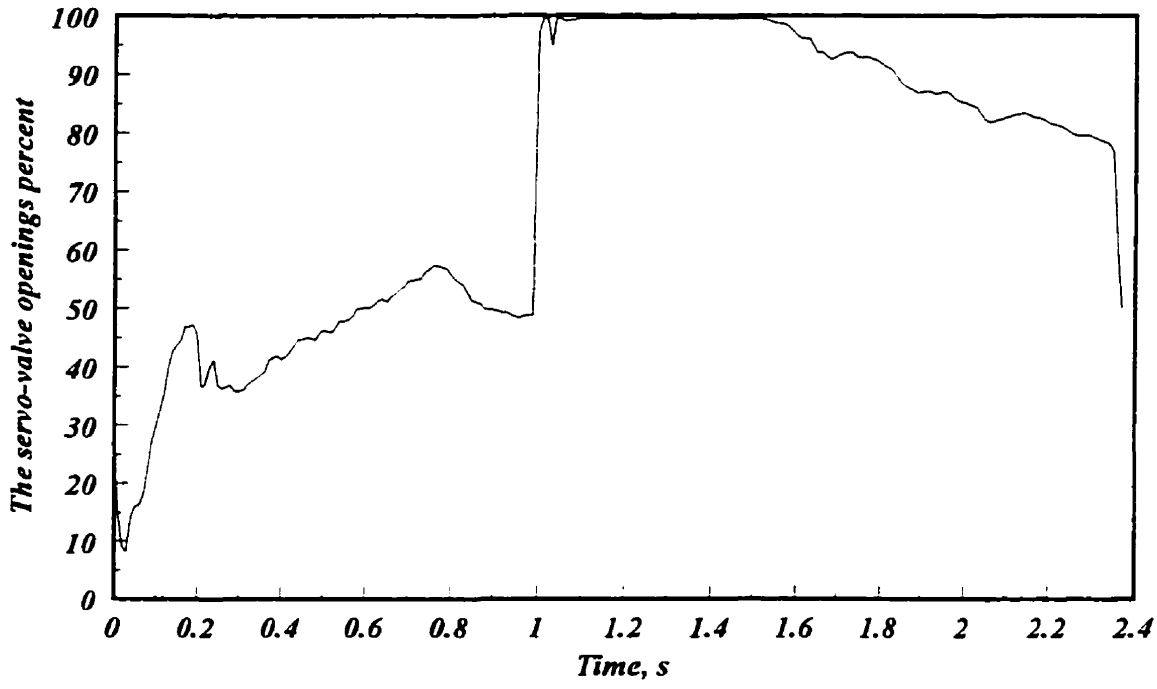


**Figure 5.24** The non-linear set point with IMC controller

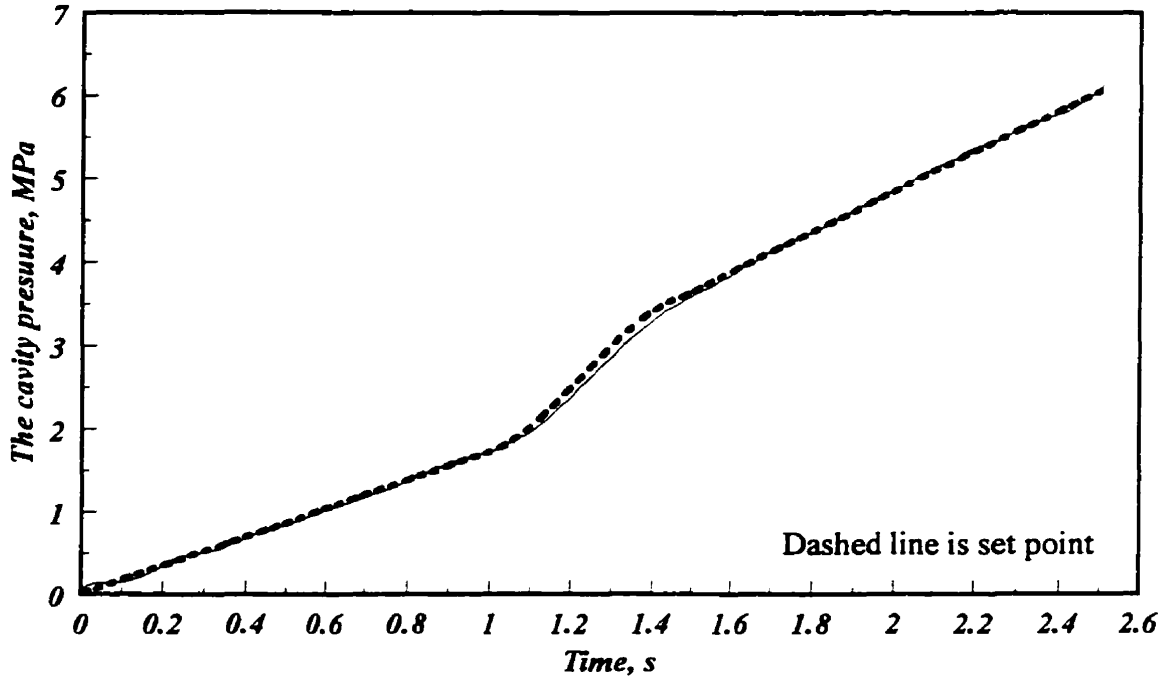


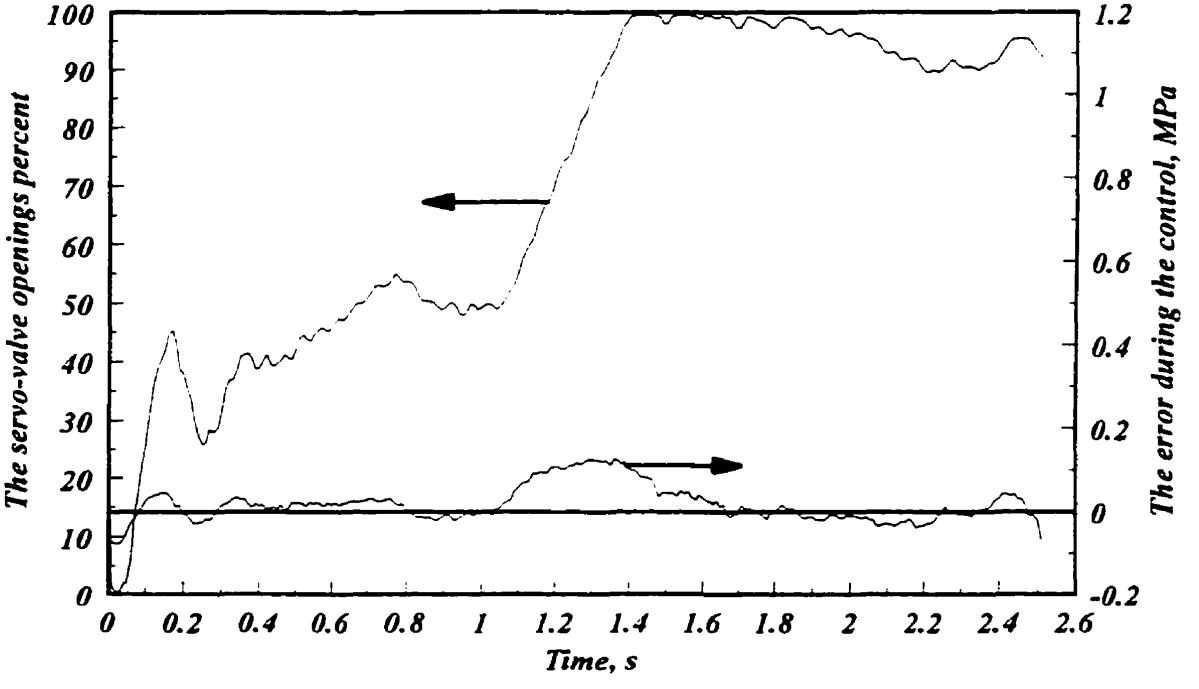


**Figure 5.25** Realistic non-linear set point result with IMC controller

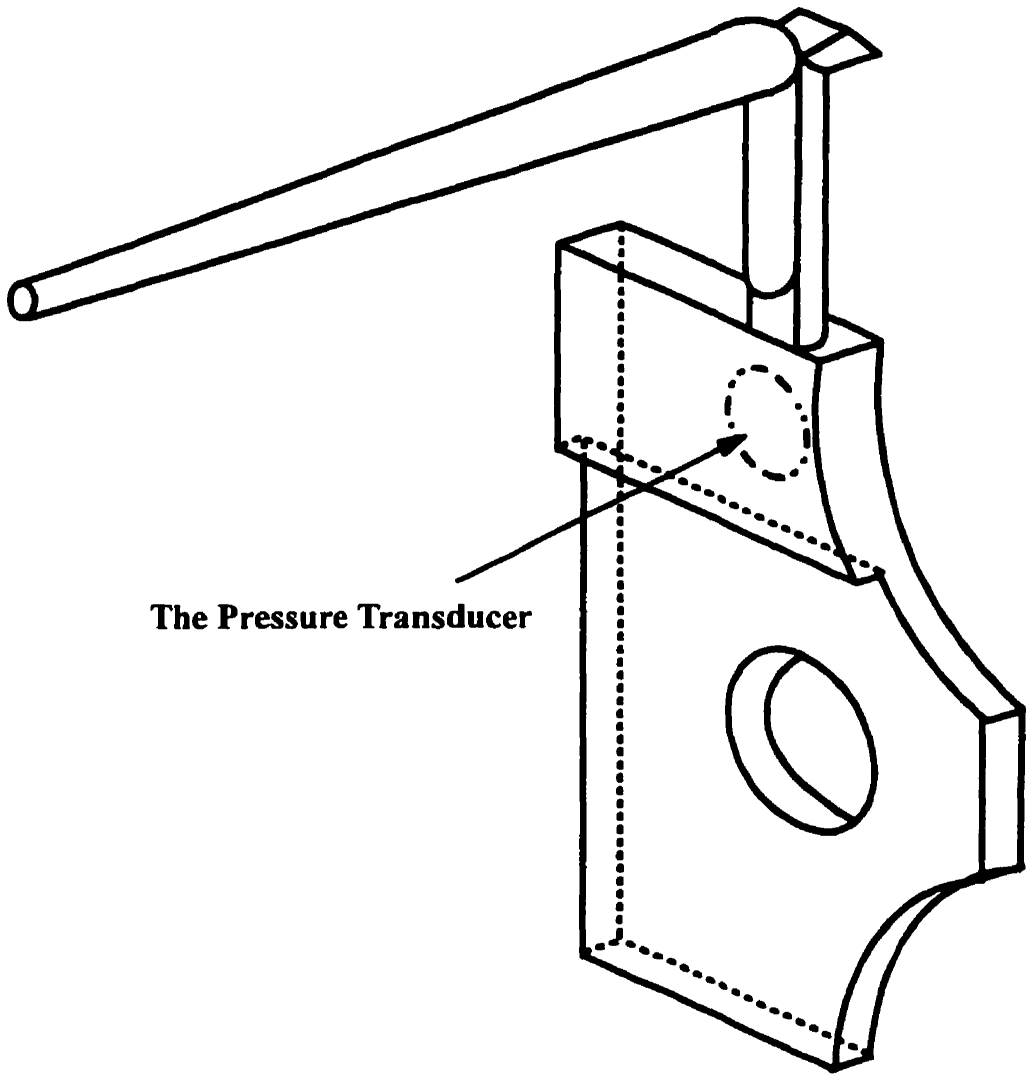


**Figure 5.26** Schematic of the irregular mold cavity

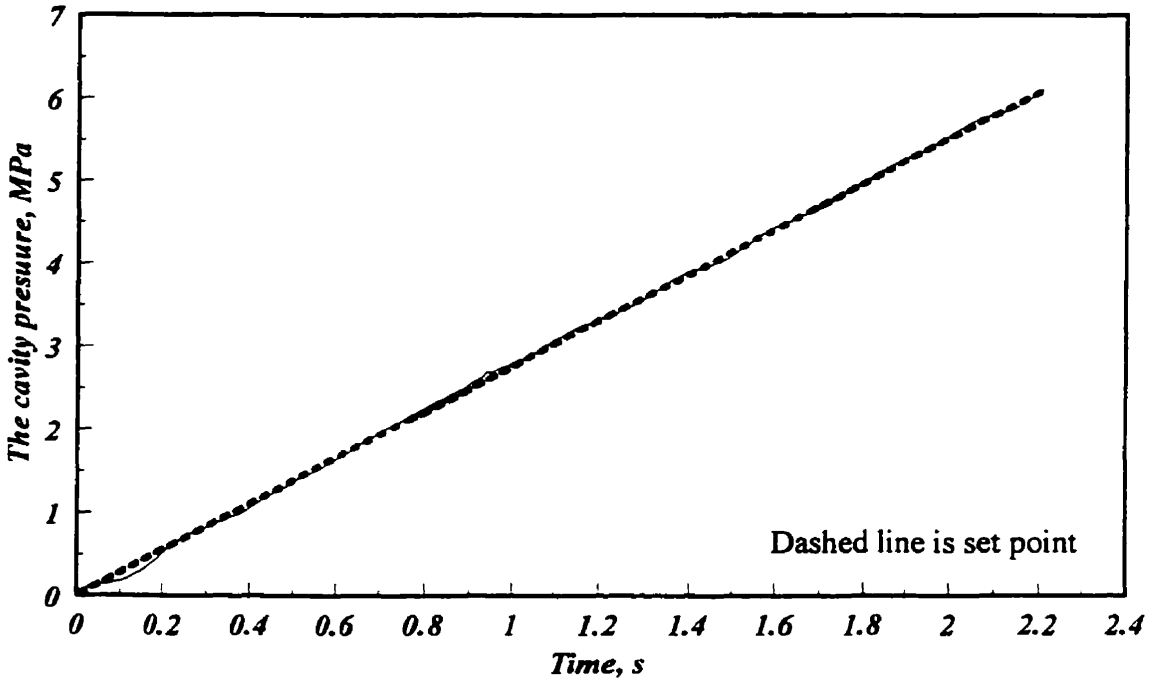


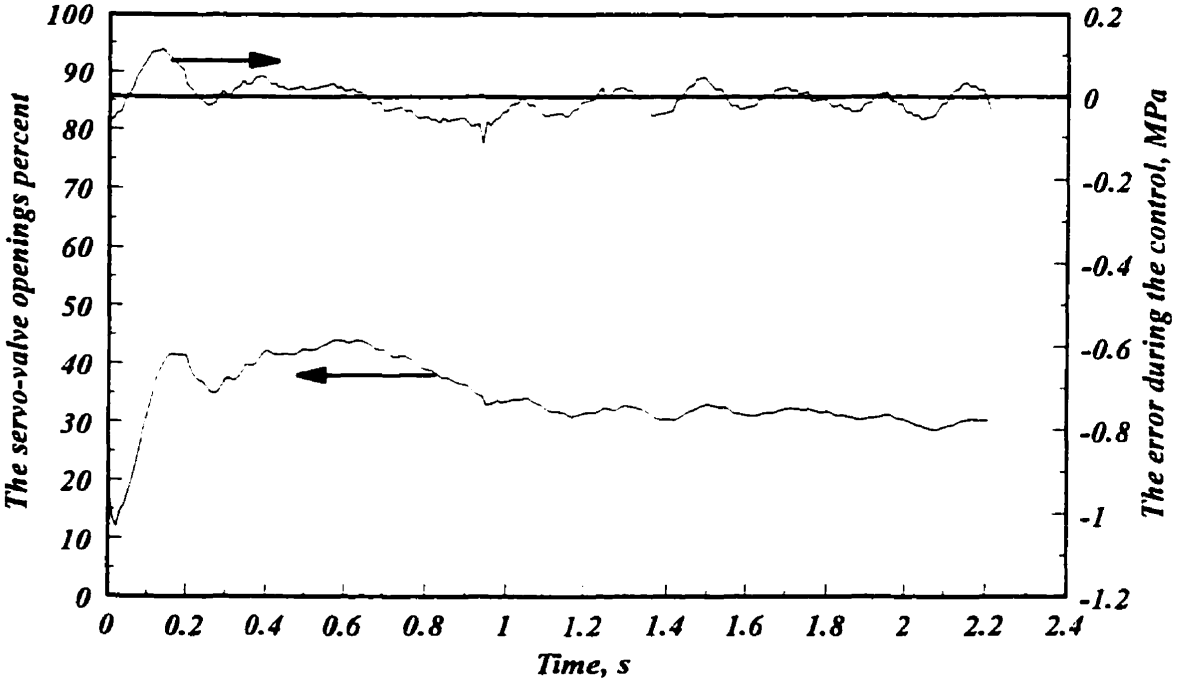


**Figure 5.27** IMC controller with irregular cavity, a $_{IMC}$=0.7

| | |
|---|---|
| Zero | $-6.395\times10^{-4}$ |
| First pole | $-57.618+33.77\times i$ |
| Second pole | $-57.618-33.772\times i$ |
| Third pole | $-88.781+373.945\times i$ |
| Fourth pole | $-88.781-373.945\times i$ |
| Fifth pole | $-6.578\times10^{-4}$ |

**Table 5.3** - Roots of transfer function, $i_s=40\%$, $i_R=15\%$, $t=2.3$ s

### 5.8.1 Discrete Transfer Function

The discrete form of the dynamic model for cavity pressure was derived from the corresponding continuous model utilizing the z-transform method. To discretize the transfer function, Equation (5.38) is expanded via partial fractions, as:

$$G(s) = \frac{n_1}{\tau (s-r_1)(s-r_2)(s-r_3)(s-r_4)} = \frac{n_1}{\tau}\left[\frac{As+B}{s^2-2as+a^2+b^2} + \frac{Ds+E}{s^2-2cs+c^2+d^2}\right] \tag{5.39}$$

where

$$r_1 = a+b\times i \quad , \quad r_2 = a-b\times i$$
$$r_3 = c+d\times i \quad , \quad r_4 = c-d\times i \tag{5.40}$$

and A, B, D, and E are:

$$A = \frac{2c-2a}{DEN.}$$
$$B = \frac{(2c-2a)^2-\left[a^2+b^2-(c^2+d^2)+2c(2c-2a)\right]}{DEN.}$$
$$D = \frac{2a-2c}{DEN.} \tag{5.41}$$
$$E = \frac{a^2+b^2-(c^2+d^2)+2c(2c-2a)}{DEN.}$$
$$DEN. = (c^2+d^2)(2c-2a)^2 + \left[(a^2+b^2)-(c^2+d^2)\right]\left[(a^2+b^2)-(c^2+d^2)+2c(2c-2a)\right]$$

The discretization with zero-order hold is:

$$G(z) = \frac{n_1}{\tau}\left[\frac{b_1 z^{-1}+b_2 z^{-2}}{1+a_1 z^{-1}+a_2 z^{-2}} + \frac{d_1 z^{-1}+d_2 z^{-2}}{1+c_1 z^{-1}+c_2 z^{-2}}\right] \tag{5.42}$$

where

$$
\begin{aligned}
a_1 &= -2e^{a\Delta t}\cos b\Delta t \qquad\qquad a_2 = e^{2a\Delta t} \\
b_1 &= \frac{-B}{a^2+b^2} - e^{a\Delta t}\left[\frac{A}{b}\sin b\Delta t + \frac{B}{b}\frac{a}{a^2+b^2}\sin b\Delta t - \frac{B}{a^2+b^2}\cos b\Delta t\right] \\
b_2 &= \frac{Ae^{a\Delta t}}{a^2+b^2}\left[\frac{B}{A}e^{a\Delta t} - \frac{B}{A}\cos b\Delta t - \frac{a^2+b^2+\frac{aB}{A}}{b}\sin b\Delta t\right]
\end{aligned}
\tag{5.43}
$$

and

$$
\begin{aligned}
c_1 &= -2e^{c\Delta t}\cos d\Delta t \qquad\qquad c_2 = e^{2c\Delta t} \\
d_1 &= \frac{-E}{c^2+d^2} - e^{c\Delta t}\left[\frac{D}{d}\sin d\Delta t + \frac{E}{d}\frac{c}{c^2+d^2}\sin d\Delta t - \frac{E}{c^2+d^2}\cos d\Delta t\right] \\
d_2 &= \frac{De^{c\Delta t}}{c^2+d^2}\left[\frac{E}{D}e^{c\Delta t} - \frac{E}{D}\cos d\Delta t - \frac{c^2+d^2+\frac{cE}{D}}{d}\sin d\Delta t\right]
\end{aligned}
\tag{5.44}
$$

Finally, rearrangement of this equations, with zero-order hold, gives the discretized transfer function:

$$
G(z) = \frac{g_1 z^{-1} + g_2 z^{-2} + g_3 z^{-3} + g_4 z^{-4}}{1 + h_1 z^{-1} + h_2 z^{-2} + h_3 z^{-3} + h_4 z^{-4}} \tag{5.45}
$$

The relationship for $g_1$, $g_2$, $g_3$, $g_4$, $h_1$, $h_2$, $h_3$, and $h_4$ are:

$$g_1 = \frac{n_1}{\tau}(b_1 + d_1) \qquad g_2 = \frac{n_1}{\tau}(b_1c_1 + b_2 + d_1a_1 + d_2)$$

$$g_3 = \frac{n_1}{\tau}(b_1c_2 + b_2c_1 + d_1a_2 + d_2a_1) \qquad (5.46)$$

$$g_4 = \frac{n_1}{\tau}(b_2c_2 + d_2a_2)$$

$$h_1 = c_1 + a_1 \qquad h_2 = c_2 + a_1c_1 + a_2$$

$$h_3 = a_1c_1 + a_2c_1 \qquad h_4 = a_2c_2$$

### 5.8.3 Controller Selection and Design

Some experiments were run with polystyrene. In this section, some of the results are shown to compare with polyethylene results. For the sake of brevity, only two controllers were applied: a PID ramp set-point tuned controller with the ITAE tuning and an IMC controller. The quality of the results is similar to those obtained with polyethylene. Figure 5.28 shows the experimental result for the PID ramp set-point tuned with ITAE criterion. Figure 5.29 shows the experimental result for the IMC controller with $a_{IMC}$=0.5. The error is less noisy in the polystyrene case. This means that the controller action is better for polystyrene.

## 5.9 Conclusions

The dynamics and control of cavity pressure during the filling phase was studied. A physically based model was used to study the dynamics of the process. Consequently, a linear transfer function with time-varying parameters was derived to continue the control studies. Different controllers with distinct tunings were designed. The results included adaptive PI and PID controllers for the filling phase. Experimental results indicated that the controllers yield accurate results for the injection molding of high density polyethylene and amorphous polystyrene. The IMC controller showed excellent controller action for the process. Applying the controller to an irregular cavity, with

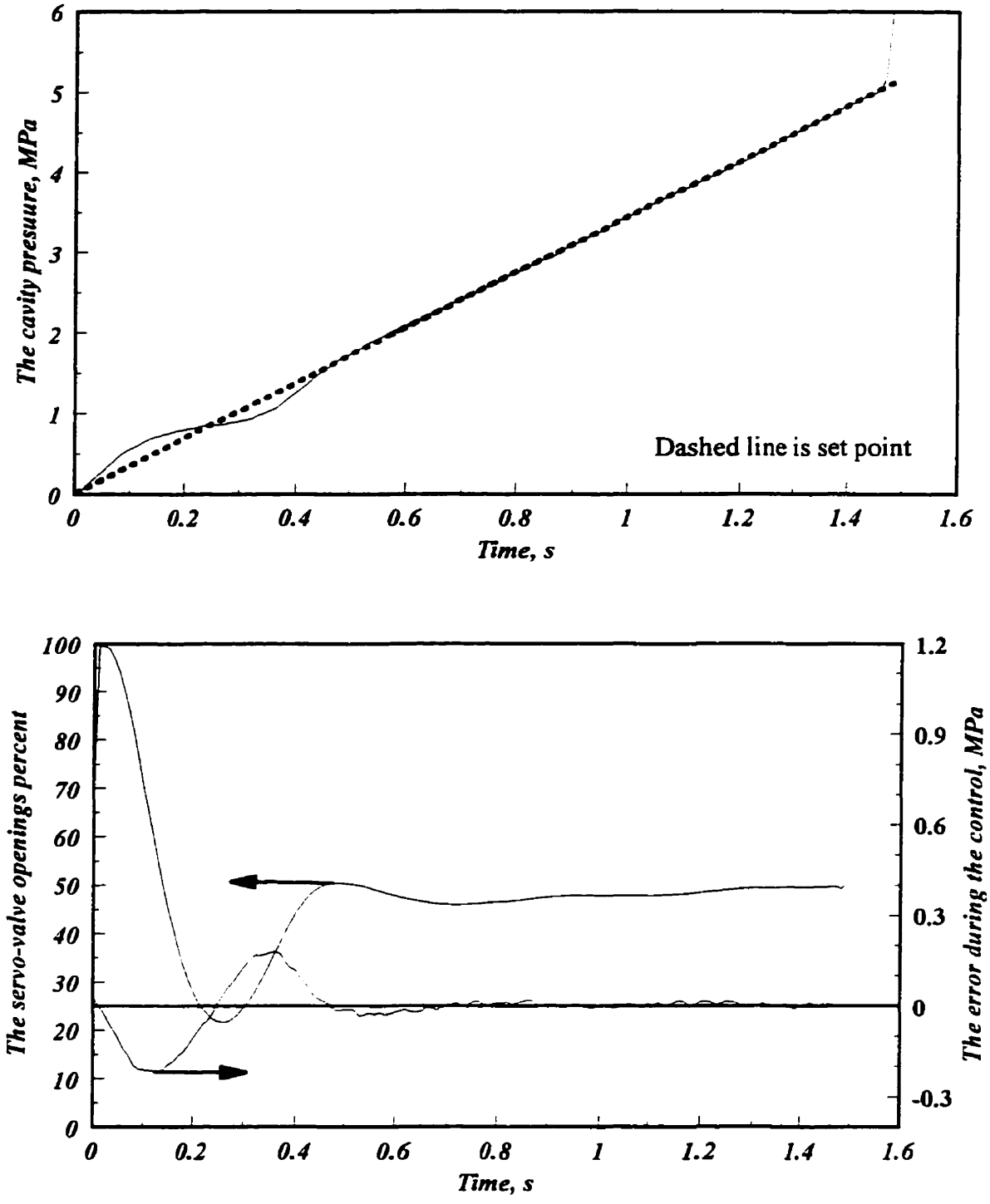


**Figure 5.28** PID ramp servoproblem tuned controller with ITAE criteria

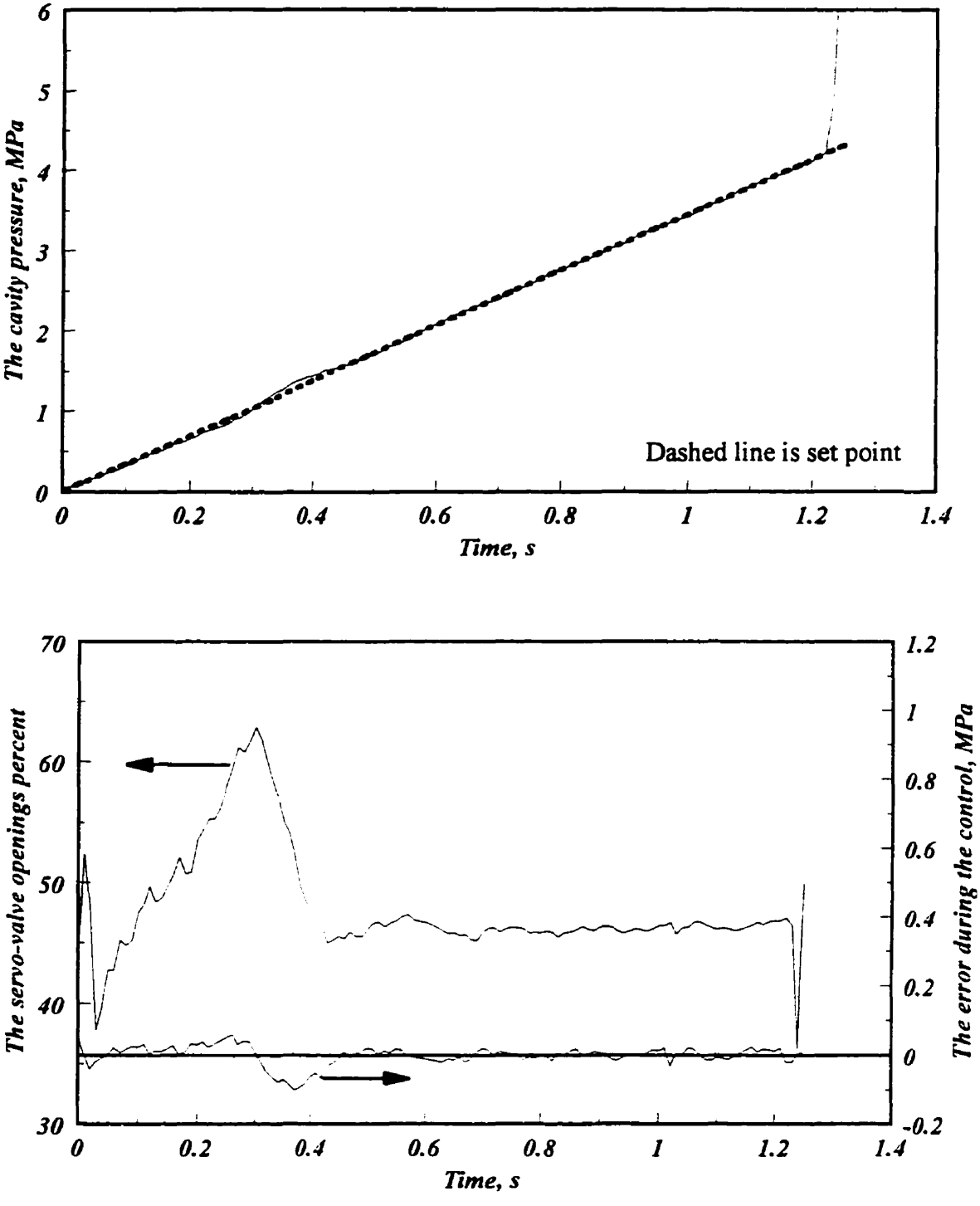


**Figure 5.29** IMC controller result for polystyrene

variable cross-section and thickness, confirmed its capacity to control complex commercial products. To the author's best knowledge, this is the first successful control of the filling phase of the injection molding process using a physically-based model.

# CHAPTER 6

# DYNAMICS AND CONTROL OF THE PACKING PHASE

## 6.1 Introduction

The melt flow rate decreases substantially after the cavity is completely filled and packing causes the pressure within the mold cavity to rise rapidly to a peak value. The peak cavity pressure is an important processing variable, as it influences the molded article quality [118]. Hence, controlling the peak cavity pressure and holding pressure is essential. In the previous chapter, the dynamics and control of the cavity pressure during the filling phase were discussed. It was also shown that the control of the cavity pressure profile during the filling phase is successful. Cavity pressure at the beginning of the packing phase will be the same as at the end of the filling phase.

This chapter deals with the following issues:

(1) Transition from the filling to the packing phase.

(2) Dynamics of the packing phase.

(3) Control of cavity pressure during the packing phase.

(4) Experimental evaluation of control alternatives.

## 6.2 Transition from Filling-to-Packing

Sequential control is vital for an automated cyclic process and is essential to the operation of injection molding machines. The filling-to-packing transition should take

place at an appropriate time which reflects the completion of the filling phase. Identification of the filling-to-packing transition has an important influence on the proper control of cavity pressure during packing [119].

Traditionally, transitional sequential actions are achieved by open loop control. Such actions are typically triggered by limit switches which detect the positions of different machine parts, together with electro-mechanical relays, which determine the various phases of the injection operation, and timers which control the phase duration and have no interaction with process itself. The result is large variability in part quality, particularly in the weight and dimensions of the molded article.

Different closed loop strategies have been suggested and evaluated to determine the transition points [120,121,122,96]. The determination of the filling-to-packing transition could be based on one or a combination of the following criteria:

(1) Ram screw position and velocity,

(2) Hydraulic pressure,

(3) Cavity pressure or its derivative.

### 6.2.1 Ram Position and Velocity Switching Criteria

Switching based on the ram position at the end of the filling phase tends to be an unreliable method, unless no cushion is used. Using cushion, by its nature, implies that the ram position at the end of the filling phase will vary from shot to shot. This variation makes ram position unsuitable for determining the point of switching to the packing phase. On the other hand, using zero cushion risks under-pack or short shots and is generally avoided by most process engineers. The same argument is valid for velocity based criteria. Therefore, switching over with the ram position and velocity as criteria does not provide an appropriate indicator of transition from the filling-to-packing phase.

### 6.2.2 Hydraulic Pressure Switching Criterion

The use of hydraulic pressure for switching over is not suitable, because the

hydraulic pressure peak can occur in the early stages of the filling phase. Moreover, the hydraulic pressure is too remote from cavity pressure and can be influenced by disturbances such as fluctuation in the polymer properties and barrel temperature. Hydraulic pressure is most suitable for transition detection when it rises steadily as the mold fills and packs. This is not the case for all molding processes, unless a relatively long filling time is used.

A combination of ram position and hydraulic pressure has been suggested as a working strategy [123]. During the filling phase, the ram position or velocity control is applied until the cavity is about 90%-98% filled without any packing. The injection pressure at this point will be used to determine the filling-to-packing transition.

### 6.2.3 Cavity Pressure or its Derivative Switching Criteria

A cavity pressure profile reflects closely the state of the material inside the mold cavity. Therefore, cavity pressure and related switch over criteria have been studied in recent years. Cavity pressure gradually increases during the filling phase and, as soon as the cavity is full, it increases rapidly to a peak value. To switch from the filling to the packing phase, the value of cavity pressure or its derivative can be used. However, there is no clear location for the placement of a melt pressure sensor. Sensors placed in the cavity near the gate have been shown to be a good choice [37,96]. The switch is actuated when the cavity pressure at a given location reaches a certain value. Unfortunately, the final value of the pressure during the filling is a function of processing conditions and, therefore, it varies. The uncertainty at the end of filling reduces the quality of control performance. On the other hand, the derivative of cavity pressure shows a large change at the end of the filling phase, and is a good indicator of the switch over point.

Investigation of the different switch over techniques has shown that significant differences in molded article repeatability are observed when different techniques are applied [124]. It appears that strategies based on the cavity pressure are the most effective ones. Criteria based on the time derivative of cavity pressure appear to be the

best for the switch point. This technique represents a general method which is not restricted to any specific machine or limited by processing conditions. Switching with regard to the time derivative of cavity pressure was chosen for this study.

## 6.3 Dynamics of Cavity Pressure

The objective of this section is to consider a dynamic model which relates the response of cavity gate pressure to the changes in the servo-valve openings. Chapter 4 gave the details of a lumped model of injection molding process which is suitable for control purposes. Particularly, section 4.3 discussed the modeling of the packing phase. The summary of the model for the packing phase is given in section 4.3.2. Incorporating the dynamics of the servo-valves, discussed in section 5.2.1, into the model, gives a description of the dynamic behavior of the injection molding process during the packing phase.

### 6.3.1 The Non-Linear State Equations for Packing

A lumped parameter model was derived in chapter 4 to describe the dynamics of the injection molding process. Each lumped parameter is like a state variable of the system. The following set gives the governing equations for the polymer melt and hydraulic oil during the packing phase:

$$
\begin{aligned}
\frac{dq_r}{dt} &= F_1 = -\frac{1}{\tau} q_r + \frac{k_v\sqrt{P_h}}{\tau}\, i_R \\
\frac{dq_s}{dt} &= F_2 = -\frac{1}{\tau} q_s + \frac{k_v\sqrt{P_s - P_h}}{\tau}\, i_S \\
\frac{dP_h}{dt} &= F_3 = \frac{\beta_h}{V_{h0} + A_h z}\{q_s - q_r - A_h v_z\} \\
\frac{dz}{dt} &= F_4 = v_Z \\
\frac{dv_z}{dt} &= F_5 = \frac{1}{M}\left[A_h P_h - A_n P_n - 2\pi\eta_0 R_n^{1-n}(L_0 + z)\frac{(s-1)^n}{(k_r^{1-s}-1)^n} v_z^n\right] \\
\frac{dP_n}{dt} &= F_6 = \frac{\beta_p}{V_{n0} - A_n z}\left[A_n v_z - \sqrt[n]{\frac{P_n - P_{gate}}{k_t}}\right] \\
\frac{dP_{gate}}{dt} &= F_7 = \frac{\beta_p}{V_t}\sqrt[n]{\frac{P_n - P_{gate}}{k_t}}
\end{aligned}
\qquad (6.1)
$$

where $F_1$ through $F_7$ are state equations, and $q_r$ and $q_s$ are hydraulic oil flow rates through relief and supply servo-valves, respectively.

The first two equations express the dynamics of the hydraulic system. The third equation is an application of the integral mass balance to the injection cylinder. Application of Newton's second law to the ram screw system yields the fifth equation. The fourth equation shows the relationship between the ram velocity and displacement. The sixth and seventh equations are the result of mass balance on the nozzle and polymer delivery system. Obviously, this is a set of non-linear ordinary differential equations. To conduct the control studies this set of equations was linearized.

## 6.4 Model Linearization

The model linearization procedure was explained in section 5.3. The same approach is used to linearize the non-linear model of the packing phase around the linearization point. The linearized model is:

$$\begin{aligned}
\frac{dQ_r}{dt} &= -\frac{1}{\tau}Q_r + \frac{a}{\tau}H + \frac{b}{\tau}R \\
\frac{dQ_s}{dt} &= -\frac{1}{\tau}Q_s - \frac{c}{\tau}H + \frac{d}{\tau}T \\
\frac{dH}{dt} &= -eQ_r + eQ_s - fZ - A_h eV \\
\frac{dZ}{dt} &= V \\
\frac{dV}{dt} &= gH - iZ - jV - kN \\
\frac{dN}{dt} &= lZ + mV - nN + nP_c \\
\frac{dP_c}{dt} &= pN - pP_c
\end{aligned} \tag{6.2}$$

The parameters a through f are defined as:

$$\begin{aligned}
a &= \frac{k_v i_{R0}}{2\sqrt{P_{h0}}} & b &= k_v\sqrt{P_{h0}} \\
c &= \frac{k_v i_{S0}}{2\sqrt{P_s - P_{h0}}} & d &= k_v\sqrt{P_s - P_{h0}} \\
e &= \frac{\beta_h}{V_{h0} + A_h z_0} & f &= \frac{\beta_h A_h (q_{s0} - q_{r0} - A_h v_{z0})}{(V_{h0} + A_h z_0)^2}
\end{aligned} \tag{6.3}$$

The parameters g through k are defined as:

$$\begin{aligned}
g &= \frac{A_h}{M} & i &= \frac{2\pi\eta_0 R_n^{1-n}(s-1)^n v_{z0}^n}{M(k_r^{1-s}-1)^n} \\
j &= \frac{2\pi\eta_0 R_n^{1-n}(s-1)^n (L_0 + z_0) n v_{z0}^{(n-1)}}{M(k_r^{1-s}-1)^n} & k &= \frac{A_n}{M}
\end{aligned} \tag{6.4}$$

The parameters l through p are defined as:

$$l = \frac{\beta_p A_n \left( A_n v_{z0} - \sqrt[n]{\frac{P_{n0} - P_{gate0}}{k_t}} \right)}{(v_{z0} - A_n z_0)^2} \qquad m = \frac{\beta_p A_n}{V_{z0} - A_n z_0}$$

$$n = \beta_p \frac{\sqrt[n]{\frac{P_{n0} - P_{gate0}}{k_t}}}{(V_{z0} - A_n z_0) n (P_{n0} - P_{gate0})} \qquad p = \beta_p \frac{\sqrt[n]{\frac{P_{n0} - P_{gate0}}{k_t}}}{V_t n (P_{n0} - P_{gate0})} \qquad \textbf{(6.5)}$$

The linearized set of equations (in Laplace transformed form) is:

$$\begin{aligned}
s\ Q_r(s) &= -\frac{1}{\tau} Q_r(s) + \frac{a}{\tau} H(s) + \frac{b}{\tau} R(s) \\
s\ Q_s(s) &= -\frac{1}{\tau} Q_s(s) - \frac{c}{\tau} H(s) + \frac{d}{\tau} T(s) \\
s\ H(s) &= -e Q_r(s) + e Q_s(s) - f Z(s) - A_h e V(s) \\
s\ Z(s) &= V(s) \\
s\ V(s) &= g H(s) - i Z(s) - j V(s) - k N(s) \\
s\ N(s) &= l Z(s) + m V(s) - n N(s) + n P_c(s) \\
s\ P_c(s) &= p\ N(s) - p P_c(s)
\end{aligned} \qquad \textbf{(6.6)}$$

Algebraic manipulation reveals the transfer function from the controlled variable (the cavity pressure at the gate) to the manipulated variable (supply servo-valve opening) is:

$$P_c(s) = \frac{pge(l+ms)}{DEN.}(d+0.2b)T(s) = \frac{n_1 s + n_2}{\tau(s-r_1)(s-r_2)(s-r_3)(s-r_4)(s-r_5)(s-r_6)}\ T(s)$$

$$\begin{aligned}
DEN. = {} & \tau s^6 + (\tau n + \tau p + \tau j + 1)s^5 \\
& + [\tau i + \tau jn + \tau jp + \tau km + n + p + j + \tau gA_h e + e(c+a)]s^4 \\
& + [\tau in + \tau ip + \tau kl + \tau kmp + jn + + jp + i + km + \tau gf + \tau gA_h en \\
& + \tau gA_h ep + gA_h e + (en + ep + ej)(c+a)]s^3 \\
& + [klp\tau + in + ip + kl + kmp + \tau gnf + \tau gpf + fg + gA_h en + gA_h ep \\
& + (ejn + ejp + ei + ekm)(c+a)]s^2 \\
& + [klp + gnf + gpf + (ein + eip + ekl + ekmp)(c+a)]s + eklp(c+a)
\end{aligned} \tag{6.7}$$

This is representation of a linear and time-invariant system and can be used for control purposes. Table 6.1 gives the numerical values of a typical transfer function for $i_s$ 40% and $i_R$ 15 % at time 6.6 s for the high density polyethylene. The system is stable due to having negative real parts in all roots. The only zero of the system is very close to the last pole of the system which practically cancels it. In other words, a fifth order transfer function can be used to describe the dynamics of the system:

$$P_c(s) = \frac{n_1}{\tau(s-r_1)(s-r_2)(s-r_3)(s-r_4)(s-r_5)}\ T(s) \tag{6.8}$$

This transfer function is used in this research.

## 6.5 Transfer Function Discretization

To discretized transfer function, Equation (6.8) is expanded to partial fractions:

$$\begin{aligned}
G(s) &= \frac{n_1}{\tau(s-r_1)(s-r_2)(s-r_3)(s-r_4)(s-r_5)} \\
&= \frac{n_1}{\tau}\left[\frac{As+B}{s^2-2as+a^2+b^2} + \frac{C}{s-r_3} + \frac{D}{s-r_4} + \frac{E}{s-r_5}\right]
\end{aligned} \tag{6.9}$$

| | |
|---|---|
| Zero | $-5.539\times10^{-5}$ |
| First pole | -42.34 + - 239.26 i |
| Second pole | -42.34 - 239.26 i |
| Third pole | -72.80 |
| Fourth pole | -10.64 |
| Fifth pole | -0.46 |
| Sixth pole | $-5.54\times10^{-5}$ |

**Table 6.1** - Roots of transfer function, $i_s$=40%, $i_R$=15%, t=6.6 s

where

$$r_1 = a + bi \qquad , \qquad r_2 = a - bi \tag{6.10}$$

and A is:

$$\begin{aligned} A = & \frac{(r_4 - r_5)(r_5^2 - 2ar_5 + a^2 + b^2)(r_4^2 - 2ar_4 + a^2 + b^2)}{DEN.} \\ & + \frac{(r_5 - r_3)(r_5^2 - 2ar_5 + a^2 + b^2)(r_3^2 - 2ar_3 + a^2 + b^2)}{DEN.} \\ & + \frac{(r_3 - r_4)(r_3^2 - 2ar_3 + a^2 + b^2)(r_4^2 - 2ar_4 + a^2 + b^2)}{DEN.} \end{aligned} \tag{6.11}$$

and B is:

$$\begin{aligned} B = & \frac{(2a - r_3)(r_5 - r_4)(r_5^2 - 2ar_5 + a^2 + b^2)(r_4^2 - 2ar_4 + a^2 + b^2)}{DEN.} \\ & + \frac{(2a - r_4)(r_3 - r_5)(r_5^2 - 2ar_5 + a^2 + b^2)(r_3^2 - 2ar_3 + a^2 + b^2)}{DEN.} \\ & + \frac{(2a - r_5)(r_4 - r_3)(r_3^2 - 2ar_3 + a^2 + b^2)(r_4^2 - 2ar_4 + a^2 + b^2)}{DEN.} \end{aligned} \tag{6.12}$$

and C, D, and E are:

$$\begin{aligned} C &= \frac{(r_5 - r_4)(r_5^2 - 2ar_5 + a^2 + b^2)(r_4^2 - 2ar_4 + a^2 + b^2)}{DEN.} \\ D &= \frac{(r_3 - r_5)(r_5^2 - 2ar_5 + a^2 + b^2)(r_3^2 - 2ar_3 + a^2 + b^2)}{DEN.} \\ E &= \frac{(r_4 - r_3)(r_3^2 - 2ar_3 + a^2 + b^2)(r_4^2 - 2ar_4 + a^2 + b^2)}{DEN.} \end{aligned} \tag{6.13}$$

and the denominator, DEN., is:

$$
\begin{aligned}
&DEN. = \\
&(r_5-r_4)(r_5^2-2ar_5+a^2+b^2)(r_4^2-2ar_4+a^2+b^2)\left[-r_3r_4r_5(2a-r_3)+r_4r_5(a^2+b^2)\right] \\
&+(r_3-r_5)(r_5^2-2ar_5+a^2+b^2)(r_3^2-2ar_3+a^2+b^2)\left[-r_3r_4r_5(2a-r_4)+r_3r_5(a^2+b^2)\right] \\
&+(r_4-r_3)(r_3^2-2ar_3+a^2+b^2)(r_4^2-2ar_4+a^2+b^2)\left[-r_3r_4r_5(2a-r_5)+r_3r_4(a^2+b^2)\right]
\end{aligned}
\tag{6.14}
$$

The discretized form of the transfer function with zero order hold is:

$$
G(z)=\frac{n_1}{\tau}\left[\frac{b_1z^{-1}+b_2z^{-2}}{1+a_1z^{-1}+a_2z^{-2}}+\frac{d_1z^{-1}}{1+c_1z^{-1}}+\frac{f_1z^{-1}}{1+e_1z^{-1}}+\frac{h_1z^{-1}}{1+g_1z^{-1}}\right] \tag{6.15}
$$

where

$$
\begin{aligned}
&a_1=-2e^{a\Delta t}\cos b\Delta t \qquad\qquad a_2=e^{2a\Delta t} \\
&b_1=\frac{-B}{a^2+b^2}-e^{a\Delta t}\left[\frac{A}{b}\sin b\Delta t+\frac{B}{b}\frac{a}{a^2+b^2}\sin b\Delta t-\frac{B}{a^2+b^2}\cos b\Delta t\right] \\
&b_2=\frac{Ae^{a\Delta t}}{a^2+b^2}\left[\frac{B}{A}e^{a\Delta t}-\frac{B}{A}\cos b\Delta t-\frac{a^2+b^2+\frac{aB}{A}}{b}\sin b\Delta t\right]
\end{aligned}
\tag{6.16}
$$

and

$$
\begin{aligned}
&c_1=-e^{r_3\Delta t} \qquad d_1=\frac{C}{-r_3}\left(1-e^{r_3\Delta t}\right) \qquad e_1=-e^{r_4\Delta t} \\
&f_1=\frac{D}{-r_4}\left(1-e^{r_4\Delta t}\right) \qquad g_1=-e^{r_5\Delta t} \qquad h_1=\frac{E}{-r_5}\left(1-e^{r_5\Delta t}\right)
\end{aligned}
\tag{6.17}
$$

Finally, rearrangement of this equation, with a zero-order hold, gives the discretized transfer function:

$$
G(z)=\frac{\alpha_1z^{-1}+\alpha_2z^{-2}+\alpha_3z^{-3}+\alpha_4z^{-4}+\alpha_5z^{-5}}{1+\beta_1z^{-1}+\beta_2z^{-2}+\beta_3z^{-3}+\beta_4z^{-4}+\beta_5z^{-5}} \tag{6.18}
$$

The relationships for $\alpha_1$, $\alpha_2$, $\alpha_3$, $\alpha_4$, $\alpha_5$ are:

$$\alpha_1 = \frac{n_1}{\tau}(b_1 + d_1 + f_1 + h_1)$$

$$\alpha_2 = \frac{n_1}{\tau}(b_1 g_1 + b_1 e_1 + b_1 c_1 + b_2 + d_1 g_1 + d_1 e_1 + d_1 a_1 + f_1 g_1 + f_1 c_1 + f_1 a_1 + h_1 e_1 + h_1 c_1 + h_1 a_1) \quad (6.19)$$

and

$$\alpha_3 = \frac{n_1}{\tau}(b_1 e_1 g_1 + b_1 c_1 g_1 + b_1 c_1 e_1 + b_2 g_1 + b_2 e_1 + b_2 c_1 + d_1 e_1 g_1 + d_1 a_1 g_1 + d_1 a_1 e_1 + d_1 a_2 + f_1 c_1 g_1 + f_1 a_1 g_1 + f_1 a_1 c_1 + f_1 a_2 + h_1 c_1 e_1 + h_1 a_1 e_1 + h_1 a_1 c_1 + h_1 a_2) \quad (6.20)$$

and

$$\alpha_4 = \frac{n_1}{\tau}(b_1 c_1 e_1 g_1 + b_1 e_1 g_1 + b_2 c_1 g_1 + b_2 c_1 e_1 + d_1 a_1 e_1 g_1 + d_1 a_2 g_1 + d_1 a_2 e_1 + f_1 a_1 c_1 g_1 + f_1 a_2 g_1 + f_1 a_2 c_1 + h_1 a_1 c_1 e_1 + h_1 a_2 e_1 + h_1 a_2 c_1) \quad (6.21)$$

$$\alpha_5 = \frac{n_1}{\tau}(b_2 c_1 e_1 g_1 + d_1 a_2 e_1 g_1 + f_1 a_2 c_1 g_1 + h_1 a_2 c_1 e_1)$$

The relationship for $\beta_1$, $\beta_2$, $\beta_3$, $\beta_4$, and $\beta_5$ are:

$$\beta_1 = g_1 + e_1 + c_1 + a_1 \qquad \beta_2 = e_1 g_1 + c_1 g_1 + c_1 e_1 + a_1 g_1 + a_1 e_1 + a_1 c_1 + a_2$$
$$\beta_3 = c_1 e_1 g_1 + a_1 e_1 g_1 + a_1 c_1 g_1 + a_1 c_1 e_1 + a_2 g_1 + a_2 e_1 + a_2 c_1 \quad (6.22)$$
$$\beta_4 = a_1 c_1 e_1 g_1 + a_2 e_1 g_1 + a_2 c_1 g_1 + a_2 c_1 e_1 \qquad \beta_5 = a_2 c_1 e_1 g_1$$

The numerical values of $\alpha$'s and $\beta$'s are graphically shown in Figure 6.1. The points, in Figure 6.1, are calculated for every 0.1 s, and solid lines are a least-squares fit to the points for use in the control algorithm. The values of these parameters are functions of time, due to the nonlinear and time-varying nature of the injection molding process.

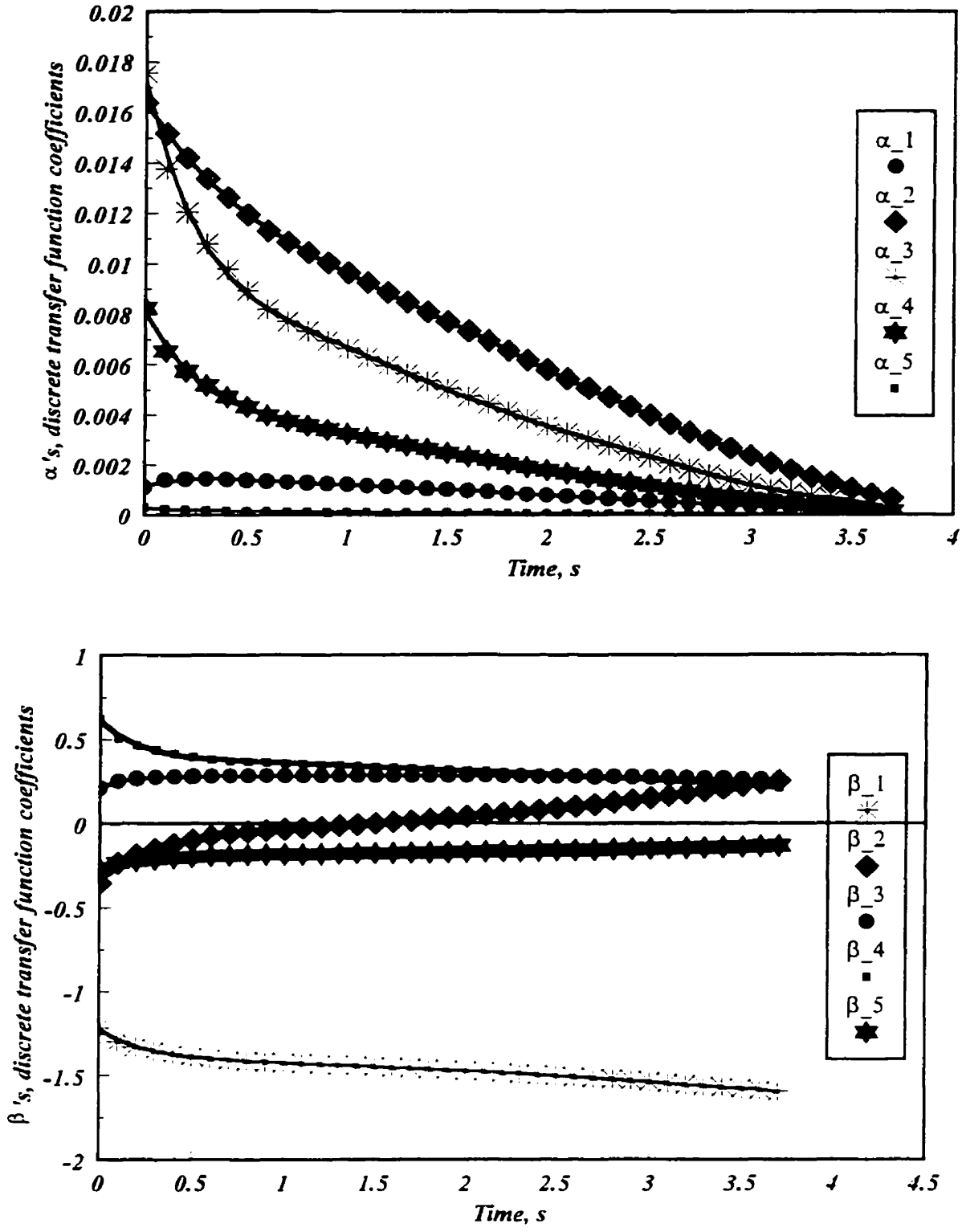


**Figure 6.1** Discrete transfer function coefficients

## 6.6 Controller Selection and Design

The results of the control studies and experiments in the filling phase showed that all PI, PID, and IMC controllers gave satisfactory results. It was expected that these controllers will also perform well in the packing phase. Thus, the PI controller was selected first for cavity pressure control during the packing phase. The results of the cavity gate dynamic model for the packing phase, presented in the previous sections, indicated the non-linear character of the process behavior. The effective design of the control loop for packing cavity pressure should compensate for this non-linearity. In the next sections, a feasible set-point profile is discussed then the different controllers are designed.

### 6.6.1 Pressure Profile of Packing Phase

Some researchers have used step change in cavity pressure as the transition from the final value in the filling phase to the final value of the packing phase [37,74]. However, this pressure profile is unrealistic and causes an inappropriate overshoot in experiments. This overshoot is reflected in structural disturbances in the final molded article. Abu Fara [37] considered a polynomial set-point for pressure profile during the packing phase. He obtained better control action with this profile. Gao [96] suggested a sum of two exponential terms after examining the open loop behavior of the system. Then, he used one exponential term for simplicity. This profile showed acceptable transition from the end of the filling phase to final value of the cavity pressure during the packing phase. The exponential cavity pressure profile is chosen as set-point in this study. The pressure profile during the packing phase is approximated by:

$$P_c = P_{FE} + (P_{PE} - P_{FE}) \times \left(1 - e^{-\frac{t - t_i}{\tau_i}}\right) \qquad (6.23)$$

where $P_{FE}$ and $P_{PE}$ are the pressure values at the end of filling and packing, respectively; $t_i$ is the filling time; $\tau_i$ is the time constant of the packing pressure profile.

### 6.6.2 PI Controller Design

The principle of a PI controller was discussed in section 5.5.2. This controller is the simplest controller which has the ability to eliminate error without any offset. This controller includes two setting parameters $k_c$ and $\tau_I$, which are controller gain and integral time constant, respectively. ITAE and ISE tuning criteria with step changes in set-point were used to calculate the optimum controller settings. The approach and calculation method are similar to those used for the filling phase. Figure 6.2 shows PI controller settings which include controller gain and integral time constant. Time zero corresponds to the beginning of the packing phase. The points, in Figures 6.2 and 6.3, are calculated from the linearized model at every 0.1 s, and solid lines are a least-squares fit to the points used in the control algorithm. During the packing phase, the controller gain increases because the process gain decreases due to solidification in the mold cavity.

### 6.6.3 PID Controller Design

This is the most popular controller in industry and normally gives good results when applied to chemical processes. The structure of this controller was explained in section 5.5.3. There are three parameters which should be determined in a manner to assure effective controller performance. The three parameters are controller gain $k_c$, integral time constant $\tau_I$, and derivative time constant $\tau_D$. Both ITAE and ISE tuning criteria have been used to calculate optimum setting parameters. Figure 6.3 shows the calculated parameters. The controller gain increases as expected. The integral time constant also increases. The derivative time constants are more or less constant for both the ITAE and ISE methods.

### 6.6.4 IMC Controller

IMC method was discussed in section 5.5.4. However, in this study, it is adaptive IMC due to the fact that coefficients of the transfer function are time-varying. The controller transfer function for the IMC method is given in Equation (5.29). Applying this equation to the packing transfer function, given in Equation (6.18),

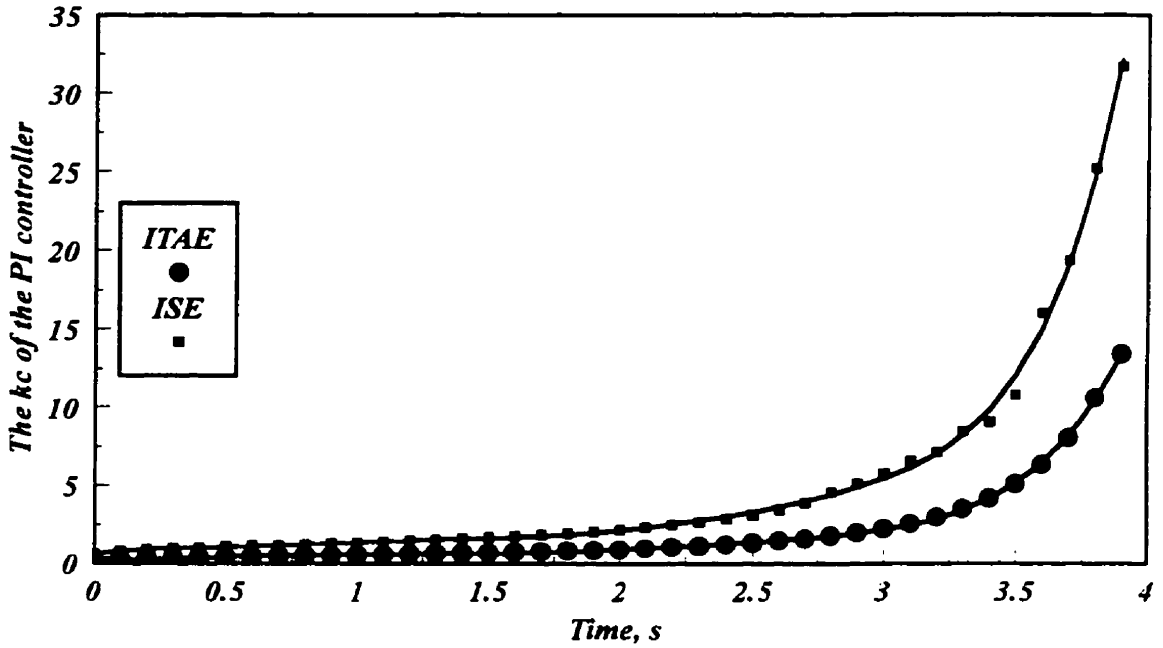


Figure 6.2a PI controller gain

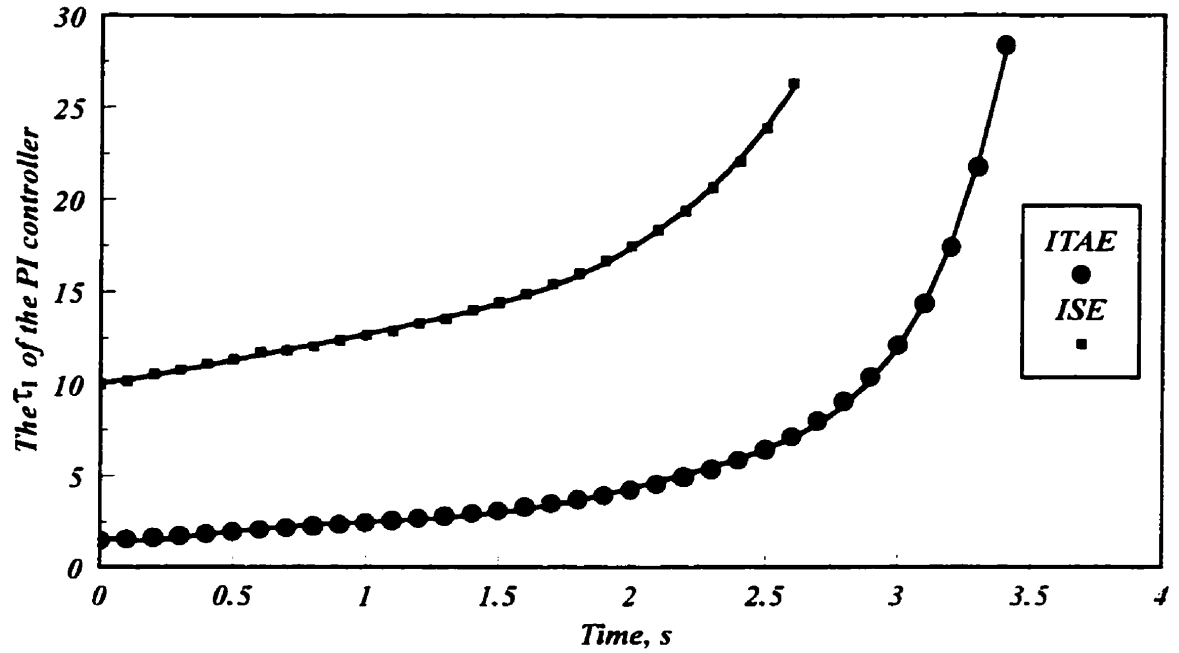


Figure 6.2b PI controller integral time constant

**Figure 6.2** PI controller settings

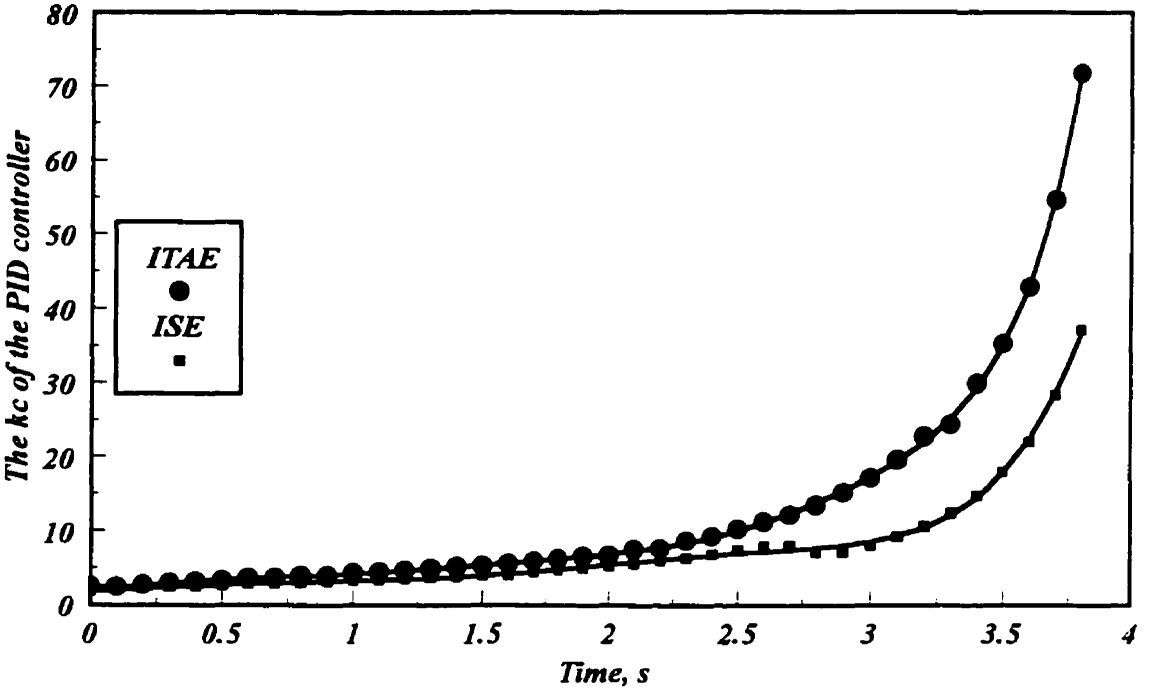


Fig. 6.3a PID controller gain

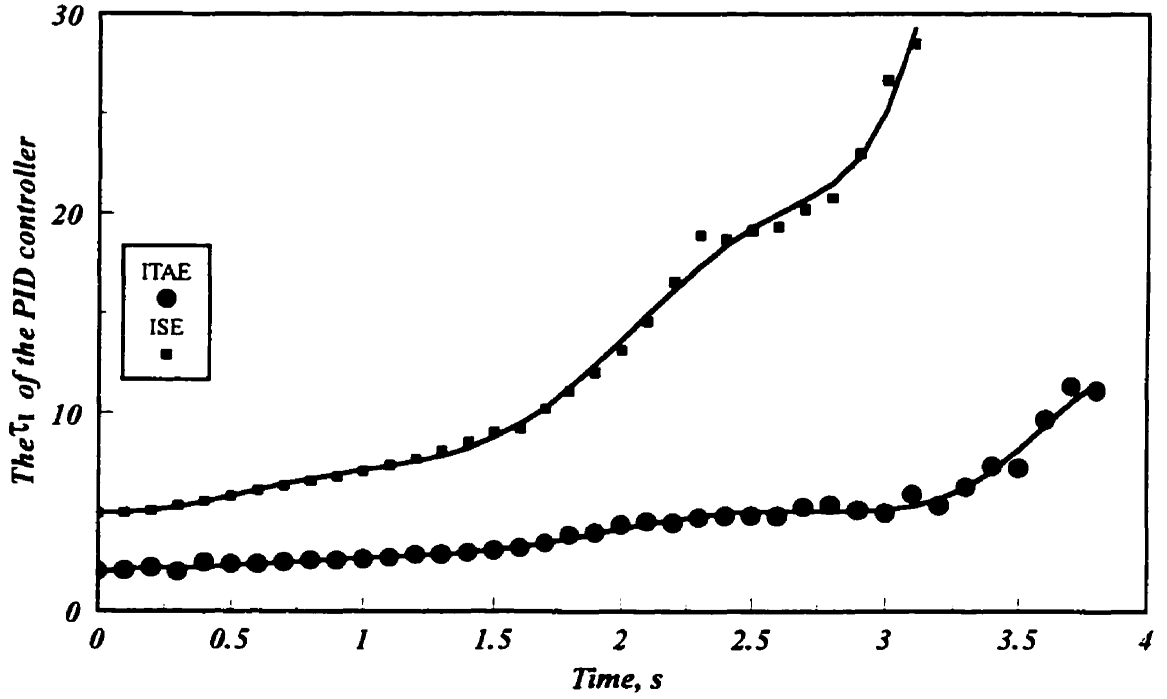


Fig. 6.3b The PID controller integral time constant

**Figure 6.3** PID controller settings

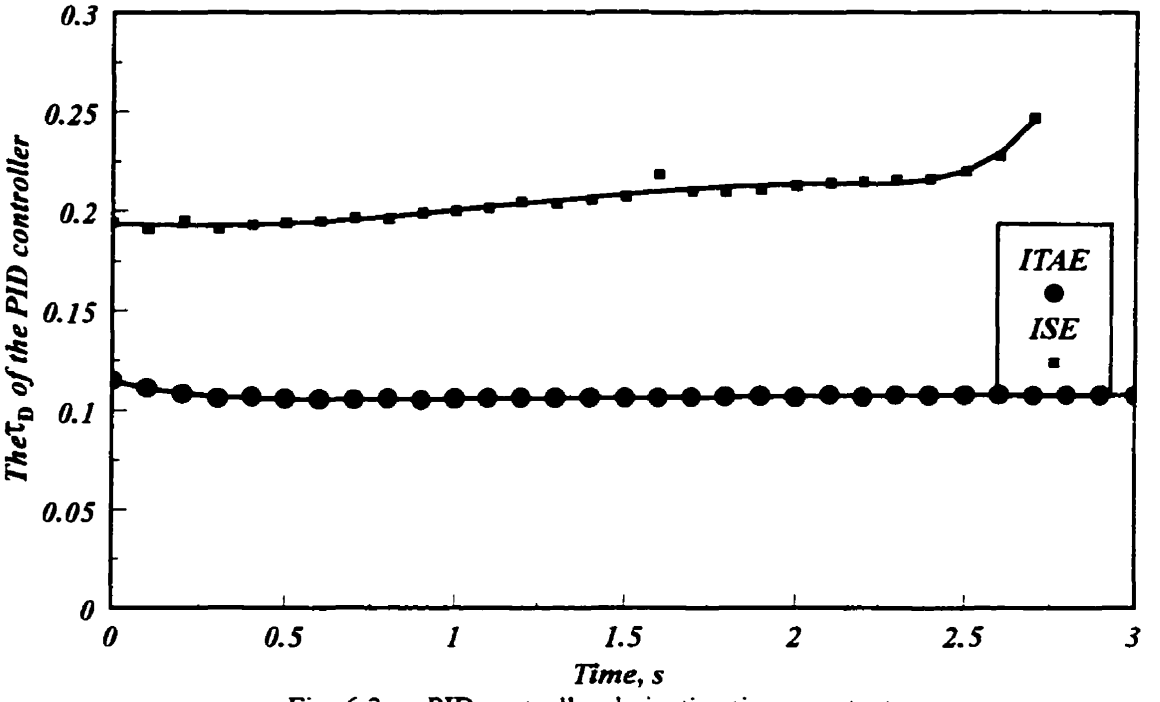


Fig. 6.3c PID controller derivative time constant

**Figure 6.3** PID controller settings

produces the IMC controller during packing:

$$G_c(z) = \frac{1-a_{IMC}}{1-z^{-1}} \times \frac{1+\beta_1 z^{-1}+\beta_2 z^{-2}+\beta_3 z^{-3}+\beta_4 z^{-4}+\beta_5 z^{-5}}{\alpha_1+\alpha_2 z^{-1}+\alpha_3 z^{-2}+\alpha_4 z^{-3}+\alpha_5 z^{-4}} \qquad (6.24)$$

where $a_{IMC}$ is an experimentally determined parameter equal to a value of 0.65 in this phase.

## 6.7 Packing Phase Control Experiments

In this section, the experimental results are shown for the high density polyethylene. These results are produced by applying the controllers for the control of cavity pressure during injection of high density polyethylene. The objective of this section is to demonstrate the feasibility of cavity pressure control during the packing phase of the injection molding cycle by performing a series of control experiments using PI, PID, and IMC controllers. Closed loop control experiments were carried out on the injection molding machine described in Chapter 3. The discretized form of the PI, PID, and IMC control laws tuned with ITAE and ISE were applied to the machine via the microcomputer system. The following experiments were performed:

(1) Control of the cavity pressure using PI, PID, and IMC controllers during the packing phase.

(2) Application of the controller with positive and negative steps in set-point.

### 6.7.1 Discretized Form of the Controllers

The discretized forms of the PI and PID controllers were given in section 5.6.1. The same equations are used in the packing phase control. The discretized IMC controller is different from that in filling control because the transfer function is different. Using the backward definition of z-transform, Equation (6.24) can be written as:

$$m(k) = m(k-1) + \frac{1}{\alpha_1}\{-\alpha_2 m(k-1) + (\alpha_2 - \alpha_3)m(k-2) + (\alpha_3 - \alpha_4)m(k-3) + (\alpha_4 - \alpha_5)m(k-4) + \alpha_5 m(k-5)\} + \frac{1-\alpha_{IMC}}{\alpha_1}\{e(k) + \beta_1 e(k-1) + \beta_2 e(k-2) + \beta_3 e(k-3) + \beta_4 e(k-4) + \beta_5 e(k-5)\} \quad (6.25)$$

## 6.8 Results and Discussion

A series of experiments were devised to test the ability and performance of the controllers. The results for the PI controller tuned with the ITAE are shown in Figure 6.4. The top figure shows the measured cavity pressure and the desired set-point. The ramp portion for times less than 2 seconds belongs to the filling phase that is controlled by the IMC controller. The cavity pressure begins to drop at about 20-21 s due to gate freezing. Thus, only the first 20 seconds of the cycle are shown in the figure. The experimental cavity pressure tracks the set-point very well. In the beginning of the packing phase, the cavity pressure is below the set-point and the controller is not fast. The lower figure shows the command sent to the servo-valve and the measured error. The error versus time is a good indicator of controller performance. It takes approximately two seconds for the error to decrease to approximately zero. The command to the servo-valve is not constant due to the controller's action. The curvature seen in the open loop cavity pressure is not seen in this figure, reflecting the controller ability to manipulate the cavity pressure. The maximum error is 1.0 Mpa and it occurs in the beginning of the packing phase where there is a step-like jump in cavity pressure. Figure 6.5 shows the performance of the PI controller tuned with ISE criterion. The measured cavity pressure is below the set-point. The performance of this controller seems to be better than the PI controller tuned with the ITAE criterion, and long time tracking is superior to the one tuned with ITAE.

Figures 6.6 and 6.7 show the PID controller performances tuned with ITAE and ISE criteria, respectively. Both controllers show very good performances. There was very little overshoot observed in the PID controller's results, which was not seen in the

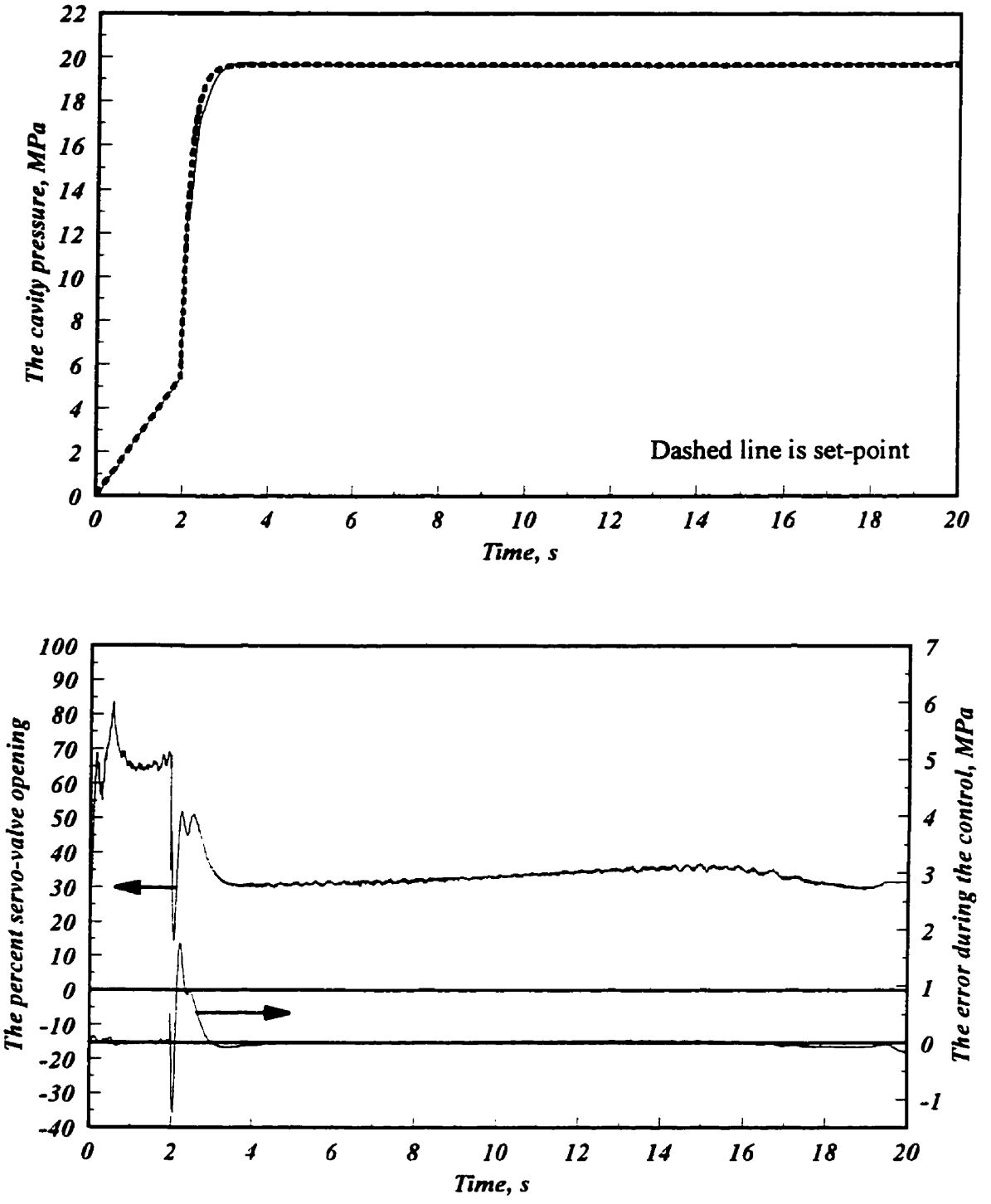


**Figure 6.4** PI controller tuned with ITAE criteria

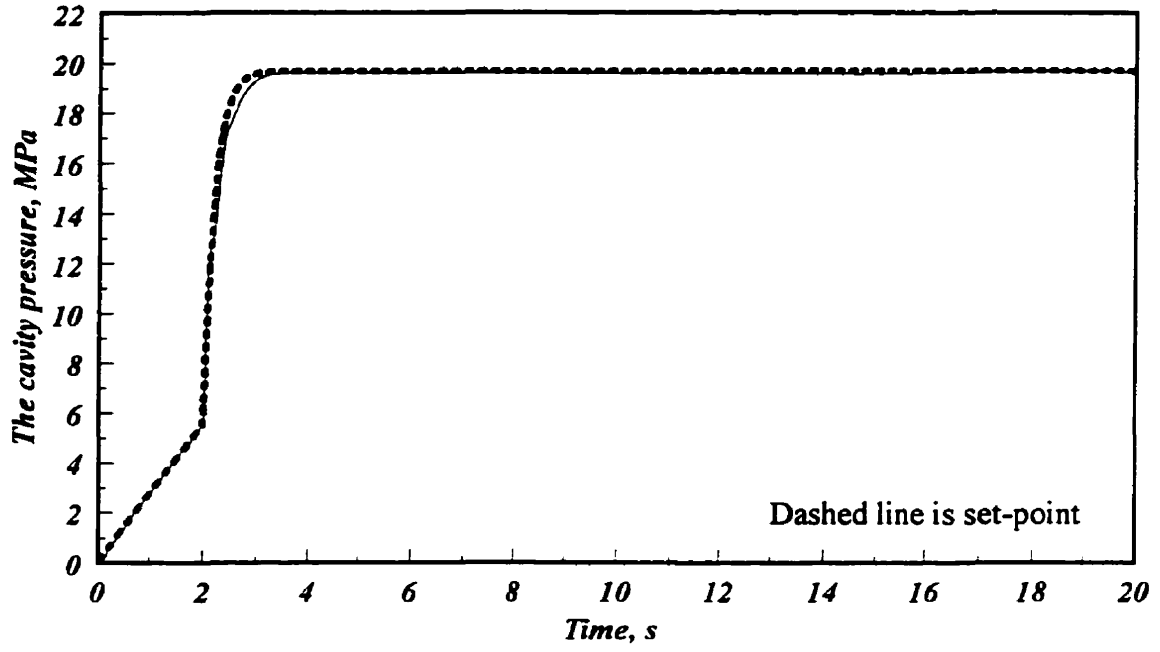


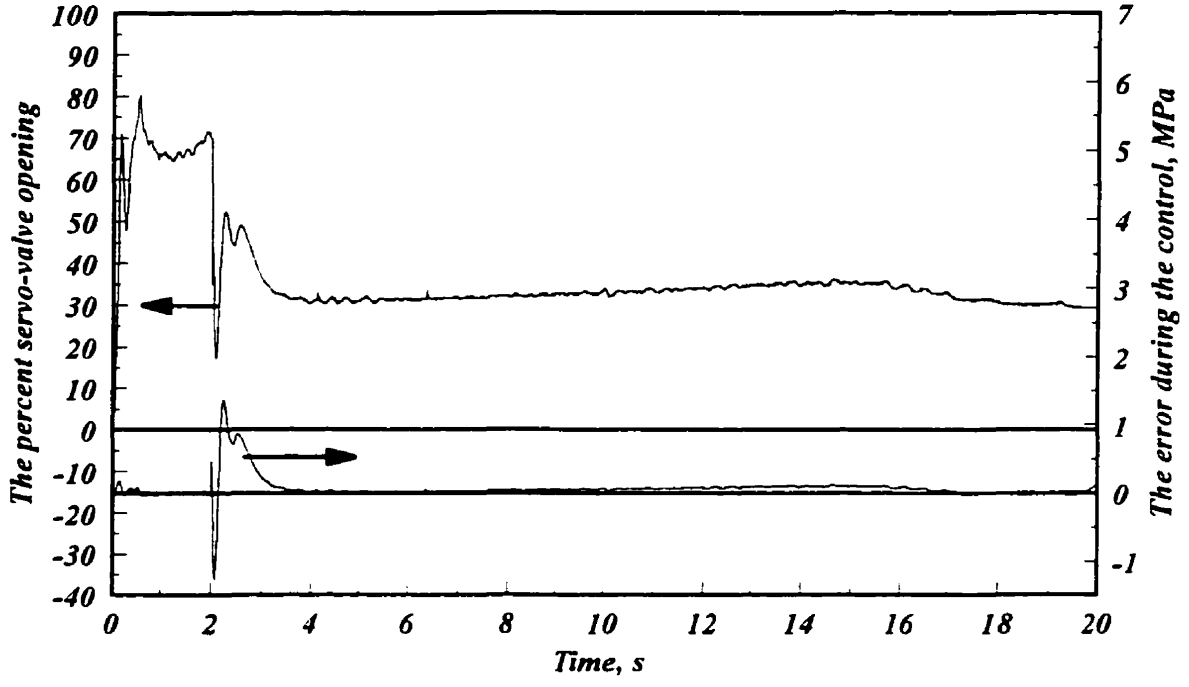


**Figure 6.5** PI controller tuned with ISE criteria

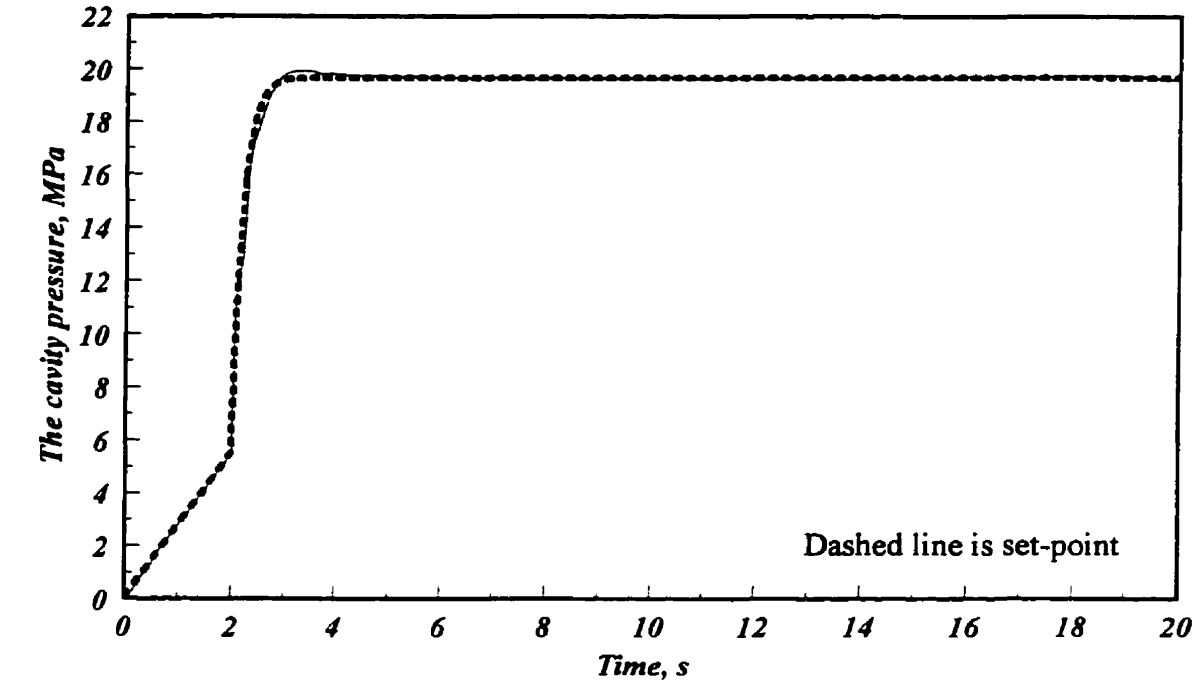


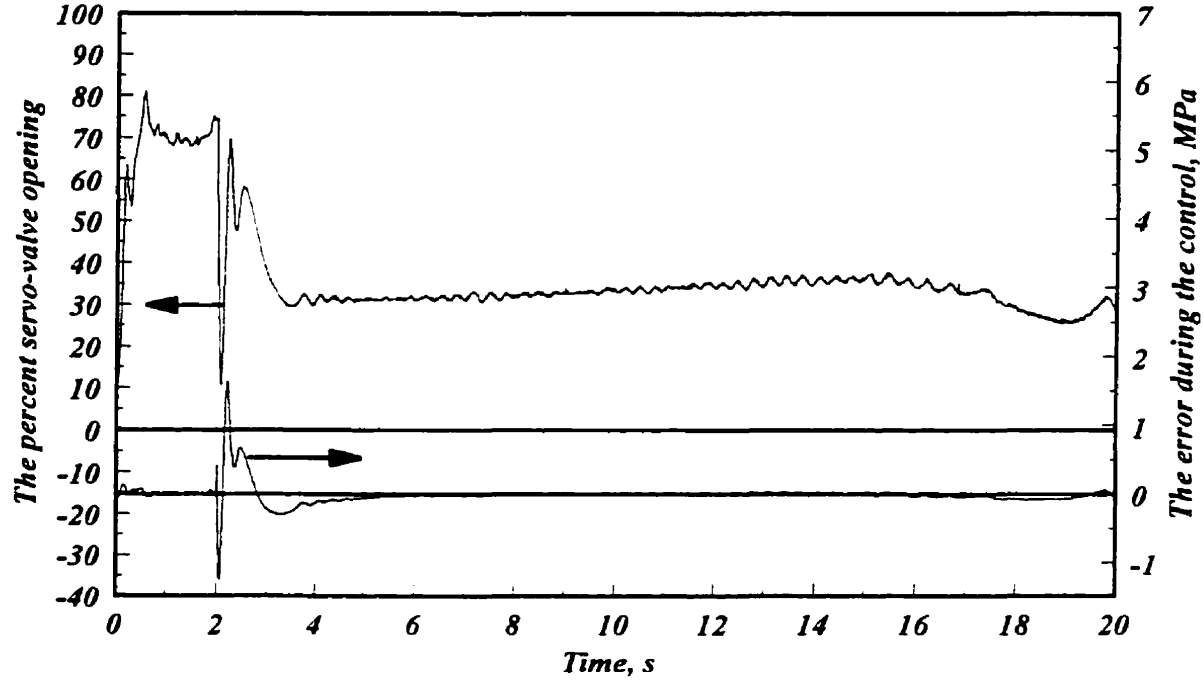


**Figure 6.6** PID controller tuned with ITAE criteria

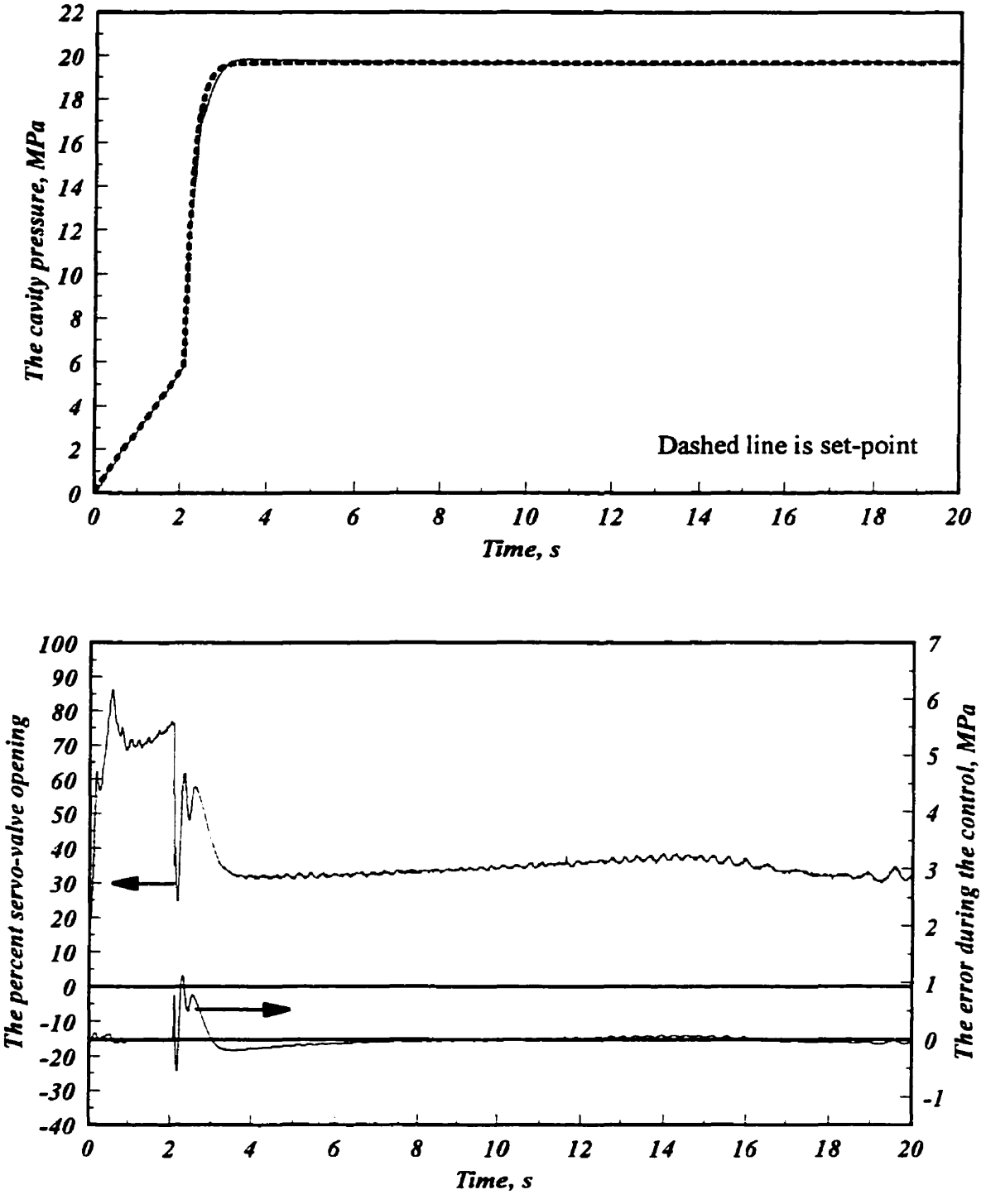


**Figure 6.7** PID controller tuned with ISE criteria

case of the PI controller. This can be attributed to the presence of derivative action in the PID controller. Long time tracking of both controllers is effective.

Figure 6.8 shows the performance of the IMC controller. The value of $a_{IMC}$ is experimentally determined to be 0.65. The performance of the IMC controller is very good. There is no overshoot or under set-point effect which are seen with the PI and PID controllers. The long time tracking ability of this controller is also very good. However, it appears that in the beginning of the packing phase the controller reacts too quickly. Thus there is evidence of saturation in controller performance. Over the long term, the command to the servo-valve fluctuates because the IMC controller reacts even to small errors. However, the magnitude of this fluctuation is only 10% opening.

For a better quantitative comparison between controller performances, the average error, maximum error, and standard deviation of error for each controller are given in Table 6.2. The average errors are close to zero, and all of them are positive except for the IMC controller. This is because of the fast reaction of the IMC controller in the beginning of the packing phase. The PI and PID controllers tuned with ISE criteria have the largest error. However, the PID controller tuned with ISE has the smallest average error. The IMC controller has the smallest standard deviation. It should be mentioned that all the controllers have small standard deviation and they have effective control over the cavity pressure. Therefore, all of them are satisfactory. The IMC controller is slightly superior for the above reasons.

Some step set-points changes were applied to the system to study the effectiveness of the response of the IMC controller. Figure 6.9 shows a step change in set-point. The step size is 1.68 Mpa. The cavity pressure response shows a very small overshoot followed by short transition time which ends in less than one second. Figure 6.10 shows the controller performance applied to negative step change in set-point. The transition duration is less than 1 second with some small overshoot.

Figures 6.11 through 6.14 show the results for cycle numbers 9, 27, 39, and 51, respectively. To have a better comparison, error of the each cycle is shown separately in Figure 6.15. The controller effectiveness does not deteriorate during this period.

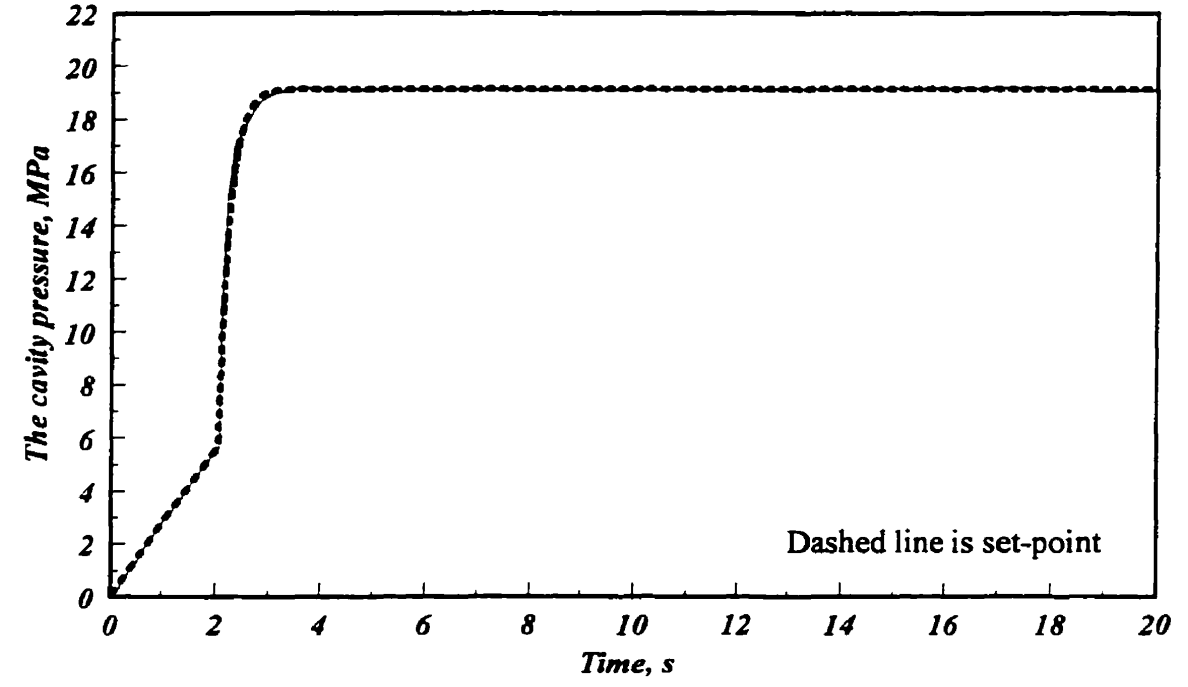


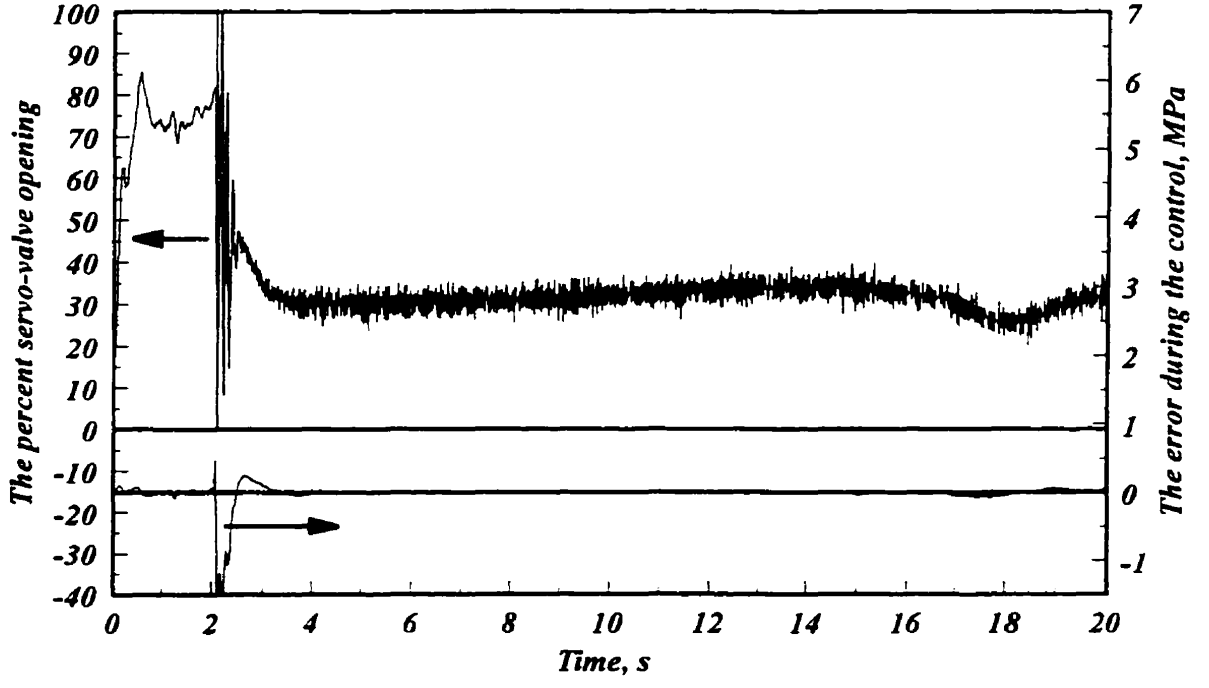


**Figure 6.8** IMC controller, a $_{IMC}$ is 0.65

| Controller type | Average error | Maximum error | Standard deviation |
|---|---|---|---|
| IMC | -0.0089 | 1.0877 | 0.1367 |
| PI, ITAE | 0.0716 | 1.3728 | 0.2015 |
| PI, ISE | 0.0269 | 1.7692 | 0.1699 |
| PID, ITAE | 0.0049 | 1.1269 | 0.1618 |
| PID, ISE | 0.0020 | 1.6496 | 0.1488 |

**Table 6.2** - Comparison between different controllers performances

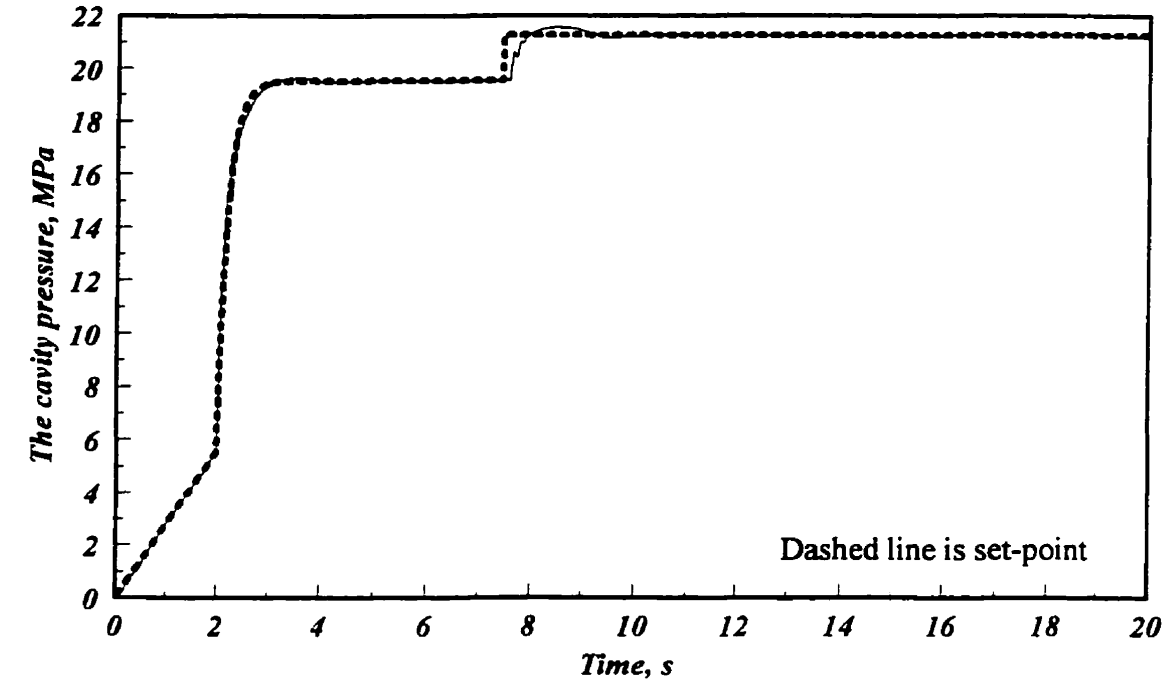


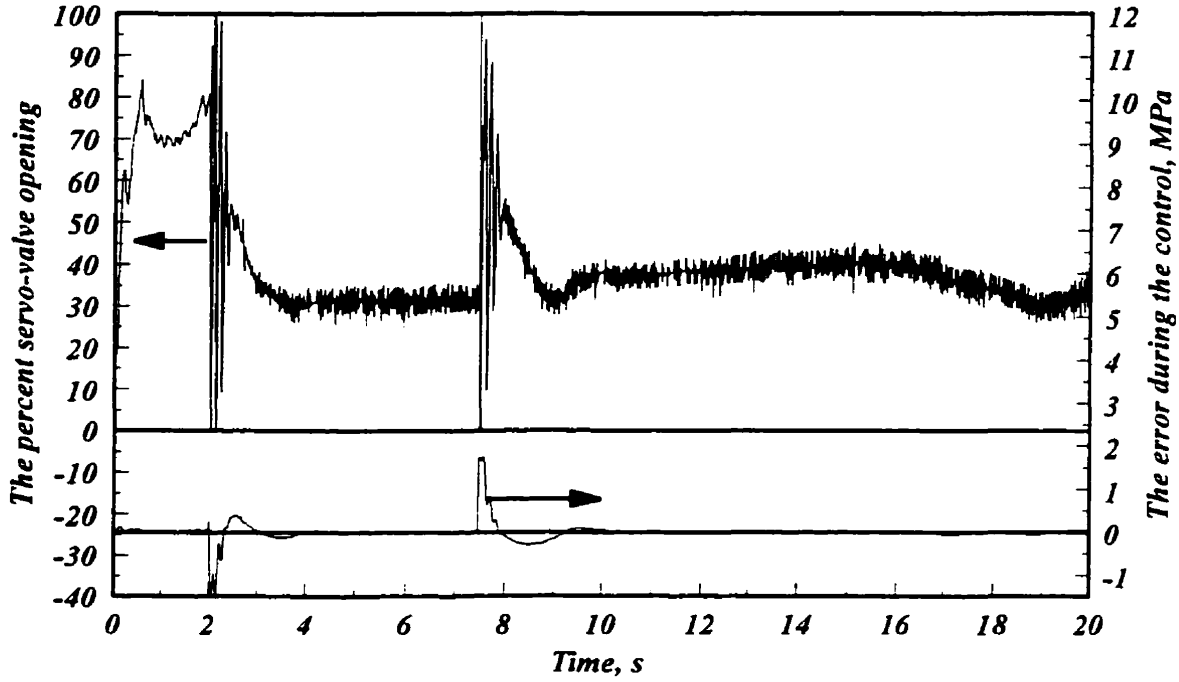


**Figure 6.9** IMC controller performance to a positive step

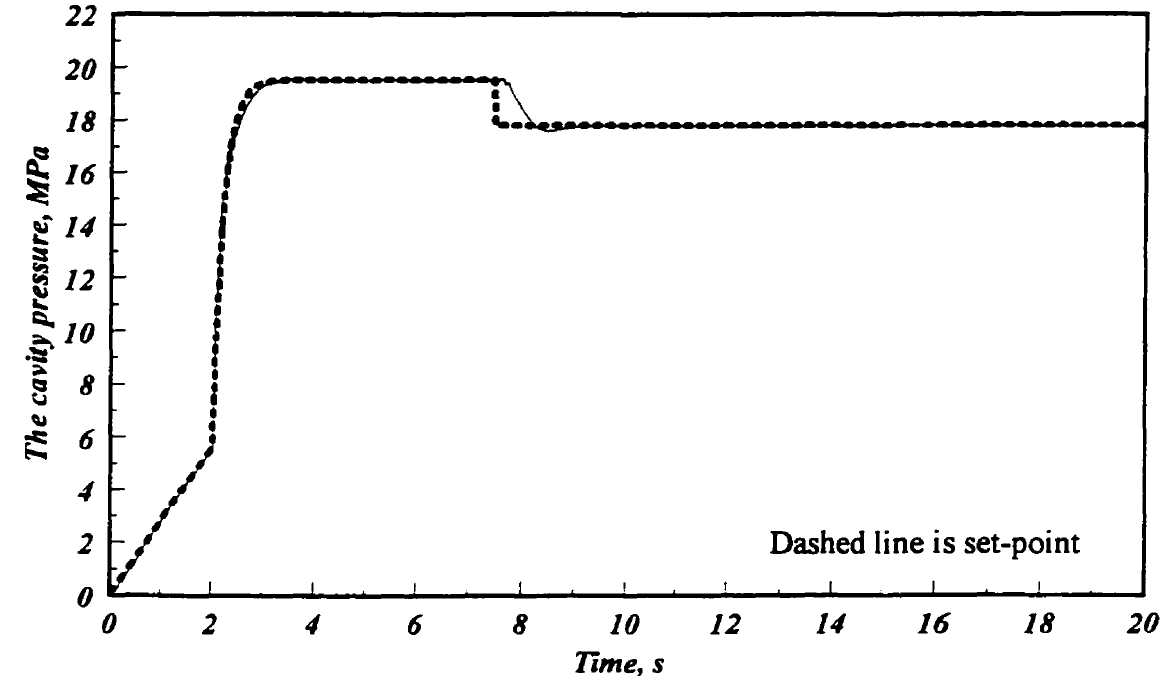


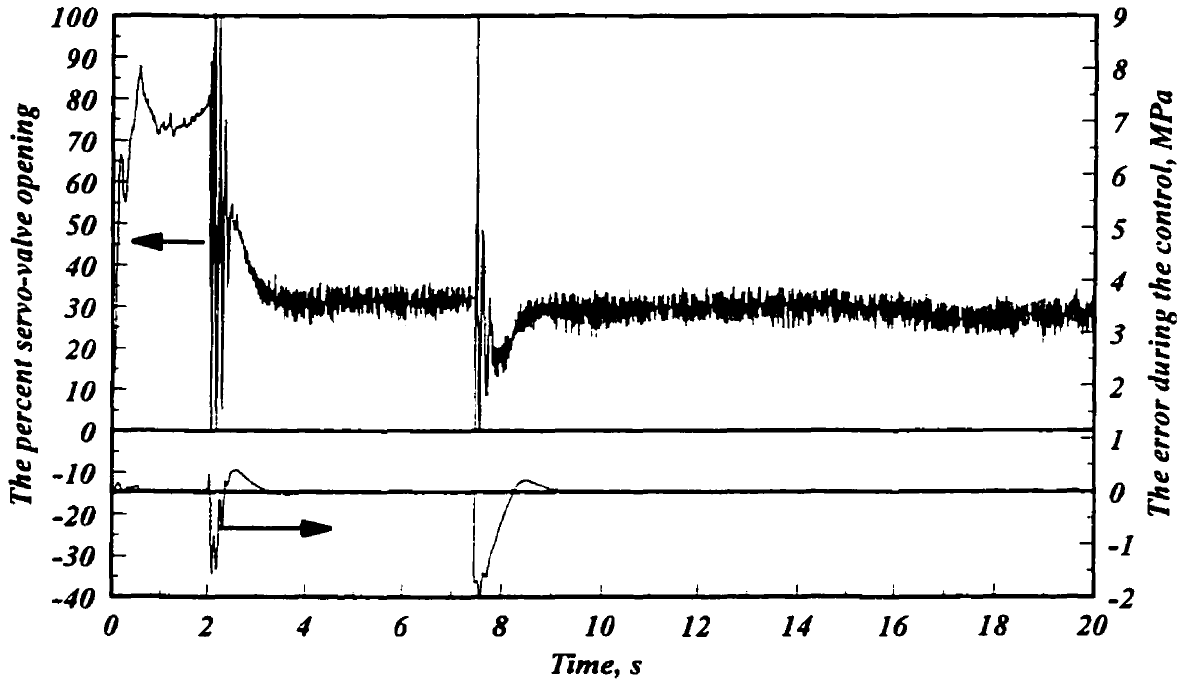


**Figure 6.10** IMC controller performance applied to a negative step

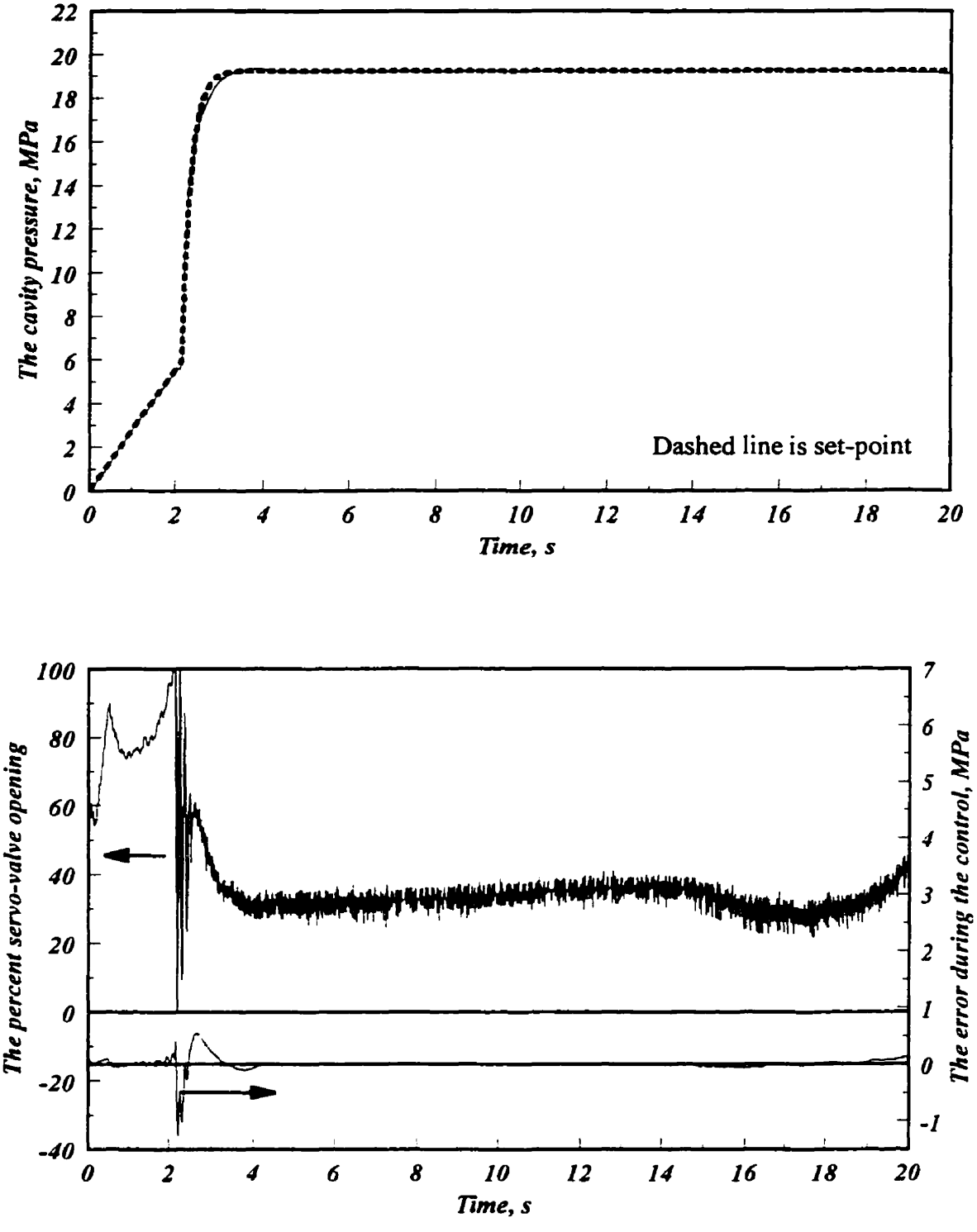


**Figure 6.11** IMC controller, cycle number 9

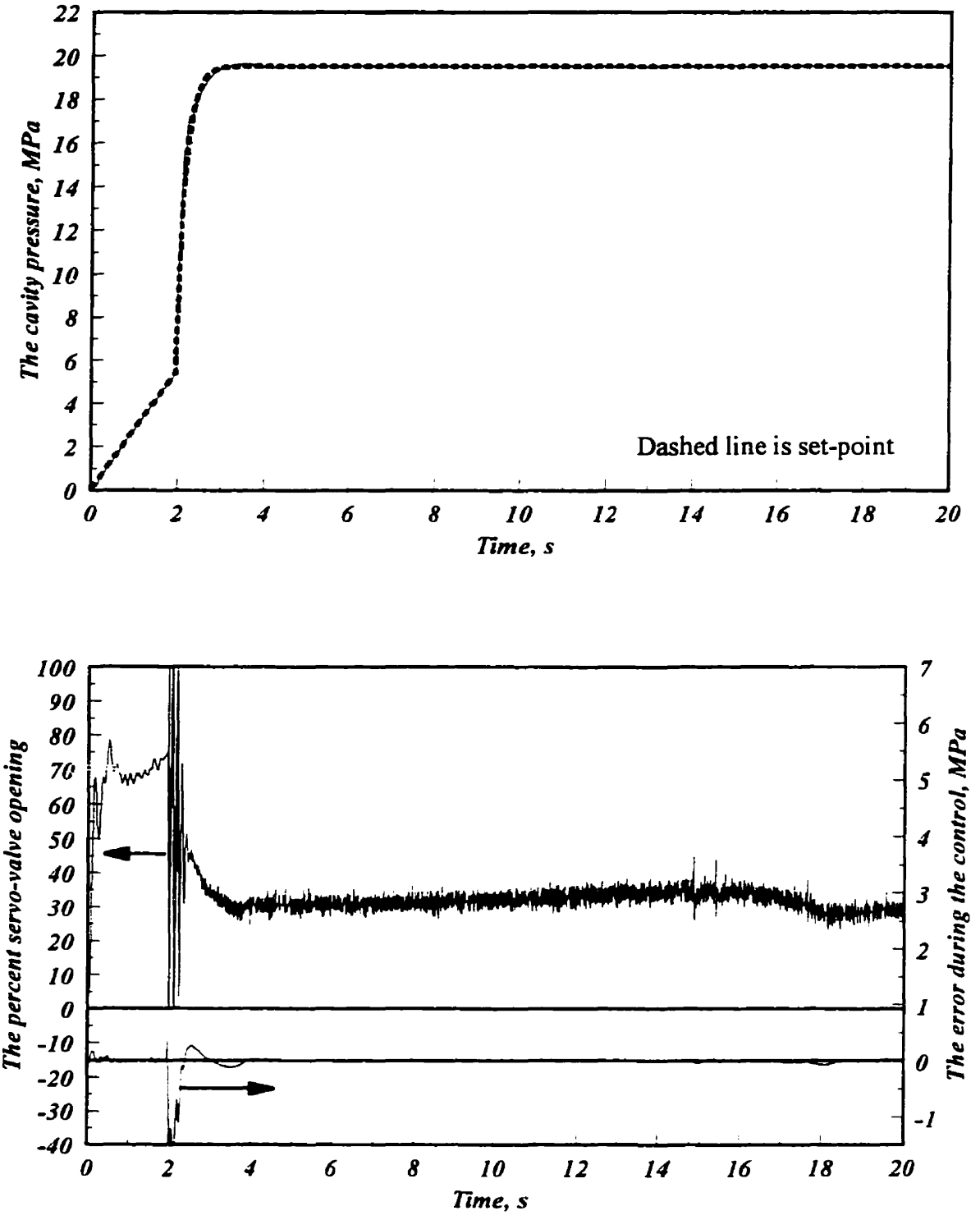


**Figure 6.12** IMC controller, cycle number 27

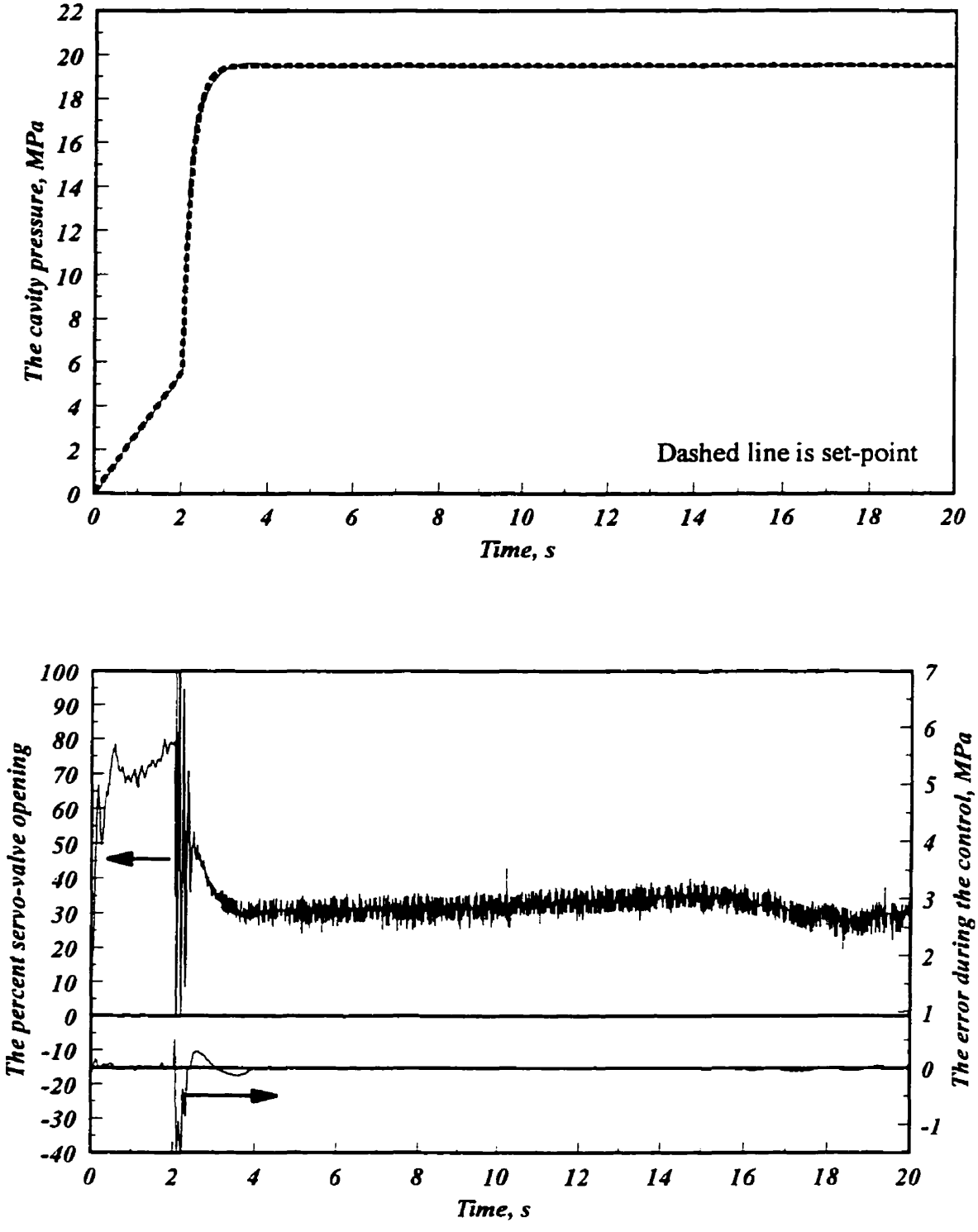


**Figure 6.13** IMC controller, cycle number 39

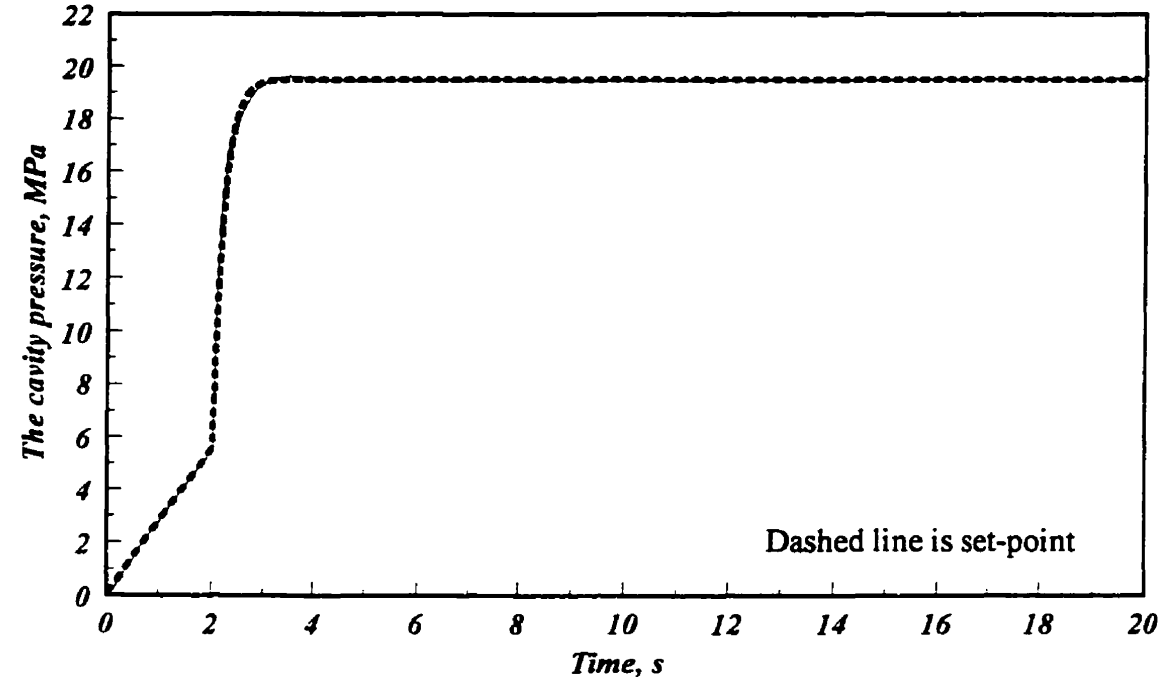


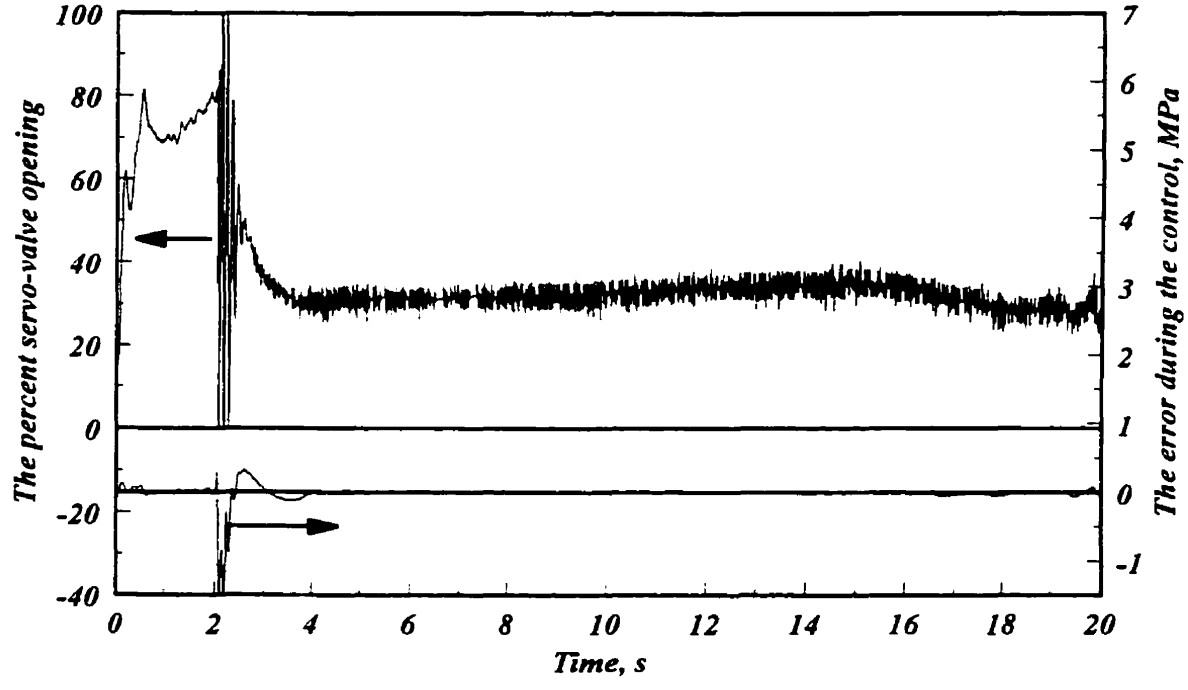


**Figure 6.14** IMC controller, cycle number 51

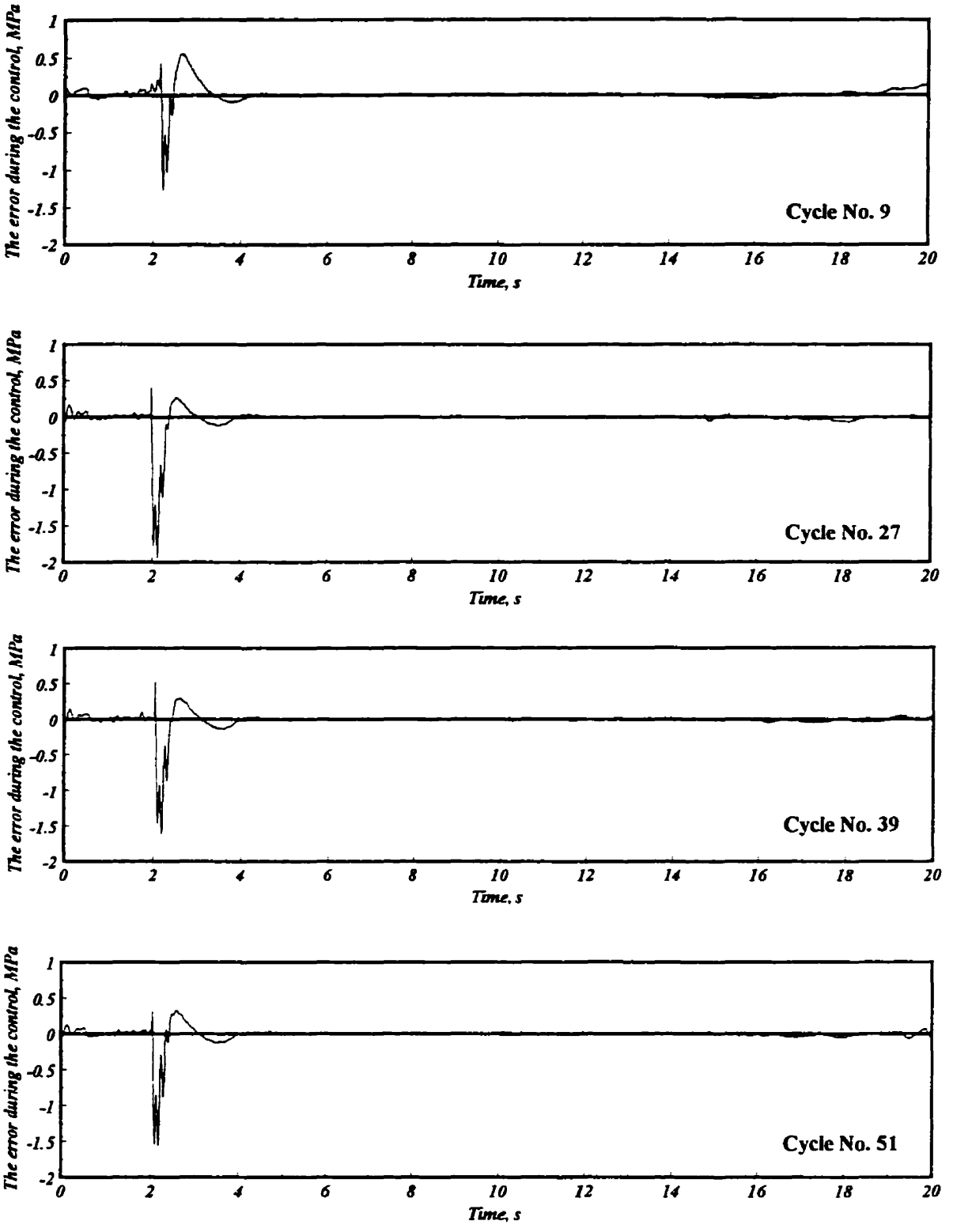


**Figure 6.15** Errors of IMC controller in different cycles

The last part of experiment, for polyethylene, was to apply the IMC controller on a cavity with irregular shape, shown in Figure 5.26. Figure 6.16 shows the result of the experiment. The cavity pressure follows the set-point in spite of small over shoot. The value of $a_{IMC}$ in this case was 0.85. The servo-valve opening is less noisy due to having larger gate in complex mold cavity.

## 6.9 Control Studies for Polystyrene

The objective of this section is to conduct the control studies using polystyrene, which is an amorphous thermoplastic polymer. The mathematical model and transfer function, derived in Equation (6.8), is also valid for polystyrene during the packing phase. This transfer function is of sixth order. Table 6.3 presents the numerical values for roots of the denominator of the transfer function. The only zero of the system can be cancelled out by the last root. Hence, the transfer function could be presented by a fifth order form such as:

$$G(s) = \frac{n_1}{\tau(s-r_1)(s-r_2)(s-r_3)(s-r_4)(s-r_5)} \tag{6.26}$$

Therefore, the above transfer function will be used to continue the control of cavity pressure during the packing phase for polystyrene.

### 6.9.1 Discrete Transfer Function

The discretized transfer function is derived from Equation (6.26) using partial fraction expansion:

$$\begin{aligned} G(s) &= \frac{n_1}{\tau(s-r_1)(s-r_2)(s-r_3)(s-r_4)(s-r_5)} \\ &= \frac{n_1}{\tau}\left[\frac{As+B}{s^2-2as+a^2+b^2} + \frac{Ds+E}{s^2-2cs+c^2+d^2} + \frac{F}{s-r_5}\right] \end{aligned} \tag{6.27}$$

where

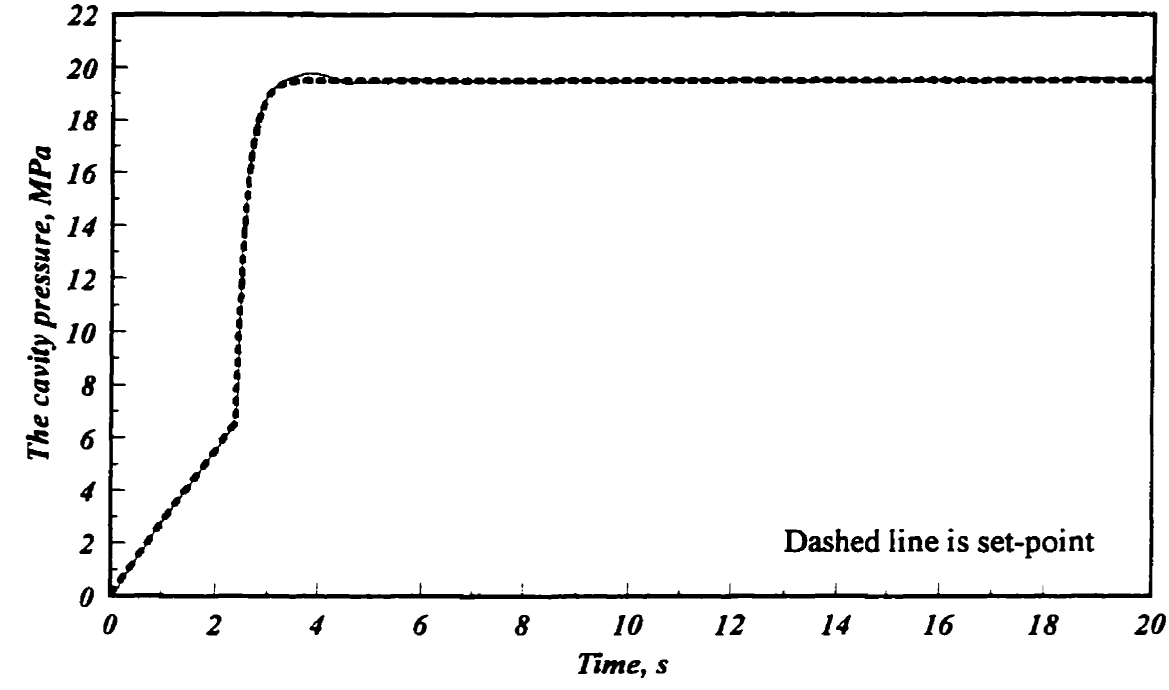


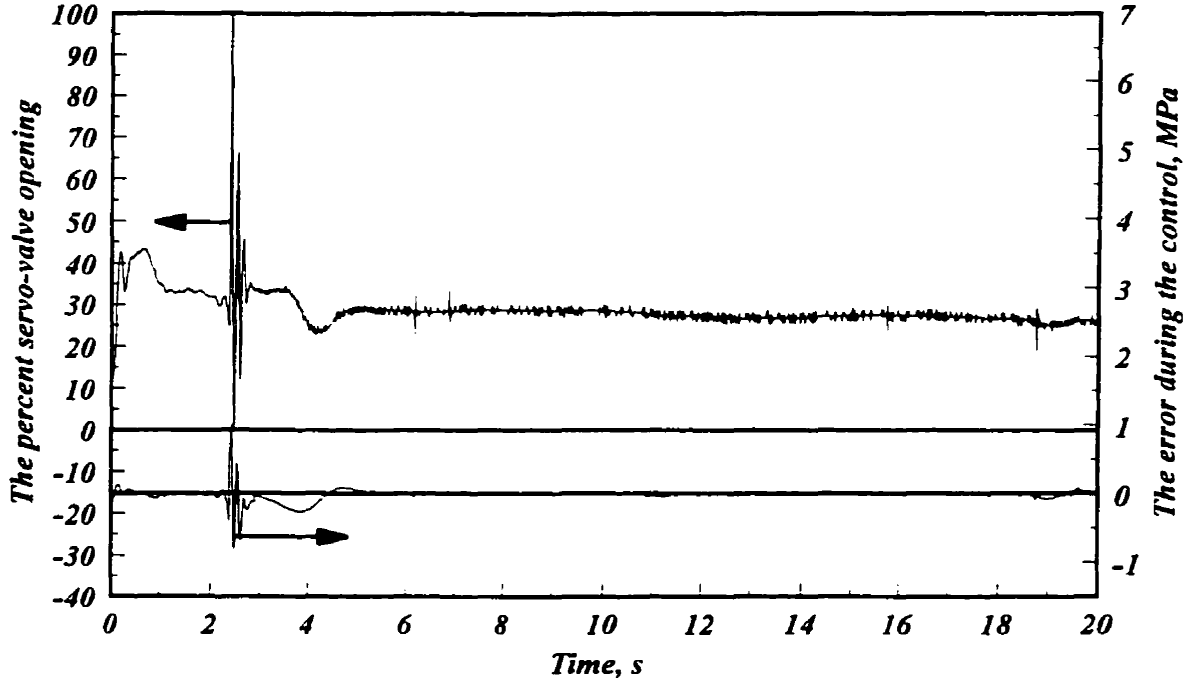


**Figure 6.16** IMC controller with irrgular cavity, a $_{IMC}$ is 0.85

| | |
|---|---|
| Zero | $-1.7791 \times 10^{-5}$ |
| First root | $-372 + 153.58 \times i$ |
| Second root | $-372 - 153.58 \times i$ |
| Third root | $-43.36 + 33.44 \times i$ |
| Fourth root | $-43.36 - 33.44 \times i$ |
| Fifth root | -0.4577 |
| Sixth root | $-1.779117 \times 10^{-5}$ |

**Table 6.3** - Roots of transfer function $i_s$=40% and $i_R$=10% at t= 4.1 s

$$r_1 = a + b \times i \quad , \quad r_2 = a - b \times i$$
$$r_3 = c + d \times i \quad , \quad r_4 = c - d \times i \tag{6.28}$$

and A is:

$$A = \frac{\left(a^2+b^2+r_5^2-2ar_5\right)\left[(a^2+b^2-c^2-d^2)-(2a-2c)(2c-r_5)\right]}{DEN.} + \frac{-(a^2+b^2-c^2-d^2-4ac+4c^2)(a^2+b^2-c^2-d^2)-(c^2+d^2)(2a-2c)^2}{DEN.} \tag{6.29}$$

and B is:

$$B = \frac{(a^2+b^2+r_5^2-2ar_5)(2a-2c)\left[(2a-2c)(2c-r_5)-(a^2+b^2)\right]}{DEN.} + \frac{(2a-r_5)(c^2+d^2)(2a-2c)+(a^2+b^2-c^2-d^2-4ac+4c^2)\times}{DEN.} \tag{6.30}$$
$$\frac{\left[(2a-r_5)(a^2+b^2-c^2-d^2)-(a^2+b^2+r_5^2-2ar_5)(2c-r_5)\right]}{DEN.}$$

and D, E, and F are:

$$D = \frac{(a^2+b^2+r_5^2-2ar_5)\left[(2a-2c)(2c-r_5)-(a^2+b^2-c^2-d^2)\right]}{DEN.}$$
$$E = \frac{(a^2+b^2+r_5^2-2ar_5)\left[(a^2+b^2-c^2-d^2-4ac+4c^2)(2c-r_5)+(c^2+d^2)(2a-2c)\right]}{DEN.} \tag{6.31}$$
$$F = \frac{(a^2+b^2-c^2-d^2-4ac+4c^2)(a^2+b^2-c^2-d^2)+(c^2+d^2)(2a-2c)^2}{DEN.}$$

and the denominator, DEN., is:

$$DEN. = (a^2+b^2+r_5^2-2ar_5)(c^2+d^2+r_5^2-2cr_5)\times \{(a^2+b^2-c^2-d^2-4ac+4c^2)(a^2+b^2-c^2-d^2)+(c^2+d^2)(2a-2c)^2\} \tag{6.32}$$

The discretized form of the transfer function with zero-order hold is:

$$G(z)=\frac{n_1}{\tau}\left[\frac{b_1z^{-1}+b_2z^{-2}}{1+a_1z^{-1}+a_2z^{-2}}+\frac{d_1z^{-1}+d_2z^{-2}}{1+c_1z^{-1}+c_2z^{-2}}+\frac{f_1z^{-1}}{1+e_1z^{-1}}\right] \tag{6.33}$$

where

$$\begin{aligned}
a_1&=-2e^{a\Delta t}\cos b\Delta t & a_2&=e^{2a\Delta t}\\
b_1&=\frac{-B}{a^2+b^2}-e^{a\Delta t}\left[\frac{A}{b}\sin b\Delta t+\frac{B}{b}\frac{a}{a^2+b^2}\sin b\Delta t-\frac{B}{a^2+b^2}\cos b\Delta t\right] \\
b_2&=\frac{Ae^{a\Delta t}}{a^2+b^2}\left[\frac{B}{A}e^{a\Delta t}-\frac{B}{A}\cos b\Delta t-\frac{a^2+b^2+\frac{aB}{A}}{b}\sin b\Delta t\right]
\end{aligned} \tag{6.34}$$

and

$$\begin{aligned}
c_1&=-2e^{c\Delta t}\cos d\Delta t & c_2&=e^{2c\Delta t}\\
d_1&=\frac{-E}{c^2+d^2}-e^{c\Delta t}\left[\frac{D}{d}\sin d\Delta t+\frac{E}{d}\frac{c}{c^2+d^2}\sin d\Delta t-\frac{E}{c^2+d^2}\cos d\Delta t\right] \\
d_2&=\frac{De^{c\Delta t}}{c^2+d^2}\left[\frac{E}{D}e^{c\Delta t}-\frac{E}{D}\cos d\Delta t-\frac{c^2+d^2+\frac{cE}{D}}{d}\sin d\Delta t\right]
\end{aligned} \tag{6.35}$$

where

$$e_1=-e^{r_5\Delta t} \qquad f_1=\frac{F}{-r_5}\left(1-e^{r_5\Delta t}\right) \tag{6.36}$$

Finally, rearrangement of the above equations, with zero-order hold, gives the discretized transfer function:

$$G(z)=\frac{\alpha_1z^{-1}+\alpha_2z^{-2}+\alpha_3z^{-3}+\alpha_4z^{-4}+\alpha_5z^{-5}}{1+\beta_1z^{-1}+\beta_2z^{-2}+\beta_3z^{-3}+\beta_4z^{-4}+\beta_5z^{-5}} \tag{6.37}$$

The relationship for $\alpha_1$, $\alpha_2$, $\alpha_3$, $\alpha_4$, $\alpha_5$ are:

$$\alpha_1 = \frac{n_1}{\tau}(b_1 + d_1 + f_1)$$
$$\alpha_2 = \frac{n_1}{\tau}(b_1 c_1 + b_2 + b_1 e_1 + a_1 d_1 + d_2 + d_1 e_1 + c_1 f_1 + a_1 f_1) \tag{6.38}$$

and

$$\alpha_3 = \frac{n_1}{\tau}(b_1 c_2 + b_2 c_1 + b_1 c_1 e_1 + b_2 e_1 + a_2 d_1 + d_2 a_1 + a_1 d_1 e_1 + d_2 e_1 + c_2 f_1 + a_1 c_1 f_1 + a_2 f_1) \tag{6.39}$$

and

$$\alpha_4 = \frac{n_1}{\tau}(b_2 c_2 + b_1 c_2 e_1 + b_2 c_1 e_1 + d_2 a_2 + a_2 d_1 e_1 + d_2 a_1 e_1 + a_1 c_2 f_1 + a_2 c_1 f_1)$$
$$\alpha_5 = \frac{n_1}{\tau}(b_2 c_2 e_1 + d_2 a_2 e_1 + a_2 c_2 f_1) \tag{6.40}$$

The relationship for $\beta_1$, $\beta_2$, $\beta_3$, $\beta_4$, and $\beta_5$ are:

$$\beta_1 = c_1 + a_1 + e_1 \qquad \beta_2 = c_2 + a_1 c_1 + a_2 + c_1 e_1 + a_1 e_1$$
$$\beta_3 = a_1 c_2 + a_2 c_1 + c_2 e_1 + a_1 c_1 e_1 + a_2 e_1 \tag{6.41}$$
$$\beta_4 = a_2 c_2 + a_1 c_2 e_1 + a_2 c_1 e_1 \qquad \beta_5 = a_2 c_2 e_1$$

### 6.9.2 Experimental Results for Polystyrene

The same approach as polyethylene is used to design the controller for polystyrene during the packing phase. Some of results are shown in this section. The PID controller tuned with the ITAE criterion is used. Figure 6.17 shows the result of this controller. The result for the control of the filling phase is also shown in the figure. In general, the cavity pressure follows the set-point very well. The amplitude of servo-valve command is less and even far from saturation. Figure 6.18 shows the result of the IMC controller.

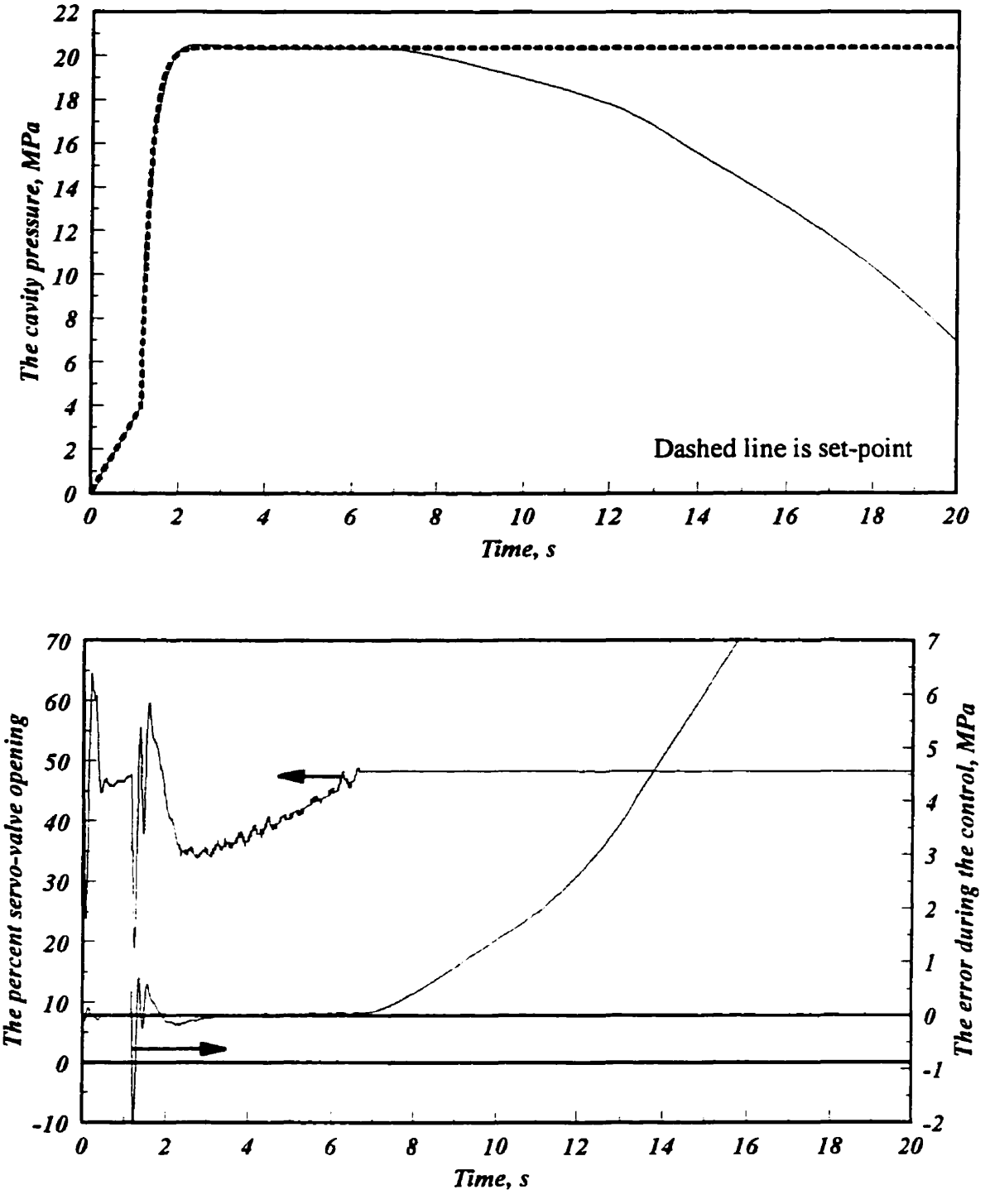


**Figure 6.17** PID controller tuned with ITAE criteria for polystyrene

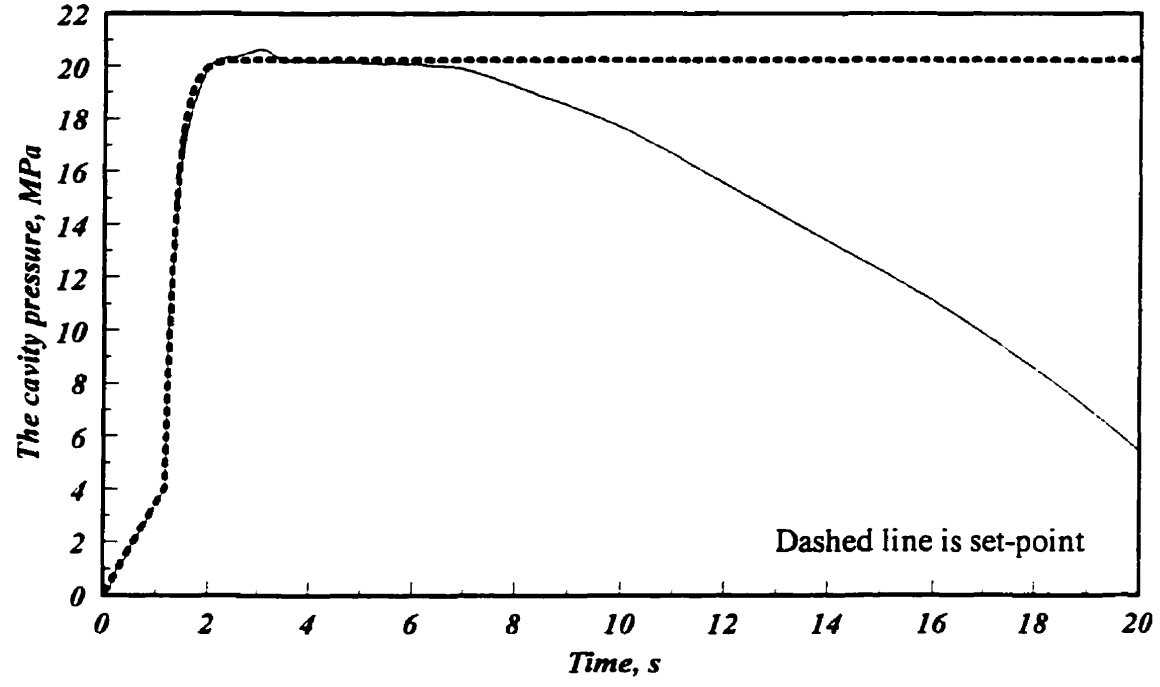


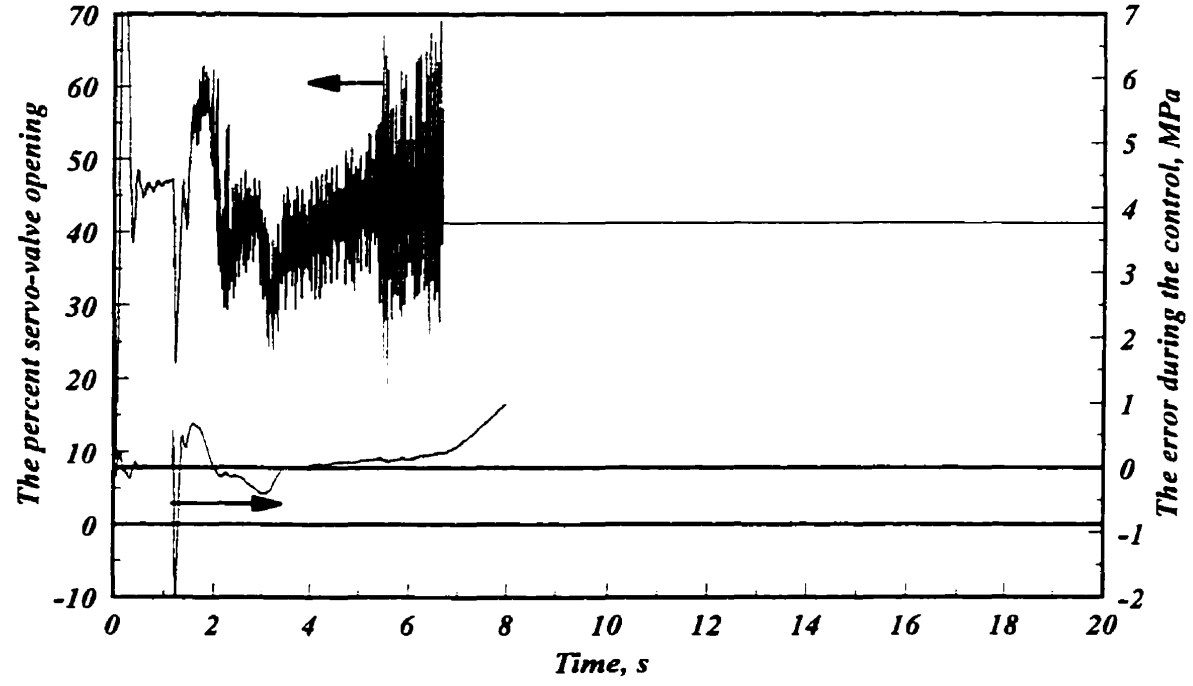


**Figure 6.18** IMC controller, a $_{IMC}$ is 0.65 for polystyrene

There is a small overshoot in the beginning of the packing phase which can be attributed to the fast response of the IMC controller reaction.

## 6.10 Conclusions

The dynamics and control of cavity pressure of the packing phase were studied. A physically based model was used to study the dynamics of the process. Consequently, a linear transfer function with time-varying parameters was derived to continue the control studies. Different controllers with distinct tuning criteria were designed. The result were adaptive PI and PID controllers. Experimental results indicate that these controllers yield good control for the injection molding of high density polyethylene and polystyrene. The IMC controller shows excellent controller action for the process. To the best knowledge of the author, this is first successful control of the injection molding process using a physically-based model.

# CHAPTER 7

# CONCLUSIONS AND RECOMMENDATIONS

## 7.1 Conclusions

The two main objectives of this research work were first to construct a physically based dynamic model of an injection molding machine. The second objective was to employ this model to study and apply different strategies to control the cavity pressure throughout the filling, and packing and holding phases. These objectives were realized successfully.

With respect to the cavity pressure profile, the injection molding process can be divided into three distinct phases: filling, packing, and cooling. A physically based model has been developed for each of these phases. This lumped theoretical model was developed for the whole injection molding machine. This model was derived by applying constitutive laws, as necessary, to various parts of the process and machine. The machine was divided into subsystems for the sake of modeling simplicity to obtain a lumped model. These subsystems are: the hydraulic system, injection cylinder, ram screw, nozzle, and polymer delivery system including mold cavity. The model was applied to the three process phases: filling, packing, and cooling. The overall model was validated by experimental testing of two polymers possessing very different processing characteristics. The polymers were a semi-crystalline high density polyethylene and an

amorphous polystyrene.

It was found that the model had to be constructed with attention to the following factors: the hydraulic subsystem had to incorporate all elements: piping, elbows, filters, and valves. Polymer melts were non-Newtonian and viscoelastic fluids although they are often modelled as simple fluids. Both effects had to be accounted for to give an accurate model during the filling phase. It was necessary to incorporate the viscoelastic phenomenon in describing the converging flow in the nozzle and radial flow part in the mold cavity, but it was neglected in the slightly diverging flow in the sprue. It was necessary to include the solidification of polymer melt in the polymer delivery system during the packing phase. This solidification plays an important role in the accuracy of the model.

The physically based model was employed to derive a dynamic model which relates the servo-valve opening (manipulated variable) to the cavity pressure (controlled variable). The physically based non-linear and time-varying model was transformed to a set of piece-wise linear transfer function form for the purposes of the control studies. The dynamic model was applied to design and evaluate control schemes for the injection molding cycle. The adaptive design approach of classical controllers such as PI and PID as well as the model based IMC method were used to design various controllers for the process.

The experimental evaluation of the controllers was conducted on a reciprocating single screw injection molding machine. Model validation was carried out from the open loop experiments with different values for supply and relief servo-valves for polyethylene and polystyrene. Controller design verification was obtained from the following set of experiments. Adaptive PI, PID, IMC controllers, tuned with different criteria, were applied to the filling phase of a rectangular mold cavity. The results indicated that the controllers could yield accurate action for the injection molding of high density polyethylene and amorphous polystyrene. The IMC controller showed the best performance. A non-linear set-point was used during the filling phase. The controllers were used with a mold cavity with complex geometry. The controller behavior was

evaluated over many cycles approaching mass production. Hence, the controller can be used in industrial injection molding machines and complex molds.

The same approach was used to pursue the packing phase control studies. During the packing phase, adaptive PI, PID, IMC controller were applied to study controller performance. Control results were very good. The IMC controller showed superior performance. Controller behavior was studied during the packing phase in mass production. The controller results with a complex geometry mold cavity showed controller ability for operation under practical molding conditions.

## 7.2 Claims for Original Work

This work has examined the physically-based modeling and control of the cavity pressure in the injection molding cycle. Particular contributions may be stated as follows:

(1) The present study is the first to derive a simple dynamic model including normal stress effects and solidification of polymer melt in the polymer delivery system, during the filling phase.

(2) The present study is the first to derive a simple model including normal stress effects and solidification of polymer melt in the polymer delivery system, during the packing phase.

(3) The present study is the first to achieve a transfer function which relates cavity pressure to the hydraulic system, during the filling phase.

(4) The present study is the first to achieve a transfer function which relates cavity pressure to the hydraulic system, during the packing phase.

(5) An adaptive control strategy was employed to achieve successful cavity pressure control during the filling and packing phases of the injection molding cycle.

## 7.3 Recommendations

Implementation of a graphic user interface to the computer control code will make the software more user friendly. To achieve a more reliable control on the injection

molding machine, it is suggested to investigate a multivariable scheme for critical variables such as cavity pressure, melt temperature, and mold temperature. Also, investigation of the relationship between molded article properties such as part weight, shrinkage, or residual stresses with the set-point of these variables is required.

Applying modern control methods such as fuzzy logic, neural networks, or artificial intelligence may improve the robustness of the process. Combining artificial intelligence with a physically-based controller can give learning feature to system and may increase the ability and robustness of the controller in rejecting noises.

# NOMENCLATURE

| | |
|---|---|
| $a_{IMC}$ | Low pass filter parameter, used in IMC method |
| A | Area |
| $A_{0,1,2,3}$ | Coefficients in filter pressure-flow behavior, in Equation (4.16) |
| $A_4$ | Constant defined in Equation (4.9) |
| $A_f$ | Cross-sectional area in front of flow |
| $A_h$ | Injection cylinder cross-area |
| $A_n$ | Nozzle cross-area |
| $A_t$ | Hydraulic system pipe cross-area |
| B(T) | Constant in Tait equation of state |
| $c_s$ | Controller bias signal |
| c(t) | Controller output |
| $C_{23,2h,s2}$ | Coefficient for pressure-flow behavior in hydraulic, in equation (4.17) |
| $C_{p,pm,ps}$ | Heat capacity, polymer melt and solid heat capacity, respectively |
| e(t) | Measured error at time t |
| E | Constant defined in Equations (4.23) |
| E(k) | Error at sampling time k |
| $\Delta E/R$ | Power-law constants |
| f | Power law index for $N_1$, in Equation (4.23) |
| $f_v$ | Friction force against the ram |
| $F_{1\text{-}6}$ | State equation in the set of governing equations |
| g | Acceleration of gravity |
| $g_{1\text{-}4}$ | Coefficient of nominator polynomial in filling discretized transfer function |
| $G_c$ | Controller transfer function |
| $G_c^*$ | Internal model controller transfer function |
| $\tilde{G}$ | Modeled process transfer function in IMC method |
| $\tilde{G}_+$ | Unstable part of process transfer function |
| $\tilde{G}_-$ | Stable part of process transfer function |
| h | Convection heat transfer coefficient, in Equation (4.37) |
| $h_{1\text{-}4}$ | Coeff. of denominator polynomial in filling discretized transfer function |

| | |
|---|---|
| H | Half thickness of the mold cavity |
| $H_g$ | Half thickness of the gate |
| $i_R$ | Relief servo-valve opening percent |
| $i_s$ | Supply servo-valve opening percent |
| I | Constant defined in equation (4.23) |
| ISE | Integral of the square error |
| ITAE | Integral of the time weighted absolute error |
| $k, k_{m,s}$ | Thermal conductivity and thermal conductivity of melt and solid |
| $k_a$ | Pre-exponential factor, equation (4.7) |
| $k_{23}$ | Head loss coefficient between points 2 & 3 |
| $k_c$ | Gain of controller |
| $k_{ct}$ | Pressure-flow coefficient between nozzle and pressure transducer |
| $k_n$ | Nozzle pressure-flow coefficient |
| $k_{n1}$ | Nozzle pressure-flow coefficient for the first part of the nozzle |
| $k_r$ | Radius ratio of screw to nozzle |
| $k_{s2}$ | Head loss coefficient between points s & 2 |
| $k_t$ | Total pressure-flow coefficient |
| $k_v$ | Servo-valve constant |
| $L, L_0$ | Screw length and its initial length, respectively |
| $L_{23,2h,s2}$ | Pipe length between points 2 & 3, 2 & h, and s & 2, respectively |
| $L_c$ | Cavity length |
| $L_{exc}$ | Length of heat exchanger in the hydraulic system |
| $L_g$ | Length of the gate |
| $L_{n1,n2,n3}$ | Nozzle lengths in the first, second, and third parts, respectively |
| $L_r$ | Length of the runner |
| M | Ram screw mass |
| M(k) | Controller output at sampling time k |
| M(t) | Thickness of the polymer melt part during the cooling |
| n | Power-law index |

| | |
|---|---|
| $n_{1,2}$ | Coefficient of nominator polynomial of transfer function |
| $n_t$ | Number of tubes in the shell and tube heat exchanger |
| N | Nozzle pressure deviation variable |
| $N_1$ | The first normal stress difference |
| $P_{2,3}$ | Pressures at point 2 and 3, respectively |
| $P_c$ | Cavity pressure, and cavity pressure deviation variable in control |
| $P_{FE}$ | Pressure at the end of filling phase |
| $P_{gate}$ | Gate pressure |
| $P_h$ | Hydraulic pressure |
| $P_n$ | Nozzle pressure |
| $P_{PE}$ | Pressure at the end of packing phase |
| $P_s$ | Supply pressure, pressure before supply servo-valve |
| q | Flow rate between points s and 2 |
| $q_2$ | Flow rate between points 2 and 3 |
| $q_h$ | Oil flow into the injection cylinder |
| $q_p$ | Polymer flow rate |
| $Q_{r,s}$ | Relief and supply servo-valve flow deviation variables, respectively |
| r | Radius |
| $r_{1,6}$ | Roots of denominator polynomial in transfer function |
| $r_i$ | Solid and melt interface radius in the sprue |
| $\Delta r$ | Radial interval |
| R | Relief servo-valve deviation variable |
| $R_1$ | Radius in the beginning of the radial part of the cavity |
| $R_{exc}$ | Radius of the tube in the shell and tube heat exchanger |
| $R_h$ | Radius of the tube in the hydraulic system |
| $R_m$ | Radius of the melt part |
| $R_{n,r,s1,s2}$ | Nozzle, runner, beginning and end of sprue radiuses, respectively |
| $R_t$ | Radius of the tube in the hydraulic system |
| s | Inverse of power law index 1/n, and Laplace variable in control study |

| | |
|---|---|
| $s(t)$ | Solid skin thickness in the cavity |
| $t$ | Time |
| $\Delta t$ | Time interval |
| $t_i$ | Filling time |
| $T$ | Temperature, supply servo-valve deviation variable in control |
| $T_o$ | Temperature at time zero |
| $T_b$ | Barrel temperature |
| $T_i$ | Initial temperature |
| $T_m$ | Melting temperature of polymer |
| $T_{melt}$ | Polymer melt temperature |
| $T_{mold}$ | Mold temperature |
| $T_s$ | Polymer solid temperature |
| $u$ | Input to dynamic model in Equation (5.6) |
| $U$ | Flow velocity |
| $v, v_o$ | Specific volume and its value at atmospheric pressure in Tait equation |
| $v_z$ | Ram screw velocity |
| $V$ | Ram screw velocity deviation variable |
| $V_{avg}$ | Average velocity |
| $V_{h,h0}$ | Injection cylinder volume, and its initial volume, respectively |
| $V_{n,n0}$ | Nozzle volume, and its initial volume, respectively |
| $V_p$ | Instantaneous volume of the cavity filled by the polymer |
| $V_t$ | Total volume of the polymer delivery system |
| $w_c$ | Width of the cavity |
| $x$ | State equation vector in Equation (5.5) |
| $y_{2,3,f,s}$ | Height of the points 2, 3, s, f |
| $z$ | Ram screw displacement, z-transform variable in control |
| $Z$ | Ram screw displacement deviation variable |
| $\alpha, \alpha_{m,s}$ | Thermal diffusivity and thermal diffusivity of polymer melt and solid |
| $\alpha_{1\text{-}5}$ | Coeff. of nominator polynomial in packing discretized transfer function |

| | |
|---|---|
| $\alpha_{2,f,h}$ | Kinematic energy correction factor in point 2, f, and h, respectively |
| $\beta_{1\text{-}5}$ | Coeff. of denominator polynomial in packing discretized transfer function |
| $\beta_{h,p}$ | Hydraulic oil, and polymer bulk modulus, respectively |
| $\dot{\gamma}$ | Shear rate |
| $\eta$ | Polymer viscosity |
| $\eta_0$ | Polymer viscosity at $\dot{\gamma}=1$ |
| $\lambda$ | Constant defined as $\alpha.\Delta t/\Delta r^2$ |
| $\mu$ | Hydraulic oil viscosity |
| $\rho$ | Polymer density |
| $\rho_o$ | Hydraulic oil density |
| $\rho_s$ | Polymer solid density |
| $\tau$ | Time constant of the servo-valve dynamic behavior |
| $\tau_D$ | Derivative time constant |
| $\tau_I$ | Integral time constant |
| $\psi$ | Coefficient in normal stress equation, Equation (4.23) |
| $\omega$ | Converging angle in the convergence part of the nozzle |

# REFERENCES


1. Saechtling, H., "International Plastics Handbook for the Technologist, engineer, and user", Hanser Publisher, 1995

2. Fenner, R. T., "Principles of Polymer Processing", Chemical Publishing Co., New York, 1979

3. Ljung L., and T. Glad, "Modeling of Dynamic Systems", Prentice Hall Inc., 1994

4. Barrie I. T., "Understanding How an Injection Mold Fills", SPE Journal, vol. 27, P.64, August 1971

5. Donovan, R. C., D. E. Thomas, and L. D. Leversen, "An Experimental Study of Plasticating in a reciprocating screw injection mold machine", Polym. Eng. Sci., vol. 11, No. 5, P.353, 1971

6. Donovan, R. C.,"A Theoretical Melting Model for a Reciprocating-Screw Injection Molding Machine", Polym. Eng. Sci., vol. 11, No. 5, P.361, 1971

7. Williams, G. and Lord A., "Mold-Filling Studies for the Injection Molding of Thermoplastic Materials. Part I: The Flow of Plastic Material in Hot- and Cold-Walled Circular Channels", Polym. Eng. Sci., vol. 15, No. 8, P.553, 1975

8. Lord, A. H., and G. Williams, "Mold-Filling Studies for the Injection Molding of Thermoplastics Materials. Part II: The Transient Flow of Plastic Material in the Cavities of Injection-Molding Dies", Polym. Eng. Sci., vol. 15, No. 8, P.569, 1975

9. Kamal, M. R., Y. Kuo, and P. H. Doan, "The Injection Molding Behavior of Thermoplastics in Thin Rectangular Cavities", Polym. Eng. Sci., vol. 15, No. 12, P.863, 1975

10. Ryan M. E., and T. S. Chung, "Conformal Mapping Analysis of Injection Mold Filling", Polym. Eng. Sci., vol. 20, No. 9, P.642, 1980

11. Kamal M. R., P. G. Lafleur, "Computer Simulation of Injection Molding", Polym. Eng. Sci., vol. 22, No. 17, P. 105, 1982

12. Lafleur P. G., M. R. Kamal, "A Structure-Oriented Computer Simulation of the Injection Molding of Viscoelastic Crystalline Polymers Part I: Model with Fountain Flow, Packing, Solidification", Polym. Eng. Sci., vol. 26, No. 1, P.92, 1986

13. Kamal M. R., P. G. Lafleur, "A Structure-Oriented Computer Simulation of the Injection Molding of Viscoelastic Crystalline Polymers Part II: Model Predictions and Experimental Results", Polym. Eng. Sci., vol. 26, No. 1, P. 103, 1986

14. Gogos C. G., C. F. Huang, and L. R. Schmidt, "The Process of Cavity Filling Including the Fountain Flow in Injection Molding", Polym. Eng. Sci., vol. 26, No. 20, P.1457, 1986

15. Titomanlio, G., S. Piccarolo, and G. Levati, "On the Packing-Holding Flow in the Injection Molding of Thermoplastics Polymers", J. of Applied Polymer Science, vol. 35, P.1483, 1988

16. Kamal M. R., S. K. Goyal, E. Chu, "Simulation of Injection Mold filling of Viscoelastic Polymer with Fountain Flow", AICHE J., vol. 34, No. 1, P. 94, January 1988

17. Huilier, D., C. Lenfant, J. Terrisse, and R. Deterre, "Modeling the Packing Stage in Injection Molding of Thermoplastics", Polym. Eng. Sci., vol. 28, No. 24, P.1637, 1988

18. Chiang, H. H., C. A. Hieber, and K. K. Wang, "A Unified Simulation of the Filling and Post-filling Stages in Injection Molding. Part I: Formulation", Polym. Eng. Sci., vol. 31, No.2, P.116, 1991

19. Chiang, H. H., C. A. Hieber, and K. K. Wang, "A Unified Simulation of the Filling and Post-filling Stages in Injection Molding. Part II: Experimental Verification", Polym. Eng. Sci., vol. 31, No. 2, P.125, 1991

20. Kamal, M. R., and T. D. Papathanasiou, "Filling of a Complex-Shaped Mold with a Viscoelastic Polymer, Part I and Part II",Polym. Eng. Sci., vol. 33, No.

4, P.400, 1993

21. Titomanlio G., V. Speranzo, and V. Brucato, "On the Simulation of Thermoplastics Injection Moulding Process", Intern. Polymer Processing, No. 1, P.55, 1995

22. Shankar, A., and Paul F. W., "A Mathematical Model for the Evaluation of Injection Molding Machine Control", Trans. of the ASME, J. of Dynamic systems, Measurement, and Control, vol. 104, P.86, March 1982

23. Wang, K. K., S. F. Shen, C. Cohen, C. A. Hieber, T. H. Kwon, and R. C. Rickeston, "Computer-Aided Design and Fabrication of Molds and Computer Control of Injection Molding", Progress Report No.11, Injection Molding Project, Cornell University, Ithaca, New York

24. Chiu, C. P., M. C. Shih, and J. H. Wei, "Dynamic Modeling of the Mold Filling Process in an Injection Molding Machine", Polym. Eng. Sci., vol. 31, No. 19, P.1417, 1991

25. Wei, J. H., C. C. Chang, and C. P. Chiu, "A Nonlinear Model of a Servo-Pump Controlled Injection Molding Machine", Polym. Eng. Sci., vol. 34, No. 11, P.881, 1994

26. Woll, S. L. B., and D. J. Cooper, "A Dynamic Injection Molding Process Model for Simulating Mold Cavity Pressure Patterns", To be published in Polym. Eng. Sci.

27. Stephanopoulos, G., "Chemical Process Control, An Introduction to Theory and Practice", Prentice-Hall Inc., 1984

28. Seborg, D. E., T. F. and Edgar, D. A. Mellichamp, "Process Dynamics and Control", Wiley and Sons, 1989

29. Ljung, L., "System Identification, Theory for the User", Prentice Hall Inc., 1987

30. Paulson, D. C., "Guide to Injection Machine Control", SPE Journal, vol. 27, P.37, Jan. 1971

31. Keyes, D. L., "State of the Injection Molding Process Control", P.50, ANTEC 1974

32. Jordan, T. J., F. L. Laczko, R. T. Maher, and H. T. Plant, "Understanding and Controlling the Injection Molding Process", Modern Plastics, P.96, Sept. 1972

33. Peter, J. W., "Prelude to Automated Process Control", SPE J., vol. 28, P.57, Aug. 1972

34. Allen, E. O., and D. A. Vanputte, "Know All Your Molding Variables", Plastics Eng., P.37, July 1974

35. Mahoney, F. E., "Taking a Direct Route to Process Control", Modern Plastics, P.74, Oct. 1974

36. Plant, H. T., and R. T. Maher, "A Preliminary Analysis of the Injection Molding Process and Factors Effecting Part Size Control", P.74, ANTEC 1975

37. Abu Fara, D., "Control of Nozzle and Cavity Pressure during Filling and Packing in Thermoplastic Injection Molding", Ph.D Thesis, McGill University, Montreal, Canada, 1988

38. Davis, M. A., "Servocontrolled Injection Molding", P.618, ANTEC 1976

39. Paulson, D. C., "Closed Loop Process Control Brings Tenfold Gain in Molded-Part Accuracy", Modern Plastics, P.60, Aug. 1979

40. Sanschagrin, B., "Process Control of Injection Molding", Polym. Eng. Sci., vol. 23, No. 8, P.431, 1983

41. Agrawal, A. R., I. O. Pandelidis, and M. Pecht, "Injection Molding Process Control - A Review", Polym. Eng. Sci., vol. 27, No. 18, P.1345, 1987

42. Patterson, W. I., M. R. Kamal, and V. G. Gomes, "Dynamic Modeling and Control of Melt Temperature in Injection Molding", P.754, ANTEC 1985

43. Kamal, M. R., W. I. Patterson, and V. G. Gomes, "An Injection Molding Study, Part I: Melt and Barrel Temperature Dynamics", Polym. Eng. Sci, vol. 26, No.

12, P.854, 1986

44. Gomes, V. G., W. I. Patterson, and M. R. Kamal, "An Injection Molding Study. Part II: Evaluation of Alternative Control Strategies for Melt Temperature", Polym. Eng. Sci., vol. 26, No. 12, P.867, 1986

45. Ruscitti, G., "The Measurement and Control of Nozzle Melt Temperature in Thermoplastics Injection Molding",M.Eng. Thesis, McGill University, Montreal, Canada, 1993

46. Lu, C. H., and C. C. Tsai, "Multivariable Self-Tuning Temperature Control for Plastic Injection Molding Process", Intern. IEEE/IAS Conf. on Industrial Automation and Control, P.702, 1995

47. Bulgrin, T. C., and T. H. Richards, "Application of Advanced Control Theory to Enhance Molding Machine Performance", IEEE Transaction on Industry Applications", vol. 31, No.6, P.1350, Nov./Dec. 1995

48. Abu Fara, D., "The Dynamics of Injection Hydraulics in Thermoplastics Injection Molding", M.Eng., McGill University, Montreal, Canada, 1983

49. Wang, K. K., S. F. Shen, C. Cohen, C. Hieber, and A. I. Isayev, Progress Report # 10, Injection Molding Project, Cornell University, Ithaca, New York, 1984

50. Pandelidis, I. O., A. R. Agrawal, "Self-Tuning Control of RAM Velocity in Injection Molding", P.235, ANTEC, 1987

51. Pandelidis I. O., A. R. Agrawal, "Optimal Anticipatory Control of Ram Velocity in Injection Molding", Polym. Eng. Sci., vol. 28, No. 3, P.147, 1988

52. Zhang C. Y., J. Leonard, and R. G. Speight, "Adaptive Controller Performance Used for Ram Velocity Control during Filling Phase", P. 593, ANTEC 1996

53. Shankar, A., "Dynamic Modeling and Control of Injection Molding Machines", Ph.D Thesis, Carnegie Institute of Technology, Carnegie-Mellon University, Pittsburgh, USA, 1977

54. Speight R. G., J. B. Hull, and P. D. Coates, "Control of Polymer Melt Flow Front Position during the Injection Molding Process", P. 588, Antec 1995

55. Gao, F., W. I. Patterson, M. R. Kamal, "Dynamics and Control of Surface and Mold Temperatures in Injection Molding", Intern. Polymer Processing, VIII, P.147, 1993

56. Patterson, W. I., M. R. Kamal, and F. Gao, "Mold Temperature Measurement and Control", P.227, ANTEC 1990

57. Harry, D. H., "Injection Molding Machine Control Algorithm", P.383, ANTEC 1991

58. Kamal, M. R., W. I. Patterson, D. Abu Fara, "A Study of Injection Molding Dynamics", P.658, ANTEC 1983

59. M. R. Kamal, W. I. Patterson, D. Abu Fara, and A. Haber, "A Study in Injection Molding Dynamics", Polym. Eng. Sci., vol. 24, No. 9, P.686, 1984

60. Kamal, M. R., W. I. Patterson, N. Conley, D. Abu Fara, and G. Lohfink, "Dynamics and Control of Pressure in the Thermoplastics Injection Molding", P.189, ANTEC 1986

61. Kamal, M. R., W. I. Patterson, N, Conley, D. Abu Fara, and G. Lohfink, "Dynamics and Control of Pressure in the injection Molding of Thermoplastics", Polym. Eng. Sci., vol. 27, No. 18, P.1403, 1987

62. Haber, A., and M. R. Kamal, "The Dynamics of Peak Cavity Pressure in Injection Molding", P.107, ANTEC 1986

63. Haber, A., and M. R. Kamal, "The Dynamics of Peak Cavity Pressure in Injection Molding", Polym. Eng. Sci., vol. 27, No. 18, P.1411, 1987

64. Abu Fara, D., W. I. Patterson, and M. R. Kamal, "Cavity Pressure in Injection Molding During Filling, Packing, and Holding", P.221, ANTEC 1987

65. Abu Fara, D., M. R. Kamal, and W. I. Patterson, "Comprehensive Strategies for Sequential Closed-Loop Pressure Control throughout the Injection Molding

Cycle", P.239, ANTEC 1990

66. Smud, S. M., D. O. Harper, K. W. Leffew, "Advanced Process Control for Injection Molding", Polym. Eng. Sci., vol. 31, No. 15, P.1081, 1991

67. Wu, J. L., S. J. Chen, and R. Malloy, "Development of an On-Line Cavity Pressure-Based Expert System for Injection Molding Process", P.444, ANTEC 1991

68. Chiu, C. P., J. H. Wei, and M. C. Shih, "Adaptive Model Following Control of the Mold Filling Process in an Injection Molding Machine", Polym. Eng. Sci., vol. 31, No. 15, P.1123, 1991

69. Srinivasan, K., T. Srinivasan, and G. P. Maul, "Improvements in Closed Loop Control of Thermoplastic Injection Molding Processes", P.343, ANTEC 1991

70. Gao, F., W. I. Patterson, and M. R. Kamal, "Adaptive Control of Cavity Pressure during Filling", P.565, ANTEC 1993

71. Gao, F., W. I. Patterson, and M. R. Kamal, "Cavity Pressure Dynamics and Self-Tuning Control for Filling and Packing Phases of Thermoplastics Injection Molding", Polym. Eng. Sci., vol. 36, No. 9, P.1272, 1996

72. Patterson, W. I., F. Gao, and M. R. Kamal, "Control of Cavity Pressure during Packing", P.701, ANTEC 1994

73. Kamal, M. R., F. Gao, and W. I. Patterson, "Cavity Pressure Control During Cooling", P.706, ANTEC 1994

74. Hu, J., and J. H. Vogel, "Dynamic Modeling and Control of Packing Pressure in Injection Molding", Transaction of the ASME, J. of Eng. Materials and Technology, vol. 116, P.244, 1994

75. Seaman, C. M., A. A. Desrochers, and G. F. List, "Multi-objective Optimization of a Plastic Injection Molding Process", IEEE Transaction on Control Systems Technology, vol. 2, No. 3, P.157, Sep. 1994

76. Ljung, L., "System Identification Toolbox, for use with MATLAB", MathWorks Inc., 1991

77. Coates, P. D., and R. G. Speight, "Toward Intelligent Process Control of Injection Molding of Polymers", Proceeding of the Institution of Mechanical Engineers Part B- J. of Eng. Manufacture, vol. 209, No. 5, P.357, 1995

78. Ricketson, R. C., and K. K. Wang, "Injection Molding Process Control Based on Empirical Models", P.231, ANTEC 1987

79. Wang, P. J., and K. K. Wang, "Adaptive On-Line Process Control of Injection Molding Using PVT Model", P.2336, ANTEC 1991

80. Devos, P., F. Laurent, J. Pabiot, and M. Ryckebusch, "New and Autoadaptive Process Control on Plastic Injection Molding", P.2209, ANTEC 1992

81. Yakemoto, K., T. Sakai, Z. Maekawa, and H. Hamada, "Adaptive Holding Pressure Control Based on the Prediction of Polymer Temperature in a Mold Cavity", P.2192, ANTEC 1993

82. Varela A. E., W. I. Patterson, and M. R. Kamal, "Estimation of Melt Temperature and Part Weight in Injection Molding from Cavity Surface Temperature Measurements", P. 384, ANTEC 1995

83. Varela A. E., M. R. Kamal, and W. I. Patterson, "A Method for Estimating Bulk Melt Temperature and Part Weight in Injection Molding of Amorphous Thermoplastics", Advances in Polymer Tech., vol. 15, No.1, P.17, 1996

84. Varela, A., "Estimation and Control of Part Weight and Relevant Process Parameters in Injection Molding of Amorphous Thermoplastics", Ph.D Thesis, McGill University, Montreal, Canada, 1996

85. Taghizadegan S., "Statistical Process Control of Injection Molding Simulation Based on an Experimental Study", P. 598, ANTEC 1996

86. Haber, A., "Microprocessor Control System for the Injection Molding Process", M.Eng. Thesis, McGill University, Montreal, Canada, 1982

87. Gao, F., "Measurements, Dynamics and Control of the Mold Temperature of Injection Molding", M.Eng. Thesis, McGill University, Montreal, Canada, 1989

88. Dynisco, "Plastic Melt Pressure Transducer", Dynisco Bulletin B81, 1994

89. New York Ltd., "Plastic Melt Pressure Transducer/Transmitter", GP:50 New York Ltd., Bulletin 113, Rev 5, 1995

90. Chander Engineering Co., Manufactures of Physical Property Testing Instruments, Tulsa, Oklahoma, Catalogue 23-1

91. Fusser, H. B., "A Man-Machine Interface for PC-Controlled Injection Molding", M.Eng. Thesis, McGill University, Montreal, Canada, 1991

92. Gao, F., H. B. Fusser, M. R. Kamal, and W. I. Patterson, "A Versatile System for the Control of Injection Molding", ANTEC, P.1887, 1992

93. Didsbury, K., P. N. Leroux, and J. M. Ostrander, "QNX 4.1 Operating System, User's Guide", Quantum Software Systems Ltd., Kanata, Canada, 1992

94. Didsbury, K., P. N. Leroux, and J. M. Ostrander, "QNX 4.1 Operating System, System Architecture", Quantum Software Systems Ltd., Kanata, Canada, 1992

95. Didsbury, K, P. N. Leroux, and J. M. Ostrander, "QNX 4.1 Operating System, Utilities Reference", Quantum Software Systems Ltd., Kanata, Canada, 1992

96. Gao, F., "The Control of Cavity Pressure throughout the Injection Molding Cycle", Ph.D Thesis, McGill University, Montreal, Canada, 1993

97. Moy, F., "Microstructure and the Distribution of Tensile Properties in Injection Molded Polyethylene", Ph.D Thesis, McGill University, Montreal, Canada, 1980

98. Chu, E. F.-H., "A Comprehensive Integrated Computer Simulation of the Injection Molding Process for Thermoplastics", Ph.D Thesis, McGill University, Montreal, Canada, 1992

99. Du Pont Information Data Sheet, " Sclair 2908, Injection Molding Polyethylene Resin"

100. Product Data Sheet, "Styron 685D, Polystyrene Resins", Dow Plastics, Dow Chemical Canada Inc.

101. White, F. E., "Fluid Mechanics", McGraw-Hill Inc., New York, 1979

102. Tadmor, Z., and I. Klein, "Engineering Principles of Plasticating Extrusion", Van Norstrand Reinlod Co. 1970

103. Moog Electrohydraulic Servo-valve Manual, Moog A076 and 760 series, Catalog 762 686, Moog Inc.

104. Moog Pressure Line Filter, HP010 & HP020, Catalog 605 682, Moog Inc.

105. Tadmor, Z., C. G. Gogos, "Principles of Polymer Processing", John Wiley & sons, 1979

106. Oka, S., "The Steady Slow Motion of a Viscous Fluid through a Tapered Tube", J. of the Physical Society of Japan, vol. 19, No. 8, p.1481, August 1964

107. Oka, S., and A. Takami, "The Steady Slow Motion of a Non-Newtonian Liquid through a Tapered Tube", Japanese J. of Applied Physics, vol. 6, No. 4, p.423, April 1967

108. Kwon, T. H., S. F. Shen, and K. K. Wang, "Pressure Drop of Polymeric Melts in Conical Converging Flow: Experiments and Predictions", Polym. Eng. Sci., vol. 26, No. 3, p. 214, 1986

109. Cogswell, F. N., "Converging Flow of Polymer Melts in Extrusion Dies", Polym. Eng. Sci., vol. 12, No.1, p.64, 1972

110. Carnahan, B., "Applied Numerical Methods", Wiley Inc., New York, 1969

111. Lafleur P. G., "Computer Simulation of the Injection Molding of Viscoelastic Crystalline Thermoplastics", Ph.D Thesis, McGill University, Montreal, Canada, 1983

112. Wang K. K., C. Cohen, C. Hieber, Progress Report # 15, Injection Molding Project, Cornell University, Ithaca, New York, 1990

113. Encyclopedia of Polymer Science and Engineering, Second Edition, vol. 16, John Wiley & sons, 1989

114. Technical Report, Moog Controls, Industrial Division, New York, 14052-3300

115. Grace, A., "Optimization Toolbox for Use with MATLAB", The Math Works Inc., 1994

116. Morari, M., E. Zafiriou, "Robust Process Control", Prentice-Hall, Englewood, Cliffs, NJ, 1989

117. Fu, M., A. W. Olbrot, and M. P. Polis, "Comments on Optimal Gain for Proportional-Integral-Derivative Feedback", IEEE Control System Magazine, P. 100, January 1989

118. Crawford, R. , V. Klewpatinod, and P. P. Benham, "A study of Injection Molding Parameters and their Influence on Mechanical Properties", Plastics and Rubber: Processing, Dec., p.133, 1978

119. Malloy, K., S. J. Chen, and S. A. Orroth, "A Study of Injection to Holding Pressure Switch-Over Techniques Based on Time, Position or Pressure", p.33, ANTEC, 1987

120. Thayer, W. J., "Is There an Optimum Control for Injection Molding?", Plastics World, p.45, March 1975

121. Thayer, W. J., and M. A. Davis, "Controls for Injection Molding of Thermoplastics", Advances in Plastics Technology, p.28, July 1981

122. Bozzelli, J. W., and J. Cardinal, "Process Control on Injection Molding Machines: What is the Correct Hydraulic Response during Switch over from 1st to 2nd Stage?", P.584, ANTEC 1996

123. Qin Zou, P. E., and A. Gabriel,"Evaluation of the Fill-to-Pack Transfer Method: Position vs Velocity", p.637, ANTEC 1995

124. Malloy, R. A., S. J. Chen, and S. A. Orroth, "A Study of Injection to Holding Pressure Switch-over Techniques Based on Time, Position or Pressure", SPE Technical Papers, vol. 33, P.225, 1987

# APPENDIX A

## TRANSDUCER SPECIFICATION AND CALIBRATION

The pressure transducers used in this study were Dynisco models PT435A, PT422A, and GP:50-142. Specifications of the transducers are given in references [88,89].

Calibration of the pressure transducers was performed using a high pressure dead-weight tester [90]. It represents a source of accurate pressure. The calibration procedure of the manufacture was followed. The calibration was performed in psi as working units (1 Pa = $1.45 \times 10^{-4}$ psi). The output of a pressure transducer is proportional to its excitation voltage. The excitation voltage equals 10 volts: the transducer output range is 0-30 mv. Hence, a line is fitted to data in the following form:

$$P = Slope \times mv + Intercept \qquad \textbf{(A.1)}$$

where slope and intercept are found by curve fitting on the experimental data. The calibration by linear regression and shown in Figures A.1 and A.2.

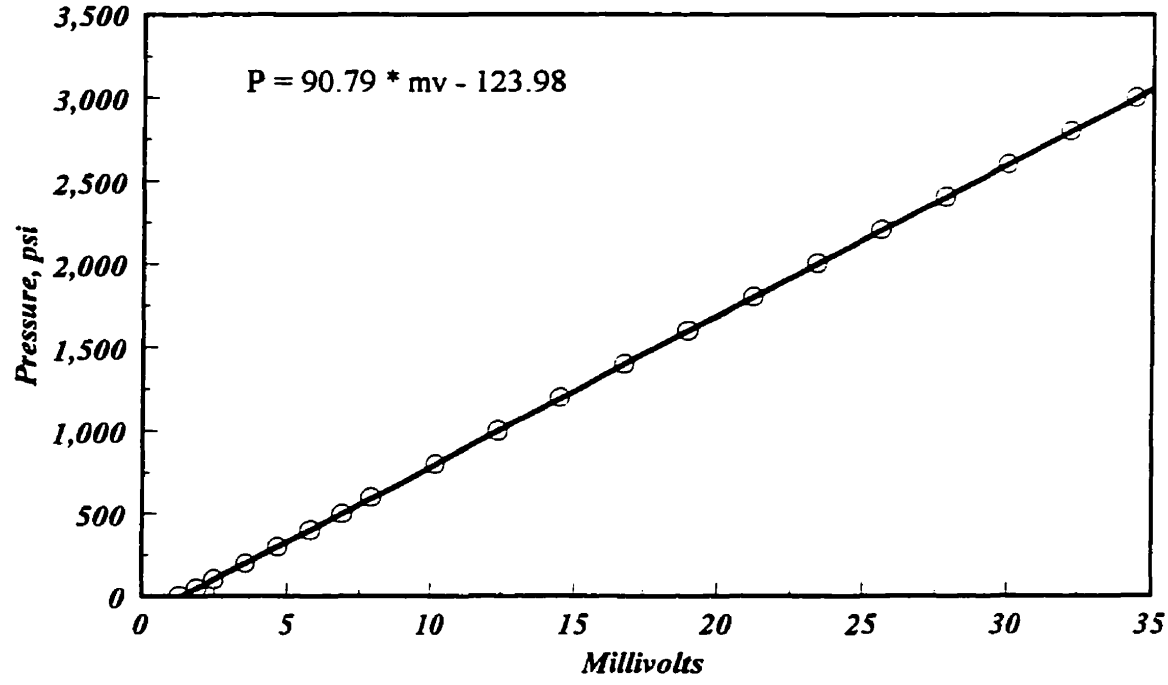


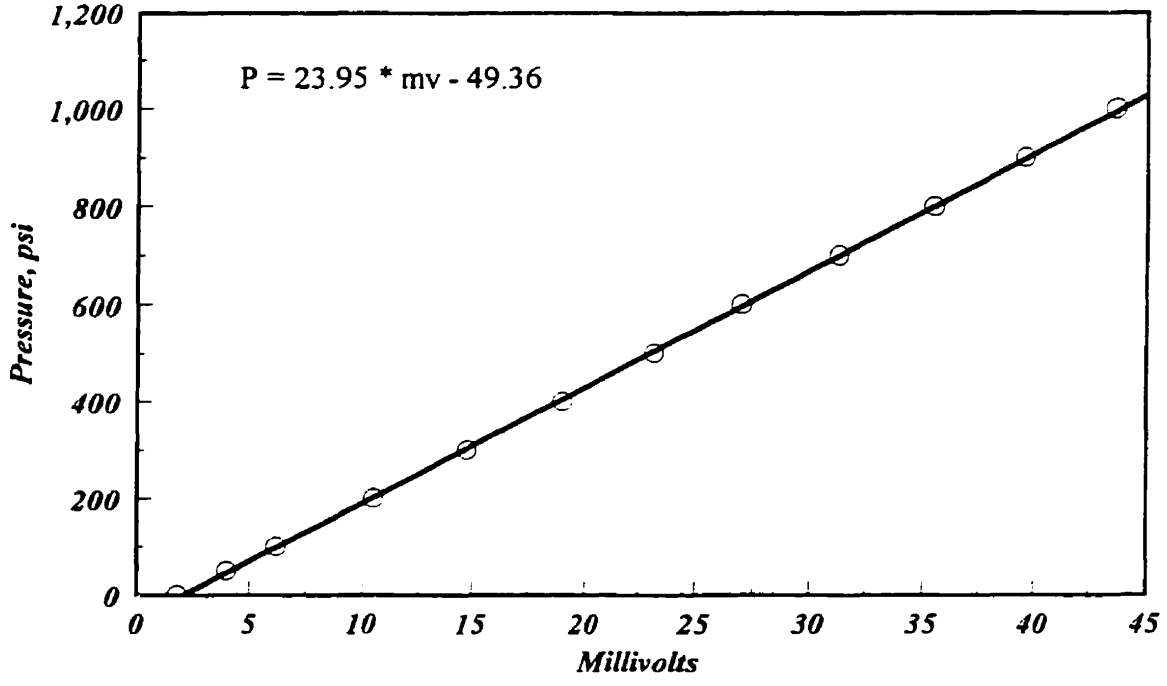


**Figure A.1** Calibration curves for the supply and injection cylinder PT

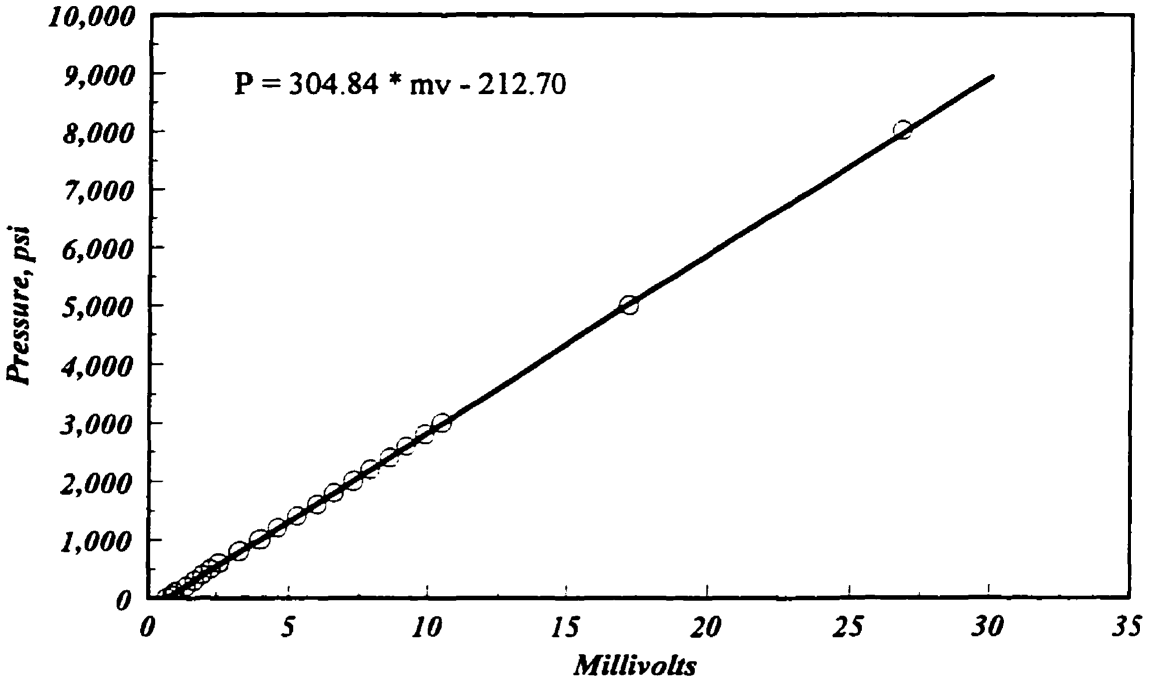


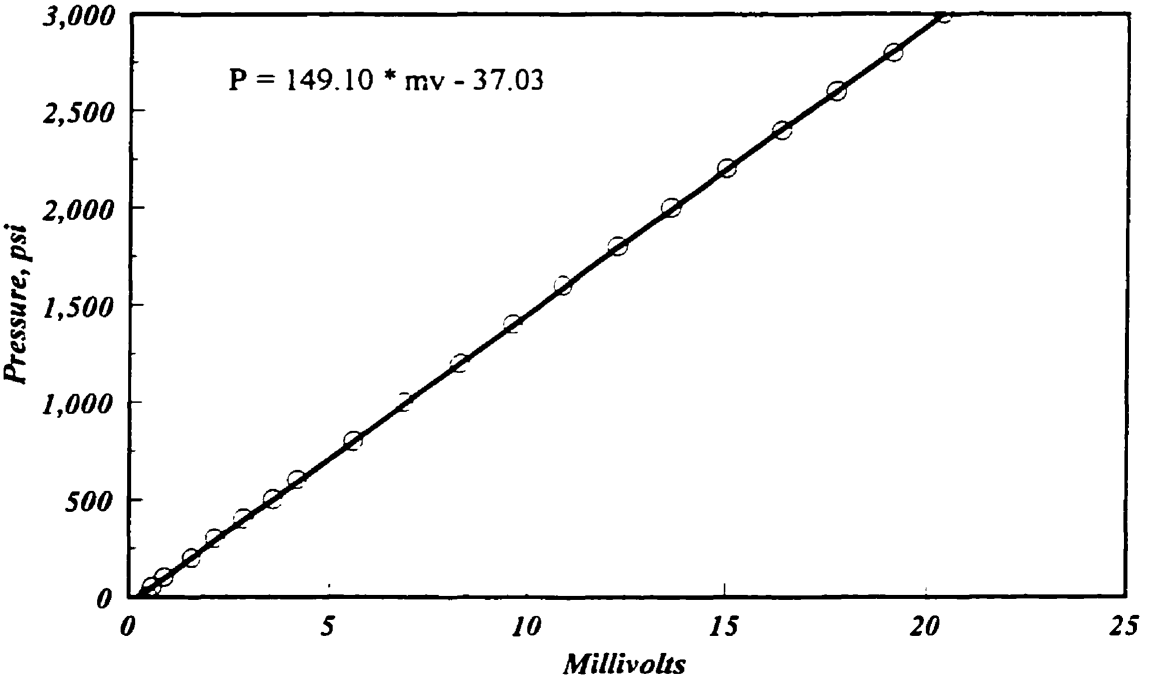


**Figure A.2** Calibration curves for the nozzle and cavity gate PT

# APPENDIX B

# INJECTION MOLDING MACHINE GEOMETRY

The list of injection molding machine geometry is presented in this appendix. For simplicity, the parameters are categorized into three groups: the hydraulic system geometry, and polymer delivery system geometry.

## B.1 The Hydraulic System Geometry

| | |
|---|---|
| $L_{s2}$ | 1.55 m |
| $L_{2h}$ | 1.26 m |
| $L_{23}$ | 4.18 m |
| $L_{exc}$ | 0.6 m |
| $R_{exc}$ | 0.005 m |
| $R_h$ | 0.0525 m |
| $R_t$ | 0.0075 m |
| $y_2$ | 0.52 m |
| $y_s$ | 0 m |
| $y_h$ | 0.96 m |
| $y_3$ | 0.34 m |
| $k_{23}$ | 23 |
| $k_{s2}$ | 2 |
| $\alpha$ | 2 |

## B.2 The Polymer Delivery system geometry

| | |
|---|---|
| $L_{n1}$ | 0.075 m |
| $L_{n2}$ | 0.052 m |
| $L_{n3}$ | 0.016 m |
| $L_s$ | 0.1 m |
| $L_r$ | 0.018 m |
| $L_g$ | 0.006 m |
| $R_n$ | 0.0175 m |
| $R_{s1}$ | 0.003 m |
| $R_{s2}$ | 0.005 m |
| $R_r$ | 0.0036 m |
| $A_g$ | $6.5 \times 10^{-6}$ m$^2$ |
| $w_c$ | 0.061 m |
| H | 0.0015 m |

# APPENDIX C

## PRESSURE DROP IN CONICAL CONVERGING FLOW

A formula for estimating pressure drop in a conical converging channel has been derived based on a power-law fluid model with normal stress effect incorporated. A $\theta$-averaged force balance has been first introduced. Figure B.1 shows schematic of flow geometry. Assuming that there is one velocity element in r-direction, the momentum balance in r-direction gives:

$$\frac{\partial(p+\tau_{rr})}{\partial r} = -\rho v_r \frac{\partial v_r}{\partial r} - \frac{2\tau_{rr} - \tau_{\theta\theta} - \tau_{\varphi\varphi}}{r} - \frac{1}{r}\frac{\partial \tau_{r\theta}}{\partial \theta} - \frac{\cos\theta}{r\sin\theta}\tau_{r\theta} \qquad \text{(C.1)}$$

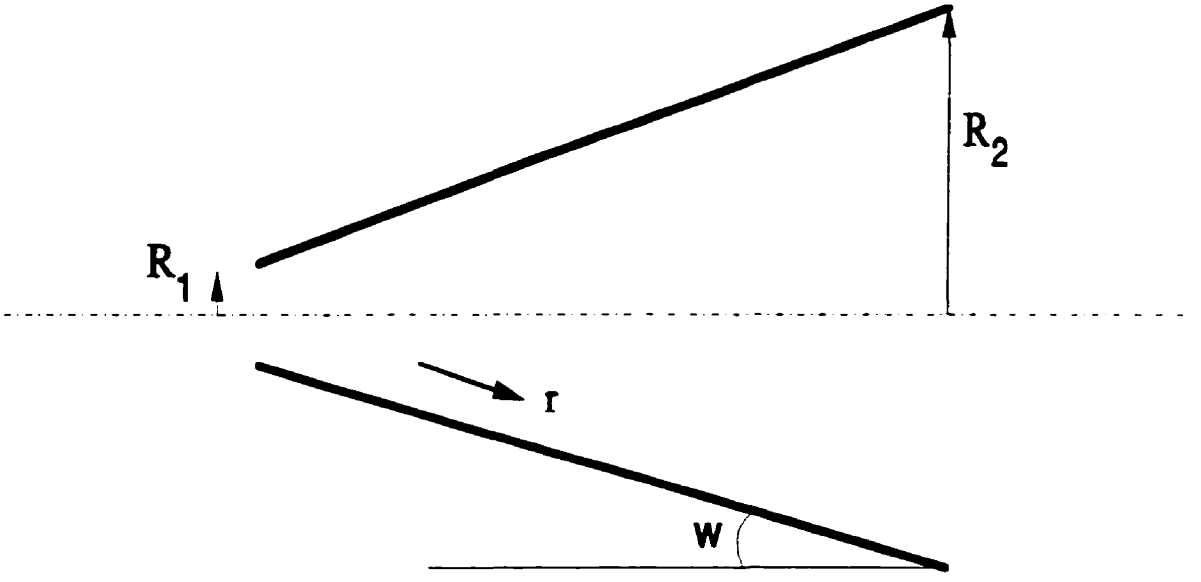


**Figure C.1** Schematic of flow geometry

The nominator of the third term in right hand side of Equation (C.1) can written as:

$$2\tau_{rr}-\tau_{\theta\theta}-\tau_{\varphi\varphi}=2(\tau_{rr}-\tau_{\theta\theta})+(\tau_{\theta\theta}-\tau_{\varphi\varphi})=2N_1+N_2=2N_1 \qquad \text{(C.2)}$$

It assumed that the second normal stresses difference is negligible. $p+\tau_{rr}$ is called P. An average pressure drop in each cross sectional area is defined as:

$$\bar{P}=(P+\tau_{rr})_{avg}=\frac{\int_0^{\omega}2\pi\sin\theta\cos\theta\,(P+\tau_{rr})\,d\theta}{\int_0^{\omega}2\pi r^2\sin\theta\cos\theta\,d\theta} \qquad \text{(C.3)}$$

To calculate average pressure it is necessary to determine the following relationship:

$$\int_0^{\omega}2\pi r^2\sin\theta\cos\theta\frac{\partial P}{\partial r}d\theta=-\int_0^{\omega}\rho v_r\frac{\partial v_r}{\partial r}2\pi r^2\sin\theta\cos\theta\,d\theta-\int_0^{\omega}4\pi rN_1\sin\theta\cos\theta\,d\theta \qquad \text{(C.4)}$$
$$-\int_0^{\omega}2\pi r\frac{\partial\tau_{r\theta}}{\partial\theta}\sin\theta\cos\theta\,d\theta-\int_0^{\omega}2\pi r\cos^2\theta\,\tau_{r\theta}d\theta$$

The result of these integrals are calculated by using Leibnitz rule for differentiating an integral. The velocity profile is [108]:

$$-r^2v_r(\theta)=f(\theta)=\frac{q}{2\pi I}\times\left[1-\left(\frac{\sin\theta}{\sin\omega}\right)^2\right] \qquad \text{(C.5)}$$

where I is:

$$I=\int_0^{\omega}\left[1-\left(\frac{\sin\theta}{\sin\omega}\right)^{\frac{1}{n}+1}\right]\sin\theta\,d\theta=\frac{2}{3}\frac{(1-\cos\omega)^2(1+2\cos\omega)}{\sin^2\omega}\frac{n+1}{3n+1} \qquad \text{(C.6)}$$

It should be mentioned the same result can be provided by changing the velocity in a pipe from cylindrical coordination to spherical coordination. The first normal stresses

difference is provided by power-law:

$$N_1 = \psi \dot{\gamma}^{f} = \psi \left( \frac{1}{r} \frac{\partial v_r}{\partial r} \right)^{f} \tag{C.7}$$

Substitution of Equations (C.3), (C.5), and (C.7) in Equation (C.4) gives:

$$\pi r^2 \sin^2\omega \frac{\partial \bar{P}}{\partial r} = \int_0^{\omega} 4\pi r \psi \left[ \frac{s+1}{r^3} \frac{q}{2\pi I} \right]^{f} \frac{\cos^{f}\theta \sin^{\frac{f}{n}}\theta}{\sin^{\frac{(n+1)f}{n}}\omega} \sin\theta\cos\theta\, d\theta$$

$$- \int_0^{\omega} \rho \frac{f(\theta}{r^2} \times \frac{2f(\theta)}{r^3} 2\pi r^2 \sin\theta\cos\theta\, d\theta + \int_0^{\omega} 2\pi r \cos^2\theta \eta_0 \left[ \frac{s+1}{r^3} \frac{q}{2\pi I} \right]^{n} \frac{\cos^{n}\theta \sin\theta}{\sin^{n+1}\omega} d\theta \tag{C.8}$$

$$+ 2\pi r \sin\omega \cos\omega\, \eta_0 \left[ \frac{s+1}{r^3} \frac{q}{2\pi I} \right]^{n} \frac{\cos^{n}\omega \sin\omega}{\sin^{n+1}\omega}$$

Calculating the result of integrals in this equation provides:

$$\frac{\partial \bar{P}}{\partial r} = -\frac{2\rho(s+1)}{r^5} \left( \frac{q}{2\pi I} \right)^2 \frac{(n+1)^2}{(3n+1)(4n+2)}$$

$$+ \frac{4\psi E (s+1)^{f}}{\sin^{2+f(1+1/n)}\omega} \left[ \frac{q}{2\pi I} \right]^{f} \frac{1}{r^{3f+1}} + \frac{2\eta_o (s+1)^{n}}{\tan\omega} \left[ \frac{q}{2\pi I \tan\omega} \right]^{n} \frac{1}{r^{3n+1}} \tag{C.9}$$

$$+ \frac{2\pi (s+1)^{n} (1 - \cos^{n+3}\omega)}{(n+3)\sin^{n+3}\omega} \left[ \frac{q}{2\pi I} \right]^{n} \frac{1}{r^{3n+1}}$$

where E is:

$$E = \int_0^{\omega} \cos\theta^{f+1} \sin\theta^{fn+1} \, d\theta \tag{C.10}$$

In the last step, the integration of this equation regarding r results the final pressure drop:

$$\begin{aligned}
\Delta\bar{P} = & \frac{-\rho(n+1)^3}{4n(3n+1)(2n+1)} \left(\frac{1}{2\pi I}\right)^2 q^2 \\
& + \frac{4\psi E}{3f \sin^{2+f+fn}\omega} \left(\frac{n+1}{n}\right)^f \left[\frac{1}{2\pi I}\right]^f \left(\frac{1}{R_1^{3f}} - \frac{1}{R_2^{3f}}\right) q^f \\
& + \frac{2\eta_0}{3n\tan\omega} \left(\frac{n+1}{n}\right)^n \left[\frac{1}{2\pi I}\frac{1}{\tan\omega}\right]^n \left(\frac{1}{R_1^{3n}} - \frac{1}{R_2^{3n}}\right) q^n \\
& + \frac{2\eta_0(1-\cos\omega)}{3n(n+3)\sin^{n+3}\omega} \left(\frac{n+1}{n}\right)^n \left[\frac{1}{2\pi I}\right]^n \left(\frac{1}{R_1^{3n}} - \frac{1}{R_2^{3n}}\right) q^n
\end{aligned} \tag{C.11}$$

# APPENDIX D

# PROPERTIES OF THE POLYMERS

This appendix is devoted to description of some of the physical and processing properties of the materials used in the present study. Two resins were used which are a injection molding grade high density polyethylene resin, Sclair 2908 supplied by Nova Chemicals, and polystyrene, Styron 685D supplied by Dow Chemical. In the two following sections the properties of these two resins are listed.

## D.1 Polyethylene Characterization

This resin was commonly designated as EX2 in earlier studies in this department. The properties and injection molding behavior of EX2 have been subjected of extensive studies in our group. The methods used to characterize the material have been described in detail elsewhere [97,98,111]. Some relevant properties of the resin, supplied by the manufacturer, are listed in Table 3.7. The relevant thermoplastics data, transport properties and other characteristics of this resin, employed in this study, are listed below. These data were obtained from the above refrences.

(a) Viscosity, $\eta$, Pa.s

$$\eta = k_a e^{-\frac{\Delta E}{RT}} \dot{\gamma}^{n-1} \qquad \text{(D.1)}$$

where n = 0.822

$k_a = 13.92\ kg.s^{a-2}/m$

$\Delta E/R = 2{,}167.4\ K$

(b) Thermal conductivity, k, W/m.K

$$k = \sum_{i=0}^{m} A_i (T - 273.15)^i \qquad \textbf{(D.2)}$$

where for the solid phase,

$m = 5$

$A_o = 5.1528 \times 10^3$

$A_1 = -1.1389 \times 10^2$

$A_2 = 3.6453$

$A_3 = -5.758 \times 10^{-2}$

$A_4 = 4.2367 \times 10^{-4}$

$A_5 = -1.1766 \times 10^{-6}$

and for the liquid phase,

$m = 3$

$A_0 = -2.6526 \times 10^3$

$A_1 = 0.9418 \times 10^2$

$A_2 = -5.6777 \times 10^{-1}$

$A_3 = 1.1607 \times 10^{-3}$

(c) Specific heat, $C_p$, J/kg.K

$$C_p = B_0 + B_1 T \qquad \textbf{(D.3)}$$

where $B_0 = 0.7314 \times 10^3$

$B_1 = 3.6314$

(d) Density, $\rho$, $kg/m^3$

$$\rho = \sum_{i=0}^{2} A_i P^i \qquad \textbf{(D.4)}$$

where P is pressure in Pa, and

| Temp. Range, °C | $A_0$ | $A_1 \times 10^6$ | $A_2 \times 10^{15}$ |
|---|---|---|---|
| ≤ 140 | 799.8 | 1,023.3 | -4,025.5 |
| 140 - 150 | 793.1 | 1,123.7 | -5,432.1 |
| 150 - 160 | 790.7 | 966.0 | -2,797.7 |
| 160 - 170 | 785.2 | 972.6 | -2,797.7 |
| 170 - 180 | 777.3 | 1,123.5 | -4,657.2 |
| 180 - 190 | 772.9 | 1,1017.3 | -2,954.4 |
| 190 - 200 | 765.9 | 1,051.8 | -2,991.4 |

(e) The first normal stresses difference, Pa

$$N_1 = \psi \dot{\gamma}^{f} \qquad \textbf{(D.5)}$$

where

| Temperature, °C | f | $\psi$ |
|---|---|---|
| 160 | 2.494 | 311.89 |
| 170 | 2.5613 | 364.16 |
| 180 | 2.4019 | 252.29 |

## D.2 Polystyrene Characterization

Some related properties, provided by Dow Chemical, mentioned in Table 3.8. This section, thermoplastics and transport properties are listed [112,113].

(a) Density, kg/m$^3$, T = °C

$$\rho = 1{,}086.5 - 6.19\times10^{-1} T + 1.36\times10^{-4} T^2 \qquad \textbf{(D.6)}$$

(b) Heat Capacity, $C_p$, J/mol.K

(c) Bulk modulus, $\beta_p$, MPa

3330 - 3660

$$\begin{aligned} 200<T<360\,K \quad & C_p = 7.7551\times10^{5}\,T^{-2} + 0.53447\,T - 41.58 \\ 373<T<600\,K \quad & C_p = 0.2653\,T + 95.12 \end{aligned} \tag{D.7}$$

(d) Thermal conductivity and diffusivity, k and $\alpha$, W/m.k and $m^2/s$, respectively

| Temp., K | k | $\alpha\times10^{-8}$ |
|---|---|---|
| 300 | 0.154 | 12.35 |
| 400 | 0.160 | 8.28 |
| 500 | 0.164 | 8.02 |

(e) Rheological behaviour, viscosity, $kN.s/m^2$

$$\eta = 10.8\,e^{-0.022(T°C-200)}\,\dot{\gamma}^{n-1} \tag{D.8}$$

(f) The first normal stresses difference, Pa

$$N_1 = 378.7423\times\dot{\gamma}^{1.326} \qquad at \qquad T=220°C \tag{D.9}$$

(g) P-V-T behavior, Tait equation of state

$$v(T,P) = v_0(T)\left(1 - 0.0894\ln\left[1 + \frac{P}{B(T)}\right]\right) \tag{D.10}$$

where

$$v_0(T) = \begin{cases} b_{1,l} + b_{2,l}\bar{T} & \text{if } T > T^* \\ b_{1,s} + b_{2,s}\bar{T} & \text{if } T \le T^* \end{cases}$$

$$B(T) = \begin{cases} b_{3,l} e^{-b_{4,l}\bar{T}} & \text{if } T > T^* \\ b_{3,s} e^{-b_{4,s}\bar{T}} & \text{if } T \le T^* \end{cases} \qquad \textbf{(D.11)}$$

$$\bar{T} = T - b_5$$

The transition temperature $T^*$ at a given pressure is given by the intersection of the v-T isobaric lines in the liquid and solid states.

| $b_{1,l}$ $m^3/kg$ | $b_{2,l}$ $m^3/kg.°C$ | $b_{3,s}$ $N/m^2$ | $b_{4,l}$ $°C^{-1}$ | $b_5$ °C |
|---|---|---|---|---|
| $1.0071\times10^{-3}$ | $5.789\times10^{-7}$ | $2.021\times10^{8}$ | $3.01\times10^{-3}$ | 150 |
| $b_{1,s}$ $m^3/kg$ | $b_{2,s}$ $m^3/kg.°C$ | $b_{3,s}$ $N/m^2$ | $b_{4,s}$ $°C^{-1}$ | |
| $9.86\times10^{-4}$ | $2.422\times10^{-7}$ | $2.26\times10^{8}$ | $1.363\times10^{-3}$ | |

**Table D.1** - Constants for the double-domain Tait equation of state

# IMAGE EVALUATION
# TEST TARGET (QA-3)

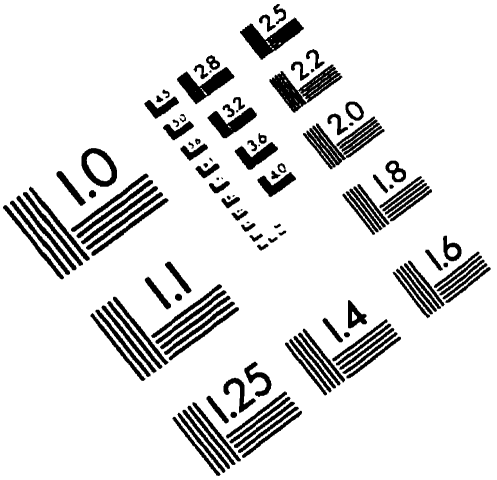


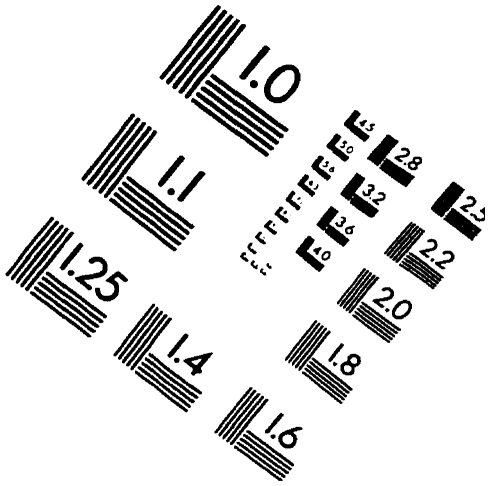


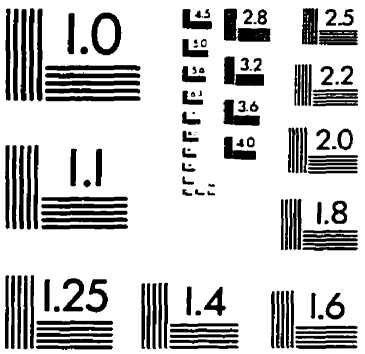


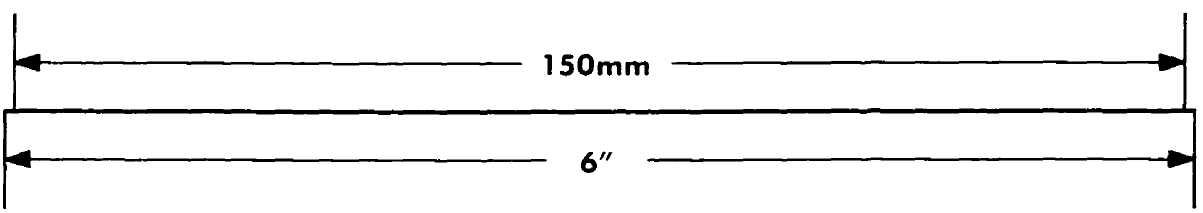


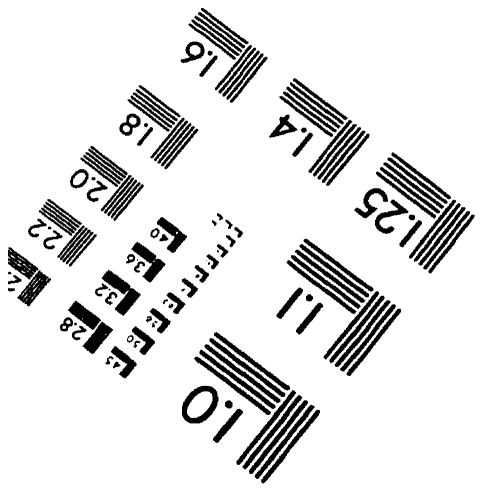


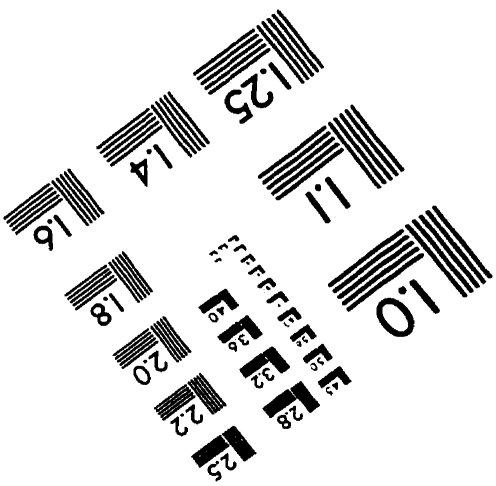


APPLIED IMAGE, Inc
1653 East Main Street
Rochester, NY 14609 USA
Phone: 716/482-0300
Fax: 716/288-5989